THE JOURNAL
OF
CHEMICAL PHYSICS

VOLUME 20, NUMBER 2 FEBRUARY, 1952

Dipole Moments Derived from Force Constants and Ionic Refractions

CHR. KNAKKERGAARD MØLLER
Chemical Laboratory, Royal Veterinary and Agricultural College, Copenhagen, Denmark

For simple hydrogen compounds an approximate formula is derived which correlates the dipole moments of the H-bonds with the corresponding stretching force constant, bond length, and ionic refraction—and which contains only a single adjustable parameter.

IT has been suggested in a previous paper[1] that there may be a certain simple connection between the force constants of some bonds involving hydrogen and the ionic refractions of the atoms to which the hydrogen is bonded, and the diminution of the force constants in the series HF, HCl, HBr, and HJ was explained as due to the polarizing influence of the proton on the halide ion. Now, it seems likely that the variation of the dipole moments in these molecules may also be described in terms of the polarizability of the halide ions,[2] and, considering only simple H-compounds, it will be shown in the following how it is possible on the basis of a very simple model to "predict" reasonable values for the dipole moments from knowledge of the force constants and ionic refractions.

In order to compare the force constants K_{ij} proper we refer them to the same standard bond length, say 1A, by means of a formula:[1]

$$K_{ij}\cdot d_{ij}=C_{ij}\cdot 10^{-8}, \tag{1}$$

where d_{ij} is the bond length. The reduced force constants C_{ij} obtained in this way, for simple H-bonds, can be shown roughly to obey the relation:[1]

$$C_{ij}=(8.8-0.23A_j)\cdot 10^5 \text{ dynes/cm}, \tag{2}$$

where A_j is the ionic refraction of the atom to which H is bonded. The term involving A_j is to be interpreted as follows. The vibrating proton induces in the halide ion an electric moment the magnitude of which varies in phase with the vibrations. As the induced moment represents potential energy there must be a force component acting on the proton which depends on the polarizability—and so on A_j—of the halide ion. Let us introduce a screening factor σ characteristic of each bond (and so of the bond length) which factor is practically constant for small variations in the bond length about the characteristic equilibrium position. It can then easily be shown[1] that the polarizability of the halide ion "j" contributes to the force constant:

$$-\tfrac{1}{2}\alpha_j\left(\frac{\partial^2 E^2}{\partial x^2}\right)_{x=d_{ij}}=-\frac{3A_j}{8\pi N}\left\{\frac{\partial^2}{\partial x^2}\left(\frac{e\sigma}{x^2}\right)^2\right\}_{x=d_{ij}}$$

$$=-\frac{3\cdot 20A_j}{8\pi N}\cdot\frac{e^2\sigma^2}{d_{ij}^6}, \tag{3}$$

where $\alpha_j=3A_j/4\pi N$ is the polarizability, e the elementary charge $4.80\cdot 10^{-10}$ esu, and $N=6.03\cdot 10^{23}$.

Without polarization the reduced force constants should be about $8.8\cdot 10^5$ dynes/cm. Identifying the deviations herefrom with the above calculated electrostatic contribution, also referred to the standard bond length 1A, we get with C_{ij} in 10^5 dynes/cm

$$\sigma^2/d_{ij}^5=0.110\cdot(8.8-C_{ij})\cdot 10^{40}/A_j,$$

or with d_{ij} in A, K_{ij} in 10^5 dynes/cm and A_j in cm^3:

$$3A_j\sigma/4\pi N d_{ij}^3=0.131(8.8/d_{ij}-K_{ij})^{\frac{1}{2}}A_j^{\frac{1}{2}}. \tag{4}$$

While in the case of vibrations we consider the proton alone being responsible for the *changes* in polarization, in order to calculate the mean value of the absolute polarization of the halide ion we must also take into account the influence of an eventual electron cloud about the proton. Hence to this purpose we reckon with a net charge $<4.80\cdot 10^{-10}$ about the protonic center—but use the screening factor from (4). The difficulty is to determine this net charge. If it has any

[1] A. Langseth and C. K. Møller, Acta Chem. Scand. 4, 937 (1950).
[2] P. Debye, *Polar Molecules* (Dover Publications, New York, 1946).

TABLE I. Comparison of bond moments obtained from (5) and from experimental data.

Bond (compound)	d_{ij}	K_{ij} 10^5 dynes/cm	A_j cm³	μ_{ij} calc D	μ_{ij} exp[a] D
HF	0.92A	9.7	2.2	1.66	1.91[b]
HCl	1.28A	5.15	8.45	1.15	1.03
HBr	1.41A	4.11	11.84	0.86	0.78
HJ	1.60A	3.14	18.47	0.37	0.38
HO (H_2O)	1.02A	7.6	4.06	1.34	1.51
HS (H_2S)	1.33A	4.25	15.0	0.53	0.68
HSe (H_2Se)	1.53A	3.37	17.3	0.44	0.3*
HN (H_3N)	1.01A	6.86	7	0.96	1.31
HP (H_3P)	1.45A	3.33	18	0.21	0.36
HAs (H_3As)	1.56A	2.81	20	0.04	0.10
HC (H_4C)	1.09A	5.45	12	0.53	0.4

* Obtained from the dipole moment given for H_2Se in Gmelins Handbuch.
[a] Linus Pauling, *Nature of the Chemical Bond* (Cornell University Press, Ithaca, 1945).
[b] N. B. Hannay and C. P. Smyth, J. Am. Chem. Soc. **68**, 171 (1946).

sense to speak about the charge of an atom in a molecule we may presumably imagine the atom core embedded in an electron cloud of about the same volume as in the free atom and with a definite mean charge. Instead of using a new protonic net charge for each compound as basis for the calculation of dipole moments we shall assume the same charge all over, and account for the differences in polarizability (or ionic character) by subtracting the moments induced in the X-ion by the proton. As our starting point we may then choose a molecule where the hydrogen-bonded atom is non-polarizable, i.e., the bond mainly having ionic character. The nearest we can come to this is in HF. But even here we do not know the charge on the hydrogen atom. However, we may consider this magnitude as a parameter which we put equal to $1.80\cdot10^{-10}$ esu—in order to get a reasonable agreement with the experimentally determined values of the dipole moments.

Some justification for this choice may be given by the following argument. The more ionic character we give the HX-bond and the shorter we make it the bigger is the force constant. We then tentatively assume that it is possible to determine its value in HF from purely electrostatic considerations.—As the force constant is determined by the curvature of the potential curve this assumption does not imply that homopolar forces are not operative in the bond formation. We imagine the proton as center of a uniform negative space charge with radius $a=0.53$A (the Bohr radius) and a total charge ϵ' which we want to determine. We consider this electron cloud as attached to the halide ion. Now it is well known that a positive charge e inside a sphere, uniformly filled with negative space charge, will execute harmonic vibrations[3] and the force constant is determined by

$$K=\epsilon'\cdot e/a^3.$$

Inserting $K=9.7\cdot10^5$ dynes/cm, $a=0.53$A and $e=4.80\cdot10^{-10}$ esu we get $\epsilon'=-3.00\cdot10^{-10}$ esu so that the net charge on the hydrogen atom is $\epsilon=1.80\cdot10^{-10}$ esu.

Assuming furthermore the same uniform distribution over the whole molecule—with radius 1.36A—we calculate the total number of electrons in it to be $(1.36/0.53)^3\cdot(3.00/4.80)=10.7$; actually it should be 10.—These are certainly very rough approximations and it may be fortuitous that we get the wanted values—presumably several neglected effects cancel each other.

We are now able to calculate the dipole moments of the simplest H-bonds from:

$$\mu_{ij}=\epsilon d_{ij}-\sigma\epsilon\alpha_j/d_{ij}^2=\epsilon d_{ij}(1-3\sigma A_j/4\pi N d_{ij}^3),$$

or using (4) and putting $\epsilon=1.80\cdot10^{-10}$ esu:

$$\mu_{ij}=1.80\cdot d_{ij}\{1-0.131(8.8/d_{ij}-K_{ij})^{\frac{1}{3}}A_j^{\frac{1}{3}}\}\text{ debyes,}\quad(5)$$

where d_{ij} is in A, K_{ij} in 10^5 dynes/cm, and A_j in cm³. Where the ionic refractions are known they are taken from[2] or from Gmelin's *Handbuch der Anorganischen Chemie*. For CH_3^-, NH_2^-, PH_2^-, and AsH_2^- they are obtained from (2), inserting the known values for d_{ij} and K_{ij}.[4] In this way we get $A(CH_3)\approx12$, $A(NH_2)\approx7$, $A(PH_2)\approx18$, and $A(AsH_2)\approx20$. Too much reliance should not, of course, be put on these values; that may be the explanation that the calculated dipole moment for the N—H bond does not agree very well with the experimental one. As for the dipole moment of the C—H bond its direction as obtained here is opposite that calculated by Coulson.[5] On the whole the agreement between calculated and experimental bond moments is not bad, considering the roughness of the procedure and the uncertainties inherent in the ionic refractions and the stretching force constants. (See Table I.)

It should be noted that the final formula (5) correlates the dipole moment with magnitudes which it is possible to measure by physical methods, except, perhaps, for the factor $1.80\cdot10^{-10}$. But even this factor seems to have a physical sense and in fact it seems not necessary to resort to the more dubious concept of electronegativity.

ACKNOWLEDGMENT

I wish to thank the director of the laboratory, Professor A. Tovborg Jensen, for interest in this work and Dr. Chr. Højendahl for kind criticism.

[3] See e.g., G. Joos, *Theoretical Physics* (Blackie and Sons, London, 1946).
[4] See e.g., W. Gordy, J. Chem. Phys. **14**, 305 (1946).
[5] C. A. Coulson, Trans. Faraday Soc. **38**, 433 (1942).

The Reaction of Ethyl Radicals with Deuterium

M. H. J. WIJNEN* AND E. W. R. STEACIE
Division of Chemistry, National Research Council, Ottawa, Canada

(Received August 20, 1951)

The reaction of ethyl radicals with deuterium has been studied. The ethyl radicals were produced by photodecomposition of diethyl ketone. As activation energy was found $E=13.3\pm0.5$ kcal. From this value it may be concluded that the activation energy is about 11.5 ± 1 kcal for the reaction of ethyl radicals with hydrogen.

INTRODUCTION

THE fact that there is little quantitative information about the reactions of ethyl radicals of the type

$$C_2H_5+RH=C_2H_6+R$$

is mainly due to the uncertainty of the mechanisms by which ethyl radicals are produced. More complete investigations of two photochemical sources of ethyl radicals have been made recently. Of these two sources, diethyl mercury[1] and diethyl ketone,[2,3] the latter is far more convenient for use as an ethyl source since its vapor pressure and its thermal stability are considerably greater than those of diethyl mercury.

EXPERIMENTAL

The apparatus was mainly the same as used in the photolysis of diethyl ketone.[2] The deuterium was brought into the reaction cell through a hot palladium tube and mixed thoroughly with the diethyl ketone by letting the gas expand several times in a 200 cc bulb. The analysis system contained a silica gel trap, a pump-down liquid nitrogen trap, a modified Ward still[4] and a combined Toepler pump and gas burette. The reaction products and the excess diethyl ketone were adsorbed on silica gel cooled by liquid nitrogen, and the main part of deuterium was pumped off. The C_2 and the C_4 fractions were then condensed in the pump-down trap and CO and the rest of the D_2 were removed. The C_2 fraction was finally pumped off at $-175°C$, measured in the gas burette, and analyzed by a mass spectrometer. After a few runs it became clear that part of the C_4 fraction, even at room temperature, was withheld by the silica gel. No attempt was therefore made to measure the amount of C_4 produced in subsequent runs.

As light source, the full radiation from a Hanovia *S*500 medium pressure arc was used.

The diethyl ketone was obtained from the Eastman Kodak Company and was distilled once in vacuum before use. The deuterium was prepared by Dr. L. C. Leitch of this laboratory and contained 4 percent HD.

RESULTS

In Table I are given the results obtained for mixtures of diethyl ketone and deuterium under various conditions. The total pressures in column 3 are given in mm at 0°C. The ratio of diethyl ketone pressure to deuterium pressure is given in column 4. In experiments 29 and 30 the intensity of the light source was cut down by the use of neutral density filters to 10 percent (29) and 26.5 percent (30) of the intensity used in all other experiments. In Table II are given the results obtained with mixtures of diethyl ketone and deuterium in the presence of an excess of helium.

DISCUSSION

The reaction mechanism for the photolysis of diethyl ketone in the presence of D_2 may be given by

$$C_2H_5COC_2H_5+h\nu=2C_2H_5+CO \quad (1)$$

$$C_2H_5+C_2H_5=C_4H_{10} \quad (2)$$

$$C_2H_5+C_2H_5=C_2H_6+C_2H_4 \quad (3)$$

$$C_2H_5+C_2H_5COC_2H_5=C_2H_6+C_2H_4COC_2H_5 \quad (4)$$

$$C_2H_5+D_2=C_2H_5D+D \quad (6)$$

$$D+C_2H_5COC_2H_5=HD+C_2H_4COC_2H_5 \quad (7)$$

$$C_2H_4COC_2H_5=C_2H_4+CO+C_2H_5. \quad (5)$$

Reactions (1) to (5) form the reaction mechanism for the photolysis of diethyl ketone alone and have been discussed in a previous paper.[2]

If reaction (5) is excluded temporarily then we may write

$$\frac{R_{C_2H_5D}}{R_{C_2H_6-C_2H_4}}=\frac{k_6(C_2H_5)(D_2)}{k_4(C_2H_5)(C_2H_5COC_2H_5)} \quad (I)$$

or

$$\frac{k_6}{k_4}=\frac{R_{C_2H_5D}}{R_{C_2H_4-C_2H_4}}\frac{(C_2H_5COC_2H_5)}{(D_2)} \quad (II)$$

In the above expressions $R_{C_2H_6-C_2H_4}$ denotes the rate of ethane formation by reaction (4) only. This is obtained by subtracting the amount of ethylene from the total amount of ethane.

* National Research Council of Canada Postdoctorate Fellow, 1949–1951.

[1] K. J. Ivin and E. W. R. Steacie, Proc. Roy. Soc. (London) (to be published).

[2] Kutschke, Wijnen, and Steacie, J. Am. Chem. Soc. (to be published).

[3] M. H. J. Wijnen and E. W. R. Steacie, Can. J. Chem. (to be published).

[4] D. J. LeRoy, Can. J. Research, **B28**, 492 (1950).

TABLE I. Photolysis of diethyl ketone in the presence of D_2. Composition of C_2 fraction.

Exp No.	Temp °C	Total press mm at 0°C	P_{DK}/P_{D_2}	C_2 formed mm³ (N.T.P.)	% C_2H_5D	% C_2H_6	% C_2H_4	$\frac{R_{C_2H_5D}}{R_{C_2H_6-C_2H_4}}\cdot 10^2$	$\frac{k_6}{k_4}\cdot 10^2$
21	54	76	0.252	52	0.6	64.8	33.5	1.92	4.84
19	87	76.5	0.261	80	0.85	78.6	20.5	1.46	3.81
15	136	94	0.173	43.5	3.3	81.6	15.1	4.96	8.58
17	136	69.5	0.256	57.5	2.74	87.1	10.1	3.56	9.1
25	152	81.7	0.264	78	3.4	90.0	6.7	4.08	10.8
29	176.5	74.5	0.262	172	5.7	92.4	1.9	6.3	16.5
30	176.5	76	0.26	145	5.4	91.5	3.2	6.12	15.9
31	176.5	77	0.26	78	4.6	87.4	8.1	5.8	15.1
32	176.5	79	0.376	78	3.6	89.9	6.6	4.3	16.1
33	176.5	77	0.096	86	11.3	79.2	9.4	16.2	15.5
26	180	84	0.254	106	4.7	90.7	4.7	5.46	13.9
27	200	79.5	0.254	118	6.5	88.5	5.0	7.78	19.7
11	216	40.8	0.63	90	4.65	83.6	11.6	6.45	40.6
12	216	44.5	0.26	128	8.6	81.3	10.1	12.1	31.4
13	216	61.5	0.18	130	10.7	74.8	14.5	17.7	31.8
14	216	67.7	0.35	88	7.8	82.7	9.5	10.6	37.1
28	216	80.5	0.255	96	9.5	83.5	6.9	12.4	31.6
22	257	71.5	0.25	205	12.4	77.6	10.0	18.3	45.7
23	257	22.6	0.254	122	15.7	75.0	9.2	23.8	60.5
24	257	80	0.264	177	11.6	79.0	9.7	16.7	44
48	286.5	74.5	0.284	252	11.9	75.6	12.5	18.8	53.4

The amount of ethylene produced by reaction (5), increases with increasing temperature and decreasing intensity. The influence of the intensity has been studied in experiments 29, 30, and 31. In experiment 29 the intensity was cut down to 10 percent and in experiment 30 to 26.5 percent of the intensity used in experiment 31. The results obtained for k_6/k_4 (column 10, Table I) are the same, within experimental error, in spite of considerable change in the percentage of ethylene in the C_2 fraction.

It has been shown in a previous investigation[2] of the photolysis of diethyl ketone that the ratio C_2/C_4 increases with increasing temperature and decreasing intensity. This explains why reaction (5) has little or no influence on $R_{C_2H_6-C_2H_4}$. The ethyl radicals formed by reaction (5) will almost certainly react with diethyl ketone to form ethane, so that for each C_2H_4 molecule formed by reaction (5) another C_2H_4 molecule is formed by reaction (4). It is, therefore, justifiable to ignore reaction (5).

Equation (II) indicates that k_6/k_4 is independent of the ratio $(C_2H_5COC_2H_5)/(D_2)$. The experiments at 216°C and experiments 31, 32, and 33 show that this is true.

If $(C_2H_5COC_2H_5)/(D_2)$ is kept constant then $R_{C_2H_5D}/R_{C_2H_6-C_2H_4}$ should be constant at constant temperature. This is shown by experiments 12, 28 and 22, 24. The high value for k_6/k_4 in experiment 23 may be due to the very low pressure used in this experiment.

In the above reaction scheme we did not consider the possibility of a reaction between the C_2H_5 radicals and the D atoms. The following reactions are theoretically possible

$$C_2H_5+D=C_2H_5D^* \quad (8)$$

$$C_2H_5D^*=C_2H_5+D \quad (9)$$

$$C_2H_5D^*=C_2H_4D+H \quad (10)$$

$$C_2H_5D^*=C_2H_4+HD \quad (11)$$

$$C_2H_5D^*=CH_3+CH_2D \quad (12)$$

$$C_2H_5D^*+M=C_2H_5D+M. \quad (13)$$

Of these reactions, only reactions (10), (11), and (13) could lead to erroneous results in the estimation of the activation energy of the reaction $C_2H_5+D_2$. If reaction (10) occurred to an appreciable amount, it should be possible to detect $C_2H_4D_2$ as a reaction product, but no trace of it was found. If reactions (11) and (13) occurred, the ratio $R_{C_2H_5D}/R_{C_2H_6-C_2H_4}$ would be

TABLE II. Photolysis of diethyl ketone in the presence of D_2 and He. Composition of C_2 fraction.

No.	Temp °C	Total press mm at °C	P_{He} mm at °C	P_{DK}/P_{D_2}	C_2 formed in mm³ (N.T.P.)	% C_2H_5D	% C_2H_6	% C_2H_4	$\frac{R_{C_2H_5D}}{R_{C_2H_6-C_2H_4}}\cdot 10^2$	$\frac{k_6}{k_4}\cdot 10^2$
8	92	129	85.5	0.314	55	1.05	69.5	29.5	2.63	8.25
1	146	108	72	0.371	78	2.0	77.3	20.7	3.53	13.1
2	146	113	74	0.396	67	1.8	79.4	18.8	2.71	10.7
7	160	158	120	0.357	90	2.6	83.6	13.7	3.72	13.3
5	192	123	83	0.364	154	3.4	84	12.7	4.77	17.4
6	218	125	84	0.372	130	5.6	86	8.4	7.22	26.8
4	242	116	78	0.368	170	7.1	83.2	9.7	9.66	3.56

changed by the presence of a foreign gas. A few experiments were therefore made using an excess of helium (Table II). The results do not differ from those obtained from experiments in the absence of helium.

In Fig. 1, $\log k_6/k_4$ is plotted against $1/T$. The open circles represent the values of Table I (no helium present); the filled circles give the values of Table II (excess helium present).

From Fig. 1 we obtain as activation energy for the reaction

$$C_2H_5+D_2=C_2H_5D+D. \qquad (6)$$

$E_6=E_4+5.9\pm0.5$ kcal$=13.3\pm0.5$ kcal.†

Accepting as collision diameters $\sigma_{D_2}=2.8\ 10^{-8}$ cm and $\sigma C_2H_5=4.10^{-8}$ cm and as steric factor for reaction (4) $P_4\simeq 3.\ 10^{-4}$ [2]) we obtain for the steric factor of reaction (6) $P_6\simeq 10^{-3}$.

No other values were found in the literature for the activation energy of reaction (6). If, however, we compare this reaction with the reaction,

$$C_2H_5+H_2=C_2H_6+H, \qquad (14)$$

then it seems logical that the large difference in zero point energy between H_2 and D_2 will lead to a difference in activation energy between reactions (6) and (14) of the order of 1–2 kcal. We suggest, therefore, as activation energy for reaction (14) $E_{14}=11.5\pm1$ kcal. Estimates of the activation energy for reaction (14) have been given by Leermakers[5] ($E_{14}>15$ kcal), Moore and Taylor[6] ($E_{14}=9\pm2$ kcal) and by Jungers and Taylor[7] ($E_{14}>11$ kcal). Our estimate is, therefore, in reasonable agreement with earlier work. If we consider the difference in bond dissociation energy between the CH_3-H and C_2H_5-H bonds it is clear that the activation energies for the reactions of ethyl radicals with H_2 and D_2 should be higher than the activation energies for the similar reactions with methyl radicals. Our results are, therefore, not consistent with the values obtained by Anderson, Davison, and Burton[8] for the activation energies of the reactions of methyl radicals with hydrogen (12.1 kcal; 13.7 kcal) and deuterium (13.2 kcal; 14.8 kcal). Recent work done in this laboratory by Dr. T. G. Majury[9] leads, however, to much lower values than those obtained by Anderson, Davison, and Burton for the reaction of methyl radicals with hydrogen and deuterium.

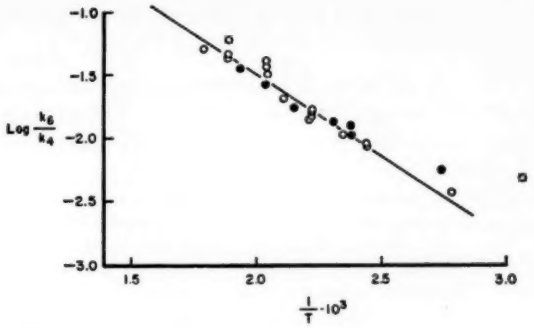

FIG. 1. Arrhenius plot of k_6/k_4.

Another check on the proposed value for E_{14} may be obtained from the activation energy of the reaction

$$C_2H_6+H=C_2H_5+H_2, \qquad (15)$$

E_{15} has been given as 9 kcal by Trost and Steacie[10] and as 7.2 kcal by Trenner, Morikawa, and Taylor.[11] Recent experiments by Darwent[12] indicate an activation energy for reaction (15) of about 6 kcal. Trost and Steacie's value has been based on an assumed steric factor of 0.1 for reaction (15). A lower steric factor will reduce their value of E_{15}.

$$H+C_2H_6 \underset{E_{14}}{\overset{E_{15}}{\rightleftharpoons}} C_2H_5+H_2.$$

Accepting $E_{14}=11.5\pm1$ kcal we obtain for reaction (15) $E_{15}=11.5\pm1-(102.5-98)=7\pm1$ kcal which is thus consistent with earlier estimates of the activation energy of reaction (15).

ACKNOWLEDGMENT

The authors wish to thank Miss Frances Gauthier and Dr. F. P. Lossing for the mass spectrometer analyses.

† Assuming $E_4=7.4$ kcal, as found in previous work. (See reference 2.)

[5] J. A. Leermakers, J. Am. Chem. Soc. **55**, 4508 (1933).
[6] W. J. Moore and H. S. Taylor, J. Chem. Phys. **8**, 396 (1940).
[7] J. C. Jungers and H. S. Taylor, J. Chem. Phys. **6**, 325 (1938).
[8] Anderson, Davison, and Burton, Disc. Faraday Soc. (April, 1951).
[9] T. G. Majury and E. W. R. Steacie, unpublished results.
[10] W. R. Trost and E. W. R. Steacie, J. Chem. Phys. **16**, 361 (1948).
[11] Trenner, Morikawa, and Taylor, J. Chem. Phys. **5**, 203 (1937).
[12] B. deB. Darwent (unpublished results).

On the Early Stages of Condensation of Rare-Gas Type Molecules*

SIDNEY G. REED, JR.
The Catholic University of America, Washington, D. C., and the U. S. Naval Ordnance Laboratory, White Oak, Silver Spring, Maryland†

(Received August 13, 1951)

The early stages of condensation are treated from the standpoint of the associative equilibrium of single molecules and stable molecular aggregates. Formulas are presented for partition functions from which one can calculate standard chemical potentials and concentrations of specified configurations of up to 8 molecules having a Lennard-Jones (6–12) interaction. Numerical results are given for nitrogen. It appears that nitrogen aggregate concentrations fall steeply with decreasing temperature. Results of this procedure, using a restricted region of phase space, are compared with those obtained with no restrictions for 2 and 3 molecule aggregates.

1. INTRODUCTION

CONDENSATION in a vapor free of dust and ions must start with the formation of very small molecular aggregates. The aggregates containing a given number n of molecules can form, in general, a number of relatively stable isomeric configurations, all of which are present in different concentrations at equilibrium. In theories of the kinetics of condensation the aggregates have been supposed to undergo a critical stage of growth for some value or range of values of n for which their concentration is a minimum.[1] The formation of these critical aggregates, or nuclei, is the bottleneck for the growth process. When the aggregates contain a sufficiently large number of molecules, they may be considered spherical droplets for which, at temperature T, a vapor pressure p is determined according to the Thomson formula

$$kT\ln(p/p_0)=2\gamma m/\rho r, \tag{1}$$

where γ is the surface tension, m the mass, r the radius, and ρ the density. The vapor pressure over a plane surface of the condensed phase is p_0.

In many discussions of the beginnings of condensation, Eq. (1) has been extrapolated to apply to nuclei which were supposed to contain only a few molecules. This procedure has been recognized to be unsound for a number of reasons, which may be summarized as follows:

(a) The thermodynamic equilibrium of aggregates with single molecules depends, in general, on the concentration of aggregates. As the aggregates increase in size, the importance of their concentration diminishes, and for droplets it is altogether negligible.[2]

(b) The division of properties of matter into bulk and surface properties depends on the short range of molecular interaction forces. In the case of droplets, one can speak of this difference being located in a layer of thickness of roughly twice this range, about 5 to 10A. Aggregates containing only a few molecules are not more than 3 to 4 times this range in diameter. The definition of r becomes ambiguous in extrapolation of Eq. (1) to such aggregates, and it is difficult to see how anything but an artificial extension of the concept of surface tension could be made for them. In the range of droplet radii for which γ can be defined macroscopically, it is expected to decrease with decreasing radius.[3]

The approach chosen here is to consider the equilibrium of single molecules with aggregates containing only a few molecules, using the methods of statistical mechanics and thermodynamics.[4] Previous work in this direction, for aggregates containing more than 2 molecules, has either involved, in part, one of the macroscopic extrapolations just discussed[5] or used only bond energies, not free energies.[6] For each value of n, calculation is made here for only one of the relatively stable isomeric configurations. This is a symmetrical configuration of low energy in which the molecules are supposed to rotate freely and to make simple harmonic vibrations around their equilibrium positions. The potential energy of two molecules distant r cm is presumed to be given by the Lennard-Jones formula

$$\varphi(r)=4\epsilon[(\sigma/r)^{12}-(\sigma/r)^6], \tag{2}$$

where ϵ and σ are constants for a specific molecule. The minimum of $\varphi(r)$ occurs at $r=r_0=1.122\sigma$. The aggregates and single molecules are treated as independent constituents of a perfect gas mixture. On these assumptions the partition functions of aggregates containing 2, 3, 4, 5, 6, and 8 molecules are expressed in terms of ϵ, σ, and parameters determined by the geometry. Using these, standard chemical potentials, and for given temperature and concentration of single molecules, concentrations of these aggregates can be

* Parts of this paper are based on a portion of a thesis submitted in partial fulfillment of the requirements for the degree of Doctor of Philosophy in the Catholic University of America.

† Present address, Physics Department, Loyola University, New Orleans 18, Louisiana.

[1] R. Becker, Disc. Faraday Soc. **5**, 55 (1949).

[2] W. H. Rodebush, Chem. Revs. **44**, 269 (1949).

[3] R. C. Tolman, J. Chem. Phys. **17**, 333 (1949); J. Kirkwood and F. P. Buff, J. Chem. Phys. **17**, 338 (1949); **18**, 991 (1950).

[4] J. E. and M. G. Mayer, *Statistical Mechanics* (John Wiley and Sons, Inc., New York, 1940).

[5] W. Band, J. Chem. Phys. **7**, 324 (1939); J. Frenkel, *Kinetic Theory of Liquids* (Oxford University Press, London, 1946); O. K. Rice, J. Chem. Phys. **15**, 314 (1947).

[6] H. G. Stever, private communication; G. C. Benson and R. Shuttleworth, J. Chem. Phys. **19**, 130 (1951).

computed. Numerical results of this procedure, making the further approximations of including only nearest neighbor interactions and neglecting stretching of the aggregates due to their rotation, are presented for nitrogen. The aggregate concentrations so found may be regarded as estimates of nuclei concentrations used in discussions of condensation kinetics.[1,7]

By taking into account only small harmonic vibrations around equilibrium positions of the molecules in an aggregate, arrangements very different from equilibrium are assumed negligibly rare, and some error is made in the partition function. The general expression for the partition function which does not involve this assumption may be written as a phase integral in $3n$ dimensions but has proved very difficult to evaluate for $n>3$. For the cases $n=2$ and 3 some comparison can be made, as shown in the appendix, between ratio of partition functions found by our approximate procedure and those obtained using the general expression. Although the comparison may be regarded as satisfactory as to numerical agreement, the interpretation of this is not quite clear.

2. THERMODYNAMIC CONSIDERATIONS

If aggregates of all kinds and single molecules present in a large volume V are in equilibrium, we have

$$\mu_n = n\mu_1, \tag{3}$$

where μ_n is the chemical potential of a single n-aggregate, and μ_1 that of a single molecule. Isomeric aggregates have equal chemical potentials. On the basis of our assumptions we can write

$$\mu_n = \mu_n^\dagger + kT\ln c_n, \tag{4}$$

where $\mu_n^\dagger$ is the standard chemical potential of the n-aggregate and c_n its concentration, measured in number of n-aggregates per cc. According to the definition[8]

$$\mu_n^\dagger = -kT\ln(Q_n/V), \tag{5}$$

where Q_n is the partition function of the aggregate. We suppose Q_n to be separable into a product of the partition functions of the individual molecules within the aggregate and the partition function of the aggregate as a whole. The internal partition function of the molecules is assumed to be unaffected upon condensation to form the aggregate. The partition function of the aggregate proper is designated in the following as Q_n for simplicity, and is taken to be separable into a product of translational, rotational, vibrational, and energy contributions. Then $\mu_n^\dagger$ is separable into a sum of corresponding contributions. Of all the isomeric configurations for a given n, those having smallest $\mu_n^\dagger$ will have largest concentrations.

From Eqs. (3) and (4) we can write

$$\ln c_1 = -(\mu_1^\dagger - \mu_n^\dagger/n)/kT + (\ln c_n)/n, \tag{6}$$

which exhibits the fact that c_1 depends on $\mu^\dagger_n$ and c_n through their nth roots. As n increases, therefore, c_1 will become effectively independent of c_n and only the contributions to $\mu_n^\dagger$ of order n will matter. These are, of course, the vibration and energy contributions which, for very large n, go over into the chemical potential μ_0 of one molecule in the localized bulk phase.

It is convenient to refer values of μ_1 to those at saturation for the same temperature,

$$\mu_1 = \mu_0 + kT\ln(c_1/c_0). \tag{7}$$

The quantity $\ln(c_1/c_0)=\ln(p_1/p_0)=s$ is a measure of the under- or supersaturation. From Eqs. (3), (4), and (7) we have, for the concentration of the n-aggregate

$$c_n = \exp n(s + (\mu_0 - \mu_n^\dagger/n)/kT). \tag{8}$$

3. THE PARTITION FUNCTION

A. Statistical Formulas

The different contributions to the partition function of an aggregate of molecules having the interaction (2) can be expressed in terms of parameters depending only on ϵ and σ, and on constants depending on the geometry. These parameters are the (dimensionless) wavelength[9]

$$\Lambda = h/\sigma(m\epsilon)^{\frac{1}{2}}$$

and the (dimensionless) temperature

$$\tau = kT/\epsilon,$$

where m is the mass of a single molecule. The translational partition function of an n-aggregate may now be written

$$(Q_n)_k = V\sigma^{-3}(2\pi n)^{\frac{3}{2}}(\Lambda\tau^{-\frac{1}{2}})^{-3}. \tag{9}$$

The classical rotational partition function for a rigid dumb-bell is

$$(Q_2)_r = 4\pi^2 IkT/h^2,$$

which can be written

$$(Q_2)_r = 2.518\pi^2(\Lambda\tau^{-\frac{1}{2}})^{-2}. \tag{10}$$

For nonlinear aggregates, $n>2$,

$$(Q_n)_r = \pi^{\frac{1}{2}}(A_nB_nC_n)^{\frac{1}{2}}\zeta_n^{-1}(8\pi^2kT/h^2)^{\frac{3}{2}},$$

where A_n, B_n, C_n are the three principal moments of inertia and ζ_n is the symmetry number. Putting

$$(A_nB_nC_n)^{\frac{1}{2}} = 1.413\delta_n(m\sigma^2)^{\frac{3}{2}},$$

where δ_n is a pure number depending on the geometry, we have

$$(Q_n)_r = 31.96\pi^{7/2}\delta_n\zeta_n^{-1}(\Lambda\tau^{-\frac{1}{2}})^{-3}. \tag{11}$$

[7] M. Volmer, *Kinetik der Phasenbildung* (Steinkopf, Dresden, 1939).

[8] Reference 4, p. 128.

[9] J. de Boer, Physica **14**, 139 (1948).

TABLE I. Symmetrical configurations used in calculation.

No. of molecules	Configuration	No. of bonds
2	dumb-bell	1
3	equilateral triangle	3
4	tetrahedron	6
5	trigonal bipyramid	9
6	octahedron	12
8	double tetrahedron	18

The vibrational partition function can be expressed as

$$(Q_n)_v=\prod_j(1-\exp(-h\nu_n^{(j)}/kT))^{-1}, \quad (12)$$

where

$$2\pi\nu_n^{(j)}=(\varphi''(r_0)/m)^{\frac{1}{2}}\cdot a_n^{(j)}$$

and

$$h\nu_n^{(j)}/kT=1.203(\Lambda\tau^{-1})a_n^{(j)},$$

the $a_n^{(j)}$ being (for $n>2$) $3n-6$ numbers determining the natural frequencies. For $n=2$, $a_2=2^{\frac{1}{2}}$. In the approximation of including only nearest neighbor interactions, the zero point energy of the aggregate is

$$U_n^0=-[\beta_n\epsilon-\textstyle\sum_j(h\nu_n^{(j)}/2)], \quad (13)$$

where β_n is the number of bonds of (assumed) length r_0. For the energetic contribution to the partition function

$$(Q_n)_\epsilon=\exp(-U_n^0/kT),$$

we can write

$$(Q_n)_\epsilon=\exp[\tau^{-1}(\beta_n-0.602\Lambda\textstyle\sum_j a_n^{(j)})]. \quad (14)$$

B. Description of Aggregates

The configurations listed in Table I were selected for aggregates containing up to 8 molecules. The 8 molecule aggregate, called in Table I a double tetrahedron, is formed by adding to a tetrahedron four more molecules in equilibrium positions with respect to triangular faces.

The values of the constants ζ_n, δ_n, and β_n for these configurations are given in Table II.

The values of β_n, ζ_n, and δ_n were obtained from elementary geometric considerations. Values of $a_n^{(j)}$ for $n=2$, 3 and 4 were found from the literature.[10] An application of the method of symmetry coordinates[11] was made to obtain $a_n^{(j)}$ for $n=5$, 6 and 8. The spectrum for $n=6$ was also obtained by a modification of the procedure of Eucken and Sauter.[12]

From Table II it can be seen that there are accidental degeneracies occurring, for $n=6$ and 8. A coupling of vibrational modes is expected in such a case, because the weak intermolecular forces will lead to anharmonicities. Our calculation neglects any such coupling, as also the coupling of rotation and vibration.

[10] G. Herzberg, *Infrared and Raman Spectra* (D. Van Nostrand Company, Inc., New York, 1945).
[11] Reference 10, p. 145.
[12] A. Eucken and F. Sauter, Z. physik. Chem. **B26**, 463 (1934).

4. NUMERICAL RESULTS FOR NITROGEN

Calculations of the concentrations c_n were made for nitrogen, using Eq. (8), the formulas of Section 3, and the values $\Lambda=0.225$ and $\epsilon/k=96.6°K$.[9] In computing μ_0, the vapor has been assumed to be a perfect gas, with the pressure of the equilibrium bulk phase for a given temperature, obtained from Keesom and Bijl.[13] Only the translational part of the partition function of the vapor molecules was used, in accordance with the assumption of free rotation in the condensed aggregates. The results are given in Table III for five values of τ and for $s=0$. Concentrations for higher values of s may be obtained, according to Eq. (8), by adding $0.434ns$ to each value in Table III. Concentrations of single molecules, $n=1$, are also given for comparison.

From Table III it appears that the concentrations decrease rapidly with τ and that this decrease is more steep for the larger aggregates. The concentrations for $\tau=1.0$ are quite large. In this connection it should be recalled that the calculation was performed assuming the system of aggregates and single molecules could be regarded as a mixture of perfect gases, and that μ_0 could be computed taking the vapor to be a perfect gas. Both of these assumptions fail for the high densities at $\tau=1.0$. Conditions are apparently too near the critical point, which occurs for $\tau=1.3$.

TABLE II. Constants for configurations of Table I.

n	β_n	ζ_n	δ_n	$a_n^{(j)}$ (Integers in parentheses indicate degeneracy of preceding frequency)
2	1	2	...	2
3	3	6	$2^{\frac{1}{2}}$	3, $(\frac{3}{2})$ (2)
4	6	12	$2^{\frac{1}{2}}$	1(2), 2, 2(3)
5	9	6	$(242/36)^{\frac{1}{2}}$	0.2(2), 1.27(2), 1.49(2), 1.5, 2.12, 0.39
6	12	24	8	1(2), 1(3), 2, 2(3), $(\frac{3}{2})$ (3)
8	18	12	$(68/9)^{\frac{1}{2}}$	0.2(3), 0.97(3), 1(2), 1.07(3), 1.70(2), 2.20(3), 1.34, 2.20

5. DISCUSSION

Gilmore[14] has made a comparison of the values of chemical potentials of nitrogen aggregates obtained by our procedure with those found using formulas involving various extrapolations of macroscopic surface tension. Agreement is reported with the results of some of his formulas, when the surface tension correction of Tolman[3] is not used. The data are unfortunately too meagre to allow conclusions to be drawn about the relative worth of the various surface tension extrapolations.

Table III gives concentrations of only one configuration for each n. A rough estimate of total concentration of all relatively stable n-aggregates can be obtained by simply enumerating all configurations having about the same number of nearest neighbor bonds,

[13] Keesom and Bijl, Physica **4**, 305 (1937).
[14] F. R. Gilmore, thesis, California Institute of Technology (1951).

and assigning the same c_n from Table III to each. In this way the total concentration of 6-aggregates is estimated roughly to be twice c_6 of the table, and that of 8-aggregates as 8 times c_8 of the table.[15]

Second neighbor interactions have two partly compensating effects. The nearest neighbor bond lengths are slightly shortened, increasing the potential energy of the aggregate, while the second neighbor interactions themselves lower the potential energy. The second of these predominates, but is found to alter the chemical potentials by only a few percent when taken into account.

The author wishes to thank Professor Karl F. Herzfeld for much advice and encouragement, Dr. R. Becker for helpful discussion, and Miss D. Ericson for assistance with computation.

APPENDIX

For the cases $n=2$ and 3 the evaluations of the general expression for the partition function are implicit in calculations of second and third virial coefficients such as have been performed by Hirschfelder's group.[16]

TABLE III. $\mathrm{Log}_{10}c_n$ for nitrogen as function of $\tau=T/96.6$, for $s=\ln(p_1/p_0)=0$. Values for $s\neq 0$ may be obtained by adding $0.434ns$. Units of c_n are no. per cc.

n \ $\tau=$	0.3	0.4	0.6	0.8	1.0
1	11.9	15.1	18.4	19.9	20.8
2	5.0	10.7	16.1	18.8	17.8
3	−2.5	5.7	13.5	17.4	19.9
4	−10.4	0.3	11.6	15.0	17.8
5	−16.6	−4.3	8.1	13.6	17.2
6	−26.2	−11.1	3.5	10.0	14.6
8	−39.9	−20.1	−0.5	9.8	15.5

To connect our approach to that of the theory of nonideal gases,[4,17] one uses Eq. (4) for $n=1$,

$$\mu_1=\mu_1^{\dagger}+kT\ln c_1.$$

Now the total number N of molecules is

$$N=\sum_n nN_n, \tag{15}$$

where N_n is the number of n-aggregates, and in equilibrium

$$N_n/N_1{}^n=\mathbf{Q}_n/\mathbf{Q}_1{}^n, \tag{16}$$

where the $\mathbf{Q}$ are the exact partition functions. Therefore

$$c=N/V=\sum_n n(\mathbf{Q}_n/V)(V/\mathbf{Q}_1)^n c_1{}^n, \tag{17}$$

where $\mathbf{Q}/V$ is independent of V. Then c_1 can be expressed as a power series in c. The deviations from the ideal gas behavior in the chemical potential are given by $kT\ln(c_1/c)$. Developing this in powers of c with the help of Eq. (17) and calculating the equation of state, it is possible to relate $\ln(\mathbf{Q}_2/\mathbf{Q}_1)$ with the second virial coefficient, and $\ln(\mathbf{Q}_3/\mathbf{Q}_2)$ with the second and third virial coefficients. These relations are

$$\ln(\mathbf{Q}_2/\mathbf{Q}_1)=\ln(-B^{(0)}(\tau))+\ln[(2\pi)^{5/2}/3\Lambda^3] \tag{18}$$

and

$$\ln(\mathbf{Q}_3/\mathbf{Q}_2)=\ln(\mathbf{Q}_2/\mathbf{Q}_1)+\ln 2[1-C^{(0)}(\tau)/4(B^{(0)}(\tau))^2], \tag{19}$$

where $B^{(0)}$ and $C^{(0)}$ are the reduced virial coefficients tabulated in reference 15.

TABLE IV. Comparison of exact and approximate calculation.

τ	$\log_{10}(\mathbf{Q}_2/\mathbf{Q}_1)$ (virial coeff)	$\log_{10}(Q_2/Q_1)$ (harm vibr)	$\log_{10}(\mathbf{Q}_3/\mathbf{Q}_2)$ (virial coeff)	$\log_{10}(Q_3/Q_2)$ (harm vibr)
0.3	4.084	3.731	...*	...*
0.4	4.005	3.850	...	...
0.6	3.922	3.849	...	...
0.8	3.888	3.921	4.175	3.527
1.0	3.867	4.013	4.178	3.620

* No data in reference 15.

In Table IV we present the exact classical values from Eqs. (18) and (19) and the results of our calculation assuming harmonic vibrations, for the range of τ for which our other calculations have been made. The quantities listed are logarithms to base 10 rather than natural logarithms.

The exact $\mathbf{Q}$ calculated from virial coefficients differs on two points from the approximate Q obtained assuming only simple harmonic vibrations. Since the potential curve flattens out for large displacements outward from the minimum, the exact $\mathbf{Q}$ should exceed Q. On the other hand, $\mathbf{Q}$ also measures the effect of those molecules which have a positive relative energy, i.e., which are not bound. This effect will decrease $\mathbf{Q}$, since a region of space is excluded for the molecules' passage, and even in the attractive region they move faster, and occupy this region less often than in the absence of such forces. Unfortunately these two effects are not separated, and the comparison of $\mathbf{Q}$ and Q is not as useful for our purposes as might be hoped.

In reference 15 the third virial coefficient has been calculated only down to $\tau=0.7$. It is clear from the graphs of the virial coefficients[18] as functions of τ that in the region of interest to us, the difference between calculated third virial coefficients is large because the slopes are so steep there. The comparison for Q_2/Q_1 seems satisfactory, on the whole. For $\tau\gtrsim 0.8$, Q_2/Q_1 is larger than $\mathbf{Q}_2/\mathbf{Q}_1$, which seems to indicate the predominance of the second of the two effects just discussed. For Q_3/Q_2 this seems to be the case in the whole range here considered.

[15] The configurations can be enumerated according to the symmetry classes. For example, for $n=8$ we have 1 of group T_d, used in computing Table III, 1 of D_{6h} (hexagonal bipyramid), 2 of C_3, 4 of C_2.

[16] R. B. Bird and E. L. Spotz, University of Wisconsin CM-599, Project NOrd 9938 (1950).

[17] J. de Boer, Phys. Soc. Reports on Progress in Physics, XII (1949).

[18] Reference 15, p. 35 and p. 92.

The Frictional Coefficient for Flexible Chain Molecules in Dilute Solution*

LEO MANDELKERN AND PAUL J. FLORY
Department of Chemistry, Cornell University, Ithaca, New York
(Received July 12, 1951)

The frictional coefficient, f_0, of a polymer molecule in dilute solution is assumed to vary directly as an average linear dimension of the chain. From this assumption equations are developed, as follows, which are analogous to those used successfully in the interpretation of intrinsic viscosity measurements; $f_0/\eta_0 = K_f M^{\frac{1}{3}}\alpha$ and $K_f = P(\langle r_0^2\rangle/M)^{\frac{1}{2}}$ where α represents the factor by which the actual root-mean-square end-to-end distance exceeds the unperturbed distance $(\langle r_0^2\rangle)^{\frac{1}{2}}$, M is the molecular weight, η_0 the viscosity of the medium, and P should be a universal constant.

Data in the literature on the dependence on molecular weight of sedimentation constants and diffusion coefficients, extrapolated to infinite dilution confirm the conclusions drawn from these equations.

RECENT investigations[1–6] of the intrinsic viscosities of a wide variety of flexible chain molecules have shown that in dilute solution the polymer molecule may be replaced by an equivalent hydrodynamic sphere, in so far as its frictional effects are concerned. In particular, these results show unequivocally that the radius of this effective sphere varies directly with an average linear dimension of the polymer, such as the root-mean-square beginning-to-end distance of the chain. This has been shown to hold over wide variations in temperature and molecular weight and for a variety of polymer types, each in a number of solvents. According to the theory for the configuration of real polymer chains,[1,3] the intrinsic viscosity, $[\eta]$, is governed by the following equations:

$$[\eta] = KM^{\frac{1}{2}}\alpha^3, \tag{1}$$

$$K = \Phi(\langle r_0^2\rangle/M)^{\frac{3}{2}}, \tag{2}$$

$$\alpha^5 - \alpha^3 = 2\psi_1 C_M(1-\Theta/T)M^{\frac{1}{2}}. \tag{3}$$

Φ appears to be a universal constant the same for all polymers, and $(\langle r_0^2\rangle)^{\frac{1}{2}}$ is the root-mean-square distance from beginning to end of the chain in the absence of perturbances caused by interaction between remotely connected segments. α represents the factor by which the actual root mean-square end-to-end distance $(\langle r^2\rangle)^{\frac{1}{2}}$ exceeds the unperturbed distance in a particular solvent at a given temperature. ψ_1 is an entropy parameter and C_M is calculable according to theory from $M/\langle r_0^2\rangle$. Θ is the critical temperature at which phase separation occurs for a polymer of infinite molecular weight in the given solvent.

Similarly, it can be expected that the frictional coefficient, f_0, will also vary as an average linear dimension of the polymer chain. If η_0 is the viscosity of the medium, then in analogy with Eqs. (1) and (2) we may write:

$$f_0/\eta_0 = K_f M^{\frac{1}{3}}\alpha, \tag{4}$$

where

$$K_f = P(\langle r_0^2\rangle/M)^{\frac{1}{2}}, \tag{5}$$

and P, like the Φ of the corresponding viscosity relation, should be a universal constant the same for all polymers. Just as K can be determined by measuring $[\eta]$ at a temperature $T=\Theta$ where $\alpha=1$, so K_f should be obtainable by measuring f_0/η_0 at $T=\Theta$. Substituting Eq. (5) in (4), and noting that $(\langle r_0^2\rangle)^{\frac{1}{2}}\alpha = (\langle r^2\rangle)^{\frac{1}{2}}$,

$$P = (f_0/\eta_0)(\langle r^2\rangle)^{-\frac{1}{2}}. \tag{6}$$

Hence, P may be established by determining the frictional coefficient f_0 and the root-mean-square end-to-end distance $(\langle r^2\rangle)^{\frac{1}{2}}$ (as obtained, for example, from light scattering dissymmetry measurements) in the same solvent and at the same temperature. This method corresponds to that employed in the evaluation of Φ from $[\eta]$ and $(\langle r^2\rangle)^{\frac{1}{2}}$.[3]

Equations (1), (2), (4), and (5) can be combined to give

$$f_0/\eta_0 = P\Phi^{-\frac{1}{3}}(M[\eta])^{\frac{1}{3}}. \tag{7}$$

Experimental verification of Eq. (7) depends on the determination of f_0 through measurement of either the sedimentation constant or the diffusion coefficient with appropriate extrapolation to infinite dilution.

The Svedberg[7] equation for the sedimentation velocity constant, s_0, at infinite dilution is given by:

$$s_0 = (M/\mathbf{N})(1-\bar{v}\rho)/f_0, \tag{8}$$

where s_0 is the rate of sedimentation at infinite dilution in a unit centrifugal field, $\mathbf{N}$ is Avogadro's number, $\bar{v}$ the partial specific volume of the solute and ρ the density of the solution. Combining with Eq. (7)

$$s_0([\eta]^{\frac{1}{3}}/M^{\frac{1}{3}}) = \mathbf{N}^{-1}\Phi^{\frac{1}{3}}P^{-1}(1-\bar{v}\rho)/\eta_0. \tag{9}$$

* This work was carried out at Cornell University as part of a research program supported by the Allegany Ballistics Laboratory, Cumberland, Maryland, an establishment owned by the United States Navy and operated by the Hercules Powder Company under Contract NOrd 10431.

[1] P. J. Flory, J. Chem. Phys. **17**, 303 (1949).
[2] T. G. Fox, Jr., and P. J. Flory, J. Phys. Colloid Chem. **53**, 197 (1949).
[3] P. J. Flory and T. G. Fox, Jr., J. Am. Chem. Soc. **73**, 1904 (1951).
[4] T. G. Fox, Jr., and P. J. Flory, J. Am. Chem. Soc. **73**, 1909 (1951).
[5] T. G. Fox, Jr., and P. J. Flory, J. Am. Chem. Soc. **73**, 1915 (1951).
[6] P. J. Flory and T. G. Fox, Jr., J. Polymer Sci. **5**, 745 (1950).
[7] T. Svedberg and K. O. Pedersen, *The Ultracentrifuge* (Oxford University Press, Oxford, England, 1940), p. 10.

Since $\bar{v}\rho$ is essentially constant, according to Eq. (9) $s_0([\eta]^{\frac{1}{3}}/M^{\frac{1}{3}})$ for a given polymer-solvent system should be independent of M. Furthermore, the value of $s_0([\eta]^{\frac{1}{3}}/M^{\frac{1}{3}})\eta_0/(1-\bar{v}\rho)$ should be the same for *all* randomly coiled polymers, regardless of the solvent and temperature.

For the purpose of testing the validity of the conclusions drawn from Eq. (9) measurements of s_0 and $[\eta]$ in the same solvent are required for *fractions* of a given polymer covering a wide range in molecular weight. The recently published work of Newman and Eirich[8] for polystyrene fractions and that of Singer[9] for cellulose acetate fractions appear to be suitable for this purpose. The results of the calculations are given in Table I.

To avoid the effects of random errors in the molecular weights given by Newman and Eirich, molecular weight values were recalculated from the intrinsic viscosities in methyl ethyl ketone as given by these authors. The intrinsic viscosity-molecular weight relation of Ewart and Tingey[10] was used for this purpose. Values of the intrinsic viscosities in toluene (not reported by Newman and Eirich) were calculated from these molecular weights by means of a recently published relation.[5] In confirmation of Eq. (9), the quantity $(s_0[\eta]^{\frac{1}{3}}/M^{\frac{1}{3}})$ is observed to be a constant within experimental error for each polymer solvent pair, independent of the molecular weight of the fraction. The agreement is particularly good among the polystyrene data.

The value of the quantity $\Phi^{\frac{1}{3}}P^{-1}$ can also be calculated if the partial specific volume of the solute is known. Heller and Thompson[11] give $\bar{v}$ for polystyrene at high dilution in several solvents: $\bar{v}=0.913$ in toluene and approximately 0.925 in methyl ethyl ketone. For cellulose acetate we assume that $\bar{v}$ is equal to the specific volume of the bulk polymer as obtained by linearly extrapolating to 20° from specific volume-temperature data taken above the glassy state transition. Using recently reported specific volume-temperature data on cellulose acetate,[12] the value of $\bar{v}$ obtained in this manner is 0.741. In Table II are given the results of the calculation of $\Phi^{\frac{1}{3}}P^{-1}$ from the averages of $(s_0[\eta]^{\frac{1}{3}}/M^{\frac{1}{3}})$ for each set of data in Table I using the above partial specific volumes.

TABLE I. Calculation of $s_0([\eta]^{\frac{1}{3}}/M^{\frac{1}{3}})$ for polystyrene and cellulose acetate.

Polystyrene: MW	in methyl ethyl ketone $s_0([\eta]^{\frac{1}{3}}/M^{\frac{1}{3}})\times10^{17}$	in toluene $s_0([\eta]^{\frac{1}{3}}/M^{\frac{1}{3}})\times10^{17}$
1,240,000	25.3	13.6
830,000	25.0	13.4
519,000	26.6	13.4
254,000	25.6	13.9
	av: 25.6	13.6
Cellulose acetate in acetone		
194,000	54.0	
130,000	59.5	
53,000	59.0	
11,000	50.3	
	av: 57.5[a]	

[a] Since the molecular weight, 11,000, of the lowest fraction corresponds to a degree of polymerization of only about forty, it was not included in the average.

TABLE II. Calculation of $\Phi^{\frac{1}{3}}P^{-1}$.

Polymer	Solvent	$\Phi^{\frac{1}{3}}P^{-1}\times10^{-6}$
Polystyrene	Methyl ethyl ketone	2.59
Polystyrene	Toluene	2.31
Cellulose acetate	Acetone	2.75
		av: 2.55±.20

The remarkably close agreement among the values for the three systems supports the theory set forth above including the conclusion that P, as well as Φ, is a universal constant. In the preceding material we have assumed only that the radius of the equivalent hydrodynamic sphere required by the frictional coefficient is proportional to an average linear dimension such as $(\langle r^2\rangle)^{\frac{1}{2}}$. Similarly, the radius of the equivalent sphere required by the viscosity is found to be proportional to $(\langle r^2\rangle)^{\frac{1}{2}}$.[3-5] If the further assumption is made that the two equivalent spheres are identical in size, then $\Phi^{\frac{1}{3}}P^{-1}$ may be calculated from Einstein's equation for the viscosity of a solution of spheres and Stokes's law for the frictional coefficient of a sphere. The value thus found is 2.1×10^{6}.

The universal constants Φ and P can be estimated also from the hydrodynamic theories of Kirkwood and Riseman.[13,14] As has been pointed out recently[3] the value of Φ thus obtained is 3.6×10^{21}. P can be obtained from their expression for f_0.

$$f_0=Z\zeta/[1+(8\lambda_0/3)Z^{\frac{1}{2}}], \tag{10}$$

where $\lambda_0=\zeta/(6\pi^3)^{\frac{1}{2}}\eta_0 b\alpha$, Z is the number of chain atoms in the polymer molecule, b is the effective bond length, and ζ is a frictional constant for the chain unit in the fluid medium. The intramolecular linear expansion factor α, disregarded by Kirkwood and Riseman and by others, is here included in the denominator of the expression for λ_0. It follows, from the fact that since the Kirkwood-Riseman function $\lambda_0 Z^{\frac{1}{2}}F(\lambda_0 Z^{\frac{1}{2}})$ is very nearly at its asymptotic value,[14] $\lambda_0 Z^{\frac{1}{2}}$ is at least 20.[13] Therefore unity in the denominator of Eq. (10) may be neglected compared with $(8/3)\lambda_0 Z^{\frac{1}{2}}$. Hence

$$f_0/\eta_0=(\tfrac{3}{8})(6\pi^3)^{\frac{1}{2}}Z^{\frac{1}{2}}b\alpha. \tag{11}$$

to an approximation which is negligible.

[8] S. Newman and F. Eirich, J. Colloid Sci. **5**, 541 (1950).
[9] S. Singer, J. Chem. Phys. **15**, 341 (1947).
[10] R. H. Ewart and H. C. Tingey, Abstracts of ACS meeting, Atlantic City, 1947.
[11] W. Heller and A. C. Thompson, J. Colloid Sci. **6**, 57 (1951).
[12] L. Mandelkern and P. J. Flory, J. Am. Chem. Soc. **73**, 3206 (1951).
[13] J. G. Kirkwood and J. Riseman, J. Chem. Phys. **16**, 565 (1948).
[14] Two revisions are required in the Kirkwood-Riseman interpretation of intrinsic viscosity. The intramolecular expansion factor α^3 must be introduced, and, as experiments demonstrate beyond question, their function $\lambda_0 Z^{\frac{1}{2}}F(\lambda_0 Z^{\frac{1}{2}})$ must be assigned a value indistinguishable from its asymptotic limit.

Thus, their equations for $[\eta]$ and f_0 are of the same forms as Eqs. (1) and (4), and they can be combined to give Eqs. (7) and (9). Therefore, the fact that the radius of the effective hydrodynamic sphere varies as a linear dimension of the polymer chain can be deduced from their theory in the limit of sufficiently large frictional interaction. Equations (7) and (9) provide a basis for correlating the frictional coefficient and sedimentation constant with molecular weight, which is to be preferred over the previously postulated linear dependence of s_0 on $M^{\frac{1}{2}}$.[15,16] The latter fails to take account of the dependence of α on M. Comparison of Eq. (11) with (4) and (5) gives 5.1 as the value of P, and $\Phi^{\frac{1}{3}}P^{-1}$ should equal 3.0×10^6. However, the best experimental data to date[3] indicate that $\Phi\cong2.1\times10^{21}$. Using this value of Φ with the calculated P gives $\Phi^{\frac{1}{3}}P^{-1}\cong$ to 2.5×10^6 in almost exact agreement with the experimental results of Table II.

The diffusion coefficient at infinite dilution, D_0, is related to f_0 as follows:

$$D_0=kT/f_0. \tag{12}$$

[15] Newman, Riseman, and Eirich, Proceedings of the International Colloquium on Macromolecules (1949), p. 161.

[16] A. Peterlin, J. Polymer Sci. **5**, 473 (1950). Peterlin's expression for f_0 can be obtained directly from Eq. (10) by using Stokes' law for the frictional coefficient of the chain unit.

Combining with Eq. (7):

$$D_0\eta_0(M[\eta])^{\frac{1}{3}}=kTP^{-1}\Phi^{\frac{1}{3}}. \tag{13}$$

Vallet[17,18] has shown on the basis of measurements on polystyrene fractions in several solvents that $D_0\eta_0$ is proportional to $(M[\eta])^{-\frac{1}{3}}$, which corresponds to constancy of $\Phi^{\frac{1}{3}}P^{-1}$. He has pointed out also that the sizes of the equivalent spheres calculated from diffusion measurements using Stokes' law for the frictional coefficient are comparable with those computed from viscosity measurements using Einstein's equation. As has been pointed out recently,[19] existing values of D_0 are subject to errors resulting from faulty extrapolation previously used. For this reason calculations of $\Phi^{\frac{1}{3}}P^{-1}$ from diffusion data have not been included here.

An expression analogous to Eq. (13) for the rotary diffusion constant of flexible chain molecules at infinite dilution may be obtained in an entirely similar manner.

Note added in proof: A treatment similar to the one given here has been carried out recently for proteins (H. A. Scheraga and L. Mandelkern, to be published) in terms of an effective hydrodynamic ellipsoid, with results which simplify the correlation of the frictional coefficient with the intrinsic viscosity.

[17] G. Vallet, Compt. rend. **230**, 1353 (1950).

[18] G. Vallet, J. Chim. phys. **47**, 649 (1950).

[19] L. Mandelkern and P. J. Flory, J. Chem. Phys. **19**, 984 (1951).

THE JOURNAL OF CHEMICAL PHYSICS VOLUME 20, NUMBER 2 FEBRUARY, 1952

Random Flight with Multiple Partial Correlations

C. M. TCHEN
National Bureau of Standards, Washington, D. C.

(Received May 4, 1950)

The fundamental statistical properties of a linear polymer can be best studied by a more general model of random flight *with multiple partial correlations*. Results show that the problems of free rotation and symmetrically restricted rotation in polymers correspond to one and two partial correlations, respectively. The present study of the correlation function by means of difference equations enables one to carry out the generalization to higher orders of partial correlations. The mean square value of the distance r between the ends of the chain is studied for both finite and infinite number of links, and for multiple partial correlations. It is shown that the case of one partial correlation corresponds to a Markoff chain, and the distribution of r is found to be normal.

1. INTRODUCTION

We consider a random flight of n paths each having a constant length b. We assume that certain partial correlations can exist between the paths. The first problem is to find the mean square distance between the end of the nth path and the origin of the flight. This is an analog to the problem of the distance between the ends of a linear polymer chain. Therefore we can speak identically of random flight or chain, path or link. The case of free rotation in a long chain molecule was studied by Eyring,[1] Kuhn,[2] Sadron,[3] and Kubo,[4] and the case of hindered rotation by Debye, Bresler, Frenkel,[5] Taylor,[6] and Benoît.[7] Results show that these cases correspond to the problems of random flight with one and two partial correlations, respectively. The simple method developed here will give more generally valid results than theirs, including all the cases they have considered, and enables us to carry out the generalization to higher degrees of partial correlations.

The second problem is to find the distribution func-

[1] H. Eyring, Phys. Rev. **39**, 746 (1932); see also Guth and Mark, Sitzber. Akad. Wiss. Wien **9**, 445 (1934).

[2] W. Kuhn, Kolloid Z. **68**, 2 (1934); **76**, 258 (1936).

[3] C. Sadron, J. chim. phys. **43**, 12 (1946).

[4] R. Kubo, J. Phys. Soc. (Japan) **3**, 119 (1948).

[5] S. E. Bresler and J. I. Frenkel, Acta Physicochim. URSS **11**, 485 (1939).

[6] W. J. Taylor, J. Chem. Phys. **15**, 412 (1947).

[7] H. Benoît, J. chim. phys. **43**, 9 (1946).

tion in the case of a large number of paths. It is well known that a random walk without correlation takes a normal distribution. We shall calculate the distribution in a random walk with a correlation of the type c^{j-i} between the ith and jth paths, where c is a partial correlation. Applications of those problems can be found not only in polymer statistics, but also in turbulent motion where the fluctuating velocity is a random function with correlation.

2. CORRELATION FUNCTION AND MEAN SQUARE DISTANCE BETWEEN THE TWO ENDS OF A CHAIN

In three dimensions consider a chain $A_0, A_1 \cdots A_i \cdots A_n$ of n links forming n vectors labeled $\mathbf{b}_0, \mathbf{b}_1 \cdots \mathbf{b}_i, \cdots \mathbf{b}_{n-1}$, and having all a constant length b. The vector A_0A_n denoted by $\mathbf{r}$ can be written as follows:

$$\mathbf{r}=\sum_{i=0}^{n-1}\mathbf{b}_i.$$

Its mean square is

$$\langle r^2\rangle=\sum_{i=0}^{n-1}\sum_{j=0}^{n-1}\langle \mathbf{b}_i\cdot\mathbf{b}_j\rangle. \tag{1}$$

Here $\langle\cdots\rangle$ denotes the mean value or expectation. We introduce a correlation function between $\mathbf{b}_i$ and $\mathbf{b}_j$ defined by

$$R(i,j)=\langle \mathbf{b}_i\cdot\mathbf{b}_j\rangle/b^2.$$

If the effects of the ends are neglected, the correlation function will not depend on i and j separately, but on their difference $s=j-i$. Consequently (1) reduces to

$$\langle r^2\rangle=b^2\sum_{i=0}^{n-1}\sum_{j=0}^{n-1}R(j-i). \tag{2}$$

By means of a transformation of coordinates from i, j into s, j such that $s=j-i$, (2) can be transformed into

$$\langle r^2\rangle=2b^2\sum_{s=1}^{n-1}\sum_{j=s}^{n-1}R(s)+b^2\sum_{j=0}^{n-1}R(0). \tag{3}$$

If we call

$$\langle r_0^2\rangle=nb^2$$

the mean square distance between the ends of a chain without correlation, when n is large,

$$S=\sum_{s=1}^{n-1}R(s), \tag{4}$$

the area of the correlation curve, and

$$M=\sum_{s=1}^{n-1}sR(s), \tag{4a}$$

the moment of the correlation curve, (3) can be written as follows:

$$\langle r^2/r_0^2\rangle=1+2(S-M/n). \tag{5}$$

For n very large

$$\langle r^2/r_0^2\rangle=1+2S. \tag{5a}$$

As $S-M/n$ is positive, formulas (5) and (5a) show that a correlation gives rise to an inflation in the configurations of the chain.

3. PARTIAL CORRELATIONS AND CORRELATION FUNCTION

The partial correlation c_k is defined by

$$c_k=\langle \mathbf{b}_i\cdot\mathbf{b}_{i+k}\rangle/b^2=\cos\angle\,\mathbf{b}_i\mathbf{b}_{i+k}, \tag{6}$$

provided $\cos\angle\,\mathbf{b}_i\mathbf{b}_{i+j}=0$ for $j<k$. Here $\angle\,\mathbf{b}_i\mathbf{b}_{i+k}$ represents the angle between $\mathbf{b}_i$ and $\mathbf{b}_{i+k}$.

It is the purpose of this section to find the expression of the correlation function from given partial correlations. Once the correlation function is determined, it is then an easy matter to compute $\langle r^2\rangle$ by applying formula (5). Since (6) is at the same time the expression for the correlation function provided $c_j=0$ for $j<k$, we can write

$$R(k)=c_kR(0),$$

or if the end effect is neglected

$$R(k+s)=c_kR(s). \tag{7}$$

Here $R(0)=1$. If any partial correlation equals unity, we have

$$R(k)=1, \tag{8}$$

for all k.

First take the case of one partial correlation c_1. R is governed by

$$R(1+s)=c_1R(s). \tag{9}$$

Next take the case of two partial correlations c_1 and c_2. The correlation function which must satisfy the conditions (7), (8), and (9) will have the following difference equation:

$$R(2+s)=c_1(1-c_2)R(1+s)+c_2R(s), \tag{10}$$

or

$$R(2+s)=\sum_{j=1}^{2}\sigma_{j,2}R(2+s-j),$$

with

$$\sigma_{1,2}=c_1(1-c_2),\quad \sigma_{2,2}=c_2.$$

By iteration we obtain the following difference equations for the correlation function containing k partial correlations:

$$\left.\begin{aligned} R(k+s)&=\sum_{j=1}^{k+s}\sigma_{j,k+s}R(k+s-j) \quad \text{for} \quad s<0,\\ R(k+s)&=\sum_{j=1}^{k}\sigma_{j,k}R(k+s-j) \quad \text{for} \quad s\geqslant 0,\end{aligned}\right\} \tag{11}$$

with

$$\sigma_{j,k}=c_j(1-c_{j+1})(1-c_{j+2})\cdots(1-c_k).$$

Let us apply the general difference equations (11) to the

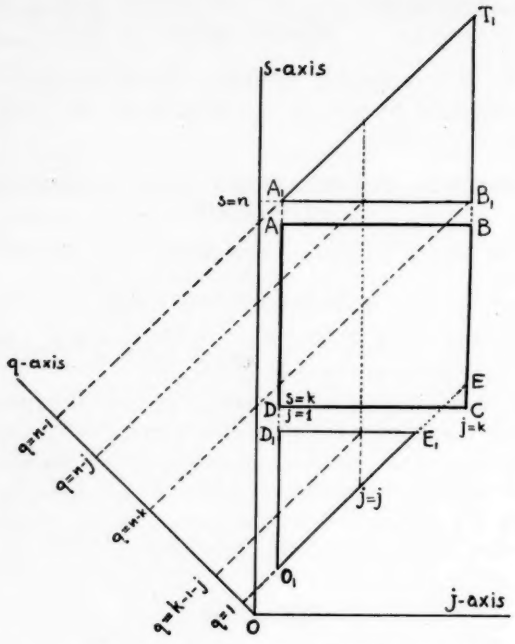

FIG. 1. Areas covering the set of points involved in the double summation of $\sigma_{j,k}R(s-j)$.

following three examples with one, two, and k partial correlations.

(a) Case of One Partial Correlation, $k=1$

Equation (11) reduces to (9) which gives

$$R(s)=c_1{}^s.$$

After substitution of this expression into (5) we obtain

$$\frac{\langle r^2\rangle}{\langle r_0{}^2\rangle}=\frac{1+c_1}{1-c_1}-\frac{2c_1(1-c_1{}^n)}{n(1-c_1)^2}\equiv m(c_1). \tag{12}$$

$m(c_1)$ is used for the sake of abbreviation to represent the whole expression (12). For large n (12) reduces to

$$\frac{\langle r^2\rangle}{\langle r_0{}^2\rangle}=\frac{1+c_1}{1-c_1}. \tag{12a}$$

(b) Case of Two Partial Correlations, $k=2$

Equation (11) reduces to (10) which gives the solution,

$$R(s)=B_1\rho_1{}^s+B_2\rho_2{}^s, \tag{13}$$

where ρ_1, ρ_2 are roots of the characteristic equation,

$$\rho^2-c_1(1-c_2)\rho-c_2=0,$$

and B_1, B_2 are

$$B_1=\frac{c_1-\rho_2}{\rho_1-\rho_2},\quad B_2=-\frac{c_1-\rho_1}{\rho_1-\rho_2},$$

as determined by the boundary conditions of $R(s)$.

Substitution of (13) into (5) gives

$$\frac{\langle r^2\rangle}{\langle r_0{}^2\rangle}=B_1m(\rho_1)+B_2m(\rho_2), \tag{14}$$

where the function m is defined by (12). For large values of n (14) simplifies to

$$\frac{\langle r^2\rangle}{\langle r_0{}^2\rangle}=\frac{1+c_1}{1-c_1}\frac{1+c_2}{1-c_2}. \tag{14a}$$

(c) Case of k Partial Correlations with Large n

The calculations of $\langle r^2/r_0{}^2\rangle$ from (5a) reduce to the calculations of S by means of R to be calculated from Eq. (11). It is convenient to divide $S=S_1+S_2$ into two parts:

$$S_1=\sum_{s=1}^{k-1}\sum_{j=1}^{s}\sigma_{j,s}R(s-j),$$

$$S_2=\sum_{s=k}^{n-1}\sum_{j=1}^{k}\sigma_{j,k}R(s-j),$$

because (11) gives two different formulas for R.

By a transformation of coordinates from $s-j$ into q, S_1 can be transformed into

$$S_1=\sum_{q=1}^{k-2}\sum_{j=1}^{k-1-q}\sigma_{j,q+j}R(q)+\sum_{j=1}^{k-1}c_j. \tag{15}$$

S_2 can be divided into the following elements:

$$S_2=\Omega_1-\Omega_2-\Omega_3+\Omega_4,$$

where S_2, Ω_1, Ω_2, Ω_3 are summations of $\sigma_{j,k}R(s-j)$ over the set of points covering the following areas, respectively (see Fig. 1): $ABCD$, $O_1ET_1A_1$, $A_1B_1T_1$, $O_1D_1E_1$, and Ω_4 is the value of $\sigma_{j,k}R(s-j)$ at the point $j=k$, $s=k$. They are calculated as follows:

(1) In the system of coordinates q, j, Ω_1 is found to be

$$\Omega_1=S\sum_{j=1}^{k}\sigma_{j,k}.$$

It is easy to prove

$$1-\sum_{j=1}^{k}\sigma_{j,k}=\prod_{j=1}^{k}(1-c_j)\text{ say }J_k.$$

Hence

$$\Omega_1=S(1-J_k).$$

(2) In the new coordinates, we have

$$\Omega_2=\sum_{q=n-k}^{n-1}\sum_{j=n-q}^{k}\sigma_{j,k}R(q)$$

$$\Omega_3=\sum_{q=1}^{k-2}\sum_{j=1}^{k-1-q}\sigma_{j,k}R(q)$$

$$\Omega_4=c_k.$$

Ω_2 vanishes if n increases indefinitely, while the number of partial correlations k remains finite. The sum $S=S_1+S_2$ gives then

$$J_k S=\sum_{j=1}^{k} c_j+\Omega_5,$$

where

$$\Omega_5=\sum_{q=1}^{k-2}\sum_{j=1}^{k-1-q}\sigma_{j,\,q+j}R(q)-\Omega_3.$$

After substitution of S, (5a) gives

$$\frac{\langle r^2\rangle}{\langle r_0^2\rangle}=\Phi_1-2\Phi_2/J_k+2\Omega_5/J_k. \tag{16}$$

Here

$$\Phi_1=\prod_{j=1}^{k}(1+c_j)/\prod_{j=1}^{k}(1-c_j),$$

$$\Phi_2=c_1c_2c_3+c_1c_2c_4+\cdots+c_1c_2c_3c_4c_5+\cdots.$$

Φ_2 is the sum of combinatory products of odd numbers of partial correlations, beginning with products of three partial correlations. Ω_5 is easily computed for not too large values of k:

$$\begin{aligned}&\text{for}\quad k=1,\quad \Omega_5=0;\\ &\text{for}\quad k=2,\quad \Omega_5=0;\\ &\text{for}\quad k=3,\quad \Omega_5=c_1^2(1-c_2)c_3.\end{aligned}$$

Hence for $k=3$

$$\langle r^2/r_0^2\rangle=\frac{1+c_1}{1-c}\frac{1+c_2}{1-c_2}\frac{1+c_3}{1-c_3}-\frac{2c_1c_2c_3}{(1-c_1)(1-c_2)(1-c_3)}+\frac{2c_1^2c_3}{(1-c_1)(1-c_3)}. \tag{17}$$

Formula (17) degenerates to (12a) and (14a), respectively, for the cases of one and two partial correlations. If the partial correlations are small so that the third-order terms are negligible compared with unity, the general formula (16) simplifies to the following form:

$$\langle r^2/r_0^2\rangle=\prod_{j=1}^{k}(1+c_j)/\prod_{j=1}^{k}(1-c_j), \tag{18}$$

valid for large n and for an arbitrary finite number k of partial correlations.

4. DISTRIBUTION FUNCTION IN A CORRELATED CHAIN

In the case of a random chain without correlation, the different links are independent. It is well known that the distance between the two ends of the chain takes a normal distribution, and has a mean square value proportional to the number of links n, provided n increases indefinitely. If the links are correlated, we have shown that the mean square distance is still proportional to n, with a coefficient of proportionality depending on the correlation. It is obvious that the linear proportionality with n does not imply necessarily a normal distribution. However, we shall show in the following that, if the correlation which covers the whole chain has a decreasing trend, such as a correlation of the type c^{j-i} between the ith and jth links, a normal distribution will result. Here c is the partial correlation. It is to be remarked that a correlation c^{j-i} for a discontinuous chain corresponds to a correlation $e^{-l/\lambda}$ between two points separated by a curvilinear length l on a continuous chain. Here

$$\lambda=\lim_{b=0}\frac{b}{1-c}.$$

At the limit $b=0$, c tends to unity.

Consider in the x, y plane a chain of n links. Since the length of the link is immaterial to the distribution function, it can be taken as unity. Two consecutive links make an angle $\pm\alpha$, and α is a constant. The first link can be arbitrarily placed to coincide with the x axis. Then the kth link makes an angle θ_{k-1} with the x axis, such that

$$\theta_{k-1}=\theta_{k-2}+\epsilon_{k-1}\alpha,$$

where ϵ_k are mutually independent variables having values ±1, each with probability $\frac{1}{2}$. The components of the distance between the 2 ends will be denoted by ξ, η. We have

$$\xi=\sum_{i=0}^{n-1}X_i$$

$$\eta=\sum_{i=0}^{n-1}Y_i,$$

with

$$X_i=\cos\theta_i;\quad Y_i=\sin\theta_i.$$

The relation which exists between θ_{k-1} and θ_{k-2} indicates that they belong to a Markoff process, so do also X_i and Y_i. For such random variables of the Markoff chain the central limit theorem holds, and their summations ξ and η take consequently a normal distribution at the limit $n\to\infty$.[8,9]

Here between ξ and η no correlation exists:

$$\langle\xi\eta\rangle=\tfrac{1}{2}\sum_{i=0}^{n-1}\sum_{j=0}^{n-1}(\cos\theta_i\sin\theta_j+\sin\theta_i\cos\theta_j)$$

$$=\tfrac{1}{2}\sum_{i=0}^{n-1}\sum_{j=0}^{n-1}\sin(\theta_i+\theta_j)=0.$$

Consequently the distance between the ends of the chain which is by definition the resultant of ξ and η possesses also a normal distribution at the limit $n\to\infty$.

[8] W. Doeblin, "Sur les propriétés asymptotiques de mouvements régis par certains types de chaînes simples," thesis Paris (1937).
[9] C. M. Tchen (to be published).

The Effects of Hydrostatic Pressure on the Ionic Conductivity of AgBr

S. W. KURNICK
Department of Physics, University of Chicago, Chicago 37, Illinois*
(Received August 13, 1951)

Comparison of the conductivities of pure AgBr and AgBr doped with varying concentrations of $CdBr_2$ in the intrinsic temperature range determines the concentration of defects and the mobilities of silver vacancies and interstitial ions. These quantities have been measured as a function of pressure up to 8000 kg/cm² at three temperatures below 300°C. From the pressure variation of the defect concentration, the molar volume ΔV^* of the imperfections is found to be 16 cc/mole below 300°C. An analysis of the pressure variation of the mobilities u_0 and $u_\square$ of the Ag^+ interstitial ions and of the silver vacancies, respectively, indicates that the free volumes associated with their motions are 2.7 cc/mole and 7.4 cc/mole. The value of $\Delta V^* = 16$ cc/mole is consistent with the Frenkel disorder type. At temperatures above 300°C, however, the observed value of $|\partial \ln\sigma/\partial p|$ is larger than expected from a simple Frenkel disorder type. An effort is made to interpret this behavior in terms of mixed Frenkel and Schottky defects.

INTRODUCTION

THE mechanism of ionic conductivity of AgBr has been recently subjected to review by various investigators.[1–7] Two alternative models under consideration are those of Schottky and Frenkel. The Schottky mechanism assumes that pairs of ions vacate their normal lattice sites to form new layers of the lattice either on the surface or at dislocations in the solid crystal. The vacancies so formed move through the lattice by virtue of nearest neighbors jumping into these empty sites. In a pure sample, the number of sites vacated by positive ions is equal to the number of empty sites left by negative ions. According to the Frenkel mechanism, on the other hand, an ion is removed from its normal site to an interstitial position in the lattice cell. In the most general Frenkel model, both positive and negative ions go to interstitial positions; in AgBr, however, it appears likely that only the silver ion contributes to the conduction because the larger bromide ions find it energetically difficult to move into an interstitial position.

In either case, the conductivity

$$\sigma = \Sigma e_i n_i u_i, \tag{1}$$

where n_i is the density of imperfections of the ith type with charge e_i and u_i as its corresponding mobility. For instance, in the case of the Frenkel mechanism

$$\sigma = e(n_\square u_\square + n_o u_o), \tag{2}$$

$n_\square$ and $u_\square$ are the density and mobility of the silver vacancies and n_o and u_o the density and mobility of the interstitial ions. For the Schottky disorder type, however, n_o and u_o refer instead to the bromide vacancy. In either the Frenkel or Schottky disorder type

$$n_i = A_i \exp -(\Delta G_i^o/2RT), \tag{3}$$

$$u_i = B_i/T \exp -(\Delta G_i^{o\prime}/RT). \tag{4}$$

The constants A_i, B_i, ΔG_i^o, and $\Delta G_i^{o\prime}$ depend on the ion type and mechanism considered.

The majority of investigators agree that the Frenkel mechanism is dominant in AgBr over most of the temperature range which they have studied. The question under discussion is the extent, if any, to which the Schottky mechanism contributes to the conductivity. The object of this paper is to report data on the pressure variation of the ionic conduction of pure and doped samples of AgBr. Such data permit the evaluation of the number of imperfections and their corresponding mobilities at different pressures, and, in addition, the volume change associated with the creation of these imperfections. This volume change may then be used as a criterion for determining which conductive mechanisms are effective in AgBr. Such experiments have, in fact, been performed previously on AgBr by Jost and his collaborators[8] up to pressures of 300 atmospheres. However, they assumed that only one term of Eq. (1) controls the conductivity, and that in the Frenkel model there is no volume change associated with the creation of defects.

Until recently an unambiguous evaluation of all the quantities in Eq. (1), even assuming a single disorder type, namely the Frenkel, has been impossible. The usual assumption that interstitial ions and silver vacancies have equal mobilities is unjustifiable. Fortunately, Teltow[9] has developed a technique which permits the evaluation of all the parameters in Eq. (2) by studying the variation with temperature of the conductivity of pure AgBr and AgBr doped with varying amounts of $CdBr_2$. Teltow's technique has been em-

* The actual experiments were carried out in the Institute for the Study of Metals, University of Chicago. This paper was submitted to the University in partial fulfillment for a degree of Doctor of Philosophy.

[1] J. W. Mitchell, Phil. Mag. **40**, 249 (1949).
[2] A. W. Lawson, Phys. Rev. **78**, 185 (1950).
[3] R. W. Christy and A. W. Lawson, J. Chem. Phys. **19**, 517 (1951).
[4] H. Kanzaki, Phys. Rev. **81**, 884 (1951).
[5] C. R. Berry, Phys. Rev. **82**, 422 (1951).
[6] O. Stasiw, Z. Phys. **127**, 522 (1950).
[7] J. H. Simpson, Proc. Roy. Soc. (London) **A197**, 269 (1949).
[8] W. Jost and G. Nehlap, Z. phys. Chem. **34B**, 350 (1937); W. Jost and S. Mennenöh, Z. physik. Chem. **196**, 188 (1950); S. Mennenöh, Z. Elektrochem. **54**, 433 (1950).
[9] J. Teltow, Ann. Physik **5**, 63–88 (1950).

ployed in the work described below. Without this technique, the evaluation of high pressure data would be difficult. On the other hand, Teltow's data at atmospheric pressure alone are unable to determine whether the Schottky type of imperfection is also present at temperatures close to the melting point of AgBr.

THEORY

Koch and Wagner[10] suggested the doping of silver bromide with varying concentrations of cadmium bromide to enhance the conduction by vacancies. Assuming a Frenkel disorder type, Teltow[10] utilized this technique to sort out the following contributions to the conductivity of pure AgBr: (a) the concentration of defects x_o defined as n_o/N; (b) the mobility u_o of the interstitial Ag^+ ion; (c) the mobility $u_\square$ of the vacancies. This information is obtained by measuring the ratio $1/Z$ of the conductivities of a pure AgBr sample and a sample doped with y atomic percent of Cd^{++} ions. In the intrinsic range, this ratio is given by

$$Z=[(y/2x_o)^2+1]^{\frac{1}{2}}-(\varphi-1)/(\varphi+1)(y/2x_o), \quad (5)$$

where φ is the ratio of mobilities $u_o/u_\square$. Isothermal plots of Z *vs* y are hyperbolas of the type shown in Fig. 1. In Eq. (5) it is assumed no association between the Cd^{++} ion and a vacancy takes place. Implicit in Teltow's derivation are the assumptions of electrical neutrality and dilute solution equilibrium. The former assumption implies that each Cd^{++} added to the AgBr lattice will add a vacancy if no other interactions take place. Accordingly,

$$x_\square'-x_o'=y, \quad (6)$$

where the primed quantities refer to the concentrations in doped samples. In addition, assuming a quasi-chemical equilibrium between interstitial Ag^+ ions and vacancies of the type

$$Ag_o^+ \text{ (interstitial)}+Ag_\square^+ \text{ (vacancy)} \rightleftharpoons Ag^+ \text{ (normally situated)} \quad (7)$$

the law of mass action yields, for sufficiently small values of x,

$$x'_\square x_o'=x_\square x_o=K_1. \quad (8)$$

Statistical mechanics, applied after the manner of Mott and Gurney,[11] leads to the relation

$$x_o=(N'/N)^{\frac{1}{2}}\exp-(\Delta G_F^o/2RT) \quad (9)$$

where ΔG_F^o is the work necessary to create a mole of imperfections in an infinite perfect lattice, where x_o is small, and interactions between imperfections may be neglected. N and N' are the densities of ion pairs and interstitial positions, respectively. The change in x_o with pressure at constant temperature is given by

$$\frac{\partial \ln x_o}{\partial p}=-\frac{1}{2RT}\frac{\partial}{\partial p}\Delta G_F^o=-\frac{\Delta V^*}{2RT}, \quad (10)$$

where ΔV^* is the over-all increase in volume associated with one mole of imperfections. The change in free energy ΔG_F^o, and consequently the corresponding term ΔV^*, include changes attributable to the alteration of vibrational frequencies and the expansion of the lattice in the vicinity of both the interstitial ion and the vacancy. In the derivation of the equations above, it is assumed that N'/N is not a function of either temperature or pressure.

For the change in mobilities with pressure at constant temperature

$$\frac{\partial}{\partial p}u_o(p)=-\frac{1}{RT}\frac{\partial}{\partial p}\Delta G_o'=-\frac{\Delta V_o}{RT}. \quad (11)$$

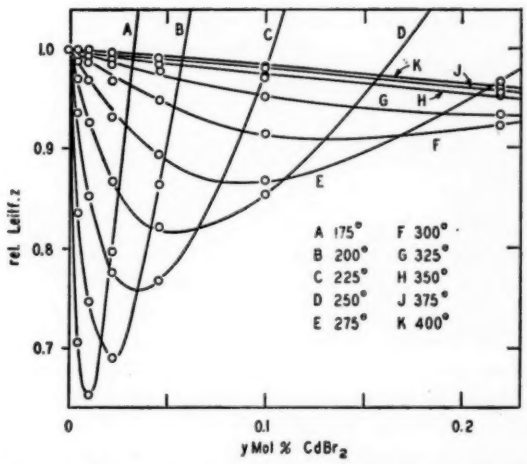

FIG. 1. Isotherms of z, the ratio of conductivities, $CdBr_2$ doped AgBr and pure AgBr, *vs* atomic percent Cd^{++} present. (After Teltow.)

A corresponding equation may be written for the change with pressure of the mobility of the vacancies. As suggested by Schottky,[12] both mobilities may differ in pressure and temperature response. The parentheses after u symbolize the pressure at which the mobility is determined; $\Delta G_o'$ is the change in free energy of the system associated with motion of an imperfection to a saddle point; ΔV_o is the change in volume accompanying the formation of the activated state as interstitial ions migrate. Again, it may be added, that the ΔG's for the mobilities include contributions from the change in vibrational frequency and lattice expansion. By use of the Einstein[13] relation between diffusion coefficient D, and mobility u, namely

$$D_i/kT=u_i/e_i. \quad (12)$$

[10] E. Koch and C. Wagner, Z. phys. Chem. **38B**, 295 (1937).
[11] N. F. Mott and R. W. Gurney, *Electronic Processes in Ionic Crystals* (Oxford University Press, London, 1946), second edition, pp. 52–53.
[12] W. Schottky, Z. Elektrochem. **45**, 33 (1939).
[13] See reference 11, p. 63.

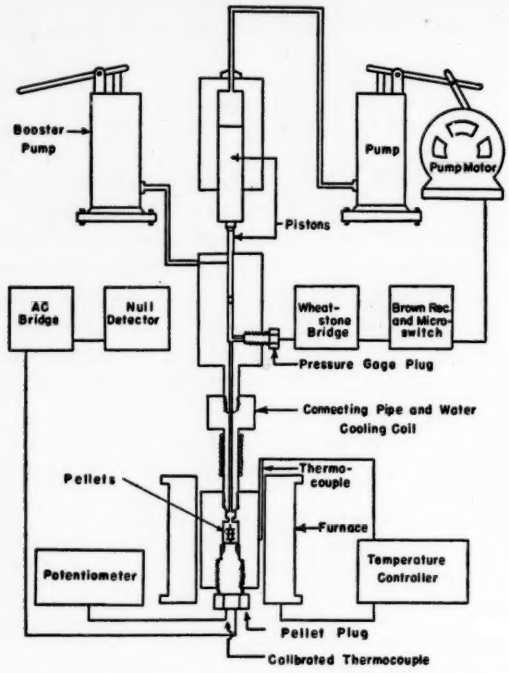

FIG. 2. Schematic diagram of apparatus.

We may easily show that B_i introduced in Eq. (4) is given by

$$B_i=(a^2\nu_i e_i)/k, \tag{13}$$

where ν_i is the frequency of vibration of the ith-type ion and a is of the order or magnitude of the lattice parameter. As will be shown later, $(\partial/\partial p)\ln B_i$ is appreciably smaller than $\Delta V_i/RT$, and consequently for a satisfactory approximation we may omit it from Eq. (11). It is apparent from the foregoing considerations that by extending Teltow's technique to high pressure it should be possible to evaluate the volume increase associated with the creation of imperfections. Since the bromide ion is several times larger than the silver ion, we may expect a detectable difference in the ΔV's observed, depending on whether the Frenkel or Schottky mechanism prevails.

The principal basis for accepting the Frenkel disorder type in the past has been the transport data of Tubandt,[14] who found no evidence for bromide ion transport up to temperatures of 300°C. However, Tubandt's results do not rule out the possibility of the Schottky disorder type provided the mobility of the bromide ion vacancies is sufficiently small compared to that of the Ag^+ vacancies below 300°C. Actually, Teltow's equations are applicable to both types of disorder, but the assumption of a Schottky disorder leads to a value of the mobility of the Br^- vacancies which would be inconsistent with Tubandt's transport experiment. We are forced to conclude, therefore, that there is little doubt that the Frenkel disorder prevails below 300°C. However, above 300°C evidence available up to the present concerning the Schottky disorder has been somewhat contradictory. Data are presented below which confirm Teltow's results below 300°C, but which seem to support the existence of the Schottky disorder also at higher temperatures.

[14] C. Tubandt, *Hand. Exptl. Physik* XII, Pt. 3 (1932).

EXPERIMENTAL PROCEDURE

High Pressure Generator

The high pressure generator is shown schematically in Fig. 2. This apparatus has been described previously;[15] however, it has been modified for this experiment in the following ways: (1) the pressure medium is a 3-centistoke silicone oil, Dow Corning 200; (2) an external furnace has been built around the lower bomb, which envelopes the specimen plug to be described later; and (3) a connecting pipe which is watercooled is provided to avoid heating the manganin wire pressure gage in the upper bomb.

Temperature Control

Since the conductivity changes about 8 percent for each °C change of temperature, it is necessary to use a proportioning temperature controller operating from a thermocouple inserted between lower bomb and furnace to maintain a sufficiently constant temperature. Because of high heat capacity of the lower bomb, the assembly has a time constant of about three hours. Under these circumstances, the temperature can be maintained constant to within $\frac{1}{2}$°C.

Specimen Plug

The specimen plug is shown in Fig. 3. To determine the quantities φ and x_o in Eq. (5) doped and pure cylindrical specimens (D) of AgBr are stacked alternately with silver electrodes (C). Because of compressibility and thermal expansion, specimens and electrodes are held in electrical contact by a stainless steel spring (B) insulated by a transite washer (A). Electrical connections are brought out from the high pressure chamber through conical pipestone packings (E) to the binding posts at (H). At a given temperature and pressure the ratio of conductivities is determined by alternately measuring the impedance of doped and pure samples with an ac bridge.

High pressure seals between the bomb (J), the specimen plug, and connecting pipe are made by the sealing rings, (F).

To measure the temperature accurately, a calibrated thermocouple (H) is inserted through a bore in the plug itself. To account for the slight temperature difference between the specimen and the position of the calibrated thermocouple, the latter is connected in series through the binding posts to an auxiliary thermocouple (designated by the dashed lines) in the high pressure chamber. This scheme measures the tempera-

[15] P. W. Bridgman, *Physics of High Pressure* (G. Bell and Sons, London, 1949), Chapter 2.

ture close to the specimen but minimizes the effect of pressure on the thermal emf observed. A temperature difference of about 2°C exists at equilibrium between the main and auxiliary thermocouples because of the heat leak through the water-cooled connecting pipe. This temperature difference may be considerably larger, of course, just after changes in pressure are made.

Both thermocouples are made of chromel-alumel, and the thermocouple is calibrated against the melting points of tin and zinc and the boiling point of water. Measured temperatures are accurate to within $\frac{1}{2}$°C over the range 100° to 431°C.

Ac Measurement of Resistance

Conductivity measurements are made by a Brown Electro-Measurement Corporation impedance bridge model 250-C at 1000 cycles. The bridge is powered by an audio-oscillator through a bridge transformer to reduce capacity effects. Balance points are detected by a General Radio null detector, type 1231-B. Capacities in parallel with the sample resistance are balanced out in all readings, and the impedance is also checked at 400 cycles. The bridge has a sensitivity of at least 0.5 percent over the range of resistances under study.

Preparation of Samples

Both pure and doped samples were prepared from a common batch of commercial silver bromide made by the Goldsmith Smelting and Refining Company, New York City. From spectrographic analysis it was estimated that the total foreign metallic impurities were about 5×10^{-4} percent. As a check, another batch of AgBr was prepared by precipitation from $AgNO_3$ and HBr. A simultaneous comparison of the conductivities of two samples from the different sources as a function of temperature and pressure revealed no appreciable discrepancies. To prepare the different solid solutions for the $CdBr_2$ doped samples, the largest concentration, 0.1 atomic percent Cd, was prepared and the other concentrations were derived by continued dilution of the 0.1 percent solution with pure AgBr. The concentrations used were 0.1, 0.05, 0.025, 0.01, and 0.005 percent.

Doped pellets were melted and cast under a pressure of some 10,000 atmospheres. They solidified with average grain size of about 0.5 mm. Pure and doped samples for the comparison measurements had dimensions of approximately 0.6 in. diameter and 0.3 in. in length. For conductivity measurements on the pure samples at temperatures above 300°C, the resistances were enhanced by casting cylinders of 0.125 in. diameter and 0.3 in. length in a smaller pellet die.

The cast pellets were then polished with metallographic finishing paper, washed in acetone and distilled water, and a thin film of silver was then evaporated on the flat surfaces.

The silver evaporated surfaces were then backed with several coats of DuPont silver paint No. 4548 and the entire pellet was baked at about 400°C for 24 hours. This baking had the dual purpose of destroying the organic material in the paint and annealing the pellets. To protect the electrode surfaces $\frac{5}{8}$-in. silver disks about 0.015 in. thick were used to back the pellets. Thus, after a pressure run, the pellets stuck to the disks and not to the main electrodes. Pellets and disks could then be removed and reused.

OBSERVATIONAL PROCEDURE

The particular reference temperatures used are chosen to give the most accurate and reproducible values of Z, the ratio of conductivities, in the intrinsic range. At the lowest temperature, 202°C, Z ratios are measured to within 1 percent reproducibility at the lower pressures, decreasing to 3 percent reproducibility at 8000

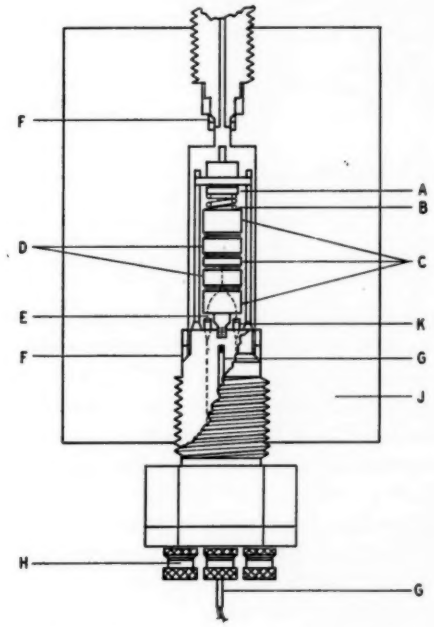

FIG. 3. Lower bomb and plug assembly.

kg/cm². At temperatures below 202°C, especially at higher pressures, conductivity readings are not reproducible. At 251° and 289°C, Z ratios reproduce to within 1 percent. From Fig. 1 it is seen that higher temperatures bring the Z values closer to unity. Since one of the ordinates of the plots which determine x_o and φ (see below) is proportional to $1/Z-Z$, 1 percent errors will become more and more significant at higher temperatures.

The reference pressures are determined by limitations in the high pressure equipment. Above 8000 kg/cm² pressure the silicone oil becomes more and more viscous and a pressure difference is created along the connecting pipe. This differential was measured at room temperature by making a high pressure run with a manganin wire pressure gage replacing the specimen plug. The pressure level 2500 kg/cm² is selected (rather than

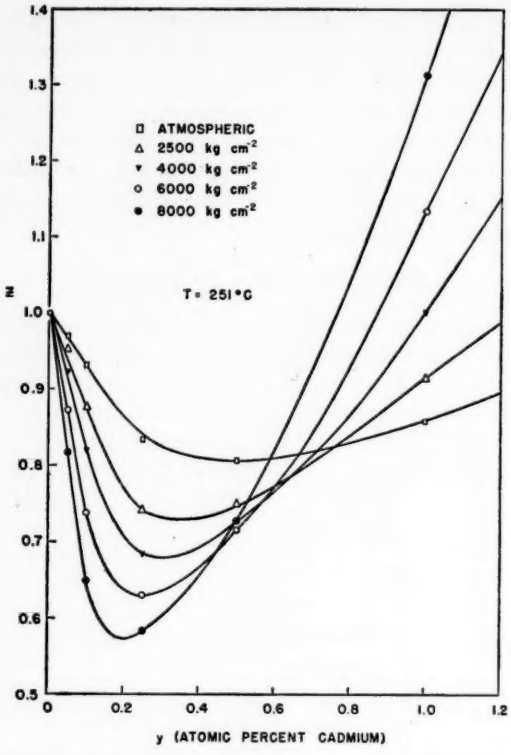

FIG. 4. The 251°C isotherm of Z *vs* y at various pressures.

2000 kg/cm²) to lower the length of travel of the piston. The procedure is to take all the high pressure readings (2500 kg/cm² and above) at one temperature, then to lower to approximately atmospheric pressure to complete the run.

For the determination of Z, a doped sample of a given concentration and a pure sample are simultaneously pressurized. The pressurized system is then brought up to one of the three reference temperatures 202°C, 251°C, or 289°C and resistance readings are taken at the high pressure levels, 2500, 4000, 6000, and 8000 kg/cm².

TABLE I. Values of the ratio of cadmium bromide doped and pure silver bromide conductivities at different temperatures and and pressures.

Temperature	y%	Pressure (kg/cm²) 0	2500	4000	6000	8000
	0.005	0.836	0.764	0.681	0.582	0.496
	0.010	0.710	0.614	0.559	0.515	0.506
202°C	0.025	0.636	0.636	0.668	0.738	0.852
	0.050	0.813	0.946	1.065	1.256	1.446
	0.10	1.426	1.824	2.220	2.709	3.184
	0.005	0.970	0.953	0.922	0.873	0.817
	0.010	0.931	0.876	0.820	0.738	0.649
251°C	0.025	0.835	0.742	0.684	0.630	0.584
	0.050	0.806	0.750	0.726	0.716	0.728
	0.10	0.859	0.915	1.000	1.133	1.314
	0.005	0.985	0.970	0.960	0.945	0.928
	0.010	0.975	0.962	0.940	0.906	0.856
289°C	0.025	0.935	0.894	0.850	0.788	0.721
	0.050	0.906	0.850	0.797	0.746	0.692
	0.10	0.887	0.837	0.827	0.829	0.896

After the high pressure readings are taken, the piston is raised beyond the booster pump inlet, the pressure is removed, and resistance readings are taken at the vapor pressure of the fluid. Pressure is then applied again by the booster pump and the piston brought down; the temperature controller is reset to the next temperature. In all cases, to arrive at a given temperature takes four hours and, in changing pressure, twenty minutes elapse before the samples come to equilibrium.

All Z readings are corrected for temperature differences between top and bottom specimens arising from heat drainage through the water-cooled connecting pipe (see Fig. 3). To determine these temperature differences at different temperatures and pressures the conductivities of two pure samples are compared. To check whether or not differences in chemical purity and grain size, as well as a temperature gradient contributes to the conductivities, the samples are reversed and rerun.

RESULTS BELOW 300°C

The Z *vs* y isotherms of Teltow are shown in Fig. 1. From these curves he derived x_o and φ from the minimum value of Z and the initial slope of $(dZ/dy)_{y\to o}$. These values, coupled with the conductivities of pure AgBr, permit evaluation of u_o and $u_\square$. These data are to be contrasted with those shown in Fig. 4, which shows the effect of high pressure on the 251°C isotherm. It is apparent that the effect of pressure is qualitatively equivalent to lowering the temperature. The situation is similar at other temperatures and the results are listed in Table I.

TABLE II. Values of concentrations x_o and ratio of mobilities φ for polycrystal samples derived by comparison of $CdBr_2$ doped and pure AgBr conductivities.

Pressure (kg cm⁻²) ×10³	T=202°C x_o%	φ	T=251°C x_o%	φ	T=289°C x_o%	φ
0	9.0×10^{-3}	7.9	3.4×10^{-2}	4.17	8.1×10^{-2}	2.75
2.5	5.5	9.8	2.2	5.52	5.3	3.57
4	4.2	11.0	1.6	6.43	4.1	4.17
6	2.9	13.0	1.1	8.00	3.0	5.05
8	1.9	15.7	0.81	10.1	2.1	6.20

The values listed in Table II were obtained by a somewhat different analysis than that employed by Teltow. It must be understood that the evaluation of data based by drawing a hyperbolic curve through the observed point is somewhat treacherous because, in general, observations are not available at the exact minimum of the hyperbola. In view of the fact that an error in locating the minimum may lead to serious discrepancies in φ and x_o, it is desirable to obtain an objective technique for evaluating data. This may be accomplished in the following fashion. We may transform Eq. (5) to the linear form

$$(X/A)+(Y/B)=1, \tag{14}$$

where $X=(1/y)[(1/Z)-Z]$ and $Y=y/Z$. In the fore-

going equation the intercepts A and B are $(1/x_o)\times[(\varphi-1)/(\varphi+1)]$ and $x_o[\varphi-(1/\varphi)]$, respectively. If now the observable quantity X is plotted against the observable Y, a straight line should be obtained if there is no association, and such a diagram provides an acid test for the assumptions underlying the theory, in addition to providing a more objective method for evaluating the data. After drawing the best line through these points, the value of the intercepts A and B are determined. In terms of these quantities, x_o and φ are determined by the following equations:

$$\sinh(\tfrac{1}{2}\ln\varphi)=\tfrac{1}{2}(AB)^{\frac{1}{2}} \tag{15a}$$

$$x_o\cosh(\tfrac{1}{2}\ln\varphi)=\tfrac{1}{2}(B/A)^{\frac{1}{2}}. \tag{15b}$$

The manner in which the experimental data are so plotted for the 251°C isotherm to determine x_o and φ is illustrated in Fig. 5. The data for 202°C and 289°C were analyzed similarly and are listed in Table II.

The behavior of the ratio of mobilities φ as a function of pressure is illustrated in Fig. 6. In this diagram is

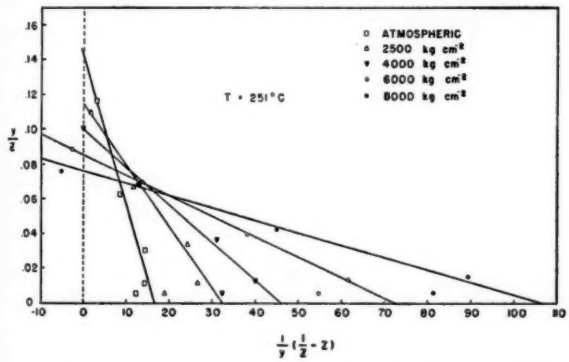

FIG. 5. The 251°C isotherm; $1/y[(1/Z)-Z]$ *vs* y/Z is used to determine the parameters x_o and φ for different pressures.

plotted $RT\ln[\varphi(p)/\varphi(o)]$ as a function of pressure for different temperatures. With recourse to Eq. (11), the slope of this curve is $\Delta V_\square-\Delta V_o$. To evaluate the effect of the pressure on the concentrations x_o, we have plotted in Fig. 7 the quantity $RT\ln(x_o(o)/x_o(p))$, the slope of which according to Eq. (10) is $\frac{1}{2}\Delta V^*$. To solve for the individual terms $\Delta V_\square$ and ΔV_o, the ratios $u_\square(o)/u_\square(p)$ and $u_o(o)/u_o(p)$ are first found from

$$\frac{\sigma(o)}{\sigma(p)}=\frac{x_o(o)}{x_o(p)}\,\frac{\varphi(o)+1}{\varphi(p)+1}\,\frac{u_\square(o)}{u_\square(p)}, \tag{16a}$$

$$\frac{u_o(o)}{u_o(p)}=\frac{\varphi(o)}{\varphi(p)}\,\frac{u_\square(o)}{u_\square(p)}, \tag{16b}$$

from which the desired quantities are then found from Eq. (11). The necessary data for the ratio $\sigma(o)/\sigma(p)$ is given in Table III for various temperatures and pressures. The values for ΔV^*, $\Delta V_\square$ and ΔV_o so derived are listed in Table IV and illustrated in Fig. 8. Furthermore, from the variation of $\ln x_o$, $T\ln u_o$ and $T\ln u_\square$ with

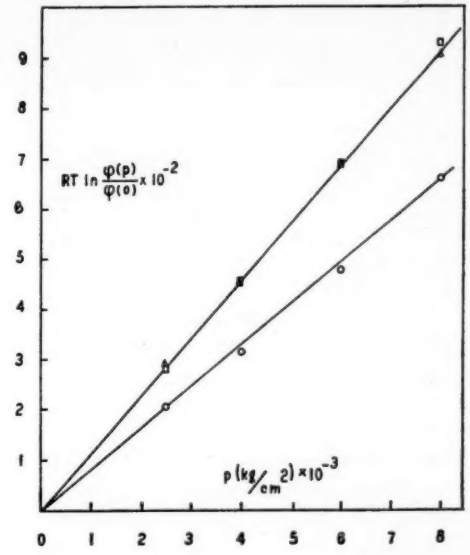

FIG. 6. The determination of $\Delta V_\square-\Delta V_o$ from the slope of $RT\ln[\varphi(p)/\varphi(o)]$ *vs* p at various temperatures: 202°C (○); 251°C (△); 289°C (□).

$1/T$ the quantities W_1, U_o, and $U_\square$ are also evaluated and listed in the same table which also contains Teltow's values.

Discussion of Results Below 300°C

In the derivation of φ and x_o from Eq. (5), the assumption is made that the association between a Cd^{++} ion and the vacancy can be neglected for concentrations of $y=0.1$ percent and less. At atmospheric pressure and 250°C Teltow found that 13 percent of the Cd^{++} ion is associated for the smallest concentrations of y (0.0046 percent) used, and that when $y=0.1$ percent about 27 percent of the associated vacancies do not

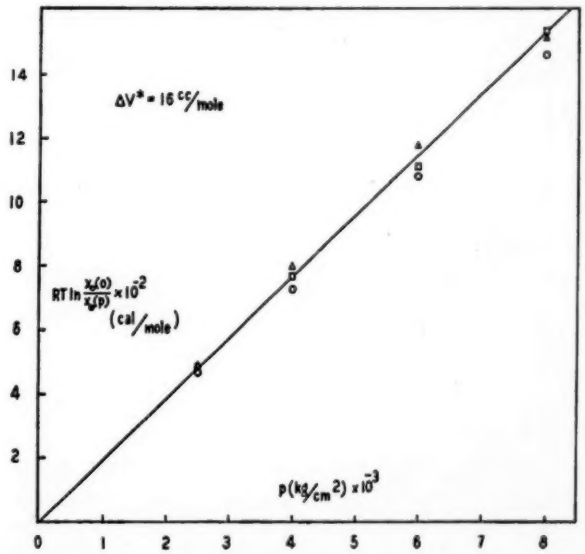

FIG. 7. The determination of $\frac{1}{2}\Delta V^*$ from the slope of $RT\ln[x(o)/x(p)]$ *vs* p at various temperatures: 202°C (○); 251°C (△); 289°C (□).

TABLE III. Relative high pressure conductivities for polycrystal and single crystal samples. Conductivity at atmospheric pressure $\sigma(o)$ is compared with that at high pressure $\sigma(p)$. Single crystal and polycrystal samples do not differ significantly at higher temperatures.

Temperature	$\sigma(o)$ $(\Omega\ cm)^{-1}$	Pressures in kg cm^{-2} 2500	4000	6000	8000
	Polycrystal				
202°C	7.35×10^{-4}	2.00	2.95	4.80	7.90
251°C	4.26×10^{-3}	2.00	2.96	4.78	7.57
289°C	1.47×10^{-2}	2.04	3.00	4.85	7.65
	Single crystal				
202°C	7.40×10^{-2}	2.01	3.01	5.32	9.00

contribute to the conductivity. The 250°C data of Teltow are plotted y/Z *vs* $1/y[(1/Z)-Z]$ in Fig. 9 to show the effects of association on concentrations of $CdBr_2$ up to 10 percent. The 251°C atmospheric data for concentration up to 0.1 percent as used in these experiments are also plotted.

Too much weight should not be put on the data for the lowest concentrations used because the effect of foreign impurities is unknown. Furthermore, both Teltow's data and our data support the assumption of no association for values of y below 0.1 percent. For this reason in Table IV we have compared the value W_1 obtained above and that of Teltow assuming no association. Although our value of 27,500 cal/mole is 1700 cal/mole smaller than his value, the agreement is satisfactory considering the experimental errors involved.

The discrepancies between the values of U_o and $U_\square$ and those of Teltow are somewhat larger than that for the W_1's. The reason for this discrepancy is that in Eq. (4) the factor preceding the exponential is assumed to be B_i/T instead of a constant as assumed by Teltow.

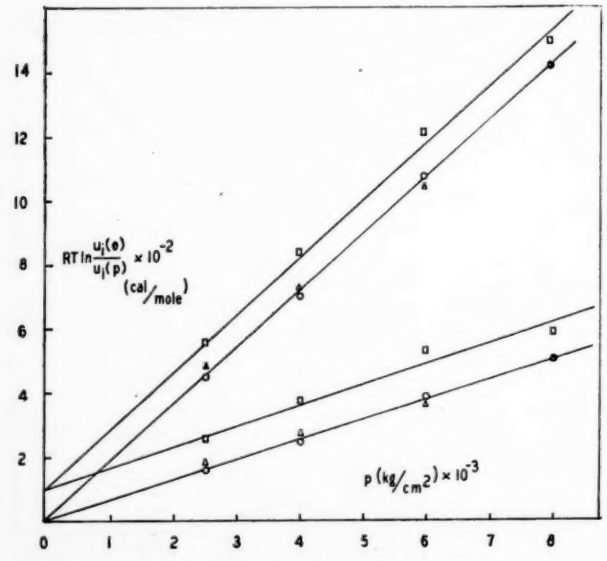

FIG. 8. The determination of $\Delta V_\square$ and ΔV_o for the temperatures 251°C and 289°C from the slope $u_\square(o)/u_\square(p)$ and $u_o(o)/u_o(p)$ *vs* p. Polycrystal samples: 251°C (Δ); 289°C (□). Single crystal: 202°C (○).

If Teltow's data are analyzed similarly the agreement is much more satisfactory.

The change in volume ΔV^* of 16 cc/mole found from the data above appears to be consistent with a Frenkel model below 300°C since it is well below the minimum value of 29 cc/mole (the molar volume of AgBr) required by a Schottky mechanism. Mott and Littleton[16] have calculated the displacement of ions adjacent to vacancies in NaCl. They found that the nearest neighbors are displaced outwards 0.07 a. Although this displacement depends on the dielectric constant, their value may be used roughly to estimate the change in volume associated with silver vacancies at 10 cc/mole. Since the silver interstitial ion will also demand an increase in volume, our experimental value of 16 cc/mole does not seem unreasonable.

TABLE IV. Summary of data.

Atmospheric pressure data	Symbol	Value	Source
Activation energy for Frenkel defects	W_1	27,500 cal/mole 29,200 cal/mole	Teltow
Activation energy for Schottky defects	W_2	>34,000 cal/mole	
Vacancy mobility energy	$U_\square$	11,200 cal/mole 8310 cal/mole	Teltow
Interstitial mobility energy	U_o	4700 cal/mole 3410 cal/mole	Teltow
Concentration at 406°C Frenkel defects alone	x_o	0.62% 1.2%	Teltow[a]
Concentrations at 406°C mixed Frenkel-Schottky defects			
(a) Interstitial ions	x_o	0.15%	
(b) Silver vacancies	$x_\square$	2.6%	
(c) Bromide vacancies	x_-	2.4%	
High pressure data			
Volume change for a mole of Frenkel defects	ΔV^*	16 cc/mole	
Free volume of Ag_o^+ mobility	ΔV_o	2.6 cc/mole	
Free volume of $Ag^+\square$ mobility	$\Delta V_\square$	7.4 cc/mole	
Volume change for a mole of Schottky defects	ΔV^{**}	38–48 cc/mole	
Anomalous expansion data to 406°C	$\frac{\delta v}{v}$		
Relative volume change with Frenkel defects alone		0.4% 0.65%	Teltow
Relative volume change with mixed Frenkel-Schottky defects		3.0–3.5%	
Anomalous expansion coefficient analyzed from Strelkow's data		2.6%	Lawson
Anomalous enthalpy data to 406°C	ΔH		
Anomalous enthalpy with Frenkel defects alone		170 cal/mole 350 cal/mole	Teltow
Anomalous enthalpy with mixed Frenkel-Schottky defects		>860 cal/mole	
From specific heats		950 cal/mole	Christy and Lawson
		<620 cal/mole	Kanzaki[b]

[a] Teltow's concentration with author's ΔV^* or W_1.
[b] Measured to melting point.

[16] N. F. Mott and M. J. Littleton, Trans. Faraday Soc. 34, 485 (1938).

Turning now to the values found for the free volumes associated with the mobilities of the imperfections it is noted their values are approximately proportional to U_o and $U\,\square$. This result does not seem to be unreasonable, since the activation energies should certainly be related to the free volumes required. However, it must be noted that these values are overestimated in Table IV for the following reasons.

It has been previously stated in the development of Eq. (11) that the term $(\partial/\partial p)\ln B_i$ is negligible compared to the terms $\Delta V_i/RT$. In terms of the potential field U_i' surrounding either the silver vacancy or interstitial ion and the compressibilities β_i of the neighborhood surrounding these imperfections, $\beta_i = 18r/(\partial^2 U_i'/\partial r^2)$ and $\partial^2 U_i'/\partial r^2 = 4\pi^2 \nu_{oi}^2 m$, where r is the distance between imperfections and neighbors and ν_{oi} is the frequency of vibration of either the interstitial ion or the neighboring silver ion of mass m. It follows that

$$(\partial \ln B_i)/\partial p \simeq -\tfrac{1}{2}\beta_i. \qquad (17)$$

By using the compressibility of AgBr, $\beta = 2\times 10^{-6}$ kg cm^{-2} and $T = 560$°K, $(\partial \ln B\,\square)/\partial p$ is 7 percent of $\Delta V\,\square/RT$, and $(\partial \ln B_o)/\partial p$ is 20 percent of $\Delta V_o/RT$. However, for the silver vacancies it may be said that $\beta\,\square$ is somewhat larger than β and for the interstitial ions β_o is smaller. The estimated error in $(\partial \ln B_i)/\partial p$ is about 10 percent of $\Delta V_i/RT$ and represents the amount by which both $\Delta V\,\square$ and ΔV_o have been overestimated. Unless otherwise noted the values of $\Delta V\,\square$ and ΔV_o used are those for which $\partial \ln B_i/\partial p$ is assumed negligible.

One of the principal discrepancies in the internal consistency of the data below 300°C is the failure of the $RT \ln(\varphi(p)/\varphi(o))$ at 202°C to agree with those at 251°C and 289°C. This effect is illustrated in Fig. 6. This discrepancy may arise for two reasons: (a) the effect of impurities is increasingly important at lower temperatures; (b) the effect of grain boundary conductivity may play an appreciable role at 202°C. Shapiro and Kolthoff[17] have already studied the effect of pressure on the conductivity of silver bromide and have concluded that at lower temperatures an appreciable contribution to the conductivity may arise from grain boundary conduction. Accordingly, to investigate this phenomenon, the conductivity of a single crystal of AgBr was investigated. It was found that at temperatures of 251°C and 289°C, regardless of pressure, the conductivity of a single crystal was identical with that of a polycrystalline sample. However, at 202°C and pressures above 5000 kg/cm², a marked deviation was found. In view of the agreement between the ΔV's derived from the 251°C and 289°C isotherms at higher pressures, we believe that the discrepancy of the ΔV's derived from the 202°C data may be ascribed to grain boundary conduction. This point of view is substantiated by the fact that the parameters derived from polycrystalline data at 289°C and 251°C, when extrapolated to 202°C and used with $\sigma(o)/\sigma(p)$ values of a single crystal of pure AgBr (see Table III), yield values for $\Delta V\,\square$ and ΔV_o which are in excellent agreement with those observed at 251°C and 289°C (Fig. 8). In this connection we must note, however, that the ΔV's computed from the 289°C isotherms at lower pressures deviates by about 10 percent from the value listed in Table IV. The reason for this discrepancy is not understood and may be the result of experimental error in the atmospheric data.

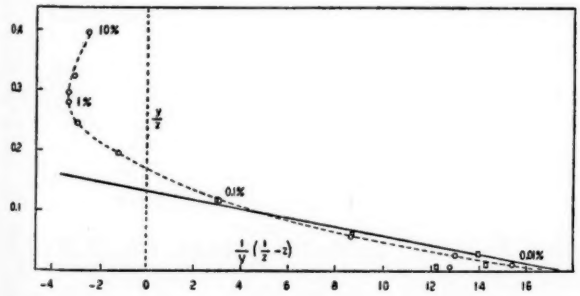

FIG. 9. Comparison of Teltow's z values for 250°C isotherm (○) and the atmospheric z values used in this experiment for 251°C (□). In this plot the effects of association of the Cd^{++} and the silver vacancies are not evident until Teltow's Cd^{++} content is greater than 0.1 percent, the highest concentration used.

[17] I. Shapiro and I. Kolthoff, J. Chem. Phys. **15**, 41 (1947).

TABLE V. Ratio of conductivities $\sigma(p)/\sigma(p_o)$, $p_o = 8{,}000$ kg cm^{-2} at temperatures 337°C and 406°C for pure silver bromide.

Temp.	337°C	406°C
$\sigma(o)$(Ω cm^{-1})	6.85×10^{-2}	4.95×10^{-1}
p(kg cm^{-2})	$\sigma(p)/\sigma(p_o)$	
0	9.28	13.1
500	7.95	...
1000	6.70	8.30
1500	5.62	...
2000	4.86	5.68
2500	...	4.73
3000	3.60	3.97
4000	2.73	2.90
5000	2.11	2.15
6000	1.64	1.66
7000	1.28	1.27
8000	1.00	1.00

RESULTS ABOVE 300°C

Although the Teltow technique is not sufficiently accurate above 300°C to yield significant data, it was deemed desirable to investigate the effects of pressure on the conductivities of pure AgBr at higher temperatures. Accordingly, pure samples were investigated to temperatures as high as 406°C. The results are tabulated in Table V and illustrated in Fig. 10. It is to be noted that the initial slope of $\ln\sigma(p)/\sigma(p_o)$ *vs* p becomes disproportionately higher as the temperature is increased. Although the parameters derived below 300°C when extrapolated to higher temperatures give reasonable agreement with the conductivity observed at 8000 kg/cm² and 406°C, these same parameters are incapable of predicting the low pressure data at high temperature.

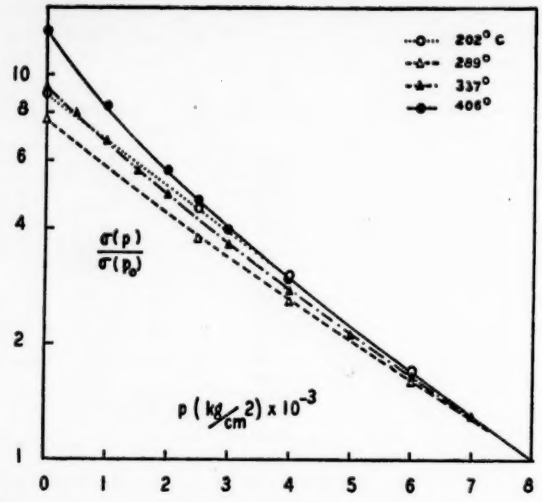

FIG. 10. Change in conductivities $\sigma(p)$ relative to $\sigma(p_o)$, $p_o = 8000$ kg/cm² for pure AgBr at different temperatures. Absolute values of $[\partial \ln\sigma(p)/\partial p]$ are greater than at 289°C because conduction is controlled more and more by vacancies than by interstitial Ag^+ ions. Below 300°C, the 202°C isotherm has a higher $|\partial \ln\sigma(p)/\partial p|$ because the shift from vacancies to interstitial Ag^+ ions as the controlled factor in the conductivity is overweighed by the change in the factor, $1/T$.

For this reason, the onset of a new phenomenon was suspected, and it appeared desirable to repeat Tubandt's experiment at 406°C. The results of this experiment are tabulated in Table VI. The net result may be summarized by saying that even at this temperature no contribution of the Br^- ion to the conductivity can be detected.

Discussion of Results Above 300°C

The discrepancy between $\sigma(o)/\sigma(p)$ at 406°C and its values below 300°C may arise from a variety of reasons: (a) the Cd^{++} ion in a silver site will associate with a silver vacancy to form a complex $Cd^{++}Ag\,\square^+$ which does not contribute to the conductivity and leads to erroneous evaluations of φ and x_o; (b) the ΔV's associated with the creation of imperfections and changes in mobilities with pressure may increase as the temperature increases; (c) a new type of interstitial site may become available, or (d) the onset of a new type of imperfection may be created in the lattice, such as Schottky defects. We shall now discuss these possibilities in order:

TABLE VI. Simplified transport experiment[a]

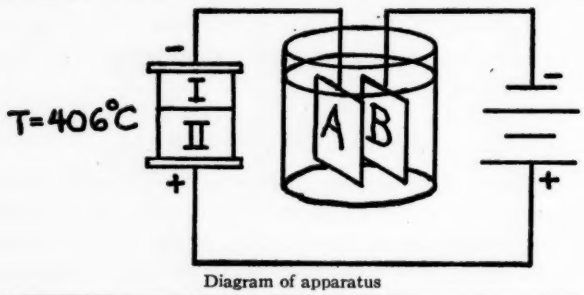

Diagram of apparatus

AgBr pellets	Weight (g) Before current passage	After current passage	Change in weight
Silver cathode+pellet I	4.0608	4.1970	0.1362
Silver anode+pellet II	10.7759	10.6393	−0.1366
Coulometer			
Silver anode (A)	5.6404	5.5042	−0.1362
Silver cathode (B)	11.7214	11.8577	0.1363

[a] Change in weight of AgBr blocks *I* and *II* is compared with the weight changes in the coulometer electrodes *A* and *B* after current passage. Equal changes in *I*, *II* and *A*, *B* show current transport by silver ions at 406°C in AgBr.

It has already been pointed out above that association between the Cd^{++} ions and the silver vacancies occur to an inappreciable extent in the concentrations used in our experiments. For this reason possibility (a) is rejected.

Assuming only a Frenkel disorder, to obtain agreement between the data at 406°C and that below 300°C, it is not only necessary to increase the $\Delta V\,\square$ from 7.4 cc to 12 cc/mole but also the extrapolated ratio of the mobilities must be decreased, over a factor of three, from 1.0 to 0.3. This decrease in φ required to obtain agreement on the basis of the Frenkel mechanism alone is far beyond the experimental error, if U_o and $U\,\square$ are independent of temperature as experimentally observed below 300°C. For this reason we pass on to the next possibility.

A new type of position energetically more unfavorable than those occupied by silver ions at lower temperatures could enhance the conductivity at higher temperatures and produce a larger expansion of the lattice. However, in the case of AgBr it would appear from symmetry considerations that there are only two possible interstitial positions: namely type A, at the center of the cell $(\frac{1}{2}, \frac{1}{2}, \frac{1}{2})$, or type B at the center of a face such as $(\frac{1}{2}, \frac{1}{2}, 0)$. In order to pass from one type A to another type A position the Ag^+ ion must surmount a col. In the case of AgBr, the col for a type A interstitial ion is a type B position, and vice versa. Under these circumstances, it is difficult to see how any new interstitial position can come into play at higher temperatures.

We are forced then to consider the final possibility, namely the onset of a Schottky mechanism. In view of the transport experiment described above it must be assumed that the Br^- vacancy mobility is small enough so that its contribution to the conductivity is negligible. In this special case, the conductivity is governed by a relation of the type

$$\sigma/eN = (K_1 u_o)/(K_1+K_2)^{\frac{1}{2}} + (K_1+K_2)^{\frac{1}{2}} u\,\square, \quad (18)$$

where K_1 is the equilibrium constant for the Frenkel mechanism and K_2 is that for the Schottky.

Since the creation of a mole of Schottky imperfections must exceed the molar volume of AgBr, namely, 29 cc, the ΔV^{**} associated with this type of disorder will be greater than that found above for the Frenkel disorder. If we assume, as noted above, that the conductivity at 406°C and 8000 kg/cm^{-2} is primarily controlled by the

Frenkel mechanism because the Schottky mechanism, with its large ΔV^{**}, is rapidly repressed by pressure, then we may endeavor to sort out the two mechanisms in the following manner: With reference to Fig. 11, we denote by A a fictitious $\sigma(p)/\sigma(p_o)]_A$ curve calculated from ΔV's derived from low temperature data. Curve B is the actually observed value for $\sigma(p)/\sigma(p_o)]_B$. Then, these curves are related by

$$(1+\varphi)\frac{\sigma(p)}{\sigma(p_o)}\Bigg]_A \frac{\sigma(p_o)}{\sigma(p)}\Bigg]_B = \left(1+\frac{K_2}{K_1}\right)^{\frac{1}{2}} + \frac{\varphi}{[1+(K_2/K_1)]^{\frac{1}{2}}}, \quad (19)$$

where $p_o = 8000$ kg/cm². Since K_1 is known, K_2 may be calculated. These values are quite sensitive to the errors in φ and K_1 and are more reliable at lower pressures where the difference between curve A and curve B is most significant. Values of K_2 so derived are plotted as curve C in Fig. 11. At zero pressure, K_2 may be in error as much as a factor of two. From K_2 a value for ΔV^{**}, the molar volume for the Schottky imperfections, is estimated to 43 cc ±5 cc, in reasonable agreement with the minimum value of ~40 cc calculated from the Mott and Littleton model. The density of the various types of imperfections at 406°C may also be estimated and are given in Table IV.

It appears worthwhile to correlate the data derived above with data on thermal expansion and specific heat, both of which increase anomalously just below the melting point of AgBr, as a result of the creation of imperfections. We may estimate the relative volume increase $\delta v/v$ associated with the creation of x □ silver vacancies, x_o interstitial Ag^+ ions, and x_- bromide vacancies from the relation

$$\delta v/v = x_o(\Delta V^*/V_o) + x_-(\Delta V^{**}/V_o), \quad (20)$$

where ΔV^* is the change in volume in Eq. 10 and ΔV^{**} is the corresponding quantity for the Schottky mechanism. Similarly, the value of the increase in the anomalous enthalpy ΔH associated with the creation of the various imperfections is given by

$$\Delta H = x_o W_1 + x_- W_2, \quad (21)$$

where W_1 and W_2 are the activation energies associated with the Frenkel and Schottky mechanisms, respectively. In order to estimate ΔH from the preceding equation, it is necessary to know the value of K_2 at more than one temperature. Although data were obtained at 337°C which in principle permits these evaluations of W_2, in practice the contribution of the Schottky imperfections at this temperature was so small as to leave the value of W_2 so derived very uncertain. Accordingly, W_2 was estimated from the slope of $\ln\sigma(o)$ *vs* $(1/T)$ in the range of temperatures just below the melting point. Since only 5–10 percent on the

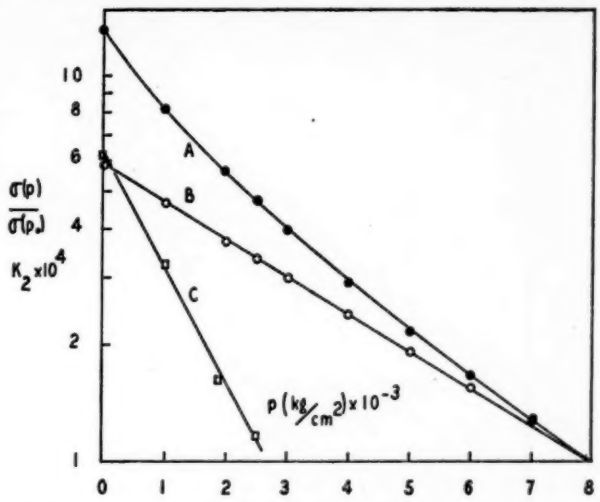

FIG. 11. Comparison of 406°C relative conductivities $\sigma(p)/\sigma(p_o)$ measured (A) and $\sigma(p)/\sigma(p_o)$ calculated (B) from ΔV^*, ΔV□, ΔV_o, and $\varphi(o)$ extrapolated to 406°C. Estimate of Schottky equilibrium constant K_2 required (*C*) for $\sigma(p)/\sigma(p_o)$ values to conform to (*A*).

defects are Ag^+ interstitial ions in this range, we have

$$W_2 \gtrsim 2(S - U\,\square), \quad (22)$$

where S is slope of $\ln\sigma(o)$ *vs* $(1/T)$. A comparison of the pure AgBr conductivities and those taken by Teltow for temperatures just below the melting point are given in Fig. 12. At lower temperatures there is good agreement but at these high temperatures Teltow's values are consistently lower. This discrepancy is larger than any possible error in temperature measurements or AgBr sample sizes. However, the slopes are in relatively good agreement. Nevertheless, the value of W_2 estimated from these graphs must be much too small or the contribution of the Schottky disorder at 289°C would be larger than that from the Frenkel. A more reasonable value for W_2 would be closer to 50,000 cal/mole. In

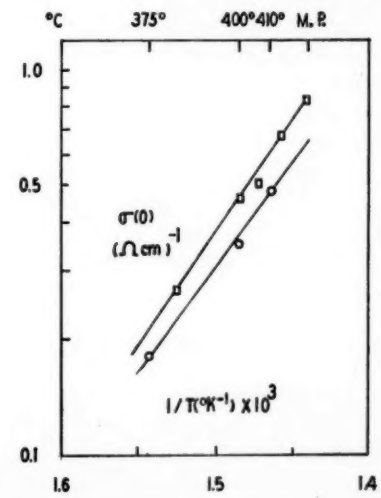

FIG. 12. High temperature atmospheric conductivities of pure AgBr $\ln\sigma(o)$ *vs* $1/T$ at temperatures just below the melting point (□). High temperature conductivities after Teltow (○).

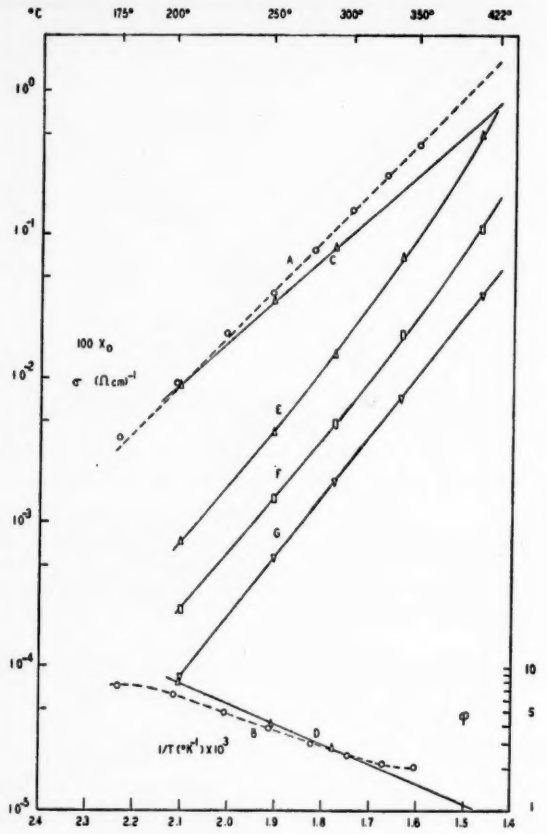

FIG. 13. Comparison of Teltow's x_o and φ values, (*A*) and (*B*), respectively, with atmospheric x_o and φ values, (*C*) and (*D*). Variation of conductivities with temperature at different pressure levels: (*E*) atmospheric; (*F*) 4000 kg/cm²; (*G*) 8000 kg/cm².

any case, the effect of double Schottky vacancies[18] has been ignored.

[18] G. J. Dienes and F. Seitz, Phys. Rev. **73**, 1260(A) (1948).

These values of $\delta v/v$, ΔH, and W_2 calculated in the manner described above are listed in Table IV, where they are compared with estimates of these quantities derived by other types of experiments.[8] In addition they are also compared with estimates of the same quantities based on the assumption of a Frenkel disorder alone. An examination of Table IV reveals that the data estimated with an assumption of a Schottky mechanism is in somewhat better agrement with thermal expansion and specific heat data than the data computed on the assumption of a Frenkel disorder alone. This agreement tends to support our interpretation of the increased slope of $\ln\sigma(o)$ *vs* $(1/T)$ just below the melting point as arising from the onset of the Schottky disorder. It might be remarked that this evidence for the existence of Schottky imperfections is substantiated by the work of O. Stasiw,[6] who has studied the optical absorption of quenched and annealed AgBr samples doped with slight concentrations of Ag_2S. On the other hand, our quantitative estimates of the number of Schottky imperfections present are considerably larger than those estimated from a comparison of x-ray lattice spacings and density measurements made by Berry.[4] High pressure conductivities and a comparison of atmospheric data with Teltow's are shown in Fig. 13.

ACKNOWLEDGMENTS

The authors wishes to express his gratitude to his sponsor, Professor A. W. Lawson, for his many constructive suggestions during the course of this investigation, and to Messrs. K. Lindholm and N. D. Nachtrieb for assistance in the construction and maintenance of the equipment. The author is also indebted to the Shell Oil Company for the award of a fellowship. This work was supported in part by funds from the Office of Naval Research.

Dielectric Constant Measurements of Chlorine Trifluoride at 9400 mc/sec*†

DALE W. MAGNUSON
K-25 Laboratories, Carbide and Carbon Chemicals Company, Oak Ridge, Tennessee
(Received July 27, 1951)

The dielectric constant of chlorine trifluoride was determined at 9400 mc/sec by measuring the change in the resonant frequency of a cavity when it is filled with the vapor. Corrections were made for the amount of dimer formed. The monomer molar polarization was best represented by $P=15.944+1882.0/T°\text{K}$ cc and the dipole moment was 0.554 Debye unit. The average dimer molar polarization was found to be 49.8 cc assuming no dipole moment.

INTRODUCTION

CHLORINE trifluoride has been investigated to a limited extent because of the reactive nature of this fluorine compound, and no references were found in the literature concerning dielectric constant or dipole moment determinations. Dielectric constant measurements were undertaken in conjunction with the infrared and Raman studies at this laboratory.[1] No assignments for the fundamental vibrational frequencies were made because the experimental data could not be fitted to the expected pyramidal model obtained from the electron diffraction data,[2] and it was expected that the value of the dipole moment might aid in the determination of the structure of this molecule. Further analysis of the infrared band contours and some of the microwave absorption spectrum[3] have indicated that the structure is not a symmetrical pyramid. A planar symmetric model would be excluded if the dipole moment were not zero.

Other investigations concerning the chemistry of this molecule have been reported.[4–6] Schmitz and Schumacher[5] have measured the equilibrium constant for the dimerization, $ClF_3+ClF_3=(ClF_3)_2$, and corrections for this would necessarily have to be made in any dielectric constant measurement. Although the amount of dimer formed would be small, the microwave dielectric constant measurements would be sufficiently accurate to yield some information concerning the dimer.

Polymerization studies of hydrogen fluoride by means of dielectric constant measurements[7] were helpful in the determination of possible polymer structures.

THEORY

The microwave method of making dielectric constant measurements consists of measuring the change in the resonant frequency of a cavity when it is filled with the dielectric. When an evacuated cavity, whose resonant frequency is ν_0, is filled with material whose dielectric constant is ϵ, the new resonant frequency, ν, is given by $\nu=\epsilon^{-\frac{1}{2}}\nu_0$. This is easily transformed to the useful expression $\epsilon-1\approx-2\Delta\nu/\nu_0$ which neglects a factor $(1+\nu_0/\nu)\nu_0/2\nu$. Hence, accurate frequency measurements are used in the dielectric constant measurements.

The molar polarization, P, is useful because it is independent of gas density, and the dipole moment is calculated from the temperature variation of the molar polarization

$$P=\frac{\epsilon-1}{\epsilon+2}\frac{M}{\rho}=\frac{4N}{3}\left(\alpha+\frac{\mu^2}{3kT}\right),$$

where M = molecular weight, ρ = gas density, N = Avogadro's number, α = molecular polarizability, μ = dipole moment, and kT has the usual designation.

In addition, an expression must be found so that corrections may be applied for the dimerization and so that the magnitude of the correction can be used to determine dimer chlorine trifluoride properties. If we define ϵ = total dielectric constant, p_m = partial pressure of monomer, p_d = partial pressure of dimer, p = total pressure, $\delta_m=(\epsilon_m-1)/p_m$, $\delta_d=(\epsilon_d-1)/p_d$, and K = equilibrium constant of dimerization, then the following relations are used to derive an expression for $(\epsilon-1)$ in terms of p, K, δ_m, and δ_d,

$$p=p_m+p_d;\quad K=p_m^2/p_d;\quad \epsilon-1=\delta_m p_m+\delta_d p_d,$$

which is

$$(\epsilon-1)=\delta_m p+(p^2-2p^3/K+5p^4/K^2\cdots)(\delta_d-\delta_m)/K.$$

For the range of pressures used in the experiments the cubic and higher terms may be neglected, and by measuring the dielectric constant at many pressures for several temperatures, experimentally determined values of the coefficients of a quadratic equation can be used to obtain the dielectric properties of the monomer and dimer.

* This document is based on work performed for the AEC by Carbide and Carbon Chemicals Company, K-25 Plant, at Oak Ridge, Tennessee.

† The results herein reported are included in a doctoral thesis submitted to the University of Tennessee.

[1] Jones, Parkinson, and Murray, J. Chem. Phys. **17**, 501 (1949).

[2] A. L. Wahrhaftig, quoted by P. W. Allen and L. E. Sutton, Acta Cryst. **3**, 46 (1950).

[3] D. F. Smith (private communication).

[4] O. Ruff and H. Krug, Z. anorg. u. allgem. Chem. **190**, 270 (1930).

[5] H. Schmitz and H. J. Schumacher, Z. Naturforsch. **2a**, 362–363 (1947).

[6] Ruff, Ebert, and Menzel, Z. anorg. u. allgem. Chem. **207**, 46 (1932).

[7] R. A. Oriani and C. P. Smyth, J. Am. Chem. Soc. **70**, 125 (1948).

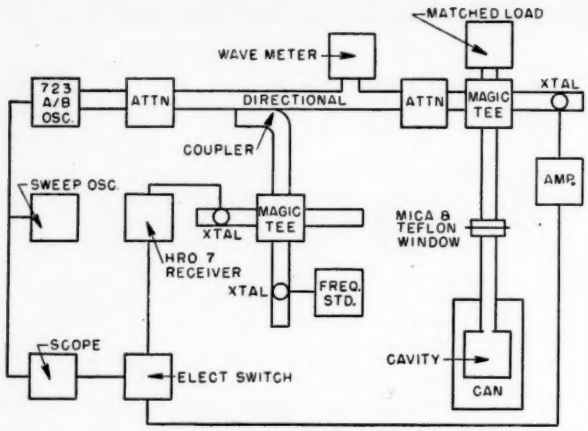

FIG. 1. Block diagram of microwave apparatus for measuring dielectric constants.

It is to be noted that the results of Schmitz and Schumacher[5] are not consistent with the effects of a nonideal gas, and they have interpreted their data as an equilibrium between monomer and dimer chlorine trifluoride. In addition, the present results at six temperatures cannot be interpreted on the basis of a Van der Waal's gas, but only as an equilibrium between the monomer and dimer.

APPARATUS

The apparatus developed at the K-25 Laboratories for dielectric constant measurements consisted of a single cavity whose resonant frequency changes were measured. An electrical block diagram is shown in Fig. 1. A frequency modulated 723A/B klystron oscillator was used to sweep over the cavity resonance by means of a saw-tooth voltage on the reflector electrode. The cavity resonance was displayed on an oscilloscope whose sweep was synchronized with the frequency modulation. The frequency of the cavity response was determined by mixing part of the klystron output with the frequency standard and detecting the beat frequency with a calibrated radio receiver (National HRO-7). The output of the receiver was displayed on the same oscilloscope by means of an electronic switch, and the beat frequency appears as another resonance pip and is aligned with the cavity resonance by tuning the receiver.

The frequency standard is similar to that of Untermeyer and Smith[8] and produces markers every 90 mc/sec in the microwave region.

The cylindrical cavity, which operates in the TE-013 mode, was machined from copper with diameter of 2.429 in. and height of 2.435 in. With an iris coupling hole 0.230 in. in diameter and 0.010 in. thick, the loaded Q was calculated to be 20,000. Experimental values of the Q were in agreement with this value. The entire cavity was surrounded by a container which was soldered to the wave guide so that changes in pressure could not deform the end plates of the cavity. The wave guide was sealed with a 10-mil Teflon window gasket backed by a 2-mil mica window. The cavity was immersed in a water bath whose temperature was controlled to ± 0.05°C by means of a mercury contact thermoregulator.

The pressure of chlorine trifluoride in the cavity was measured by comparing it to a reference air pressure by means of a calibrated differential pressure transmitter. The reference air pressure, which was variable, was measured on an absolute mercury manometer.

No changes in Q were noted upon filling the cavity with chlorine trifluoride. The loss tangent is estimated to be less than 5×10^{-6} assuming that a 10 percent change in Q would have been observed. The apparatus was not suitable for accurate Q measurements.

EXPERIMENTAL RESULTS

Procedure

The gas handling manifold and cavity were previously exposed to chlorine trifluoride so that there was no appreciable reaction during the runs.

The resonant frequency of the cavity was determined for zero pressure and for pressure increases of three to ten-cm Hg for six different temperature runs. A typical set of data is shown in Fig. 2 where the cavity resonant frequency is plotted *vs* pressure of chlorine trifluoride. The straight line drawn on the graph represents the

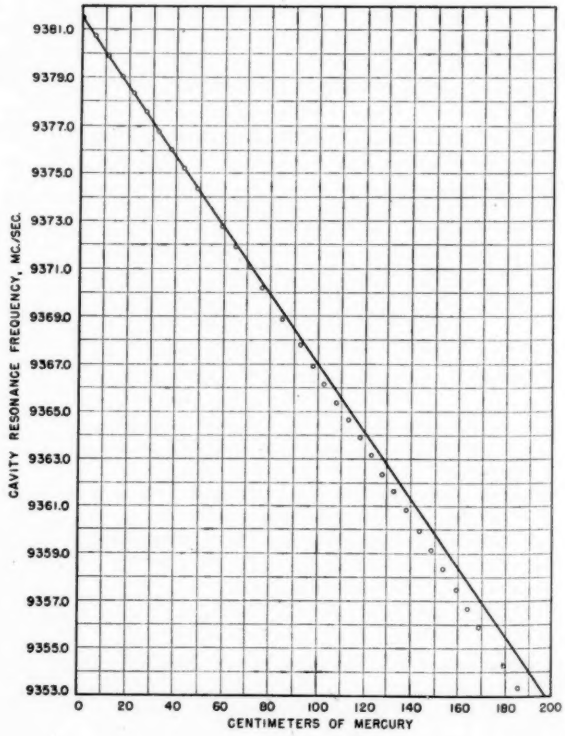

FIG. 2. Chlorine trifluoride dielectric constant measurements at 61.2°C.

[8] R. R. Untermeyer and W. V. Smith, Rev. Sci. Instr. **19**, 580 (1948).

calculated curve for monomer had there been no dimerization with increasing pressure. Pressure readings were corrected to 0° Hg density.

Calculations

For each temperature run the data were divided into three groups to solve for the coefficients of the best fit equation of the form $\nu = a_0 + a_1 p + a_2 p^2$. a_0 is the best fit value of the evacuated cavity resonant frequency and differs from the measured value by less than 0.010 mc/sec in all runs. The calculations are summarized in Table I which give the molar polarizations for chlorine trifluoride monomer and dimer at the six temperatures, 0.0, 20.0, 34.0, 40.0, 61.2, and 83.1°C. From the variation of the molar polarization of chlorine trifluoride monomer the dipole moment is calculated to be $\mu = 0.554 \pm 0.002$ Debye unit. This is plotted in Fig. 3. The equation of the line which represents the variation of the monomer molar polarization

TABLE I. Calculations of chlorine trifluoride dielectric constants.

	Monomer				
T°C	a_0 (mc/sec)	$-a_1$ mc/sec / cm Hg	δ_m (cm Hg)$^{-1}$	$(\epsilon-1)_m$	P_m (cc)
0.0	9391.000	0.188635	40.174×10^{-6}	3053.2×10^{-6}	22.811
20.0	9387.943	0.172387	36.725	3791.1	22.380
34.0	9385.769	0.162372	34.598	2629.5	22.088
40.0	9384.807	0.158283	33.732	2563.6	21.958
61.2	9381.507	0.145595	31.036	2358.8	21.571
83.1	9377.982	0.134317	28.646	2177.0	21.213

	Dimer				
T°C	$-a_2$ mc/sec / (cm Hg)^2	K (cm Hg)	δ_d (cm Hg)$^{-1}$	$(\epsilon-1)_d$	P_d (cc)
0.0	13.705×10^{-5}	1686	89.39×10^{-6}	6794×10^{-6}	50.76
20.0	8.456	2478	81.37	6184	49.59
34.0	6.566	3146	78.62	5975	50.19
40.0	5.943	3450	77.42	5884	50.39
61.2	3.980	4707	70.97	5394	49.33
83.1	1.880	6263	53.76	4086	39.81

with the inverse of the absolute temperature is $P_m = 15.944 + 1882.0/T°\text{K}$ cc and the probable error is ±0.075 cc.

The variation of the molar polarization of chlorine trifluoride dimer with the inverse of the absolute temperature is plotted in Fig. 4 along with the estimated probable error. The data are not inconsistent with a zero dipole moment for the dimer, and on this basis a weighted average of the dimer molar polarization is $P_d = (49.8 \pm 0.5)$ cc.

DISCUSSION OF RESULTS

Purity of Samples

Chlorine trifluoride is a very reactive compound and it is difficult to obtain pure material. The data were taken as soon as possible after purification by distillation. Three runs were taken on one sample whose purity was found to be 99.95 percent by means of freezing point lowering determinations. A second sample

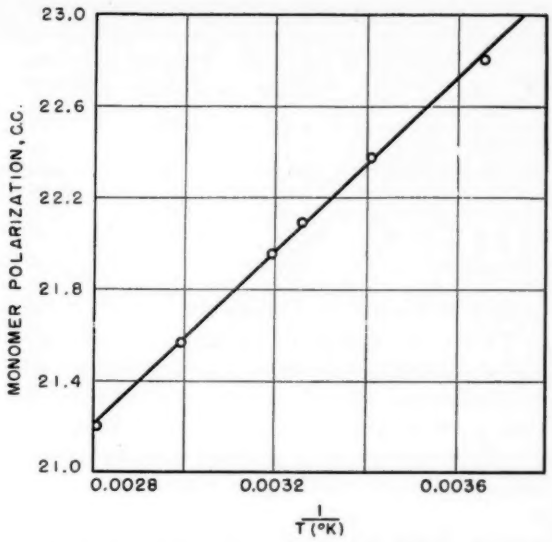

FIG. 3. Variation of the molar polarization of chlorine trifluoride monomer with temperature.

purified in a similar manner provided material for the other three runs. Previous data taken with commercial chlorine trifluoride (Harshaw Chemical Company) did not yield consistent results. In these data the impurity had a larger dielectric constant and was likely to have been hydrogen fluoride. For each temperature run the chlorine trifluoride was added to the manifold and cavity from the cylinder of purified material and it was not reused to prevent contamination.

Chlorine Trifluoride Monomer

The dipole moment of 0.554 Debye unit for chlorine trifluoride rules out the planar symmetric model similar to the structure of boron trifluoride. If we use $\angle \text{FClF} = 86°$ predicted by electron diffraction[2] and the dipole moment of chlorine monofluoride for the Cl–F bond moment of 0.881 Debye units,[9] then the dipole moment

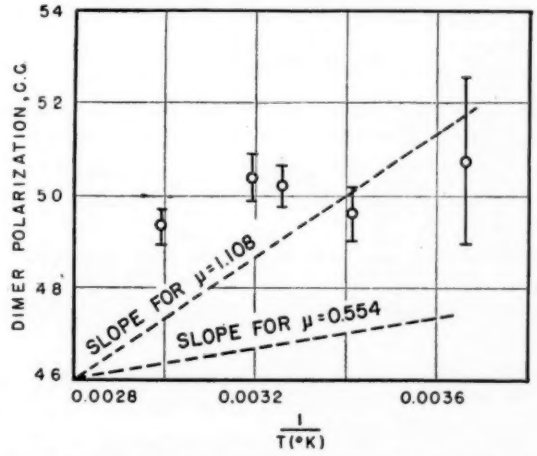

FIG. 4. Variation of the molar polarization of chlorine trifluoride dimer with temperature.

[9] Gilbert, Roberts, and Griswold, Phys. Rev. **76**, 1723 (1948).

TABLE II. Effects of chlorine trifluoride dimer.

Temp °C	Max total press cm Hg	Max dimer press cm Hg	Dimer freq shift $a_{12}p^2$ max	Percent error
0.0	45.45	1.23	0.280	3.57
20.0	101.42	4.15	0.860	1.16
34.0	135.26	5.82	1.187	0.84
40.0	133.19	5.14	1.042	0.96
61.2	185.28	7.29	1.351	0.74
83.1	39.95	0.25	0.030	33.00

of chlorine trifluoride is calculated to be 1.6-Debye units. Using the observed moments the F−Cl−F angle of a pyramidal model is predicted to be 116°. These calculations provide further tentative evidence that the present symmetrical pyramidal model is incorrect. It is recognized that these considerations are not free from fundamental objections.

Chlorine Trifluoride Dimer

The equilibrium constant of the reaction $ClF_3+ClF_3 \rightleftarrows (ClF_3)_2$ has been measured[5] at 9.5, 20.0, and 24.5°C. These data were extrapolated to the temperatures used by least squares calculation. Errors in the values of the equilibrium constant used cannot influence the monomer dielectric constant or dipole moment, but the dimer properties will be affected. Because the dimer properties are derived from a second-order effect, the errors of measurement are likely to be larger than the equilibrium constant error. The maximum partial pressures and frequency shifts caused by chlorine trifluoride are given in Table II.

The percentage errors are calculated from a total probable error of ±0.010 mc/sec in the frequency determination. These are shown also in Fig. 4.

It can be stated that the dipole moments of the two molecules are not aligned in the dimer. The calculated value for the dipole moment of the dimer is $\mu=0.50^{+0.12}_{-0.17}$ Debye unit ($\mu^2=0.250\pm0.139$). A zero moment is not inconsistent with the data.

Sources of Error

The sources of error for these dielectric constant measurements are impurities possessing different dielectric properties, and changes in the frequency standard, in receiver calibration, in pressure, and in temperature.

Impurities in the sample are the largest sources of error. It is to be pointed out that a likely impurity is hydrogen fluoride which has a larger dielectric constant. A content of 0.05 mole percent would cause only an error of 3×10^{-6} in $(\epsilon-1)$.

The 10 mc/sec crystal oscillator of the frequency standard was monitored by beating with WWV and was found to be extremely stable. A run lasted less than two hours, and the measured drift over these short periods was less than 2 cps. This corresponds to 1.9 kc/sec at 9360 mc/sec. It should be noted that a change of 5 kc/sec corresponds to a change in $(\epsilon-1)$ of 1×10^{-6}.

The receiver reproducibility alignment of the pips was ±4 kc/sec and is the limiting factor in the frequency measurements. The same error is involved in setting each of the calibration points taken above and below each frequency measurements to eliminate receiver calibration changes. The 100 kc/sec calibrating crystal introduced no appreciable error because its 300th harmonic differed from the 10 mc/sec third harmonic by less than a few hundred cycles.

For gases of high dielectric constant the frequency shift per unit pressure becomes large enough so that errors of 0.02 cm Hg are significant. For chlorine trifluoride at 40.0°C the shift is 158.3 kc/sec per cm Hg so that this error corresponds to 3 kc/sec error in frequency.

The cavity was placed in a water bath whose temperature was controlled to ±0.05°C. From the thermal expansion of copper the cavity resonant frequency should shift 132 kc/sec per °C, and this was measured to be 160 kc/sec per °C. No change in bath temperature was ever noted on a 0.1°C mercury thermometer. For a maximum long time change of 0.05°C, the resonant frequency drift would be 8 kc/sec. When the bath temperature was quickly changed, the half-time for thermal equilibrium was found to be 18 minutes. The temperature bath was maintained at the run temperature for several hours prior to starting a run to insure thermal equilibrium.

The apparatus was checked by measuring the dielectric constant of nitrogen and an average of five determinations corrected to standard conditions was $(592.6\pm0.5)\times10^{-6}$ which compares to the Birnbaum, Kryder, and Lyons[10] value of $(586.9\pm2.9)\times10^{-6}$ and the Hector and Woernley[11] value of $(579.6\pm1.0)\times10^{-6}$.

ACKNOWLEDGMENT

The writer is indebted to Dr. D. F. Smith whose valuable assistance and guidance were so freely given throughout this investigation.

[10] Birnbaum, Kryder, and Lyons, J. Appl. Phys. **22**, 95 (1951).
[11] L. G. Hector and D. L. Woernley, Phys. Rev. **69**, 101 (1943).

An Investigation of Certain Solvent Effect in Absorption Spectra*

ARTHUR L. LEROSEN AND CHARLES E. REID†
Coates Chemical Laboratories, Louisiana State University, Baton Rouge, Louisiana
(Received August 14, 1951)

A study of the solvent effects in the spectra of non-ionic compounds to whose structure a zwitter ion form makes appreciable contribution (particularly in the excited state) has revealed three distinct effects:

1. A shift of absorption bands to greater wavelength with increasing refractive index, as predicted by Kundt's rule. This is ascribed to the effect of electronic polarizability on the zwitter ion structure, and is seen unmixed with the other effects only when the solvents are hydrocarbons or aryl halides.
2. A further shift which appears with most solvents other than hydrocarbons and aryl halides, and is ascribed to orientation of molecules of nonuniform polarizability.
3. The Kuhn-Brockmann effect—a large shift which appears whenever hydrogen bonds between the solvent and solute occur. This is believed to be due to the stabilization of the zwitter ion by the electrostatic nature of the hydrogen bond.

No correlations of the spectra of phenolphthalein, *p*-rosaniline hydrochloride, or iodine with the properties of the solvent were found.

OBSERVATIONS that the absorption spectra of colored compounds in solution undergo slight displacements with change of solvent have led to several attempts to find some correlation between these shifts and the properties of the compounds involved. Kraus,[1] for example, attempted to correlate the position of the absorption bands of chlorophyll with the specific gravity of the solvent. Kundt[1] stated that a shift toward greater wavelength takes place as solvents of greater dispersion are used; however, the term "Kundt's rule" is often applied to a similar statement in which dispersion is replaced by refractive index. Vaillant concluded that the wavelength of the absorption bands varies linearly with the refractive index and density of the solvent.[2] Cennamo considered the dipole moment of the solvent to be the determining property in the case of iodine solutions.[3] Recently Brooker and Sprague, working with phenol blue, found the absorption band to shift toward greater wavelength with increasing dielectric constant of the solvent.[4]

Of these attempted correlations, Kundt's rule has received the most attention, having been supported[5] or denied[6] by several investigators; however, no systematic investigation of the problem has appeared. The present

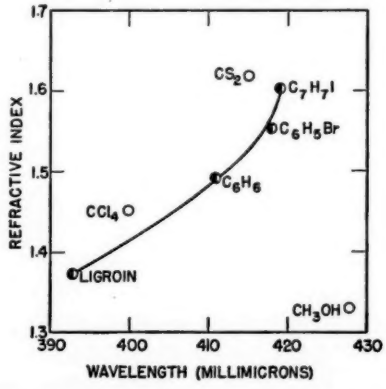

FIG. 1. Wavelength at absorption maximum of *p*-nitrosodimethylaniline *vs* refractive index of solvent. ◐ Hydrocarbons and aryl halides; ○ other solvents.

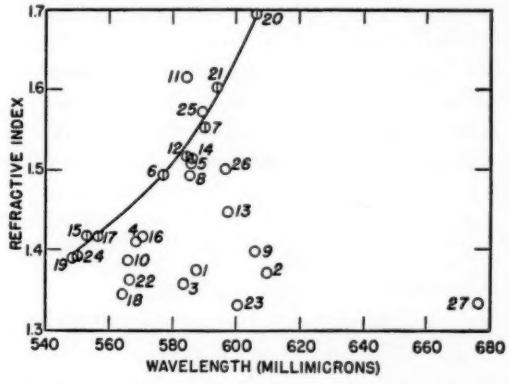

FIG. 2. Wavelength at absorption maximum of phenol blue *vs* refractive index of solvent. ◑ Hydrocarbons and aryl halides. ○ Other solvents.

1. Acetal
2. Acetic acid
3. Acetone
4. Amyl ether
5. Anisole
6. Benzene
7. Bromobenzene
8. Bromocyclohexane
9. Butanol
10. Butyl ether
11. Carbon disulfide
12. Chlorobenzene
13. Chloroform
14. *p*-Chlorotoluene
15. Cyclohexane
16. Dioxane
17. Dodecane
18. Ethyl ether
19. Heptane
20. 1-Iodonaphthalene
21. *o*-Iodotoluene
22. Isopropyl ether
23. Methanol
24. Octane
25. Phenyl ether
26. Pyridine
27. Water

* Taken from a dissertation submitted by Charles E. Reid to the graduate faculty of Louisiana State University in partial fulfillment of the requirements for the degree of Doctor of Philosophy.

† Present address: Department of Chemistry, University of Florida, Gainesville, Florida.

[1] A. Kundt, Ann. Phys. u. Chem. (Jubelband) 615–624 (1874); *ibid.* 4, 34–54 (1878).

[2] P. Vaillant, Compt. rend. **184**, 939 (1927).

[3] F. Cennamo, Nuovo cimento, Series 8, **16**, 355–359 (1939).

[4] L. G. S. Brooker and R. H. Sprague, J. Am. Chem. Soc. **63**, 3214 (1941).

[5] S. E. Sheppard, Revs. Modern Phys. **14**, 303–340 (1942).

[6] W. R. Brode, J. Phys. Chem. **30**, 56 (1926); G. Mackinney, Plant Physiol. **13**, 428 (1938); **15**, 359 (1940). R. A. Houston, *A Treatise on Light* (Longmans, Green and Company, London, 1930), sixth edition, p. 329.

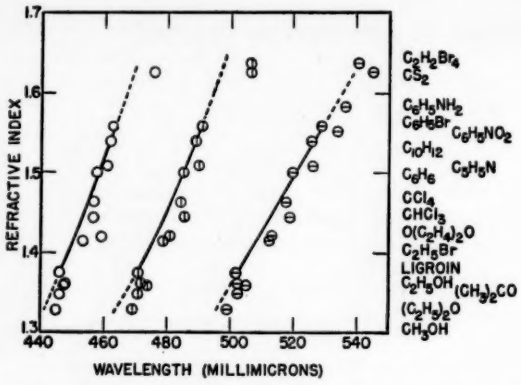

FIG. 3. Wavelength at the three absorption maxima of lycopene *vs* refractive index of solvent.

work was undertaken as a step toward remedying this deficiency.

The solutes used in the experimental work included a cationic dye, an anionic dye, several non-ionic dyes, and iodine. Measurements of absorption were made on a Beckmann photoelectric spectrophotometer. The concentrations were such as to produce an extinction coefficient of about 0.7, and the measurements were made at room temperature (approximately from 25° to 35°C).

It was found that the spectra of phenol blue, *p*-nitrosodimethylaniline, and certain carotenoids can be correlated with the refractive index of the solvent (or its dispersion) if the solvents are restricted to hydrocarbons and aryl halides. Practically all other solvents cause a shift of the spectra of these compounds to a greater wavelength than a hydrocarbon or aryl halide of the same refractive index. When solvation by hydrogen bonding between the solute and solvent is to be expected, very large shifts toward greater wavelength occur (Figs. 1–3 and Tables I, II, and IV). This last effect was expected, since it was observed by Kuhn and Brockmann in solutions of rhodoxanthin.[7] No correlation could be found with dipole moment, molar polarizability, molar refraction, or dielectric constant of the solvent. The absorption maximum of phenol blue in hydrocarbons and aryl halides follows approximately the empirical relation

$$\nu_m = [459 - 208 \log_{10}(n-1)] \times 10^{12}.$$

For phenolphthalein and *p*-rosaniline hydrochloride no correlation was found. In these compounds the shifts are relatively small, and the study of them is complicated by the fact that they dissolve only in solvents which cause solvation (Tables V and VI).

For iodine no correlation other than the well-known division into brown and violet solutions was found (Table III). This seems to depend on the presence of oxygen or nitrogen atoms in the solvent and not, despite Cennamo's conclusions,[3] on dipole moment (Table IV).

The results can be successfully interpreted qualitatively by a modification of the suggestion put forward by Brooker and Sprague.[4] These authors, finding that the absorption band of phenol blue (I) is shifted toward

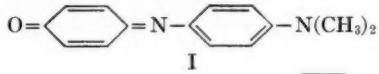

I

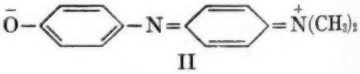

II

the red with increasing dielectric constant of the solvent, ascribed the effect of the lessening of the Coulombic energy of the zwitter ion form of phenol blue (II) by the dielectric property of the solvent. Since the zwitter ion structure contributes principally to the

TABLE I. Absorption maximum of phenol blue in various solvents.

Solvent	λ_m	n_D
Acetal	588	1.375
Acetic acid	610	1.371
Amyl ether	569	1.409
Anisole	586	1.509
Benzene	577	1.493
Bromobenzene	590	1.553
Bromocyclohexane	585	1.491
Butanol	606	1.399
Butyl ether	566	1.393
Carbon disulfide	584	1.618
Chlorobenzene	584	1.519
Chloroform	598	1.446
p-Chlorotoluene	586	1.516
Cyclohexane	553	1.419
Dioxane	571	1.417
Dodecane	557	1.417
Ethyl ether	564	1.345
Heptane	549	1.390
1-Iodonaphthalene	607	1.695
o-Iodotoluene	593	1.603
Isopropyl ether	567	1.363
Octane	550	1.391
Phenyl ether	589	1.574
Pyridine	597	1.502

TABLE II. Absorption maximum of *p*-nitrosodimethylaniline in various solvents.

Solvent	λ_m	n_D	$n_F - n_C$
1. Benzene	411	1.493	0.0167
2. Bromobenzene	418	1.555	0.0193
3. Carbon disulfide	415	1.618	0.0333
4. Carbon tetrachloride	400	1.453	0.0097
5. *o*-Iodotoluene	419	1.603	0.0234
6. Ligroin	393	1.376	0.0067
7. Methanol	428	1.331	...

TABLE III. Absorption maximum of iodine in various solvents.

Solvent	λ_m	n_D	$n_F - n_C$
1. Benzene	504	1.493	0.0167
2. Bromobenzene	506	1.553	0.0193
3. Carbon disulfide	520	1.618	0.0333
4. Carbon tetrachloride	520	1.453	0.0097
5. Chloroform	514	1.446	...
6. Dioxane	454	1.417	0.0065
7. Hexane	525	1.375	0.0064

[7] R. Kuhn and H. Brockmann, Ber. **66**, 828 (1933).

excited state rather than the ground state, this lowers the energy difference between the two. Although this appears to account satisfactorily for Brooker and Sprague's results, which were confined to the four solvents cyclohexane, acetone, methanol, and water, it breaks down seriously if a wide variety of solvents is used.

The reason for this becomes apparent upon consideration of the nature of the dielectric effect, which in a fluid is due principally to the electronic polarizability and the orientation of permanently dipolar molecules. It is not to be expected that the latter can be fully operative in the small region surrounding a dissolved molecule; here it is principally the electronic polarizability that is effective. Since electronic polarization is the phenomenon underlying refraction (at least in the visible spectrum), the absorption band should be shifted toward the red with increasing refractive index;

TABLE IV. Absorption maxima of lycopene in various solvents.*

Solvent	n_D	λm 1	2	3
1. Acetone	1.359	505	473	448
2. Aniline	1.584	537	...	...
3. Benzene	1.502	520	485	458
4. Bromobenzene	1.560	529	491	463
5. Carbon disulfide	1.628	545	506	476
6. Carbon tetrachloride	1.463	518	484	457
7. Chloroform	1.446	519	485	457
8. Dioxane	1.422	513	481	459
9. Ethanol	1.361	502	472	448
10. Ethyl bromide	1.417	512	479	453
11. Ethyl ether	1.350	502	471	446
12. Ligroin	1.376	502	471	446
13. Methanol	1.329	499	469	445
14. Nitrobenzene	1.552	534	...	...
15. Pyridine	1.509	526	490	461
16. *sym*-Tetrabromoethane	1.638	541	506	...
17. Tetralin	1.540	526	489	462

*Some of these data were determined on a visual spectrophotometer; an adjustment was made to account for systematic differences in the two procedures.

this is verified experimentally if the solvents are hydrocarbons or aryl halides.

This applies equally well to the spectra of solution of *p*-nitrosodimethylaniline and the carotenoids, which also have zwitter ion forms among their resonating structures.

The very large shifts shown when phenol blue is dissolved in water, alcohols, acetic acid, or, to a lesser extent, chloroform, and also when *p*-nitrosodimethylaniline is dissolved in methanol, are examples of the Kuhn-Brockmann effect, solvation by hydrogen bonding being inevitable in such solutions. Substantiation of this is found in the fact that alcohols cause large shifts with oxygen-containing carotenoids such as capsanthin and rhodoxanthin[7] but not with hydrocarbon carotenoids such as lycopene. If hydrogen bonding is interpreted as an electrostatic attraction of a positive hydrogen atom for a negative oxygen (or nitrogen) atom,[8] it can be seen that such bonding must stabilize the zwitter ion structure, in which the oxygen is negative. The Kuhn-Brockmann effect is clearly a consequence of this.

TABLE V. Absorption maximum of *p*-rosaniline hydrochloride in various solvents.

Solvent	λm	n_D
1. Acetone	545	1.358
2. Acetic acid	546	1.371
3. Butanol	552	1.399
4. Ethanol	549	1.360
5. Ethylene glycol	552	1.429
6. Glycerol	553	1.470
7. Isopropyl alcohol	551	1.375
8. Methanol	546	1.331
9. Propanol	552	1.385
10. Pyridine	559	1.502
11. Water	541	1.332

The smaller divergences from the hydrocarbon curve shown by ethers, alkyl halides, pyridine, and (if the solute is a hydrocarbon) alcohols, may be ascribable to an orientation effect. It is to be noted that these solvents have at least one highly polarizable bond, such as carbon-oxygen or carbon-halogen bonds.[9] In a non-uniform electrostatic field, such a molecule tends to turn so that its most polarizable portion is in the strongest part of the field. Because of this orientation the polarizability in the immediate neighborhood of the solute molecule is greater than the average polarizability for the solvent as a whole. This interpretation is believed to be preferable to an assumption that the orientation is of the same type as that which occurs when a macroscopic field is applied, the reason being that dioxane, with a dipole moment of zero, shows the effect, while the aryl halides, with large dipole moments, do not. Phenyl ether, with all bonds highly polarizable, does not exhibit this effect. That aryl halides apparently show little or no greater shift than hydrocarbons of like refractive index seems anomalous on this basis. However, the values for the polarizability of the aro-

TABLE VI. Absorption maximum of phenolphthalein in various solvents.

Solvents	λm	n_D
1. Aqueous solutions of glucose	556	1.353
	557	1.373
2. Butanol	568	1.399
3. Ethanol	564	1.360
4. Ethylene glycol	563	1.429
5. Glycerol	564	1.470
6. Isoamyl alcohol	568	1.408
7. Isopropyl alcohol	568	1.375
8. Methanol	560	1.331
9. Propanol	566	1.385
10. Water	556	1.332

[8] L. Pauling, *The Nature of the Chemical Bond* (Cornell University Press, Ithaca, New York, 1941), second edition, Chapter IX.

[9] S.-N. Wang, J. Chem. Phys. 7, 1012 (1939).

matic carbon-to-carbon bond found by Wang were based on benzene, while those for the carbon-halogen bond were based on aliphatic compounds. In the aryl halides, resonance interaction of these bonds may greatly alter their polarizabilities.

On this basis the behavior of carbon disulfide remains anomalous. The abnormally large shift of carotenoid spectra in this solvent is perhaps due to its small size, which may enable it to fill better the irregularly shaped regions around the solute molecules. However, its effect on phenol blue and *p*-nitrosodimethylaniline is in the opposite direction. Carbon disulfide is known to form addition compounds with a few complex aromatic compounds;[10] perhaps similar compounds are involved here.

The behavior of the solution of *p*-nitrosodimethylaniline in carbon tetrachloride is also anomalous.

That phenolphthalein and *p*-rosaniline hydrochloride show only small and irregular shifts is in line with this interpretation, since in ionic dyes no zwitter ion contributes to the structure of the excited state.

[10] C. F. H. Allen and A. Bell, J. Am. Chem. Soc. **64**, 1253–1260 (1942); W. König, with P. Seidel and G. Stühmer, Ber. **61B**, 2065–2074 (1928).

THE JOURNAL OF CHEMICAL PHYSICS VOLUME 20, NUMBER 2 FEBRUARY, 1952

Long-Lifetime Phosphorescence and the Diffusion Process

P. DEBYE AND JOHN O. EDWARDS
Department of Chemistry, Cornell University, Ithaca, New York

(Received September 28, 1951)

The long-lifetime phosphorescence of certain, easily oxidizable organic compounds in rigid media at the temperature of liquid nitrogen has been found to decay by an inverse power function of the time. Decay kinetics of this type have been observed previously in inorganic phosphors. Employing the diffusion equation and the observed rate law, a distribution function for electrons in the solid media is derived. Data from the experiments are discussed in relation to this theoretical treatment.

INTRODUCTION

THE long-lifetime phosphorescence of some ionic phosphors has been observed to decay by an inverse power function of the time.[1–3] This has been explained as the result of electron trapping which perturbs the hyperbolic or bimolecular type of decay. There is assumed to be a distribution of trap depths. The rate law has also been explained as being caused by absorption through the layers of phosphor. While investigating the phosphorescent emission of certain organic compounds, we had occasion to study the kinetics of the long-lifetime phosphorescence (hereafter designated Ll) of these compounds. This type of emission was observed and investigated by G. N. Lewis and his co-workers[4,5] in the course of their work on the triplet-singlet phosphorescence.[6] More recently, Linschitz and Berry[7] looked into the types of chemical structure necessary for this emission and into the emission spectrum. The spectrum of Ll was different from the triplet-singlet emission spectrum in certain cases.

The observed rate law is

$$G_e = k/t^m,$$

where G_e is the light intensity as given by the galvanometer readings, t is the time after the ultraviolet light for excitation is turned off, K is a constant which varies for each run, and m is an exponent. The constant K is the product of an apparatus factor, a rate constant, and a concentration. The exponent m, which varies with each run, will be the main subject of this paper for it is easily determined. In Fig. 1 four typical kinetic experiments are shown.

This rate law has been found to hold for inorganic and organic phosphors and it seems suitable in many types of solids. In our studies Ll has been activated in rigid molecular glasses, molecular crystals without any charged particles, and molecular crystals with large amounts of included electrolyte. The previous work[1–3] has been in ionic crystals.

Although the organic phosphor may or may not be charged, the intensity of Ll is heavily dependent on the basicity of the medium. For example aromatic amines are usually good phosphors, but their corresponding ammonium ions do not give any Ll. In similar fashion, phenolate ions are far better phosphors than the phenols. In Table I, some of the organic phosphors studied are enumerated. Assuming that one electron has been photodissociated by the radiation, data on their electronic charges before and after excitation are presented.

[1] G. R. Fonda and F. Seitz, Editors, *Solid Luminescent Materials* (John Wiley and Sons, Inc., New York, 1948).
[2] J. T. Randall and M. H. F. Wilkins, Proc. Roy. Soc. (London) (A) **184**, 366 (1945).
[3] C. Boyd, J. Chem. Phys. **17**, 1221 (1949).
[4] G. N. Lewis and D. Lipkin, J. Am. Chem. Soc. **64**, 2801 (1942).
[5] G. N. Lewis and J. Bigeleisen, J. Am. Chem. Soc. **65**, 520, 1144, 2419, 2424 (1943).
[6] This work was reviewed recently by M. Kasha, Chem. Revs. **41**, 401 (1947).
[7] H. Linschitz and M. Berry, 119th meeting of the American Chemical Society, April, 1951 at Cleveland, Ohio.

THEORETICAL

Lewis and Lipkin[4] demonstrated that the main process occurring during irradiation (in order to have Ll) is the ejection of an electron from the phosphor molecule into the surrounding solid media. Our results and those of Linschitz and Berry[7] are in agreement with this physical picture.

Consider the process which occurs during irradiation. A quantum of light is absorbed by the organic molecule and an electron is then emitted. This electron is held by the solid media around the delectronated particle, which will hereafter be called the radical. As a result of its large size, the radical is assumed to be held firmly in place by the solid solvent, and the electron slowly returns to the radical. Since the reaction rate is markedly affected by small temperature rises, the process must have a sizeable activation energy. As there is no reason to expect that the actual recombination of an electron and a radical would require an energy of activation, we feel that the kinetic results may best be explained in terms of a diffusion process and an electron distribution function.

The following symbols will be used:

D—the diffusion constant.
j—the number of jumps per second.
l—the average jump length.
s—the frequency factor.
ΔH—the activation energy.
n—the number of electrons per small volume element.
dV—the small volume element.
Δn—the change in electron concentration across the volume element.
ν—number of electrons generated per volume element per second by the exciting light.
t_0—the time that the exciting light is cut off.
t—the time after t_0.
r—the distance from the center of the sink to the volume element.
r_m—the value of r where n is at the maximum.
a—the radius of the sink.
N—the rate constant or number of recombinations per second.
F—the distribution function of electron concentration.
ρ—the dimensionless ratio, r/a.
τ—the dimensionless ratio, Dt/a^2.

For diffusion along one direction, the expression

$$D=jl^2/6,$$

is valid and j is related to the trap depth by

$$j=se^{-(\Delta H/kT)}.$$

In our derivation, we shall assume that ΔH is constant and that retrapping is a significant process. The radicals will be considered as independent, separate particles so that they may be treated as one electron sink with many electrons around it.

During irradiation, the net flow of electrons is given by

$$\partial n/\partial t=D\cdot\Delta n+\nu,$$

and at saturation this net flow is zero. After the light is turned off at time t_0, the last term, ν, drops off and the flow is now in the direction of the sink. This may be expressed as

$$\frac{\partial n}{\partial t}=D\left\{\frac{1}{r^2}\frac{\partial}{\partial r}\left(r^2\frac{\partial n}{\partial r}\right)\right\},$$

and by substitution of the dimensionless variables, we have

$$\frac{\partial n}{\partial \tau}=\frac{1}{\rho^2}\frac{\partial}{\partial \rho}\left(\rho^2\frac{\partial n}{\partial \rho}\right).$$

From our observed rate law, it may be shown that

$$(D/a^2)^m(4\pi aD)(\rho^2\partial n/\partial\rho)_{\rho=1}=N/\tau^m$$

at $r=a$.

Let us take the defining equation

$$n=F/\rho,$$

for the distribution function of electrons about the sink. If we assume the boundary condition that n be zero at $\rho=1$, that is to say, the electron meets no barrier when it arrives at the sink, we should have a function of the type,

$$F=\exp(-\lambda^2\tau)\begin{Bmatrix}\sin\lambda\rho\\ \cos\lambda\rho\end{Bmatrix}=\Phi(\lambda)\exp(-\lambda^2\tau)\sin\lambda(\rho-1),$$

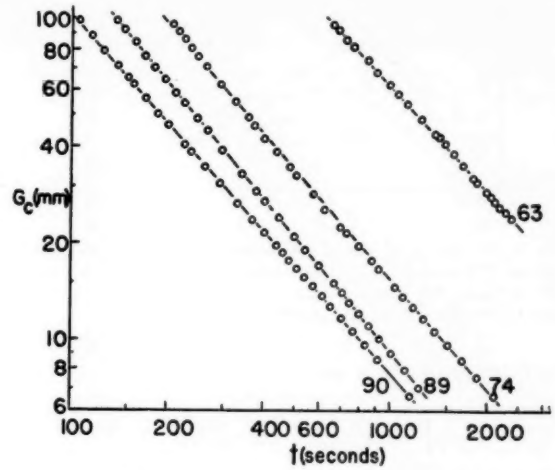

FIG. 1. Four kinetic experiments on the decay of the long-lifetime phosphorescence at the liquid nitrogen temperature: run 63, phenol in aqueous alkali; run 74, *p*-toluidine in methanol; run 89, *p*-toluidine in mixed solvent (20 percent methanol and 80 percent glycerol); run 90, tyrosine in aqueous alkali.

TABLE I. Organic phosphors and their charges.

Phosphor	E_B[a]	E_A[b]
p-toluidine diphenylamine	0	+1
sodium phenolate sodium thymolate	−1	0
disodium tyrosinate	−2	−1
bovine serum albumin in NaOH	$-n$[c]	$1-n$

[a] Electronic charge before excitation.
[b] Assumed electronic charge after excitation.
[c] n is large, probably greater than 10 in the protein.

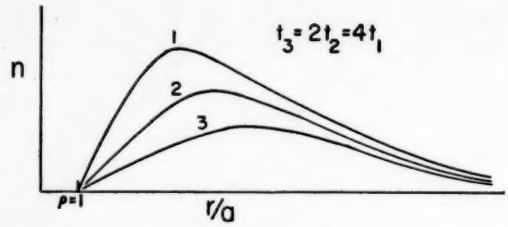

FIG. 2. A sketch of the distribution of electrons in the solid media as a function of ρ, the dimensionless distance from the center of sink. The three curves demonstrate the change in the shape of the function as the reaction proceeds.

or as is more likely, a sum of functions,

$$F=\int_0^\infty \Phi(\lambda)\exp(-\lambda^2\tau)\sin\lambda(\rho-1)d\lambda,$$

where λ is a parameter. From this, the equation

$$\frac{\partial n}{\partial \rho}=\int_0^\infty \Phi(\lambda)\exp(-\lambda^2\tau)\left\{-\frac{\sin\lambda(\rho-1)}{\rho^2}+\frac{\lambda\cos\lambda(\rho-1)}{\rho}\right\}d\lambda$$

is obtained. Multiplying through by $(4\pi aD)(D/a^2)^m(\rho^2)$ and employing our boundary condition, we have

$$\left(\frac{D}{a^2}\right)^m(4\pi aD)\int_0^\infty \lambda\Phi(\lambda)\exp(-\lambda^2\tau)d\lambda=\frac{N}{t^m},$$

from which is obtained

$$\Phi(\lambda)=(2N/4\pi aD)(\lambda^p)(a^2/D)^m.$$

By separation of variables, it may be shown that

$$p=2(m-1),$$

and our final solution is

$$n\rho=F$$

$$=\left(\frac{a^2}{D}\right)^m\left(\frac{2N}{4\pi aD}\right)\int_0^\infty \lambda^{2(m-1)}\exp(-\lambda^2\tau)\sin\lambda(\rho-1)d\lambda,$$

or

$$n=\frac{2Na^{2m}}{4\pi rD^{m+1}}\int_0^\infty \exp\left(-\frac{\lambda^2Dt}{a^2}\right)\lambda^{2(m-1)}\sin\lambda\left(\frac{r}{a}-1\right)d\lambda.$$

Making certain approximations that are valid at large values of $\rho-1/2\tau^{\frac{1}{2}}$ and at $m=1$, it is found that

$$n\cong(2Na/4\pi D^2)\{1/\rho(\rho-1)\},$$

so that the form of the distribution can be estimated for larger values of ρ. We have assumed that n is zero at $\rho=1$, so n must pass through a maximum at some intermediate value of ρ. A rough sketch of n against ρ is given in Fig. 2.

For the case of an infinitely dilute, organic phosphor, the value of m seems to be 1.00 and our equation reduces to

$$n=\frac{2Na^2}{4\pi rD^2}\int_0^\infty \exp\left(-\frac{\lambda^2Dt}{a^2}\right)\sin\lambda\left(\frac{r}{a}-1\right)d\lambda.$$

It is of interest to consider the form of the distribution function as the numerical value of the exponent m changes from 0.1 to 2.0 at a constant concentration of free radicals. The exponent increases as the maximum of n is pushed in towards the sink so that r_m approaches l in magnitude. When r_m becomes equal to l, the exponent becomes 2.0 and the process is a bimolecular recombination. As r_m gets further away from the sink, the concentration gradient is small, the amount of recombinations in unit time is small, and the rate changes little with time, for the number of electrons used up is small in unit time.

EXPERIMENTAL AND DISCUSSION

The intensity of the phosphorescence was measured by a RCA 5819 multiplier phototube coupled through an electronic power and stabilization circuit to a Rubicon type 3405 HA galvanometer. Since all of the organic molecules studied had exponential-decay emissions presumably of the triplet-singlet type, it was necessary to wait from 20 to 200 seconds after t_0 in order to take readings on the Ll phosphorescence. The phosphor was frozen in a test tube which was suspended in a Pyrex, unsilvered Dewar flask containing liquid nitrogen. All of the experiments were carried out at this temperature since the rate was immeasurably fast at the temperature of solid carbon dioxide. With a General Electric AH-6, high pressure, mercury vapor arc the phosphor could be excited through the Pyrex and the liquid nitrogen.

Generally, the decay was followed through a tenfold change in intensity, but linear plots on log-log paper have been obtained for intensity changes of more than a hundredfold. With a strong phosphor there is a large amount of activity remaining after two hours at the liquid nitrogen temperature.

Phenol and p-toluidine were purified by sublimation. The other phosphors were used without further purification.

If the physical picture is correct, the distribution of electrons about the sink should be affected by the phosphor concentration. In Table II data on the variation of m with changes in sodium phenolate concentration are presented. The solvent was water containing 1.00-M sodium hydroxide and 0.85-M sodium chloride. As expected, the value of m increases with concentration. The value of m at the lowest concentration is 1.00

TABLE II. Effect of phosphor concentration on the exponent.

Phosphor conc (molar)	m	G_{300}[a]
0.34	1.13	...
0.034	1.11	64
0.014	1.08	35
0.0068	1.07	56
0.0014	1.04	34
0.00068	1.00	15

[a] Galvanometer reading at 300 seconds.

and this value seems to be a limit for organic phosphors in a single solvent. The intensity of emission as shown by the G_{300} column is proportional to the phosphor concentration at the lower concentrations, but it seems to become independent of concentration at higher values.

It was observed that the saturation intensity of Ll is reached rapidly, for irradiation times of between 10 and 60 sec made little difference on the value of the exponent or on the phosphorescence intensity. Irradiations for times longer than a minute or two cause decreases in intensity which are presumably a result of photochemical action on the radical.

Of the 86 runs in a single solvent, 73, which is 85 percent, had m values from 0.98 to 1.13 and the range was from 0.94 to 1.40. In mixed solvents, the values ranged from 0.83 to 1.75 with no obvious pattern or maximum. Exponents from 0.1 to 2.0 have been observed with ionic phosphors.[3]

With phosphors like p-toluidine and disodium tyrosinate, additions of inert salts cause little variation in the exponent. Bovine serum albumin and other materials that can alter their charge as the amount of salt increases are phosphors in which the exponent m decreases as the amount of salt or hydroxide increases. It is our opinion that changes in the charge on the phosphor molecule can cause alterations in the electron distribution function. The decrease in exponent m is in the predicted direction for a charge effect.

The data with mixed solvents are variable and irreproducible. The results of a series of experiments on dilute p-toluidine in solvents with methanol as one component are presented in Table III. The wide variation in the exponent for solutions with the same phosphor concentration is quite surprising. The value of the exponent in these cases must depend on the molecular state of the frozen media. In mixed solvents that are perfectly homogeneous at room temperature, such phenomena as local inhomogeneities in concentration, disruption of crystal structure, and the formation of rigid glasses are possible on the sudden freezing to the temperature of liquid nitrogen.

It was found that the activated mixture, when in the state of a glassy solid, would occasionally give off a sudden burst of light and at the same time a loud cracking noise. There are several possible explanations for this. The first is that the heat released to the solid media on the relief of stresses by cracking of the solid causes an increase in diffusion rate for a short time. The second is that a new crack or boundary is formed and the electrons undergo grain boundary diffusion which is known to be faster than volume or bulk diffusion. Other effects of lesser importance are also possible e.g., triboluminescence.

TABLE III. Effect of mixed solvents on the exponent.

Vol. methanol[a]	Second solvent	m
1.00	(None)	1.09[b]
0.80	Water	1.00
0.80	Water	1.32
0.60	Water	0.96
0.60	Water	0.88
0.40	Water	1.56
0.40	Water	0.83
0.20	Water	1.59
0.20	Water	1.69
0.20	Water	1.64
0.20	Ethanol	1.43
0.20	Ethanol	1.15
0.20	Glycerine	1.17
0.20	Glycerine	1.20[c]

[a] Volume fraction of methanol.
[b] See run 74 on Fig. 1.
[c] See run 89 on Fig. 1.

Since the primary purpose of these investigations was exploratory, we have not concentrated on obtaining exact and quantitative data, but have looked into the major trends. In all, about 110 runs were carried out on various organic phosphors of the phenolate ion and aromatic amine types. All of the data are consistent with the physical picture of an electron diffusing slowly back to a radical which is held by the rigid media. Our treatment has concerned the macroscopic visualization of the decay rate law in terms of a diffusion process. No studies on the intimate nature of the electron trapping process or of the electron-radical recombination have been done.

ACKNOWLEDGMENT

The work on this project was sponsored and financed by the Army Chemical Corps through the Army Chemical Center, Maryland.

THE JOURNAL OF CHEMICAL PHYSICS VOLUME 20, NUMBER 2 FEBRUARY, 1952

The Configurational Distribution Function in Quantum-Statistical Mechanics

M. L. GOLDBERGER AND E. N. ADAMS II
University of Chicago, Institute for Nuclear Studies, Chicago, Illinois
(Received September 25, 1951)

The function $F\{N\}$ which gives the relative probability of a configuration $\{N\}$ is studied for the case of a quantum-mechanical system to which classical statistics can be applied. By means of a device originally used in quantum electrodynamics $F\{N\}$ is obtained in a new form which is very closely related to the form of the analogous classical distribution $F_{CL}\{N\}$. The new form of $F\{N\}$ shows clearly how the difference between $F\{N\}$ and $F_{CL}\{N\}$ is related to the uncertainty principle. As an illustration of the utility of the methods presented here several applications are presented. The first application is a high temperature development of $F\{N\}$ as a power series in $\hbar/kT$ which is carried through to the fourth order. The second application is the development of $F\{N\}$ as a series of configuration space integrals. A previously published low temperature development of $F\{N\}$ is obtained in a simple manner, and it is shown that all higher terms in the development can be written down explicitly by starting from the new form of $F\{N\}$. Finally, several integral equations for $F\{N\}$ are presented which give physical insight into its structure, by establishing mathematical analogies with such physical processes as neutron diffusion.

INTRODUCTION

A NUMBER of studies have been made of the relation between the statistical distribution function $F\{N\}$, which gives the relative probability of a spatial configuration $\{N\}$ of a quantum-mechanical system in thermal equilibrium with its surroundings, and the function $F_{CL}\{N\}$ which is the distribution function for the corresponding classical system. Wigner[1] has obtained an approximation for $F\{N\}$ which is valid at high temperature and in which $F\{N\}$ is expressed as the product of $F_{CL}\{N\}$ by a power series in $\hbar/kT$. Mayer and Band[2] have rederived Wigner's result in a manner which in principle permits the evaluation of all higher terms in the series development. They give an expression for $F\{N\}$ as an integral over momentum components $d^{3N}p$ of an exponential whose argument involves derivatives of the potential to all orders and all powers of such derivatives, the higher terms in this exponent being determined recursively from the lower. To obtain the nth term of the power series development for $F\{N\}$ from the integral expression it is necessary to first obtain the exponent correct to the nth power in $\hbar/kT$ by repeated use of the recursion relations, then to develop the exponential to the nth power of $\hbar/kT$, and finally to integrate over momentum. In practice the labor required to carry such a development beyond the 4th power would be prohibitive. Further, the exponent occurring in the integrand of the Mayer and Band expression for $F\{N\}$ is of such a complicated structure as to obscure the nature of the difference between the functions $F\{N\}$ and $F_{CL}\{N\}$, so that, for example, it is impossible to predict what quantum-mechanical effects are to be expected at low temperatures.

In the following paper we study the function $F\{N\}$ using a technique used by J. Schwinger[3] in treating a problem of quantum electrodynamics. In Sec. I we derive an expression for $F\{N\}$ which exhibits the essential difference between $F\{N\}$ and $F_{CL}\{N\}$ in a particularly graphic manner. $F\{N\}$ is expressed as an integral over momentum components $d^{3N}p$, an integral which differs from the corresponding integral in classical statistical mechanics only by a simple modification which is required by the uncertainty principle. The significance of the modification is discussed.

In Sec. II we show that our procedure may be altered slightly to afford a practicable means of calculating the high temperature power series development of $F\{N\}$. As an illustration of the technique the quantum correction is computed to 4th order in $\hbar/kT$.

In Sec. III we show that the form for $F\{N\}$ developed in Sec. I may be used to obtain a certain low temperature expansion in powers of the potential proposed by Green.[4] Green's result, which carries the expansion only to the first order in the potential, is here obtained in a simple manner. It is shown that the higher order terms, which Green was unable to evaluate readily using his technique, may be written down immediately; an integral expression is derived for the general term.

In Sec. IV we discuss several additional methods of attack on the problem of obtaining explicit expressions for $F\{N\}$.

SECTION I

For a system in thermal equilibrium, the probability that a given quantum state of energy E_ν is occupied is proportional to $\exp\{-\beta E_\nu\}$ where $\beta=1/kT$. The constant of proportionality is Q^{-1} where $Q\equiv\Sigma_\nu \exp\{-\beta E_\nu\}$. The function $F\{N\}$ is the unnormalized probability of the spatial configuration $\{N\}$ and is given by

$$F\{N\}=QP\{N\}=\Sigma_\nu \exp(-\beta E_\nu)\psi_\nu^*\{N\}\psi_\nu\{N\}. \quad (1.1)$$

Equation (1) can clearly be written as

$$F\{N\}=\Sigma_\nu\psi_\nu^*\{N\} \exp(-\beta\mathfrak{IC})\psi_\nu\{N\}. \quad (1.2)$$

[1] E. P. Wigner, Phys. Rev. **40**, 749 (1932).
[2] J. Mayer and W. Band, J. Chem. Phys. **15**, 191 (1947).
[3] J. Schwinger, Phys. Rev. **82**, 664 (1951), Sec. VI.
[4] H. S. Green, J. Chem. Phys. **19**, 955 (1951).

The Hamiltonian $\mathcal{H}$ will be assumed to be of the form

$$\mathcal{H}=\Sigma_J(\tfrac{1}{2}m_J)\mathbf{p}_J^2+V\{N\}, \tag{1.3}$$

in which J is a sum over particles.

We will first introduce a notation which simplfies the dimensions of the quantities appearing in our equations. Following Mayer and Band[2] we introduce

$$\begin{aligned}\lambda_J&\equiv[\hbar^2/2m_JkT]^{\frac{1}{2}};\\ \mathbf{p}_J&\equiv\lambda_J\nabla_J/i;\\ U(\mathbf{x})&\equiv\beta V\{N\};\\ H&\equiv\beta\mathcal{H}.\end{aligned} \tag{1.4}$$

In this notation the quantum relations are

$$[p_J{}^\mu, x_K{}^\nu]=(1/i)\lambda_J\delta^{\mu\nu}\delta_{JK}.$$

The expressions Eqs. (2) and (3) become

$$\begin{aligned}F\{N\}&=\Sigma_\nu\psi_\nu{}^*\{N\}e^{-H}\psi_\nu\{N\};\\ H&=-\Sigma_J\lambda_J{}^2\nabla_J{}^2+U.\end{aligned} \tag{1.5}$$

We will now discuss some properties of the operator e^{-H}. In what follows we use a many dimensional vector notation in which the operator $-i\lambda\nabla$ designates the $3N$ dimensional momentum operator, $\mathbf{x}$ the $3N$ dimensional coordinate operator. We will omit the index J on λ_J but it will be obvious how to put it back in any detailed calculation. We will examine the properties of the operator $\exp\{-(a+b)\}$ in which a and b are noncommuting operators of any sort. We write

$$u(s)=\exp\{-(a+b)s\}, \tag{1.6}$$

and notice that $u(s)$ satisfies

$$\begin{aligned}\frac{\partial u(s)}{\partial s}&=-u(s)(a+b);\\ u(0)&=1.\end{aligned} \tag{1.7}$$

We now write

$$u(s)=v(s)e^{-as}, \tag{1.8a}$$

and find that $v(s)$ satisfies the differential equation

$$\begin{aligned}\frac{\partial v(s)}{\partial s}&=-v(s)e^{-as}be^{as};\\ v(0)&=1.\end{aligned} \tag{1.8b}$$

In treating expressions such as (1.8b) the following well-known expansion is very useful

$$e^abe^{-a}=b+[a,b]+\frac{1}{2!}[a,[a,b]]+\cdots. \tag{1.9}$$

Equation (1.8b) is clearly equivalent to the integral equation

$$v(s)=1-\int_0^s ds_1v(s_1)e^{-as_1}be^{as_1}. \tag{1.10}$$

Equation (1.10) can be solved by iteration to yield

$$\begin{aligned}v(s)=1&-\int_0^s ds_1e^{-as_1}be^{as_1}\\ &+\int_0^s ds_1\int_0^{s_1}ds_2e^{-as_2}be^{as_2}e^{-as_1}be^{as_1}+\cdots.\end{aligned} \tag{1.11}$$

The series Eq. (1.11) can be expressed compactly by employing the notion of "ordered exponential" which has proven useful in quantum electrodynamics.[5] The "orderings" $[+]$ and $[-]$ are explained in detail in an appendix. Thus

$$v(s)=\exp_{[-]}\left\{-\int_0^s ds_1e^{-as_1}be^{as_1}\right\}; \tag{1.12}$$

$$e^{-(a+b)}=\exp_{[-]}\left\{-\int_0^1 dse^{-as}be^{as}\right\}e^{-a}. \tag{1.13a}$$

By an exactly analogous procedure it may be established that

$$e^{-(a+b)}=e^{-a}\exp_{[+]}\left\{-\int_0^1 dse^{as}be^{-as}\right\}. \tag{1.13b}$$

In the general result Eq. (1.13a) we will insert the special choices

$$\begin{aligned}a&=-\lambda^2\nabla^2,\\ b&=U(\mathbf{x}).\end{aligned} \tag{1.14a}$$

Equation (1.13a) then becomes

$$\begin{aligned}e^{-H}=\exp_{[-]}\Big\{&-\int_0^1 ds\exp(s\lambda^2\nabla^2)U(\mathbf{x})\\ &\times\exp(-s\lambda^2\nabla^2)\Big\}\exp(\lambda^2\nabla^2).\end{aligned} \tag{1.14b}$$

By use of the operator identity

$$\mathbf{x}\exp(s\lambda^2\nabla^2)\equiv\exp(s\lambda^2\nabla^2)[\mathbf{x}-2s\lambda^2\nabla], \tag{1.15}$$

Equation (1.14b) can be rewritten as

$$e^{-H}=\left\{\exp\left[-\int_0^1 dsU(\mathbf{x}+2s\lambda^2\nabla)\right]\right\}_{[-]}\exp(\lambda^2\nabla^2). \tag{1.14c}$$

We are now in a position to calculate $F\{N\}$. Mayer and Band have proved that because of the completeness relation the ψ_ν and the sum over ν in Eq. (1.2) can be replaced by the ψ_κ and a sum over κ for any complete orthogonal set ψ_κ of well-behaved functions. With classical statistics the sum Eq. (1.2) may be most

[5] F. J. Dyson, Phys. Rev. **75**, 487 (1949). Dyson first introduced the ordering operation. The observation that the ordered functions retained many properties of exponentials was made by J. Schwinger (unpublished).

easily carried out using plane waves as the ψ_κ in which case $F\{N\}$ becomes

$$F\{N\}=\frac{1}{N!}\int\frac{d^{3N}\kappa}{(2\pi)^{3N}}\psi_\kappa^* e^{-H}\psi_\kappa. \tag{1.16}$$

The factor of $1/N!$ is the conventional one introduced into classical statistics which takes into account in an approximate way the identity of the particles.[2] $N!$ is to be understood as $\Pi_k N_k!$ where k refers to the various groups of identical particles.

Into Eq. (1.16) we will now insert the expression e^{-H} as given by Eq. (1.14c). First we note, however, that

$$\lambda\nabla\psi_\kappa/i\equiv\psi_\kappa[\lambda\kappa+(\lambda\nabla/i)]\equiv\psi_\kappa[\mathbf{p}+(\lambda\nabla/i)]. \tag{1.17}$$

By use of Eq. (1.17) the ψ_κ on the right in Eq. (1.16) may be moved through to the left, and $\psi_\kappa^*\psi_\kappa$ may be replaced by unity. Thus, inserting Eq. (1.14c) in Eq. (1.16) and using Eq. (1.17),

$$F\{N\}=\left(\frac{1}{N!}\right)\int\frac{d^{3N}p}{(2\pi\lambda)^{3N}}\times\left\{\exp\left[-\int_0^1 ds U(\mathbf{x}+2is\lambda\mathbf{p}+2s\lambda^2\nabla)\right]\right\}_{[-]}\times\exp(-p^2). \tag{1.18}$$

We now wish to discuss Eq. (1.18) for $F\{N\}$. Because of the appearance of the ∇ operator in the function, it might appear that $F\{N\}$ is still to be considered as an operator. Actually, it is clear from (1.16) that the operator $F\{N\}$ is to be applied to 1 when it is evaluated, so the ∇ which appears as part of the argument of U operates only on the space dependence of the U's occurring in the ordered exponential. We shall later have more to say concerning the effect of the appearance ∇ in the argument of U. At this point we wish merely to make certain qualitative remarks. In the first place it may be noted that in the classical limit $\lambda\to 0$ the expression (1.18) goes over to the classical distribution function $F_{CL}\{N\}$, since the ordered exponential becomes simply the ordinary exponential e^{-U}. The expression (1.18) for $F\{N\}$ is really just the classical expression except for the displacement of the argument of $U(x)$. In order to interpret this displacement of the argument of $U(x)$ note that with our dimensionless p the uncertainty relations can be written

$$\Delta x\Delta p\sim\lambda.$$

The uncertainty in energy resulting from thermal interaction is $\Delta E\sim p^2$,

$$p\Delta p\sim p^2,$$

so $\Delta p\sim p\sim 1$, in virtue of the factor $\exp(-p^2)$. Thus the uncertainty in x is of the order

$$\Delta x\sim\lambda.$$

The difference between $F\{N\}$ as given by Eq. (1.18), and the classical distribution is just of the sort which would be expected on the basis of the uncertainty principle. As we shall see later, the displacement of the argument of $U(\mathbf{x})$ means that the potential $U(\mathbf{x})$ has been replaced by a finite distance operator with range given precisely by the "thermal uncertainty length" λ.

SECTION II

The ordered exponential expression for $F\{N\}$ given in Sec. I may be used to obtain a high temperature expansion in powers of λ by writing it in the series form Eq. (1.11). Instead of doing this, we will use a modification of the procedure of Sec. I in order to arrive more directly at the desired expansion. For this purpose we start from the form

$$F\{N\}=\frac{1}{N!}\int\frac{d^{3N}p}{[2\pi\lambda]^{3N}}\psi_\kappa^*\exp\{-[-\lambda^2\nabla^2+U]\}\psi_\kappa, \tag{2.1}$$

which can be written by use of Eq. (1.17) as

$$F\{N\}=\frac{1}{N!}\int\frac{d^{3N}p}{[2\pi\lambda]^{3N}}e^{-p^2}\times\exp\{-[-\lambda^2\nabla^2-2i\lambda\mathbf{p}\cdot\nabla+U]\}. \tag{2.2}$$

We now study the last factor in the integrand of Eq. (2.2) which we denote as $u(1)$. We define

$$u(s)\equiv\exp\{-s[-\lambda^2\nabla^2-2i\lambda\mathbf{p}\cdot\nabla+U(\mathbf{x})]\}. \tag{2.3}$$

Clearly, $u(s)$ satisfies the differential equation

$$\frac{\partial u(s)}{\partial s}=-[-\lambda^2\nabla^2-2i\lambda\mathbf{p}\cdot\nabla+U(\mathbf{x})]u(s) \tag{2.4}$$

with the boundary condition $u(0)=1$. If we write

$$u(s)=\exp(2i\lambda s\mathbf{p}\cdot\nabla)v_0(s), \tag{2.5a}$$

then

$$\frac{\partial v_0}{\partial s}=-\exp(-2is\lambda\mathbf{p}\cdot\nabla)[-\lambda^2\nabla^2+U(\mathbf{x})]\times\exp(2is\lambda\mathbf{p}\cdot\nabla)v_0, \tag{2.5b}$$

$$\frac{\partial v_0}{\partial s}=[\lambda^2\nabla^2-U(\mathbf{x}-2is\lambda\mathbf{p})]v_0,$$

$$v_0(0)=1.$$

The procedure from this point will be to remove the various orders of λ by successive substitutions. The manner in which these are to be made will become clear after another step. Denote

$$sU(\mathbf{x},s)\equiv\int_0^s ds_1 U(\mathbf{x}-2is_1\lambda\mathbf{p}). \tag{2.6}$$

We now substitute

$$v_0(s)\equiv\exp[-s\mathcal{U}(\mathbf{x},s)]v_1(s), \tag{2.7a}$$

and obtain

$$\frac{\partial v_1(s)}{\partial s}=\exp[s\mathcal{U}(\mathbf{x},s)]\lambda^2\nabla^2\exp[-s\mathcal{U}(\mathbf{x},s)]v_1(s), \tag{2.7b}$$

or using (1.9),

$$\frac{\partial v_1(s)}{\partial s}=[\lambda^2\nabla^2-2s\lambda^2(\nabla\mathcal{U}\cdot\nabla)-s\lambda^2\nabla^2\mathcal{U}+s^2\lambda^2(\nabla\mathcal{U})^2]v_1(s), \tag{2.7c}$$

$$v_1(0)=1.$$

The operators on the right in the differential Eq. (2.7c) are all of order λ^2. To order λ^2 the differential operators could be ignored, since their commutators with other terms are of order λ^4. We will carry the elimination one step further. Define

$$s\mathcal{W}(\mathbf{x},s)\equiv\int_0^s ds_1\{s_1\nabla^2\mathcal{U}(\mathbf{x},s_1)-s_1^2(\nabla\mathcal{U}(\mathbf{x},s_1))^2\}. \tag{2.8}$$

We now substitute

$$v_1(s)=\exp[-s\lambda^2\mathcal{W}(\mathbf{x},s)]v_2(s), \tag{2.9a}$$

and obtain the equation

$$\partial v_2/\partial s=\{\lambda^2\nabla^2-2s\lambda^2(\nabla\mathcal{U}\cdot\nabla)+2s\lambda^4(\nabla\mathcal{W}\cdot\nabla)-s\lambda^4\nabla^2\mathcal{W}+2s^2\lambda^4(\nabla\mathcal{U}\cdot\nabla\mathcal{W})+s^2\lambda^6(\nabla\mathcal{W})^2\}v_2, \tag{2.9b}$$

$$v_2(0)=1.$$

The functions of x in the differential equation which remains are of order λ^4 or higher, and it is clear how one proceeds to remove even higher powers of λ. In order to get the answer correct to order λ^4 it is sufficient to integrate Eq. (2.9b) with the neglect of the differential operators and of terms of order higher than λ^4. We may further simply replace $\mathcal{U}(\mathbf{x},s)$ by $U(\mathbf{x})$ since the s dependence is also of higher order in λ. Equation (2.9b) is then readily integrated to give

$$v_2(1)=1-\lambda^4\left\{\frac{1}{6}\nabla^4U-\frac{1}{12}\nabla^2(\nabla U)^2-\frac{1}{4}(\nabla U\cdot\nabla^2\nabla U)+\frac{2}{15}(\nabla U\cdot\nabla)(\nabla U)^2\right\}+O(\lambda^5). \tag{2.10}$$

The expression (2.2) for $F\{N\}$ now has been approximated by

$$F\{N\}=\frac{1}{N!}\int\frac{d^{3N}p}{[2\pi\lambda]^{3N}}\exp(-p^2)\exp(2i\lambda\mathbf{p}\cdot\nabla)\times\exp[-s\mathcal{U}(\mathbf{x},s)]\exp[-s\mathcal{W}(\mathbf{x},s)]v_2(s)|^{s=1}. \tag{2.11}$$

The exponential $\exp(2i\lambda\mathbf{p}\cdot\nabla)$ is just a displacement operator which can be applied to the expression on the right and thus removed, giving

$$F\{N\}=\frac{1}{N!}\int\frac{d^{3N}p}{[2\pi\lambda]^{3N}}\exp(-p^2)\exp[-\mathcal{U}(\mathbf{x}+2i\lambda\mathbf{p},1)]\times\exp[-\mathcal{W}(\mathbf{x}+2i\lambda\mathbf{p},1)]v_2(1). \tag{2.12}$$

Next the functions $\mathcal{U}(\mathbf{x}+2i\lambda\mathbf{p},1)$, $\mathcal{W}(\mathbf{x}+2i\lambda\mathbf{p},1)$ are developed to order λ^4. Finally, the exponential must be developed to order λ^4 and the integration over p performed. The integration over p is easily carried out by use of the relations

$$\int d^{3N}p\exp(-p^2)p^\mu p^\nu=(\pi^{3N/2}/2)\delta_{\mu\nu},$$

$$\int d^{3N}p\exp(-p^2)p^\mu p^\nu p^\lambda p^\sigma=(\pi^{3N/2}/4)[\delta_{\mu\nu}\delta_{\lambda\sigma}+\delta_{\mu\lambda}\delta_{\nu\sigma}+\delta_{\mu\sigma}\delta_{\nu\lambda}]. \tag{2.13}$$

The result of the p integration may be expressed as

$$F\{N\}=F_{CL}\{N\}\left\{1-\lambda^2\left[\frac{1}{6}\nabla^2U-\frac{1}{12}(\nabla U)^2\right]+\lambda^4\left[\frac{1}{45}(\nabla U\cdot\nabla^2\nabla U)+\frac{1}{72}(\nabla^2U)^2+\frac{1}{180}\nabla^2(\nabla U)^2+\frac{1}{288}((\nabla U)^2)^2-\frac{1}{60}\nabla^4U-\frac{1}{72}(\nabla U)^2\nabla^2U-\frac{1}{120}(\nabla U\cdot\nabla(\nabla U)^2)\right]+O(\lambda^6)\right\}. \tag{2.14}$$

The partition function obtained by integration over $\{N\}$ is

$$Q=\frac{1}{N![4\pi\lambda^2]^{3N/2}}\int d\{N\}e^{-U(x)}\left\{1-\frac{\lambda^2}{12}(\nabla U)^2+\frac{\lambda^2}{36}\times\left[\frac{1}{35}\nabla^2(\nabla U)^2+\frac{1}{8}(\nabla^2U)^2-\frac{7}{40}\nabla^4U\right]+O(\lambda^6)\right\}. \tag{2.15}$$

The calculation of the fourth-order quantum correction has been presented here to illustrate how the method of this paper may be used to reduce the labor involved in a specific calculation. The method is very flexible and can be adapted so as to have special advantages in any of a wide range of special applications. In the next section we consider another way of splitting $\exp(-H)$ which is advantageous for the study of low temperatures.

SECTION III

In a recent paper, Green[4] has discussed an extension of Wigner's original method, incorporating some work of Moyal.[6] One of his principal results is an expression for $F\{N\}$ which is valid at low temperatures. We wish to show that his results emerge directly from the expression (1.14c) and further, that we may obtained the higher terms neglected in his treatment in a very simple fashion. The form which we will present appears to have

[6] J. Moyal, Proc. Cambridge Phil. Soc. **45**, 99 (1949).

far reaching implications in low temperature problems; these implications will be discussed in a later publication.

Our starting point is a sort of unraveled form of the ordered exponential solution (1.14c). The form is one given by Schwinger, but his derivation is repeated in Appendix II since most workers in statistical mechanics are probably not familiar with Schwinger's work on electrodynamics. The form in question is

$$\begin{aligned} e^{-H}=\exp(\lambda^2\nabla^2) &- \int_0^1 ds_1 \exp[\lambda^2\nabla^2(1-s_1)]U(\mathbf{x})\exp(\lambda^2\nabla^2 s_1)+\cdots \\ &+(-)^n\int_0^1 s_1^{n-1}ds_1\int_0^1 s_2^{n-2}ds_2\cdots\int_0^1 ds_n \\ &\times\Big[\exp[\lambda^2\nabla^2(1-s_1)]U(\mathbf{x})\exp[\lambda^2\nabla^2 s_1(1-s_2)] \\ &\times U(\mathbf{x})\cdots U(\mathbf{x})\exp[\lambda^2\nabla^2 s_1 s_2\cdots s_{n-1}(1-s_n)] \\ &\times U(\mathbf{x})\exp(\lambda^2\nabla^2 s_1 s_2\cdots s_n)\Big]+\cdots. \end{aligned} \tag{3.1}$$

With this result we wish to form

$$F\{N\}=\frac{1}{[4\pi^2\lambda^2]^{3N/2}}\frac{1}{N!}\int d^{3N}p \times\exp(-i\mathbf{p}\cdot\mathbf{x}/\lambda)e^{-H}\exp(+i\mathbf{p}\cdot\mathbf{x}/\lambda). \tag{3.2}$$

The evaluation of (3.2) is easily carried out using the following relation (3.3), which may be obtained immediately by introducing a Fourier integral representation of $\delta(\mathbf{x}-\mathbf{x}_1)$.

$$\exp(\tau\nabla^2)\delta(\mathbf{x}-\mathbf{x}_1)=\frac{\exp[-(\mathbf{x}-\mathbf{x}_1)^2/4\tau]}{[4\pi\tau]^{3N/2}}. \tag{3.3}$$

If the expression (3.1) is inserted in Eq. (3.2), the integration over p *may be carried out explicitly* in every term of the series. As an illustration we do the first-order term which is the only one given by Green:

$$\begin{aligned} &\frac{1}{N![4\pi^2\lambda^2]^{3N/2}}\int d^{3N}p\int_0^1 ds_1\exp(-i\mathbf{p}\cdot\mathbf{x}/\lambda)\exp[(1-s_1)\lambda^2\nabla^2]U(x)\exp(s_1\lambda^2\nabla^2)\exp(i\mathbf{p}\cdot\mathbf{x}/\lambda) \\ &=\frac{1}{N![4\pi^2\lambda^2]^{3N/2}}\int d^{3N}p\int_0^1 ds_1\exp(-i\mathbf{p}\cdot\mathbf{x}/\lambda)\int dx_1{}^{3N}\frac{\exp[-(\mathbf{x}-\mathbf{x}_1)^2/4(1-s_1)\lambda^2]}{[4\pi(1-s_1)\lambda^2]^{3N/2}}\exp(i\mathbf{p}\cdot\mathbf{x}_1/\lambda)U(\mathbf{x}_1)\exp(s_1p^2) \\ &=\frac{1}{N![4\pi\lambda^2]^{3N/2}}\int_0^1 ds_1\int d^{3N}x_1\frac{\exp[-(\mathbf{x}-\mathbf{x}_1)^2/4s_1(1-s_1)\lambda^2]}{[4\pi s_1(1-s_1)\lambda^2]^{3N/2}}U(\mathbf{x}_1). \end{aligned} \tag{3.4}$$

The corresponding formula, Eq. (40) of Green[4] is obtained by the substitutions

$$s_1=\frac{1+Z}{2};\quad \mathbf{x}_1=\mathbf{x}+(1-Z^2\mathbf{s})^{\frac{1}{2}}, \tag{3.5}$$

except that there appear to be several typographical errors in Green's formula.

The result for $F\{N\}$ may be written quite simply if we introduce a matrix notation: We label our matrices with the coordinates $\mathbf{x}$; the potential is regarded as a diagonal matrix and we write

$$\frac{1}{[4\pi\tau\lambda^2]^{3N/2}}\exp[-(\mathbf{x}-\mathbf{x}_1)^2/4\tau\lambda^2]\equiv\langle\mathbf{x}|G\{\tau\}|\mathbf{x}_1\rangle, \tag{3.6}$$

i.e., the $(\mathbf{x}, \mathbf{x}_1)$ element of the matrix $G\{\tau\}$. Equation (3.4) becomes in this notation simply

$$\frac{1}{N![4\pi\lambda^2]^{3N/2}}\int_0^1 ds_1\langle\mathbf{x}|G\{1-s_1\}UG\{s_1\}|\mathbf{x}\rangle, \tag{3.7}$$

and matrix multiplication of the usual variety is assumed. We have then for $F\{N\}$ the following expression:

$$\begin{aligned} F\{N\}=\frac{1}{N![4\pi\lambda^2]^{3N/2}} &\times\Big[1-\sum_{n=1}^{\infty}(-)^{n-1}\int_0^1 ds_1 s_1^{n-1}\int_0^1 ds_2 s_2^{n-2}\cdots \\ &\times\int_0^1 ds_n\cdots\langle\mathbf{x}|G\{1-s_1\}UG\{s_1(1-s_2)\}U\cdots \\ &\times UG\{s_1s_2\cdots s_{n-1}(1-s_n)\}UG\{s_1\cdots s_n\}|\mathbf{x}\rangle\Big]. \end{aligned} \tag{3.8}$$

It does not appear to be possible to carry out the integrations over the s_j for the general term in a very simple fashion. We shall discuss in the subsequent publication referred to earlier the evaluation in the limit of very large λ, i.e., low temperatures. It can be verified by careful passage to the limit of $\lambda\to 0$ that (3.8) gives correctly $\exp\{-U(\mathbf{x})\}$. This method may in fact be used to obtain the power series in λ but is less suitable than our previous one.

* Notice that $[1/(4\pi\tau\lambda^2)]^{3N/2}\exp\{-[(x-x_1)^2/(4\tau\lambda^2)]\}$ is simply $\langle\mathbf{x}|\exp(\tau\lambda^2\nabla^2)|\mathbf{x}_1\rangle$ according to the ordinary rules of quantum mechanics. This furnishes an explicit form for $G\{\tau\}$.

A quantity of obvious interest in applications is the partition function Q which is obtained from $F\{N\}$ by integration over coordinates. This integration may be effected directly from Eq. (3.8); however, it is somewhat simpler to use another of Schwinger's results derived in Appendix II and given by Eq. (3.9) below. We note that Q is simply the trace of the operator e^{-H} and consequently may be evaluated in any convenient representation. Thus the trace can be evaluated in the coordinate representation in which $U(\mathbf{x})$ is known. The formula we need is

$$Tr\exp(\lambda^2\nabla^2-U)=Tr\exp(\lambda^2\nabla^2)-Tr[U\exp(\lambda^2\nabla^2)]$$
$$+\cdots+\frac{(-)^n}{n+1}\int_0^1 ds_1 s_1^{n-1}\int_0^1 ds_2 s_2^{n-2}\cdots\int_0^1 ds_n Tr$$
$$\times[U\exp[\lambda^2\nabla^2(1-s_1)]U\exp[\lambda^2\nabla^2 s_1(1-s_2)]\cdots$$
$$\times U\exp(\lambda^2\nabla^2 s_1\cdots s_n)]+\cdots. \quad (3.9)$$

Using the previously defined matrix notation, (3.9) may be written as

$$Q=\frac{1}{N![4\pi\lambda^2]^{3N/2}}\int d^{3N}x$$
$$\times\Big[1-\sum_{n=0}^{\infty}\frac{(-)^n}{n+1}\int_0^1 ds_1 s_1^{n-1}\cdots\int_0^1 ds_n$$
$$\times\langle\mathbf{x}|UG\{1-s_1\}UG\{s_1(1-s_2)\}\cdots$$
$$\times UG\{s_1\cdots s_n\}|\mathbf{x}\rangle\Big]. \quad (3.10)$$

The first three terms of Q written explicitly are

$$Q=\frac{1}{[4\pi\lambda^2]^{3N/2}}\frac{1}{N!}\int d^{3N}x$$
$$\times\Big[1-U(\mathbf{x})+\tfrac{1}{2}U(\mathbf{x})\int_0^1 du_1\int d^{3N}x^1$$
$$\times\frac{\exp[-(\mathbf{x}-\mathbf{x}^1)^2/4u_1(1-u_1)\lambda^2]}{[4\pi u_1(1-u_1)\lambda^2]^{3N/2}}U(\mathbf{x}^1)\Big]. \quad (3.11)$$

A trivial simplification has been made in the last term. It is quite evident from Eq. (3.10) that as $\lambda\to 0$, the integrand approaches $\exp\{-U(x)\}$ since the kernels G become simply unit operators. It is interesting to note that whereas $F\{N\}$ and $F_{CL}\{N\}$ are essentially different even to first order in U, the classical and quantum partition functions are identical to this order.

SECTION IV

We shall take up a different approach to the evaluation of $F\{N\}$ which is related to our "exponential" solutions but which has some advantages in giving a rather vivid physical picture of our problems. The techniques to be employed here are modeled after those used by Feynman[7] in his formulation of quantum mechanics; the equations, themselves, are very similar to equations met with in the theory of neutron slowing-down. Our starting point is the differential equation for the operator $u(s)$, namely

$$\partial u(s)/\partial s=(\lambda^2\nabla^2-U(\mathbf{x}))u(s). \quad (4.1)$$

It should be noted that $u(s)$ is an operator and does not commute, for example, with $U(\mathbf{x})$ or $\lambda^2\nabla^2$ individually; even though we write (4.1) as an ordinary differential equation, some care must be exercised in using it. These points will be emphasized further below. It is convenient to introduce in place of s the variable τ defined by

$$\tau=s\lambda^2. \quad (4.2)$$

Then

$$\partial u(\tau)/\partial\tau=(\nabla^2-U(\mathbf{x})/\lambda^2)u(\tau). \quad (4.3)$$

(Note that U/λ^2 is independent of the temperature and hence of τ.) Equation (4.3) is precisely the equation satisfied by the so-called slowing-down density in neutron diffusion.[8] The quantity τ appearing in that theory (also having the dimensions of (length)^2) is known as the age, and measures the mean square distance traveled in slowing down from birth energy to the energy of interest; $\tau=0$ corresponds to the birth energy. The term $U(\mathbf{x})/\lambda^2$ in the neutron case represents a spatially varying source or sink of neutrons. We shall exploit this analogy insofar as is feasible with $u(\tau)$ being an operator rather than simply a function of $\mathbf{x}$ and τ. Equation (4.3) is readily integrated formally in terms of the *operator* Green's function defined by

$$[(\partial/\partial\tau_1)-\nabla_1^2+U(\mathbf{x}_1)/\lambda^2]\mathbf{G}(\mathbf{x}_1,\tau_1;\mathbf{x}_2,\tau_2)$$
$$=\delta(\mathbf{x}_1-\mathbf{x}_2)\delta(\tau_1-\tau_2), \quad (4.4)$$

with the boundary condition

$$\mathbf{G}(\mathbf{x}_1,\tau_1;\mathbf{x}_2,\tau_2)\equiv 0 \quad \text{for} \quad \tau_1<\tau_2. \quad (4.5)$$

The solution of Eq. (4.3) is[9]

$$u(\tau_1)=\int d^{3N}x_2\mathbf{G}(\mathbf{x}_1,\tau_1;\mathbf{x}_2,\tau_2)u(\tau_2), \quad (4.6)$$

where, aside from being smaller than τ_1, τ_2 is arbitrary. Since (4.3) is to be solved subject to $u(0)=1$, τ_2 is conveniently taken equal to zero, so that

$$u(1)=u(\tau)|_{\tau=\lambda^2}=\int d^{3N}x^1\mathbf{G}(\mathbf{x},\lambda^2;\mathbf{x}^1,0). \quad (4.7)$$

Pictorially, we may describe (4.7) as giving the in-

[7] R. P. Feynman, Phys. Rev. **76**, 769 (1949) and Revs. Modern Phys. **20**, 367 (1948).
[8] R. E. Marshak, Revs. Modern Phys. **19**, 185 (1947).
[9] Courant and Hilbert, *Methoden der Mathematische Physik* (Interscience Publishers, Inc., New York, 1900), Vol. II.

struction of starting out with a uniform distribution as would obtain at $\tau=0$ (i.e., $\lambda=0$, or infinite temperature) and allowing the operator $\mathbf{G}$ to carry the system down to the temperature characterized by $\tau=\lambda^2$. Notice, incidentally, that the boundary condition $u(0)=1$ implies

$$\mathbf{G}(\mathbf{x}, \tau; \mathbf{x}^1, \tau)=\delta(\mathbf{x}-\mathbf{x}^1). \tag{4.8}$$

There is a very close relationship between $\mathbf{G}$ and our "ordered exponentials," but we shall not discuss the point in this paper.

The question naturally arises as to how one sets about constructing such operator Green's functions. One method of construction employs devices analogous to the "ordered exponentials." We, however, shall proceed by deriving integral equations for $\mathbf{G}$ which may be solved by iteration if by no other means. As in our earlier work there are two courses open to us, and we explore these in turn. As a first approach we relate $\mathbf{G}$ to the operator $\mathbf{D}$ defined by

$$[(\partial/\partial\tau_1)-\nabla_1^2]\mathbf{D}(\mathbf{x}_1, \tau_1; \mathbf{x}_2\tau_2)=\delta(\mathbf{x}_1-\mathbf{x}_2)\delta(\tau_1-\tau_2),$$
$$\mathbf{D}(\mathbf{x}_1\tau_1; \mathbf{x}_2, \tau_2)\equiv 0 \quad \text{for} \quad \tau_1<\tau_2. \tag{4.9}$$

Using well-known techniques, we may show that in terms of $\mathbf{D}$,

$$\mathbf{G}(\mathbf{x}_1, \tau_1; \mathbf{x}_2, \tau_2)=\mathbf{D}(\mathbf{x}_1, \tau_1; \mathbf{x}_2, \tau_2)$$
$$-\int_{\tau_2}^{\tau_1} d\tau_3 \int d^{3N}x_3 D(\mathbf{x}_1\tau_1; \mathbf{x}_3, \tau_3)(U(\mathbf{x}_3)/\lambda^2)$$
$$\times\mathbf{G}(\mathbf{x}_3, \tau_3; \mathbf{x}_2, \tau_2); \tag{4.10}$$

or

$$\mathbf{G}(\mathbf{x}_1, \tau_1; \mathbf{x}_2, \tau_2)=\mathbf{D}(\mathbf{x}_1, \tau_1; \mathbf{x}_2, \tau_2)$$
$$-\int_{\tau_2}^{\tau_1} d\tau_3 \int d^{3N}x_3 \mathbf{G}(\mathbf{x}_1, \tau_1; \mathbf{x}_3, \tau_3)(U(\mathbf{x}_3)/\lambda^2)$$
$$\times\mathbf{D}(\mathbf{x}_3, \tau_3; \mathbf{x}_2, \tau_2). \tag{4.11}$$

It is further possible to construct $\mathbf{D}$ explicitly. One may easily verify that

$$\mathbf{D}(\mathbf{x}_1, \tau_1; \mathbf{x}_2, \tau_2)$$
$$=\exp[(\tau_1-\tau_2)\nabla_1^2]\delta(\mathbf{x}_1-\mathbf{x}_2)H(\tau_1-\tau_2), \tag{4.12}$$

where $H(\tau)$ is 0 for $\tau<0$ and 1 for $\tau>0$. [$(\partial/\partial\tau)H(\tau)=\delta(\tau)$.] A less symbolic form of writing for $\mathbf{D}$ may be obtained using a Fourier integral representation of the δ function:

$$\mathbf{D}(\mathbf{x}_1, \tau_1; \mathbf{x}_2, \tau_2)=\frac{H(\tau_1-\tau_2)}{(2\pi)^{3N}}$$
$$\times\int d^{3N}k \exp[i\mathbf{k}\cdot(\mathbf{x}_1-\mathbf{x}_2)-(\tau_1-\tau_2)k^2]$$
$$\times\exp[2i(\tau_1-\tau_2)\mathbf{k}\cdot\nabla_1], \tag{4.13}$$

where we have used the elementary theorem

$$e^{(a+b)}=e^a e^b \exp\{-\tfrac{1}{2}[a, b]\}, \tag{4.14}$$

which is true provided a and b commute with their commutator. The expression for $\mathbf{D}$ given in (4.13) emphasizes the fact mentioned earlier that our Green's functions are operators. With the aid of (4.12) the fundamental integral equations may be simplified to

$$\mathbf{G}(\mathbf{x}_1, \tau_1; \mathbf{x}_2, \tau_2)=\exp[(\tau_1-\tau_2)\nabla_1^2]\delta(\mathbf{x}_1-\mathbf{x}_2)$$
$$-\int_{\tau_2}^{\tau_1} d\tau_3 \exp[(\tau_1-\tau_3)\nabla_1^2]$$
$$\times(U(\mathbf{x}_1)/\lambda^2)\mathbf{G}(\mathbf{x}_1, \tau_3; \mathbf{x}_2\tau_2); \tag{4.15}$$

$$\mathbf{G}(\mathbf{x}_1, \tau_1; \mathbf{x}_2, \tau_2)=\exp[(\tau_1-\tau_2)\nabla_1^2]\delta(\mathbf{x}_1-\mathbf{x}_2)$$
$$-\int_{\tau_2}^{\tau_1} d\tau_3 \exp[(\tau_3-\tau_2)\nabla_2^2]$$
$$\times\mathbf{G}(\mathbf{x}_1, \tau_1; \mathbf{x}_2, \tau_2)(U(\mathbf{x}_2)/\lambda^2), \tag{4.16}$$

where we have dropped the step function $H(\tau_1-\tau_2)$.

Equations (4.10) and (4.11) may be interpreted physically in the following way: $\mathbf{G}(\mathbf{x}_1, \tau_1; \mathbf{x}_2, \tau_2)$ describes the process by which the system starts out at the configuration $\mathbf{x}_2$ with "age" τ_2 and eventually reaches the configuration $\mathbf{x}_1$, and "age" τ_1; Eq. (4.10) expresses the fact that there are two routes available. Either the system "slows down" in such a way that it essentially feels no potential U (the term $\mathbf{D}(\mathbf{x}_1, \tau_1; \mathbf{x}_2, \tau_2)$), or it slows down under the influence of the potential as described by $\mathbf{G}$ to the point $(\mathbf{x}_3, \tau_3)$ where it suffers its last "collision" with U and slows down the rest of the way as a "free" system via $\mathbf{D}$. One then sums over all these intermediate points $(\mathbf{x}_3, \tau_3)$. Similarly in (4.11) the system slows down as if free to $(\mathbf{x}_3, \tau_3)$, there suffers its first potential interaction and completes its course under the influence of U via $\mathbf{G}$.

An alternative exploitation of the Green's function approach is to use the Green's function defined by

$$\left(\frac{\partial}{\partial\tau_1}+\frac{U(\mathbf{x}_1)}{\lambda^2}\right)\mathbf{K}(\mathbf{x}_1, \tau_1; \mathbf{x}_2, \tau_2)=\delta(\mathbf{x}_1-\mathbf{x}_2)\delta(\tau_1-\tau_2),$$
$$\mathbf{K}(\mathbf{x}_1, \tau_1; \mathbf{x}_2, \tau_2)\equiv 0 \quad \text{for} \quad \tau_1<\tau_2. \tag{4.17}$$

Evidently,

$$\mathbf{K}(\mathbf{x}_1, \tau_1; \mathbf{x}_2, \tau_2)$$
$$=\exp[-(\tau_1-\tau_2)U(\mathbf{x}_1)/\lambda^2]\delta(\mathbf{x}_1-\mathbf{x}_2)\delta(\tau_1-\tau_2). \tag{4.18}$$

We give only the analog of (4.15):

$$\mathbf{G}(\mathbf{x}_1, \tau_1; \mathbf{x}_2, \tau_2)=\exp[-(\tau_1-\tau_2)U(\mathbf{x}_1)/\lambda^2]\delta(\mathbf{x}_1-\mathbf{x}_2)$$
$$\times\int_{\tau_2}^{\tau_1} d\tau_3 \exp[-(\tau_1-\tau_3)U(\mathbf{x}_1)/\lambda^2]$$
$$\times\nabla_1^2\mathbf{G}(\mathbf{x}_1, \tau_3; \mathbf{x}_2, \tau_2). \tag{4.19}$$

It is clear that the first form given for $\mathbf{G}$ is the one appropriate for generating a series in powers of U,

whereas the second is the one appropriate for generating a power series in λ. We are investigating the question of developing these operator Green's functions as a computational tool. In any case we feel that they give an interesting insight into the structure of the function $F\{N\}$.

APPENDIX I

The "ordered" exponential is defined by the order of the factors in the power series expansion of $\exp\{\int_0^1 dsU(s)\}$. Consider the nth term in the power series expansion of the exponential. This term may be written

$$\frac{1}{n!}\int_0^1 ds_1\cdots\int_0^1 ds_n U(s_1)U(s_2)\cdots U(s_n). \quad \text{(AI-1)}$$

The "ordered" exponential is defined in terms of the order in which the factors $U(s_J)$ shall stand during the integrations. $[\ ]_-$ ordering means that throughout each interval of the integration the argument of the right-hand factor shall be the largest of the s_J, that of the second from the right the second largest of the s_J, etc. As an illustration we write out the term for which $n=2$.

$$\frac{1}{2!}\left[\int_0^1 ds_1\int_0^1 ds_2 U(s_1)U(s_2)\right]_- = \frac{1}{2}\int_0^1 ds_1\int_0^{s_1} ds_2 U(s_2)U(s_1) + \frac{1}{2}\int_0^1 ds_1\int_{s_1}^1 ds_2 U(s_1)U(s_2). \quad \text{(AI-2)}$$

The two integrals are equal as is seen by interchange of the dummy indices, s_1 and s_2, in one of the two. Thus

$$\frac{1}{2!}\left[\int_0^1 ds_1\int_0^1 ds_2 U(s_1)U(s_2)\right]_- = \int_0^1 ds_1\int_{s_1}^1 ds_2 U(s_1)U(s_2). \quad \text{(AI-3)}$$

By a series of similar changes of variable the general term is seen to be

$$\frac{1}{n!}\left[\int_0^1 ds_1\cdots\int_0^1 ds_n U(s_1)\cdots U(s_n)\right]_- = \int_0^1 ds_1\int_{s_1}^1 ds_2\cdots\int_{s_{n-1}}^1 ds_n U(s_1)\cdots U(s_n). \quad \text{(AI-4)}$$

The $[\ ]_+$ ordering is defined in an analogous way except that the largest value of s goes to the left. Thus

$$\frac{1}{n!}\left[\int_0^1 ds_1\cdots\int_0^1 ds_n U(s_1)\cdots U(s_n)\right]_+ = \int_0^1 ds_1\int_0^{s_1} ds_2\cdots\int_0^{s_{n-1}} ds_n U(s_1)\cdots U(s_n). \quad \text{(AI-5)}$$

It would be noted that despite the "ordering" these exponentials retain many of the important properties of the exponential function. Thus, e.g.,

$$\frac{\partial}{\partial s}\exp_{(+)}\left[\int_0^s ds' U(s')\right] = U(s)\exp_{(+)}\left[\int_0^s ds' U(s')\right];$$

$$\frac{\partial}{\partial s}\exp_{(-)}\left[\int_0^s ds' U(s')\right] = \exp_{(-)}\left[\int_0^s ds' U(s')\right]U(s);$$

$$\exp_{(+)}\left[\int_{s_2}^{s_3} ds' U(s')\right]\exp_{(+)}\left[\int_{s_1}^{s_2} ds' U(s')\right] = \exp_{(+)}\left[\int_{s_1}^{s_3} ds' U(s')\right] \quad (s_3\geqslant s_2\geqslant s_1); \quad \text{(AI-6)}$$

$$\exp_{(-)}\left[\int_{s_1}^{s_2} ds' U(s')\right]\exp_{(-)}\left[\int_{s_2}^{s_3} ds' U(s')\right] = \exp_{(-)}\left[\int_{s_1}^{s_3} ds' \dot{U}(s')\right] \quad (s_3\geqslant s_2\geqslant s_1);$$

$$\exp_{(+)}\left[\int_0^s ds' U(s')\right]\exp_{(-)}\left[-\int_0^s ds' U(s')\right] = 1.$$

APPENDIX II

The derivation of (3.1) and (3.9) which is presented here is identical to Schwinger's,[3] but is presented in detail for ease of reference and because it would appear to be applicable in a large number of problems in statistical mechanics.

The problem is to derive an expression for $\exp\times\{-(a+b)\}$ in which a, say, is regarded as a "large" operator and b a "small" one. As in the text, let

$$u(s) = e^{-(a+b)s}, \quad \text{(AII-1)}$$

$$\frac{\partial}{\partial s}u(s) = -(a+b)u(s). \quad \text{(AII-2)}$$

Introduce $v(s)$ defined by

$$u(s) = e^{-as}v(s), \quad \text{(AII-3)}$$

which satisfies the differential equation

$$\frac{\partial}{\partial s}v(s) = -e^{+as}be^{-as}v(s), \quad \text{(AII-4)}$$

subject to the obvious boundary condition $v(0)=1$. We replace (II-4) by an integral equation which incorporates the boundary condition and which may be solved by iteration:

$$v(s)=1-\int_0^s ds' \exp(as')b \exp(-as')v(s'). \quad \text{(AII-5)}$$

Carrying out the iteration, we have

$$v(s)=1-\int_0^s ds' \exp(as')b \exp(-as') + \int_0^s ds' \int_0^{s'} ds'' \exp(as')b \exp(-as') \times \exp(as'')b \exp(-as'')+\cdots. \quad \text{(AII-6)}$$

A somewhat neater form is obtained by making the substitutions $s'=ss_1$, $s''=s's_2$, $\cdots$. Making this change and forming $u(1)$ from (AII-3) we find

$$u(1)=e^{-(a+b)}=e^{-a}+(-1)\int_0^1 ds_1 e^{-(1-s_1)a}be^{-s_1a} + (-1)^2\int_0^1 s_1 ds_1 \int_0^1 ds_2 e^{-(1-s_1)a}be^{-s_1(1-s_2)a}be^{-s_1s_2a} + \cdots + (-1)^n \int_0^1 {s_1}^{n-1}ds_1 \int_0^1 {s_2}^{n-2}ds_2 \cdots \int_0^1 ds_n e^{-(1-s_1)a}be^{-s_1(1-s_2)a}b \cdots be^{-s_1s_2\cdots s_{n-1}(1-s_n)a}be^{-s_1\cdots s_na}+\cdots. \quad \text{(AII-7)}$$

If one is faced with the problem of taking the trace of $u(1)$, a further simplification can be made by virtue of the fundamental property of a trace, namely

$$Tr(AB\cdots YZ)=Tr(ZAB\cdots Y) =Tr(B\cdots YZA), \text{ etc.} \quad \text{(AII-8)}$$

Using (AII-8) one may easily verify the following equation

$$Tr\, e^{-(a+b)s}-Tr\, e^{-as}=-\int_0^1 d\alpha\, Tr[be^{-(a+\alpha b)s}]. \quad \text{(AII-9)}$$

Substituting the series (AII-7) for $\exp\{-(a+\alpha b)s\}$ we find

$$Tr\, e^{-(a+b)}=Tr\, e^{-a}+(-1)Tr\, be^{-a} + \frac{(-1)^2}{2}\int_0^1 ds_1\, Tr[be^{-(1-s_1)a}be^{-s_1a}] + \cdots + \frac{(-1)^{n+1}}{n+1}\int_0^1 {s_1}^{n-1}ds_1 \int_0^1 {s_2}^{n-2}ds_2 \cdots \int_0^1 ds_n\, Tr[be^{-(1-s_1)a}be^{-s_1(1-s_2)a}b \cdots be^{-s_1s_2\cdots s_na}]+\cdots. \quad \text{(AII-10)}$$

The Scattering of Atoms from Diatomic Molecules*

CHARLES F. CURTISS, *The Naval Research Laboratory, Department of Chemistry, University of Wisconsin*

AND

F. T. ADLER,† *Department of Physics, University of Wisconsin*

(Received June 1, 1951)

The quantum mechanics of the collision of an atom with a diatomic molecule is discussed. This is an example of the scattering of particles by a nonspherical potential field. In the region in which the atom and molecule are not interacting, the wave function for the system can be written as the product of a wave function for the free atom and that of the free molecule. By an analysis of this function one can write the asymptotic form of the true wave function in the terms of the scattering coefficients, representing the angular dependence of the transition probabilities. In a previous paper, group theoretical arguments were used to separate the rotational coordinates from the n-particle Schroedinger equation. A set of coupled differential equations for the internal wave functions was derived. In the present paper, the scattering coefficients are obtained by an analysis of the solutions of the internal wave equations involving the three coordinates specifying the internal configuration. This set of equations is transformed into a set of coupled ordinary differential equations in which the coupling is the result of the transitions in the state of the molecule. The equations are solved by a perturbation method which is valid in the case of low energy collisions in which transitions occur relatively seldom. The angular transition probabilities are obtained explicitly in terms of integrals of the interaction potential and a set of phase shifts.

IN a previous paper,[1] group theoretical arguments were used to separate the rotational coordinates from the n-particle Schroedinger equation. In the present paper, these results are used to examine the dynamics of the collision between an atom and a diatomic molecule, from the quantum-mechanical point of view. In the region in which the atom and molecule are not interacting, the wave function for the system is the product of a wave function for the free atom and that of the free molecule. In the general case of the scattering of a plane wave of atoms, the wave function consists of a plane wave of incoming atoms and a set of outgoing waves, each corresponding to a transition in the state of the molecule. The asymptotic form of the wave function can be written in terms of the scattering coefficients representing the angular dependence of the transition probabilities. These coefficients are obtained by analysis of the solution of the internal wave equations involving only the three coordinates of the relative configuration.

The set of coupled differential equations involving the three coordinates of relative configuration are transformed into a set of coupled ordinary differential equations. The coupling occurs as the result of the transitions in the state of the molecule. If the probability of a transition in the state of the molecule is small, the coupling is weak. The equations are solved by a perturbation method based on this concept. The results are applicable to the normal low energy thermal collisions but not to the high energy collisions involved in hot atom chemistry or chemical kinetics. The symmetry effects of the Pauli exclusion principle are not considered.

The transition probabilities are obtained explicitly in terms of integrals of the interaction potential and a set of phase shifts. The phase shifts are defined in terms of the solution of a particular differential equation involving the interaction potential.

THE ASYMPTOTIC FORM

Consider the motion of an atom and a diatomic molecule. In the region in which there is no interaction the wave function can be written in the form

$$\Psi^{(0)}=\exp(i\mathbf{k}_a\cdot\mathbf{r}_a)\exp(i\mathbf{k}_m\cdot\mathbf{r}_m)Z_n(\xi)Y_l^m(\theta_2,\varphi_2). \quad (1)$$

Here $\mathbf{r}_a$ and $\mathbf{r}_m$ are position vectors of the atom and center of gravity of the molecule; ξ is the separation of the atoms in the molecule; θ_2, φ_2 are the polar and azimuthal angles of the axis of the molecule with respect to space fixed axis; $\mathbf{k}_a$ and $\mathbf{k}_m$ are the wave numbers (vectorially) associated with the motion of the atom and molecule; $Z_n(\xi)$ is the harmonic oscillator wave function; $Y_l^m(\theta_2,\varphi_2)$ is a normalized spherical harmonic; and n, l, and m are the quantum numbers associated with the motion of the molecule. Let us introduce the coordinates of the center of mass of the system

$$\mathbf{r}_c=[m_1\mathbf{r}_a+(m_2+m_3)\mathbf{r}_m]/(m_1+m_2+m_3), \quad (2)$$

where m_1 is the mass of the atom; m_2 and m_3, the masses of the atoms of the molecule and a coordinate representing the relative positions,

$$\boldsymbol{\varrho}=\mathbf{r}_a-\mathbf{r}_m. \quad (3)$$

Then the wave function $\Psi^{(0)}$, Eq. (1), becomes

$$\Psi^{(0)}=\exp[i(\mathbf{k}_a+\mathbf{k}_m)\cdot\mathbf{r}_c]\times\exp\{i[(m_2+m_3)\mathbf{k}_a-m_1\mathbf{k}_m]\cdot\boldsymbol{\varrho}/(m_1+m_2+m_3)\}\times Z_n(\xi)Y_l^m(\theta_2,\varphi_2). \quad (4)$$

* This work was carried out under Contract NOrd 9938 with the Navy Bureau of Ordnance.

† Present address: Carnegie Institute of Technology, Pittsburgh, Pennsylvania.

[1] Curtiss, Hirschfelder, and Adler, J. Chem. Phys. 18, 1638 (1950).

The first factor

$$\exp[i(\mathbf{k}_a+\mathbf{k}_m)\cdot\mathbf{r}_c], \tag{5}$$

represents the motion of the center of gravity of the system. The second factor describes the relative motion in the center-of-gravity coordinate system. This factor can be written

$$\psi^{(0)}=\exp(i\mathbf{k}\cdot\boldsymbol{\rho})Z_n(\xi)Y_l^m(\theta_2,\varphi_2), \tag{6}$$

where

$$\mathbf{k}=[(m_2+m_3)\mathbf{k}_a-m_1\mathbf{k}_m]/(m_1+m_2+m_3) \tag{7}$$

represents the magnitude and direction of the relative momentum.

The expression for the wave function $\psi^{(0)}$, Eq. (6), can be written in a form which shows explicitly the dependence on the angles. The exponential factor may be expanded in the form[2]

$$\exp(i\mathbf{k}\cdot\boldsymbol{\rho})=2\pi/(2k\rho)^{\frac{1}{2}} \times\sum_L(-i)^L(2L+1)^{\frac{1}{2}}J_{L+\frac{1}{2}}(k\rho)Y_L^0(\gamma,0), \tag{8}$$

where k and ρ indicate the absolute values of the vectors and γ is the angle between $\mathbf{k}$ and $\boldsymbol{\rho}$. The addition theorem of the spherical harmonics is

$$Y_L^0(\gamma,0)=[4\pi/(2L+1)]^{\frac{1}{2}} \times\sum_\nu(-1)^L Y_L^\nu(\theta_1,\varphi_1)Y_L^\nu(\Theta,\Phi)^*, \tag{9}$$

where θ_1 and φ_1 are the polar and azimuthal angles of $\boldsymbol{\rho}$, i.e., of the line between the molecule and the atom, and Θ and Φ are the direction angles of $\mathbf{k}$, i.e., of the relative momentum (or velocity). Using Eqs. (8) and (9), Eq. (6) for the wave function ψ becomes

$$\psi^{(0)}=2\pi(2\pi/k\rho)^{\frac{1}{2}}\sum_{L,\nu} i^L Y_L^\nu(\theta_1,\varphi_1)Y_l^m(\theta_2,\varphi_2) \times Y_L^\nu(\Theta,\Phi)^*J_{L+\frac{1}{2}}(k\rho)Z_n(\xi). \tag{10}$$

This wave function is correct only in the region in which the atom and molecule are not interacting. Hence we investigate the asymptotic behavior of the function, which is

$$\psi^{(0)}\longrightarrow-\frac{2\pi i}{k\rho}\sum_{L,\nu}[e^{ik\rho}-(-1)^L e^{-ik\rho}] \times Y_L^\nu(\theta_1,\varphi_1)Y_l^m(\theta_2,\varphi_2)Y_L^\nu(\Theta,\Phi)^*Z_n(\xi). \tag{11}$$

Let us consider the scattering of a plane wave of atoms of relative momentum k_0 from a molecule in the quantum state specified by n_0, l_0, m_0. Asymptotically the wave function representing the incoming plane wave (along the z axis in the positive direction) is obtained from Eq. (11) by putting Θ equal to zero. The resulting expression is

$$-\frac{i(\pi)^{\frac{1}{2}}}{k_0\rho}\sum_L[(-1)^L\exp(ik_0\rho)-\exp(-ik_0\rho)](2L+1)^{\frac{1}{2}} \times Y_L^0(\theta_1,\varphi_1)Y_{l_0}^{m_0}(\theta_2,\varphi_2)Z_{n_0}(\xi). \tag{12}$$

[2] The spherical harmonics $Y_L^m(\theta,\varphi)$ are defined precisely in Appendix B. The definition used here is somewhat unusual. However, it is a convenient definition and is necessary in order to permit use of previous results.

The terms in $e^{ik\rho}$ and $e^{-ik\rho}$ of Eq. (11) are, of course, separately valid solutions of the wave equation, representing the two independent solutions. Asymptotically the scattered wave can contain only terms in $e^{ik\rho}$ in order to represent a wave going out from the center. Hence we can write for the scattered wave

$$-2\pi i\sum_{n,l,m,L,\nu}\frac{e^{ik\rho}}{k\rho}Y_L^\nu(\theta_1,\varphi_1)Y_l^m(\theta_2,\varphi_2)Z_n(\xi) \times\int\int f(\Theta,\Phi)_{nlm}Y_L^\nu(\Theta,\Phi)^*\sin\Theta d\Theta d\Phi. \tag{13}$$

Here $f(\Theta,\Phi)_{nl,m}$ describes the angular dependence of the scattered atoms which have caused a transition in the state of the molecule to the state specified by the quantum numbers, n, l, m. In the sum k is such a function of n and l, that the total energy of the system is conserved. (Because of the usual degeneracy in m, k is not a function of the quantum number m.) However, as usual, it is more convenient to analyze the scattered wave in terms of the spherical harmonics rather than in terms of plane waves. Hence we define

$$\alpha_{L\nu}{}^{nlm}=\int\int f(\Theta,\Phi)_{nlm}Y_L^\nu(\Theta,\Phi)^*\sin\Theta d\Theta d\Phi, \tag{14}$$

as the amplitudes of the various spherical harmonic waves. Making use of this expression and Eqs. (12) and (13) we obtain the asymptotic form of the complete wave function as

$$\psi\longrightarrow-2\pi i\sum_{n,l,m,L,\nu}Y_L^\nu(\theta_1,\varphi_1)Y_l^m(\theta_2,\varphi_2)Z_n(\xi) \times\left\{\begin{aligned}&\frac{1}{k\rho}e^{ik\rho}\left\{\alpha_{L\nu}{}^{nlm}+(-1)^L\left(\frac{2L+1}{4\pi}\right)^{\frac{1}{2}}\delta_{nn_0}\delta_{ll_0}\delta_{mm_0}\delta_{\nu 0}\right\}\\ &-\frac{1}{k\rho}e^{-ik\rho}\left(\frac{2L+1}{4\pi}\right)^{\frac{1}{2}}\delta_{nn_0}\delta_{ll_0}\delta_{mm_0}\delta_{\nu 0}\end{aligned}\right\}. \tag{15}$$

The constants $\alpha_{L\nu}{}^{nlm}$ which are now interpreted as scattering amplitudes must be obtained by considering the asymptotic form of a wave function which satisfies the requirements of the interaction potential. That is, one must obtain a valid solution of the true wave equation which is asymptotically of this form. The constants $\alpha_{L\nu}{}^{nlm}$ are thus well specified.

The wave function ψ is to be distinguished from the wave function $\psi^{(0)}$. The function $\psi^{(0)}$ represents a single plane wave of atoms approaching a molecule in the quantum state (n, l, m). The wave function ψ represents the actual situation of the incoming plane wave and the outgoing scattered waves. Because of the transitions, the state of the molecule cannot be specified.

THE SOLUTION OF THE WAVE EQUATION

It has been shown in a previous paper[1] that the wave functions in the center-of-gravity coordinate system corresponding to a total angular momentum quantum number, J, and a z-component of the angular momentum quantum number, μ, may be written in the form

$$\psi_\mu{}^J=\sum_s D^J(R)_{\mu s}{}^*\chi_s{}^J. \tag{16}$$

Here R represents a rotation which will rotate the configuration into a "standard" configuration and involves the three angular coordinates of orientation. The functions $D^J(R)_{\mu s}$ are the representation coefficients of the three dimensional rotation group. The function $\chi_s{}^J$ is a function of the internal coordinates and depends upon four additional quantum numbers: k, p, q, and j. The quantum numbers, k, p, and q are associated with the internal coordinates. The quantum number j is an external quantum number which appears because of the coupling of the equations for $\chi_s{}^J$ or more basically because only two quantum numbers were introduced in the separation of the three coordinates of orientation. It will become apparent later that j is closely related to an "orbital angular momentum," i.e., j measures the contribution of the motion of the atom to the total angular momentum. In this sense, j is the quantum-mechanical manifestation of the classical "impact parameter." Because of the vector addition of the angular momentum any one of the three quantum numbers J, q, and j is restricted to values ranging from the absolute value of the difference to the sum of the other two. However, this restriction is mathematically imposed by the properties of the functions involved, in particular by the properties of the $s_{Js}{}^{jq}$ defined later. A set of coupled differential equations for the internal functions, $\chi_s{}^J$, were derived in the previous paper.[1] A wave function for a fixed energy can be written as[3]

$$\psi=\sum_{\substack{J\mu s\\ pqj}} A_{J\mu}{}^{pqj}D^J(R)_{\mu s}{}^*\chi_s{}^J(pqj). \tag{17}$$

We will proceed to obtain an approximate solution of the equations, choose a set of $A_{J\mu}{}^{pqj}$ so that Eq. (17) is asymptotically of the form of Eq. (15) and then, by comparing terms, fix the scattering amplitudes $\alpha_{j\nu}{}^{nlm}$.

The set of coupled differential equations for the $\chi_s{}^J$ is

$$\frac{1}{\mu}\left[\frac{\partial^2}{\partial\rho^2}+\frac{2}{\rho}\frac{\partial}{\partial\rho}-\frac{1}{\rho^2}\{J(J+1)-2s^2\}\right]\chi_s{}^J+\frac{1}{M}\left[\frac{\partial^2}{\partial\xi^2}+\frac{2}{\xi}\frac{\partial}{\partial\xi}\right]\chi_s{}^J+\left\{\frac{1}{\mu\rho^2}+\frac{1}{M\xi^2}\right\}\left[\frac{\partial^2}{\partial\varphi^2}+\cot\varphi\frac{\partial}{\partial\varphi}-s^2\csc^2\varphi\right]\chi_s{}^J$$

$$+\frac{i}{\mu\rho^2}\left[\lambda_+\left\{\frac{\partial}{\partial\varphi}+(s+1)\cot\varphi\right\}\chi_{s+1}{}^J+\lambda_-\left\{\frac{\partial}{\partial\varphi}-(s-1)\cot\varphi\right\}\chi_{s-1}{}^J\right]=\frac{2}{\hbar^2}(V-E)\chi_s{}^J, \tag{18}$$

where μ and M are the reduced masses,

$$\mu=\frac{m_1(m_2+m_3)}{m_1+(m_2+m_3)}, \tag{19}$$

$$M=m_2m_3/(m_2+m_3). \tag{20}$$

λ_+ and λ_- are the numbers

$$\lambda_+=[J(J+1)-s(s+1)]^{\frac{1}{2}}, \tag{21}$$

$$\lambda_-=[J(J+1)-s(s-1)]^{\frac{1}{2}}, \tag{22}$$

and φ is the angle between the intermolecular axis and the line joining the atom and the center of gravity of the molecule. The coordinate system is illustrated in Fig. (1). The quantum numbers k, p, and q are associated with the coordinates ρ, ξ, and φ, respectively. The potential energy function V is assumed to be made up of two parts. One part is $V_\xi(\xi)$, the interaction potential of the two atoms in the molecule in the absence of the free atom. The other, $W(\rho, \xi, \varphi)$, is the collision potential and may depend in any way on the three coordinates. Thus

$$V=V_\xi(\xi)+W(\rho, \xi, \varphi). \tag{23}$$

The function $Z_p(\xi)$ of course satisfies the equation for the nonrotating free molecule,

$$-\frac{1}{M}\left[\frac{\partial^2}{\partial\xi^2}+\frac{2}{\xi}\frac{\partial}{\partial\xi}\right]Z_p(\xi)+\frac{2}{\hbar^2}V_\xi(\xi)Z_p(\xi)=\frac{2}{\hbar^2}E_pZ_p(\xi). \tag{24}$$

Here E_p is the energy associated with the vibration of the molecule.

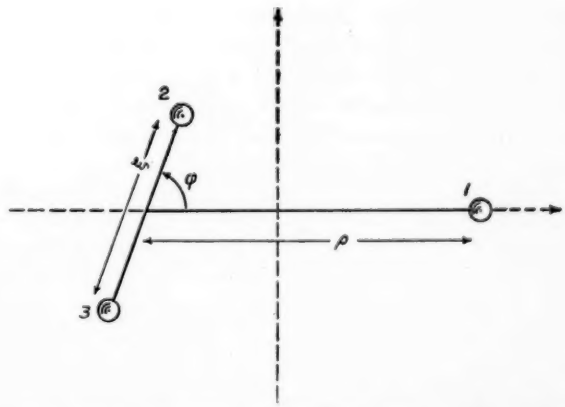

FIG. 1. The coordinates specifying the internal configuration.

[3] Because energy is conserved on collision not all terms need be included in the sum. For each set of (p, q, j) a value of k (a continuous quantum number) is chosen so that the energy is conserved.

Since the functions $Z_p(\xi)$ and $Y_q^s(\varphi, 0)$ form complete sets of functions in ξ and φ, respectively, one can expand a particular χ_s^J in a series of these functions. Thus

$$\chi_s^J(p_0q_0j_0)=\sum_{p,q} g_s^J(p_0q_0|\,pq)_{j0}Z_p(\xi)Y_q^s(\varphi, 0). \quad (25)$$

The set of Eqs. (18) then provide a set of equations for the expansion coefficients $g_s^J(p_0q_0|\,pq)_{j0}$. But rather than solving for these directly, it is more convenient to use a linear combination defined by

$$g_s^J(p_0q_0|\,pq)_{j0}=\sum_j (-i)^s s_{J0s}^{jq}G^J(p_0q_0j_0|\,pqj). \quad (26)$$

Here the s_{J0s}^{jq} are the set of numbers defined by Wigner.[4] It is shown in Appendix B that

$$\lambda_+ s_{J,0,s+1}^{jq}\left[\frac{\partial}{\partial\varphi}+(s+1)\cot\varphi\right]Y_q^{s+1}(\varphi, 0)$$
$$-\lambda_- s_{J,0,s-1}^{jq}\left[\frac{\partial}{\partial\varphi}-(s-1)\cot\varphi\right]Y_q^{s-1}(\varphi, 0)$$
$$=s_{J0s}^{jq}[J(J+1)+q(q+1)$$
$$-j(j+1)-2s^2]Y_q^s(\varphi, 0). \quad (27)$$

By using Eqs. (25) and (26) for $\chi_s^J(p_0q_0j_0)$ one can obtain from Eq. (18) a set of equations for the functions $G^J(p_0q_0j_0|\,pqj)$. By making use of the identity, Eq. (27), these become

$$\sum_{pqj}\left[\frac{1}{\mu}\left\{\frac{\partial^2}{\partial\rho^2}+\frac{2}{\rho}\frac{\partial}{\partial\rho}-\frac{j(j+1)}{\rho^2}\right\}-\frac{2}{\hbar^2}+\frac{k^2}{2\mu}\right]$$
$$\cdot s_{J0s}^{jq}G^J(p_0q_0j_0|\,pqj)Z_p(\xi)Y_q^s(\varphi, 0)=0, \quad (28)$$

where

$$\frac{\hbar^2k^2}{2\mu}=E-E_p-\frac{q(q+1)\hbar^2}{2M\xi_e^2},$$

is the translational energy of the system.[5]

Equation (28) can be simplified by making use of the orthogonality of the functions, $Z_p(\xi)^*$ and $Y_q^s(\varphi, 0)^*$. Multiplying the equation by $Z_{p'}(\xi)Y_{q'}^s(\varphi, 0)$; integrating over ξ and φ; making use of the orthogonality; and dropping the primes it follows that

$$\frac{1}{\mu}\sum_j\left[\frac{\partial^2}{\partial\rho^2}+\frac{2}{\rho}\frac{\partial}{\partial\rho}-\frac{j(j+1)}{\rho^2}+k^2\right]s_{J0s}^{jq}G^J(p_0q_0j_0|\,pqj)$$
$$=\sum_{p'q'j'}W^s(pq|\,p'q')s_{J0s}^{j'q'}G^J(p_0q_0j_0|\,p'q'j'), \quad (29)$$

where

$$W^s(pq|\,p'q')=\frac{2}{\hbar^2}\int\int W(\rho, \xi, \varphi)Z_{p'}(\xi)Z_p^*(\xi)$$
$$\times Y_{q'}^s(\varphi, 0)Y_q^s(\varphi, 0)^*\sin\varphi d\varphi d\xi. \quad (30)$$

In Appendix A it is shown that the s_{J0s}^{jq} are orthogonal in the index j, i.e.,

$$\sum_s s_{J0s}^{jq}s_{J0s}^{j'q}=\delta_{jj'}\left(\frac{2J+1}{2j+1}\right). \quad (31)$$

If Eq. (29) is multiplied by $s_{J0s}^{j''q}$ and summed over s, then it follows from this equation (dropping the primes on j'') that

$$\frac{1}{\mu}\left\{\frac{\partial^2}{\partial\rho^2}+\frac{2}{\rho}\frac{\partial}{\partial\rho}-\frac{j(j+1)}{\rho^2}+k^2\right\}G^J(p_0q_0j_0|\,pqj)$$
$$=\sum_{p'q'j'}W^J(pqj|\,p'q'j')G^J(p_0q_0j_0|\,p'q'j'), \quad (32)$$

where

$$W^J(pqj|\,p'q'j')$$
$$=\left(\frac{2j+1}{2J+1}\right)\sum_s s_{J0s}^{j'q'}s_{J0s}^{jq}W^s(pq|\,p'q'). \quad (33)$$

The set of Eqs. (32) is a set of coupled ordinary differential equations. An exact solution is difficult, but a perturbation solution may be obtained by a method similar to that used by Zener.[6] The perturbation method assumes that the coupling is weak. This is correct for low velocity collisions in which transitions in the state of the molecule occur relatively seldom.

Consider the equation

$$\left\{\frac{1}{\mu}\frac{d^2}{d\rho^2}+\frac{2}{\mu\rho}\frac{d}{d\rho}-\frac{j(j+1)}{\mu\rho^2}\right.$$
$$\left.+(k^2/\mu)-W^J(pqj|\,pqj)\right\}f=0. \quad (34)$$

Let U_{pqj}^J be the solution which is bounded at $\rho=0$ and which is normalized so that asymptotically[7]

$$U_{pqj}^J\underset{\rho\to\infty}{\longrightarrow}\frac{1}{k\rho}\sin(k\rho+\theta_{pqj}^J). \quad (35)$$

Here θ_{pqj}^J is a phase angle defined by the asymptotic form. Further let X_{pqj}^J be the solution which is asymptotically

$$X_{pqj}^J\underset{\rho\to\infty}{\longrightarrow}\frac{1}{k\rho}\exp[i(k\rho+\theta_{pqj}^J)]. \quad (36)$$

[4] Eugene Wigner, *Gruppentheorie und Ihre Andwendung auf die Quantum Mechanik der Atmospektren* (J. W. Edwards, Ann Arbor, 1944), p. 206.

[5] Here ξ_e is the equilibrium value of ξ. At this point an approximation has been made which is related to the error made in uncoupling the rotation and vibration of the molecule. A more exact treatment would yield a similar result, except that $E_p+q(q+1)\hbar^2/2M\xi_e^2$ would be replaced by the energy of the combined rotation-vibration state.

[6] C. Zener, Phys. Rev. **37**, 556 (1931).

[7] Such a solution exists if $k>0$ and if $W_J(pqj|\,pqj)$ drops off sufficiently rapidly for large ρ. This is the only physically reasonable case.

The terms on the right of Eq. (32) (except the p, q, j term) are coupling terms. These terms are nonzero in so far as transitions in the molecular state occur. Since transitions occur relatively seldom, one can approximate these terms. To the zero approximation

$$G^J(p_0q_0j_0|pqj)=\delta_{jj_0}\delta_{pp_0}\delta_{qq_0}U_{pqj}{}^J. \quad (37)$$

This represents a solution in which there are no transitions in the molecular state.[8]

Using the zero-order solution in the coupling terms of Eq. (33) one obtains the approximate equation,

$$\left\{\frac{1}{\mu}\frac{d^2}{d\rho^2}+\frac{2}{\mu\rho}\frac{d}{d\rho}-\frac{j(j+1)}{\mu\rho^2}+(k^2/\mu)-W^J(pqj|pqj)\right\}G^J(p_0q_0j_0|pqj)$$
$$=(1-\delta_{qq_0}\delta_{pp_0}\delta_{jj_0})U_{pqoj_0}{}^JW^J(pqj|p_0q_0j_0). \quad (38)$$

This equation can be solved to obtain the perturbation solution,

$$G^J(p_0q_0j_0|pqj)=\delta_{jj_0}\delta_{pp_0}\delta_{qq_0}U_{pqj}{}^J-(1-\delta_{pp_0}\delta_{qq_0}\delta_{jj_0})\mu k\times\left\{\begin{array}{l}X_{pqj}{}^J\int_0^\rho U_{pqj}{}^J(\rho')W^J(pqj|p_0q_0j_0)(\rho')\\ \times U_{pqoj_0}{}^J(\rho')\rho'^2d\rho'+U_{pqj}{}^J\int_\rho^\infty X_{pqj}{}^J(\rho')\\ \times W^J(pqj|p_0q_0j_0)(\rho')U_{pqoj_0}{}^J(\rho')\rho'^2d\rho'\end{array}\right\}. \quad (39)$$

That Eq. (39) represents an exact solution of Eq. (38) can be seen from the following arguments: By direct substitution and making use of the definition of $U_{pqj}{}^J$ as a solution of Eq. (34) one has for the left side of Eq. (38),

$$k\rho^2(1-\delta_{pp_0}\delta_{qq_0}\delta_{jj_0})W^J(pqj|p_0q_0j_0)U_{pqoj_0}{}^J\times\left[X_{pqj}{}^J\frac{dU_{pqj}{}^J}{d\rho}-U_{pqj}{}^J\frac{dX_{pqj}{}^J}{d\rho}\right]. \quad (40)$$

But from the definitions of $U_{pqj}{}^J$ and $X_{pqj}{}^J$ and Eq. (34),

$$X_{pqj}{}^J\left\{\frac{d^2}{d\rho^2}+\frac{2}{\rho}\frac{d}{d\rho}\right\}U_{pqj}{}^J-U_{pqj}{}^J\left\{\frac{d^2}{d\rho^2}+\frac{2}{\rho}\frac{d}{d\rho}\right\}X_{pqj}{}^J=0, \quad (41)$$

or rearranging

$$\frac{1}{\rho^2}\frac{d}{d\rho}\left[\rho^2\left\{X_{pqj}{}^J\frac{dU_{pqj}{}^J}{d\rho}-U_{pqj}{}^J\frac{dX_{pqj}{}^J}{d\rho}\right\}\right]=0. \quad (42)$$

Eq. (42) may be integrated to give

$$\rho^2\left\{X_{pqj}{}^J\frac{dU_{pqj}{}^J}{d\rho}-U_{pqj}{}^J\frac{dX_{pqj}{}^J}{d\rho}\right\}=c, \quad (43)$$

where c is a constant of integration. The value of c may be obtained by considering the asymptotic form of $U_{pqj}{}^J$ and $X_{pqj}{}^J$. Thus from Eqs. (35) and (38)

$$c=1/k, \quad (44)$$

and the expression (40) becomes

$$(1-\delta_{pp_0}\delta_{qq_0}\delta_{jj_0})U_{n_0l_0j_0}{}^JW^J(pqj|p_0q_0j_0), \quad (45)$$

which is identical with the right side of Eq. (38).

From Eq. (39) we obtain the asymptotic form

$$G^J(p_0q_0j_0|pqj)=-\frac{i}{2k\rho}\exp[i(k\rho+\theta_{pqj}{}^J)]\times\left[\begin{array}{l}\delta_{jj_0}\delta_{pp_0}\delta_{qq_0}[1+2i\beta^J(pqj|p_0q_0j_0)]\\ -2i\beta^J(pqj|p_0q_0j_0)\end{array}\right]+\frac{i}{2k\rho}\exp[-i(k\rho+\theta_{pqj}{}^J)]\delta_{pp_0}\delta_{qq_0}\delta_{jj_0}, \quad (46)$$

where

$$\beta^J(pqj|p_0q_0j_0)=\mu k\int_0^\infty U_{pqj}{}^JW^J(pqj|p_0q_0j_0)U_{pqoj_0}{}^J\rho^2d\rho, \quad (47)$$

represents the effect of the interaction potential.

THE SCATTERING COEFFICIENTS

A general wave function was described by Eq. (17). It is necessary to fix the coefficients, $A_{J,\mu}{}^{p,q,j}$, so that this function has the form of the wave prescribed by Eq. (15). To accomplish this let us express the angles θ_1, φ_1, and θ_2, φ_2, in terms of the rotation, R, and the angle φ. The spherical harmonics themselves form a basis for an irreducible representation of three-dimensional rotation group. Hence,

$$O_RY_l{}^m(\theta,\varphi)=\sum_{m'}D^l(R)_{m'm}Y_l{}^{m'}(\theta,\varphi), \quad (48)$$

or

$$Y_l{}^m(\theta,\varphi)=\sum_{m'}D^l(R)_{mm'}{}^*Y_l{}^{m'}(\theta',\varphi'), \quad (49)$$

where the primed coordinates are the coordinates after rotation. The equation for the $\chi_s{}^J$, Eqs. (18), were derived in a previous paper.[1] These equations depend upon the choice of the "standard configuration." The stand-

[8] The δ_{jj_0} serves to specify the particular set of j-wave functions. The solution of the wave equation without a coupling potential is accidentally degenerate in j.

ard configuration was chosen so that when the system is in this configuration, molecule one (the free atom) is on the positive z axis and molecule two is in the xz plane with positive x. Hence, if R is taken to be the rotation which takes the system into the standard configuration then the coordinates after rotation are[9] $\theta_1'=0$ (φ_1', undefined), $\theta_2'=\varphi$ and $\varphi_2'=\pi/2$. Thus from the previous equation

$$Y_j^{\nu}(\theta_1,\varphi_1)=\sum_\alpha D^j(R)_{\nu\alpha}{}^* Y_j^{\alpha}(0,0) =(-1)^j[(2j+1)/4\pi]^{\frac{1}{2}} D^j(R)_{\nu 0}{}^*, \quad (50)$$

and

$$Y_l^m(\theta_2,\varphi_2)=\sum_\alpha D^l(R)_{m\alpha}{}^* Y_l^{\alpha}[\varphi,(\pi/2)] =\sum_\alpha (-i)^\alpha D^l(R)_{m\alpha}{}^* Y_l^{\alpha}(\varphi,0). \quad (51)$$

The $D^J(R)_{\mu s}$ satisfy the orthogonality condition

$$\int D^l(R)_{\mu\nu} D^{l'}(R)_{\mu'\nu'}{}^* dR=\delta_{ll'}\delta_{\mu\mu'}\delta_{\nu\nu'}\int dR/(2l+1), \quad (52)$$

and the quantities $s_{J\mu m}{}^{jl}$ are defined so that[4]

$$\int D^J(R)_{\mu s} D^j(R)_{\nu 0}{}^* D^l(R)_{m\alpha}{}^* dR =\frac{\delta_{\mu,\nu+m}\delta_{s,\alpha}}{2J+1} s_{J,\mu-m,m}{}^{jl} s_{J0s}{}^{jl}\int dR. \quad (53)$$

It is required that the wave function described by Eq. (17) be asymptotically equal to that described by Eq. (15). Thus if Eq. (15) is equated to the asymptotic form of Eq. (17); the resulting equation multiplied by $D^{J'}(R)_{\mu's'}$; integrated over R; and use is made of the four equations just derived the result (after dropping the primes) is that

$$-i(\pi)^{\frac{1}{2}}\sum_{nlmj}(-i)^s(-1)^j(2j+1)^{\frac{1}{2}} \times s_{J,\mu-m,m}{}^{jl} s_{J0s}{}^{jl} Y_l^s(\varphi,0) Z_n(\xi) \times\begin{bmatrix} \frac{1}{k\rho}e^{ik\rho}\{\alpha_{j,\mu-m}{}^{nlm}+(-1)^j[(2j+1)/4\pi]^{\frac{1}{2}} \times\delta_{nn_0}\delta_{ll_0}\delta_{mm_0}\delta_{\mu m}\} \\ -\frac{1}{k\rho}e^{-ik\rho}[(2j+1)/4\pi]^{\frac{1}{2}}\delta_{nn_0}\delta_{ll_0}\delta_{mm_0}\delta_{\mu m} \end{bmatrix} \rightarrow\sum_{pqj} A_{J\mu}{}^{pqj}\chi_s{}^J(p,q,j). \quad (54)$$

The Eqs. (25) and (26) are used to obtain an expression for $\chi_s{}^J(p,q,j)$

$$\chi_s{}^J(p,q,j)=\sum_{p'q'j'}(-i)^s s_{J0s}{}^{j'q'} \times Y_{q's}(\varphi,0) Z_{p'}(\xi) G^J(pqj|p'q'j'). \quad (55)$$

If Eq. (55) is used for $\chi_s{}^J$ in Eq. (54), this equation multiplied by $Z_{n'}(\xi)^* Y_{l's}(\varphi,0)^*$, and use is made of the orthogonality of these functions, it follows after integration over ξ and φ that

$$-i(\pi)^{\frac{1}{2}}\sum_{mj}(-1)^j(2j+1)^{\frac{1}{2}} s_{J,\mu-m,m}{}^{jl} s_{J0s}{}^{jl} \times\begin{bmatrix} \frac{1}{k\rho}e^{ik\rho}\{\alpha_{j,\mu-m}{}^{nlm} \\ +(-1)^j\left(\frac{2j+1}{4\pi}\right)^{\frac{1}{2}}\delta_{nn_0}\delta_{ll_0}\delta_{mm_0}\delta_{\mu m}\} \\ -\frac{1}{k\rho}e^{-ik\rho}\left(\frac{2j+1}{4\pi}\right)^{\frac{1}{2}}\delta_{nn_0}\delta_{ll_0}\delta_{mm_0}\delta_{\mu m} \end{bmatrix} \rightarrow\sum_{pqjj'} A_{J\mu}{}^{pqj} s_{J0s}{}^{j'l} G^J(pqj|nlj'). \quad (56)$$

This equation is multiplied by $s_{J0s}{}^{j''l}$ and summed over the index s. Then using the orthogonality condition, Eq. (31) it follows that

$$-i(-1)^{j'}(\pi)^{\frac{1}{2}}(2j'+1)^{\frac{1}{2}}\sum_m s_{J,\mu-m,m}{}^{j'l} \times\begin{bmatrix} \frac{1}{k\rho}e^{ik\rho}\{\alpha_{j',\mu-m}{}^{nlm} \\ +(-1)^{j'}\left(\frac{2j'+1}{4\pi}\right)^{\frac{1}{2}}\delta_{nn_0}\delta_{ll_0}\delta_{mm_0}\delta_{\mu m}\} \\ -\frac{1}{k\rho}e^{-ik\rho}\left(\frac{2j'+1}{4\pi}\right)^{\frac{1}{2}}\delta_{nn_0}\delta_{ll_0}\delta_{mm_0}\delta_{\mu m} \end{bmatrix} \rightarrow\sum_{pqj} A_{J\mu}{}^{pqj} G^J(pqj|nlj'). \quad (57)$$

The constants $A_{J\mu}{}^{pqj}$ and the scattering amplitudes $\alpha_{j\nu}{}^{nlm}$ can be obtained by making use of Eq. (46) for the asymptotic form of $G^J(p_0q_0j_0|pqj)$. Equating the coefficients of $e^{-ik\rho}$ one has

$$A_{J\mu}{}^{pqj}=\delta_{pn_0}\delta_{ql_0}\delta_{\mu m_0}(2j+1)s_{J0\mu}{}^{jq}\exp(i\theta_{pqj}{}^J). \quad (58)$$

Equating the coefficients of $e^{ik\rho}$ and making use of Eq. (57) one obtains

$$2(\pi)^{\frac{1}{2}}(2j'+1)^{\frac{1}{2}}\sum_m s_{J,\mu-m,m}{}^{j'l'}\left\{\alpha_{j',\mu-m}{}^{n'l'm} +(-1)^{j'}\left(\frac{2j'+1}{4\pi}\right)^{\frac{1}{2}}\delta_{n'n_0}\delta_{l'l_0}\delta_{mm_0}\delta_{\mu m}\right\} =\delta_{\mu m_0}\sum_j(2j+1)s_{J0\mu}{}^{jl_0}\exp[i(\theta_{n_0l_0j}{}^J+\theta_{n'l'j}{}^J)] \times\begin{bmatrix}\delta_{n_0n'}\delta_{l_0l'}\delta_{jj'}[1+2i\beta^J(n'l'j'|n_0l_0j)] \\ -2i\beta^J(n'l'j'|n_0l_0j)\end{bmatrix}. \quad (59)$$

[9] In the definition of the polar coordinates adopted by Wigner (see reference 4) the azimuthal angle φ is measured from the yz plane in a positive sense toward the xz plane. This relation between the Cartesian coordinates and the polar coordinates was used in obtaining the expression for the derivations of the $D_J(R)_{\mu\nu}$ (see J. O. Hirschfelder and E. P. Wigner, Proc. Nat. Acad. Sci. **21**, 113 (1935)). These expressions in turn were used in obtaining Eqs. (18) (see reference 1). It is perhaps unfortunate that this unusual convention was adopted. However, this convention is not involved in the application of the results of this paper.

This equation is multiplied by $s_{J,\mu-m',m'}{}^{j'l'}$, and summed over all values of J. Then making use of the orthogonality relation

$$\sum_J s_{J,\mu-m',m'}{}^{j'l'} s_{J,\mu-m,m}{}^{j'l'} = \delta_{mm'}.$$

Equation (58) can be solved for the scattering amplitudes

$$\alpha_{j\nu}{}^{nlm} = \frac{\delta_{\nu,m_0-m}}{2(\pi)^{\frac{1}{2}}(2j+1)^{\frac{1}{2}}} \sum_{J,j_0} (2j_0+1) s_{J\nu m}{}^{jl} s_{Jm_0}{}^{j_0l_0} \times \exp(i\theta_{n_0l_0l_0}{}^J) \times \begin{bmatrix} \delta_{nn_0}\delta_{ll_0}\delta_{jj_0}\{\exp(i\theta_{n_0l_0j_0}{}^J) \\ -(-1)^j \exp(-i\theta_{n_0l_0j_0}{}^J)\} \\ -2i(1-\delta_{nn_0}\delta_{ll_0}\delta_{jj_0}) \\ \times \exp(i\theta_{nlj}{}^J)\beta^J(nlj\,|\,n_0l_0j_0) \end{bmatrix}. \quad (60)$$

This expression gives explicitly the scattering amplitudes. The absolute square of $\alpha_{j\nu}{}^{nlm}$ is the probability of a transition in the state of the molecule from the state (n_0, l_0, m_0) to the state (n, l, m) in a collision in which the angular dependence of the scattered wave is given by the spherical harmonic (j, ν). Each term in the sum may be interpreted, loosely, as the result of a particular type of collision. The index j_0 refers to the angular momentum of the atom with respect to the molecule before the collision. This index is a manifestation of the classical "impact parameter." From the classical point of view, because of the lack of spherical symmetry, an additional parameter is needed to describe the collision. This appears in the index, J, which measures the total angular momentum of the system. That is, the atom may approach (classically) so that its angular momentum adds to or subtracts from that the molecule. Because of the properties of the $s_{J\nu m}{}^{jl}$, it follows from Eq. (60) that J is restricted by both

$$|j-l| \leqslant J \leqslant j+l, \quad (61)$$

and

$$|j_0-l_0| \leqslant J \leqslant j_0+l_0. \quad (62)$$

Hence the sum over J is a finite sum. From the physical arguments it is clear that for reasonable potential functions the sum over j_0 converges rapidly. The actual evaluation of the scattering amplitudes for a particular potential function is being carried out.

APPENDIX A

Condon and Shortley[10] have obtained various recursion relations among the $s_{J\mu\nu}{}^{jl}$. Their Eq. (3), p. 74, written in the present notation is

$$[(J+\mu+\nu+1)(J-\mu-\nu)]^{\frac{1}{2}} s_{J\mu\nu}{}^{jl} = [(j+\mu+1)(j-\mu)]^{\frac{1}{2}} s_{J,\mu+1,\nu}{}^{jl} + [(l+\nu+1)(l-\nu)]^{\frac{1}{2}} s_{J,\mu,\nu+1}{}^{jl}. \quad (A1)$$

[10] E. U. Condon and G. H. Shortley, *The Theory of Atomic Spectra* (Cambridge University Press, London, 1935).

An analogous expression can easily be obtained (by considering the lowering operator),

$$[(J-\mu-\nu+1)(J+\mu+\nu)]^{\frac{1}{2}} s_{J,\mu,\nu}{}^{jl} = [(j-\mu+1)(j+\mu)]^{\frac{1}{2}} s_{J,\mu-1,\nu}{}^{jl} + [(l-\nu+1)(l+\nu)]^{\frac{1}{2}} s_{J,\mu,\nu-1}{}^{jl}. \quad (A2)$$

If Eq. (A2) written with μ replaced by $\mu+1$ is used to replace the first term on the right side of Eq. (A1), and if Eq. (A2) written with ν replaced by $\nu+1$ is used to replace the second, there results

$$[J(J+1)-l(l+1)-j(j+1)-2\mu\nu] s_{J,\mu,\nu}{}^{jl} = [j(j+1)-\mu(\mu+1)]^{\frac{1}{2}}[l(l+1)-\nu(\nu-1)]^{\frac{1}{2}} s_{J,\mu+1,\nu-1}{}^{jl} + [j(j+1)-\mu(\mu-1)]^{\frac{1}{2}}[l(l+1)-\nu(\nu+1)]^{\frac{1}{2}} \times s_{J,\mu-1,\nu+1}{}^{jl}. \quad (A3)$$

It has been shown elsewhere[11] that the coefficients satisfy the relation

$$s_{J\mu\nu}{}^{jl} = (-1)^{J+j+\nu}\left(\frac{2J+1}{2j+1}\right)^{\frac{1}{2}} s_{j,\mu+\nu,-\nu}{}^{Jl}. \quad (A4)$$

Thus from Eq. (A3)

$$[J(J+1)+l(l+1)-j(j+1)-2\mu\nu] s_{J,\mu-\nu,\nu}{}^{jl} = [J(J+1)-\mu(\mu+1)]^{\frac{1}{2}}[l(l+1)-\nu(\nu+1)]^{\frac{1}{2}} s_{J,\mu-\nu,\nu+1}{}^{jl} + [J(J+1)-\mu(\mu-1)]^{\frac{1}{2}}[l(l+1)-\nu(\nu-1)]^{\frac{1}{2}} \times s_{J,\mu-\nu,\nu-1}{}^{jl}. \quad (A5)$$

Wigner[3] has shown that the coefficients satisfy the orthogonality relation

$$\sum_\mu s_{J,\mu,m-\mu}{}^{jl} s_{J',\mu,m-\mu}{}^{jl} = \delta_{J,J'}. \quad (A6)$$

From the identity, Eq. (A4), it follows that another orthogonality condition holds,

$$\sum_s s_{J,m,s-m}{}^{jl} s_{J,m,s-m}{}^{j'l} = \delta_{jj'}(2J+1)/(2j+1). \quad (A7)$$

APPENDIX B

The treatment in this paper and the previous paper[1] is based on the group theory presented by Wigner.[4] In particular we have used his explicit form of the representation coefficients and the coefficients $s_{J\mu\nu}{}^{jl}$. Because of the relation of the representation coefficients to the spherical harmonics, Eq. (50), it is necessary to use a consistent definition of the spherical harmonics. Thus we define

$$Y_l{}^m(\theta,\varphi) = i^{|m|-m}\left[\frac{(2l+1)(l-|m|)!}{4\pi(l+|m|)!}\right]^{\frac{1}{2}} P_l{}^m(\theta) e^{-im\varphi}; \quad (B1)$$

where

$$P_l{}^m(\theta) = P_l{}^{-m}(\theta) = \frac{\sin^m\theta}{2^l l!}\frac{d^{l+m}}{d(\cos\theta)^{l+m}}\sin^{2l}\theta; \quad m \geqslant 0. \quad (B2)$$

[11] To be published.

Differentiating Eq. (B2), one obtains the relation

$$P_l^{m+1}=-\frac{dP_l^m}{d\theta}+m\cot\theta P_l^m;\quad m>0. \tag{B3}$$

Thus from Eq. (B1)

$$[(l+m+1)(l-m)]^{\frac{1}{2}}Y_l^{m+1}(\theta,0)$$
$$=-\frac{d}{d\theta}Y_l^m(\theta,0)+m\cot\theta Y_l^m(\theta,0);\quad m>0, \tag{B4}$$

or since

$$Y_l^m(\theta,\varphi)=(-1)^mY_l^{-m}(\theta,\varphi)^*, \tag{B5}$$

$$[(l+m)(l-m+1)]^{\frac{1}{2}}Y_l^{m-1}(\theta,0)$$
$$=\frac{d}{d\theta}Y_l^m(\theta,0)+m\cot\theta Y_l^m(\theta,0);\quad m<0. \tag{B6}$$

A standard recursion relation[12] among the $P_l^m(\theta)$ is

$$P_l^{m+1}(\theta)+(l-m+1)(l+m)P_l^{m-1}(\theta)$$
$$=2m\cot\theta P_l^m(\theta);\quad m\geqslant 1. \tag{B7}$$

Thus from Eq. (B1)

$$[(l+m+1)(l-m)]^{\frac{1}{2}}Y_l^{m+1}(\theta,0)$$
$$+[(l+m)(l-m+1)]^{\frac{1}{2}}Y_l^{m-1}(\theta,0)$$
$$=2m\cot\theta Y_l^m(\theta,0);\quad m\geqslant 1. \tag{B8}$$

or using Eq. (B5) the same expression is valid for $m\leqslant -1$. Since the expression is trivially correct for $m=0$, it is valid for all integer m.

[12] See, for example, E. Jahnke and F. Emde, *Tables of Functions* (Dover Publications, New York, 1945), p. 114.

Using Eq. (B8), Eq. (B4) becomes

$$[(l+m)(l-m+1)]^{\frac{1}{2}}Y_l^{m-1}(\theta,0)$$
$$=(d/d\theta)Y_l^m(\theta,0)+m\cot\theta Y_l^m(\theta,0);\quad m\geqslant 0, \tag{B9}$$

and Eq. (B6) becomes

$$[(l+m+1)(l-m)]^{\frac{1}{2}}Y_l^{m+1}(\theta,0)$$
$$=-\frac{d}{d\theta}Y_l^m(\theta,0)+m\cot\theta Y_l^m(\theta,0);\quad m\leqslant 0. \tag{B10}$$

From Eqs. (B4) and (B10), one has for all m

$$[(l+m)(l-m+1)]^{\frac{1}{2}}Y_l^m(\theta,0)$$
$$=-\left[\frac{d}{d\theta}-(m-1)\cot\theta\right]Y_l^{m-1}(\theta,0), \tag{B11}$$

and from Eqs. (B6) and (B9) for all m

$$[(l+m+1)(l-m)]^{\frac{1}{2}}Y_l^m(\theta,0)$$
$$=\left[\frac{d}{d\theta}+(m+1)\cot\theta\right]Y_l^{m+1}(\theta,0). \tag{B12}$$

Then from Eq. (A5)

$$[J(J+1)+l(l+1)-j(j+1)-2\mu s]s_{J,\mu-s,s}{}^{jl}Y_l^s(\theta,0)$$
$$=[J(J+1)-\mu(\mu+1)]^{\frac{1}{2}}s_{J,\mu-s,s+1}{}^{jl}$$
$$\times\left[\frac{d}{d\theta}+(s+1)\cot\theta\right]Y_l^{s+1}(\theta,0)$$
$$-[J(J+1)-\mu(\mu-1)]^{\frac{1}{2}}s_{J,\mu-s,s-1}{}^{jl}$$
$$\times\left[\frac{d}{d\theta}-(s-1)\cot\theta\right]Y_l^{s-1}(\theta,0). \tag{B13}$$

Photochemical Oxidation-Reduction and Photocatalysis. The Photochemical Activity of $FeCl_4^-$ in Alcohol as Oxidizing Agent and as Catalyst

G. J. Brealey and Norbert Uri*
Department of Chemistry, University of Manchester, Manchester, England
(Received July 16, 1951)

A true photocatalytic reaction in which the concentration of the sensitizer remains constant is described in this paper. It is shown that $FeCl_4^-$ acts as a photocatalyst for the oxidation of alcohol by thionine. In the absence of thionine $FeCl_4^-$ is the oxidizing agent. A mechanism is put forward which includes (1) photoexcitation, primary dark back reaction and separation of the primary product, (2) oxidation of the CH_3CHOH radical by $FeCl_4^-$, (3) reaction between two CH_3CHOH radicals, (4) oxidation of $FeCl_4^-$ by thionine. The latter occurs because of a considerable shift in the oxidation-reduction potential by the complexing of both ferric and ferrous iron. Various constants and constant ratios are evaluated from the experimental results.

A NEW interpretation of the absorption spectra of ferric salt solutions was worked out and some predictions on their photochemistry were made by Rabinowitch.[1] Recently Evans and Uri[2] have experimentally confirmed the occurence of free radicals in irradiated aqueous ferric salt solutions. The free radicals produced can lead to the initiation of polymerization of vinyl compounds[3] or oxidation of organic substrates.[4] In a preliminary note[5] our observations on the phenomena of the photoreduction of $FeCl_4^-$ in alcohol were reported both in the absence and in the presence of thionine. In the latter case $FeCl_4^-$ acts as photocatalyst for the reduction of thionine by alcohol. This effect occurs because of a shift in the oxidation-reduction potential of 0.5 volt of the ferric-ferrous system in alcohol on addition of sufficient excess of chloride ion.

EXPERIMENTAL

The materials used were: AnalaR ferric chloride (anhydrous) B.D.H.; lithium chloride (B.D.H.) purified by centrifuging the alcoholic solutions, purity test by measurement of absorption spectrum; thionine (B.D.H.),

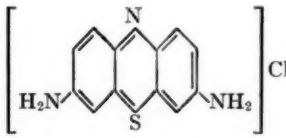

recrystallized twice from dilute hydrochloric acid. (Acidic stock solutions of thionine in alcohol were kept in the dark in Pyrex vessels; the latter precaution was taken as a result of the experience reported by Epstein, Karush, and Rabinowitch.[6]) AnalaR perchloric acid (B.D.H.). Absolute alcohol (clinical) not less than 99.5 percent C_2H_5OH. The light source was: A ME/D 250-watt high pressure mercury vapor lamp (compact source); a box model supplied by B.T.H. was used for all experiments unless otherwise stated. The light was condensed by a plain-convex quartz lens to a nearly parallel beam.

Isolation of Spectral Lines

(a) 365 mμ. 3 mm Chance OX 1 filter, 1 cm of $CuSO_4 \cdot 5H_2O$ solution (125 g $CuSO_4 \cdot 5H_2O$ (B.D.H. AnalaR)/liter) in a rectangular quartz cell.

(b) 313 mμ. 2 mm Chance OX 7 filter, 5 cm nickel sulfate solution (400 g $NiSO_4 \cdot 7H_2O$ (B.D.H. AnalaR)/liter) in a square quartz cell +1 cm of potassium biphthalate solution (5 g KH-phthalate (B.D.H. AnalaR)/liter) in a rectangular cell.

(c) 254 mμ. A low vapor pressure mercury lamp was used with a relative output of 98 percent of 254 mμ and a filter of 1 cm 4 M CH_3COOH, (B.D.H. AnalaR).

The reaction cell was made of quartz and was of square cross section. Its dimensions were 5 cm×5 cm ×1.03 cm (thickness of solution layer). It had two outlet tubes with B14 joints. Solutions were deaerated with nitrogen purified from traces of oxygen by passing it through alkaline sodium hydrosulfite+sodium anthraquinone 2-sulfonate.

Chemical Actinometry

Recrystallized uranyl oxalate (B.D.H.) was used. Standard solutions were prepared in accordance with the specifications given by Bowen.[7] The accuracy of the method was ±2 percent. Gauzes of different transmissions were used for variation of light intensity.

The reaction was followed by measuring the absorption of the light from a parallel beam produced by a small tungsten lamp (run from a 6-volt (120 amp/hr) accumulator with rheostat) with condenser lens and iris diaphragm. We used Ilford filters for the isolation of spectral regions suitable for measuring ferric chloride

* Present address: Institute of Radiobiology and Biophysics, University of Chicago, Chicago 37, Illinois.

[1] E. Rabinowitch, Revs. Modern Phys. **14**, 112 (1942); E. Rabinowitch and W. H. Stockmayer, J. Am. Chem. Soc. **64**, 335 (1942).

[2] M. G. Evans and N. Uri, Nature **164**, 404 (1949); J. Soc. Dyers and Colourists **65**, 709 (1949).

[3] Evans, Santappa, and Uri, J. Polymer Sci. **7**, 243 (1951).

[4] Bates, Evans, and Uri, Nature **166**, 869 (1950).

[5] Brealey, Evans, and Uri, Nature **166**, 959 (1950).

[6] Epstein, Karush, and Rabinowitch, J. Opt. Soc. Am. **31**, 77 (1941).

[7] E. J. Bowen, *Chemical Aspects of Light* (Oxford University Press, Oxford, 1946).

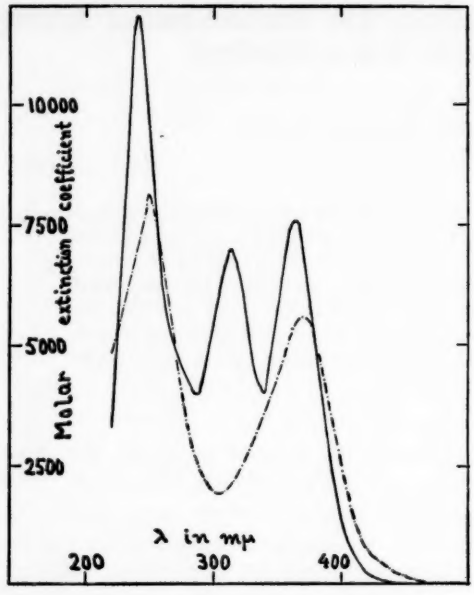

FIG. 1. Absorption spectra of $FeCl_4^-$ and $FeCl_3$ in alcohol (in the near U. V.) Fully drawn: $[FeCl_3]=0.956\times10^{-4}$ M; [LiCl] =0.4 M; $[HClO_4]=0.96\times10^{-2}$ M; $H_2O=1$ percent. Dotted: $[FeCl_3]=0.956\times10^{-4}$ M; $[HClO_4]=0.96\times10^{-2}$ M; $H_2O=1$ percent. No lithium chloride.

and thionine concentrations. In most experiments the light transmission was measured with a phototube (RCA 931A)-multiplier unit designed and constructed in this laboratory by Mr. Trowse and Mr. Nelson.

Analysis

For the purpose of photometric calibration ferric chloride solutions in alcohol were standardized by the Zimmerman Reinhardt method after evaporation of the alcohol. Lithium chloride solutions were standardized argentometrically. The purity of the thionine was checked by microanalysis (for elements) and spectrophotometrically. The Unicam SP-500 spectrophotometer was used throughout this work.

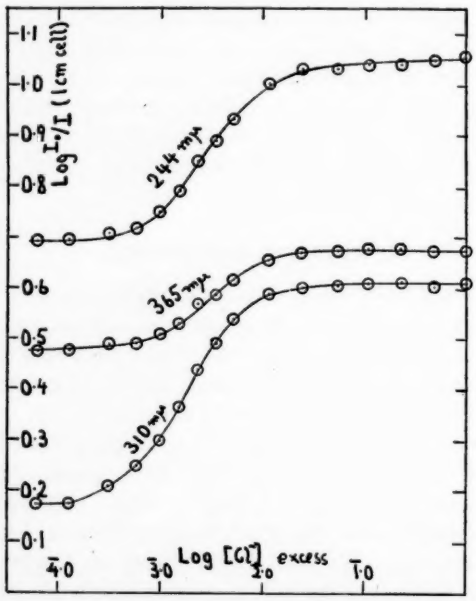

FIG. 2. Effect of LiCl on the optical density of $FeCl_3$ solutions. $[FeCl_3]=0.90\times10^{-4}$ M; $[HClO_4]=0.96\times10^{-2}$ M; $H_2O=1$ percent.

Results

(1) *Ferric Chloride Complexes in Alcohol and Their Absorption Spectra*

The absorption spectrum of $FeCl_3$ in 99 percent ethyl alcohol at a perchloric acid concentration of 10^{-2} M is given in Fig. 1, (dotted curve). At concentrations $<10^{-4}$ Beer's Law is obeyed and there is no evidence of dimerization. The absorption curve for $FeCl_3$ was obtained from a solution of 10^{-4} M $FeCl_3$. At higher concentrations $\leftrightharpoons10^{-3}$ M the optical density is no longer a linear function of concentration; this can be accounted

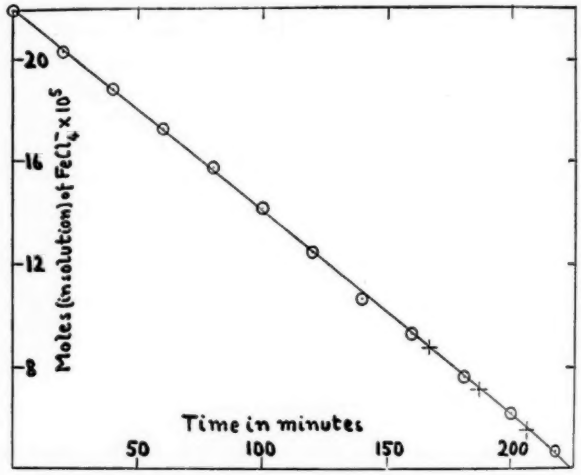

FIG. 3. Zero-order photoreduction of $FeCl_4^-$ (concentration range: 10^{-2} to 10^{-3} M). $[HClO_4]=1.04\times10^{-2}$ M; [LiCl]=0.4 M; Initial $FeCl_4^-$: ⊙ 0.994×10^{-2} M; + 0.398×10^{-2} M; $H_2O=1$ percent. Lamp output=quanta absorbed=2.55×10^{-6} $Nh\nu$/min.

for by formation of Fe_2Cl_6, which has been postulated in some organic solvents, e.g., ethyl acetate. On the addition of lithium chloride the absorption spectrum in alcohol changes as a result of the formation of $FeCl_4^-$. Figure 1 (fully drawn curve) shows the spectrum of $FeCl_4^-$ obtained from a solution at a LiCl concentration of 0.4 M. The dependence of the optical density at three wavelengths (244 mμ, 310 mμ, 365 mμ) on the lithium chloride concentration is plotted in Fig. 2. The optical density increases until a constant value is reached at a certain lithium chloride concentration ($\sim10^{-2}$ M). Above this concentration the spectrum obtained shows similar peaks to those of ferric chloride in concentrated aqueous hydrochloric acid or in ether extracts of aqueous solutions of ferric chloride in 6 N hydrochloric acid. These peaks were also observed by Metzler and Myers.[8] The species present in the ether

[8] D. E. Metzler and R. J. Myers, J. Am. Chem. Soc. 72, 3776 (1950).

extract and also in 12 N aqueous hydrochloric acid was considered to be $FeCl_4^-$ (Nekrasov and Ovsyankina[9]). The peak at 310 mμ is apparently specific for $FeCl_4^-$ and becomes fully pronounced in alcohol above LiCl concentrations of 10^{-2} M.

An attempt to verify the formula $FeCl_4^-$ was made by plotting $\log[FeCl_4^-]/[FeCl_3]$ evaluated from the absorption spectra against log[LiCl]. A straight line was obtained with a slope of ~1.4 instead of the expected slope of 1. This deviation might be due to partial solvolysis of $FeCl_3$ (reducing the Cl:Fe ratio in $FeCl_3$) or to the formation of Fe_2Cl_6.

The stability of $FeCl_4^-$ complex in ethyl alcohol is not markedly effected either by addition of water up to 10 vol percent (in contrast to the assumption we make on the $FeCl_4^=$ complex) or by addition of 60 percent aqueous perchloric acid up to a concentration of 0.75 N. (The maximum decrease in the intensity of the bands is ~5 percent.)

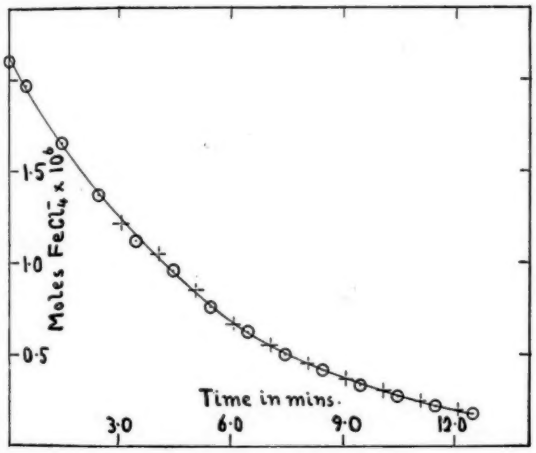

FIG. 4. Photoreduction of $FeCl_4^-$ (concentration range 10^{-4} to 10^{-5} M). Initial $[FeCl_4^-]$: ⊙ 0.956×10^{-4} M; + 0.55×10^{-4} M; $[HClO_4]=1.04\times10^{-2}$ M; [LiCl]=0.40 M; H_2O=1 percent. Volume of solution=22 ml. Lamp output=1.81×10^{-6} $Nh\nu$/min.

(2) *The Photoreduction of $FeCl_4^-$ by Ethyl Alcohol (in the Absence of Thionine)*

(a) *At a concentration range of 10^{-2} M to 10^{-3} M.*—Figure 3 shows that the photoreduction (with the 365 mμ line) of $FeCl_4^-$ under these conditions is a zero-order one. The solution was completely absorbing during 95 percent of the course of the reaction and the linearity of the graphs (in Fig. 3) is at least as good as the constancy of the lamp output. Another experiment with an initial concentration of 4×10^{-3} M $FeCl_4^-$ gave a reaction curve (also shown in Fig. 3 by crosses) which was practically identical with the lower part of the line of the experiment with the initial 10^{-2} M $FeCl_4^-$ concentration. The identity of the two curves and their linearity would indicate the absence of a back reaction resulting from accumulation of ferrous ion. The results were well reproducible. We evaluated the quantum efficiency for the disappearance of $FeCl_4^-$ as 0.31 (±3 percent).

[9] B. V. Nekrasov and V. V. Ovsyankina, J. Gen. Chem. (U.S.S.R.) **8**, 573 (1941).

TABLE I. The dependence of the quantum efficiency on the $FeCl_4^-$ concentration.

$[FeCl_4^-]\times10^5$ moles/liter	γ
7.33	0.215
5.78	0.205
4.54	0.199
3.50	0.195
2.57	0.189
2.02	0.178

Experimental Conditions. $[FeCl_4^-]=0.956\times10^{-4}$ M; $[HClO_4]=1.05\times10^{-2}$ M; [LiCl]=0.40 M; H_2O=1 percent; Volume of solution=22 ml; ($I=3.01\times10^{-6}$ $Nh\nu$/min).

(b) *At a concentration range of 10^{-4} M to 10^{-5} M $FeCl_4^-$.*—In this concentration range the light absorption for the 1-cm cell is no longer complete, and the change in the absorption fraction has to be taken into account. It was then observed that the net quantum efficiency (the correction for the absorption fraction having been made) was no longer constant but decreases with decreasing $FeCl_4^-$ concentration. The results of the reaction measured under these conditions are given in Fig. 4. Again it is noticeable that with an experiment which was started with about half the original concentration the curve obtained is identical with the lower half of the former experiment, indicating the lack of a secondary back reaction or any positive or negative autocatalysis. The variation of the quantum efficiency with decreasing $FeCl_4^-$ concentration (evaluated from a similar experiment) is given in Table I.

The dependence of the quantum yield on the light intensity (with 365 mμ) is shown in Fig. 5. The initial ferric concentration was the same (2.5×10^{-5}) in the different experiments; the photoreduction was followed to a concentration of 5×10^{-6} M $FeCl_4^-$ and $d[FeCl_4^-]/dt$ determined at 1.20×10^{-5} M $FeCl_4^-$ and 0.72×10^{-5} M

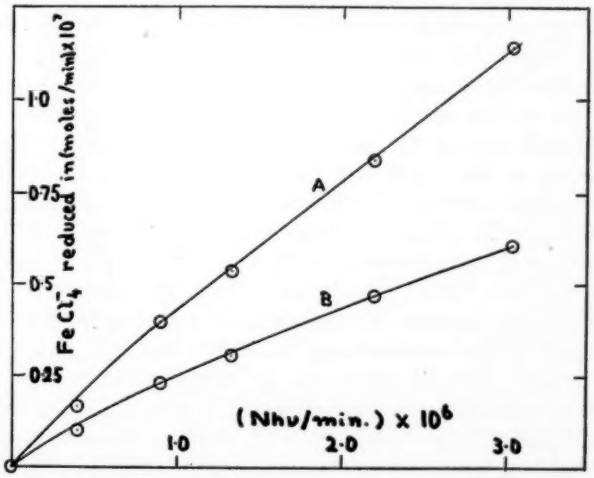

FIG. 5. Effect of light intensity on the photoreduction of $FeCl_4^-$. Final concentration: A—$FeCl_4^-$ conc: 1.20×10^{-5} M (k_ϵ=0.191); B—$FeCl_4^-$ conc: 0.72×10^{-5} M (k_ϵ=0.120). The initial concentration of $FeCl_4^-$ was 2.39×10^{-5} M. $[HClO_4]=1.05\times10^{-2}$ M; [LiCl]=0.40 M; H_2O=1 percent, vol=22 ml.

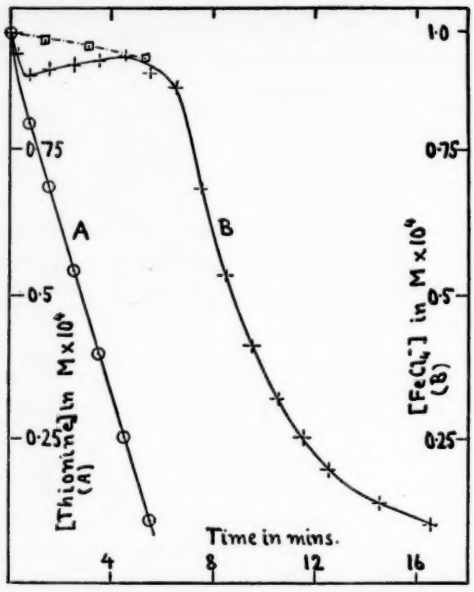

FIG. 6. Photobleaching of thionine (concentration of $[FeCl_4^-] = \sim 10^{-4}$ M). Initial $[FeCl_4^-]$ (curve A) 0.956×10^{-4} M; Initial [thionine] (curve B) 0.956×10^{-4} M; $[HClO_4] = 1.05 \times 10^{-2}$ M; [LiCl] = 0.4 M; H_2O = 1 percent, vol = 22 ml; ($I = 3.01 \times 10^{-6}$ $Nh\nu$/min).

$FeCl_4^-$ from the slope of the reaction curve. These reaction rates were plotted against the light intensity. The graph (Fig. 5) shows a measurable deviation from linearity. The quantum efficiency increases considerably but by less than a factor of two at the lowest intensities.

(3) *The Reduction of $FeCl_3$*

The photoreduction of $FeCl_3$ by ethyl alcohol is less clear-cut, as $FeCl_4^-$ is formed by liberation of Cl^- ions in the course of the reaction. The partial dimerization is an additional complicating factor. A graphical presentation shows the course of the photoreduction with an initial concentration of 10^{-4} M $FeCl_3$ in the range where Beer's Law is obeyed and an experiment started at about half the initial concentration (marked by crosses) gave again an identical curve with the lower part of the original one, indicating that no product formed during the reaction effected its course. The shape of the curve and the decrease of the quantum efficiency with time are similar to the observations made with $FeCl_4^-$. The maximum quantum efficiency (with 365 mμ) was, however, 0.58, i.e., considerably larger than with $FeCl_4^-$. At larger initial concentrations of $FeCl_3$ the reaction kinetics become very confused as a result of (a) nonobeyance of Beer's law, presumably because of dimerization and (b) formation of $FeCl_4^-$ in the course of the reaction resulting from liberation of the chloride ions by the photoreduction. Some reliance may, however, be placed on the initial quantum efficiency of $FeCl_3$ disappearance which was approximately 1.15. As this quantum efficiency was more than double the lowest observed, and some additional support for the dimerization of $FeCl_3$ was thus obtained.

(4) *The Depencence of the Quantum Efficiency on the Wavelength*

The three peaks of the absorption spectrum of $FeCl_4^-$ nearly coincide (accidentally) with the intense mercury lines at 254 mμ, 313 mμ, and 365 mμ. We measured the quantum efficiency with solutions containing 10^{-2} M $FeCl_4^-$, as under these conditions the maximum value is obtained which is independent of concentration at this order of molarities. There was no change in the order of the reaction caused by the variation of the wavelength; a zero-order reaction was observed in all cases. The values obtained—using the uranyl oxalate actinometer—were: 0.31 for 365 mμ, 0.49 for 313 mμ, and 0.58 for 254 mμ.

(5) *The Stoichiometry of the Reaction*

In order to investigate the final products of the overall reaction we irradiated a solution of 10^{-1} M $FeCl_4^-$ in alcohol until the ferric ion was quantitatively reduced. We showed that the oxidation product was acetaldehyde (by characterization with dimedone) and determined it quantitatively as the 2–4 dinitrophenylhyrazone. The yield of acetaldehyde was 97 percent of the theoretical, the empirical correction factor being allowed for. This is on the assumption that two moles of ferric ion are reduced for one mole of acetaldehyde formed. As a result of technical difficulties in the analysis we did not investigate or determine the final products, formed in experiments with the low initial concentrations of 10^{-4} M $FeCl_4^-$, where we reported some deviation in the quantum efficiency.

(6) *The System $FeCl_4^-$—Alcohol in the Presence of Thionine*

There is neither a thermal nor a photochemical reaction of thionine with alcohol under our conditions. Thionine is bleached, however, during the irradiation of the preceding system because of its reduction by the ferrous complex formed.

(a) *Concentration range 10^{-4} M to 10^{-5} M.* We irradiated (with 365 mμ) the system $[FeCl_4^-] = 10^{-4}$ M, $[HClO_4] = 10^{-2}$ M, [thionine] = $\sim 10^{-4}$ M, ethyl alcohol = 99 vol percent. The bleaching of thionine was observed by measuring light absorption with green light. Figure 6 shows that the reduction is a zero-order one from 5 percent to 95 percent bleaching. Simultaneously the reduction of $FeCl_4^-$ was studied by measuring light absorption at 365 mμ. With this wavelength and concentrations the absorption of $FeCl_4^-$ is predominant, but a correction is necessary for the absorption of thionine and its reduction products. Curve B in Fig. 6 (crosses) shows the disappearance of $FeCl_4^-$ allowing for the absorption of thionine and leucothionine but neglecting the unknown contribution to the light absorption by semithionine. It is seen from the figure that to a first approximation the concentra-

tion of $FeCl_4^-$ remains constant, while the thionine is reduced; subsequently, $FeCl_4^-$ is itself reduced, and the course of the reaction is similar to that in the absence of thionine.

(b) *Concentration range 10^{-2} M to 10^{-3} M.* Figure 7 shows that the bleaching of thionine in the system $[FeCl_4^-]=10^{-2}$ M, $[HClO_4]=10^{-2}$ M, [thionine] $=4\times10^{-5}$ M when irradiated with 365 mμ (over 99.5 percent of the light is, under these conditions, absorbed by $FeCl_4^-$) is of zero order, initially. When the leucodye accumulates there is some deviation from the zero-order reaction which is caused by the equilibrium of the redox system; thionine+ferrous complex⇌leucothionine+ferric complex.

DISCUSSION

(1) The Primary Step

The large molar extinction coefficient ($\epsilon=5000-12000$) in the light absorption of $FeCl_4^-$ in the near U.V. and its photochemical activity suggest by comparison with various ion pair complexes[1] an "electron transfer" spectrum. There are a number of possibilities as to how the primary electron transfer occurs: (a) an electron transfer involving a solvent molecule in the solvation layer in accordance with Farkas and Farkas[10] (J. Franck[11] assumed that in this case the electron is spread out over the solvation layer as a whole).

(a) $FeCl_4^-(CH_3CH_2OH)\xrightarrow{h\nu}FeCl_4^{=}(CH_3CH_2OH)^+$

or

(b) $FeCl_4^-(HOH)\xrightarrow{h\nu}FeCl_4^{=}(HOH)^+$

(c) $FeCl_4^-$ solvated $\xrightarrow{h\nu}FeCl_3^-$, Cl (solvated).

The primary excitation process could, however, not effect the kinetics because (a) $(CH_3CH_2OH)^+$ would split into $H^+ + CH_3\dot{C}HOH$ radical, (b) HOH^+ splits into $H^+ + OH$ radical. OH radical reacts with CH_3CH_2OH to give $HOH + CH_3\dot{C}HOH$, (c) Cl reacts with CH_3CH_2OH to give $HCl + CH_3\dot{C}HOH$; $FeCl_3^-$ would react with Cl^- to give $FeCl_4^{=}$. The final result of the excitation will therefore be the same, *viz.*, the production of $FeCl_4^{=}$ and $CH_3\dot{C}HOH$ radical.

The kinetics show (as in the case of $Fe^{3+}OH^-$ and $Fe^{3+}Cl^-$) that there is a primary dark back reaction independent of subsequent reactions of the free radicals. There is thus a constant fraction which the maximum quantum efficiency cannot exceed. We do not yet know the qualitative interpretation of the variation of the quantum yield with wavelength. It is possibly caused by electronic transitions to different excited states. For the sake of convenience we shall formulate the primary step as $FeCl_4^-(CH_3CH_2OH)\xrightarrow{h\nu}FeCl_4^{=}(H^+, CH_3\dot{C}HOH)$. The experimental results fit the following mechanism:

1. Photoexcitation and primary dark back reaction:

$$FeCl_4^-(H-\underset{\displaystyle CH_3}{\underset{|}{C}}HOH) \underset{k_d}{\overset{h\nu(k_\epsilon I)}{\rightleftharpoons}} FeCl_4^{2-}(H^+;\ \underset{\displaystyle CH_3}{\underset{|}{C}}HOH)$$

(primary product = A).

2. Separation of the primary product:

$$FeCl_4^{2-}(H^+;\ \underset{\displaystyle CH_3}{\underset{|}{C}}HOH)\xrightarrow{k_s}FeCl_4^{2-}+H^+ + \underset{\displaystyle CH_3}{\underset{|}{C}}HOH.$$

3. Reduction of $FeCl_4^-$ by the free radical:

$$CH_3\underset{\displaystyle H}{\underset{|}{C}}-OH + FeCl_4^- \xrightarrow{k_1} CH_3\underset{\displaystyle H}{\underset{|}{C}}=O + H^+ + FeCl_4^{2-}.$$

4. Combination of free radicals:

$$2CH_3C\cdot HOH\xrightarrow{k_2}\text{products}.$$

Stationary state kinetics based on the preceding scheme (assuming $dA/dt=0$, $\{d[CH_3\cdot\dot{C}HOH]/dt\}=0$) leads to the following equation:

$$\gamma-\frac{k_s}{k_d+k_s}=\frac{k_1C(V)^{\frac{1}{2}}}{(k_2k_\epsilon I)^{\frac{1}{2}}}\left(\frac{2k_s}{k_d+k_s}-\gamma\right)^{\frac{1}{2}},$$

where $C=|FeCl_4^-|$, $V=$volume, and γ (net quantum yield) $=\{d[FeCl_4^-]/dt\}\cdot V/k_\epsilon I$.

In the concentration range which is discussed in Section 2(a) (of the results), i.e., $[FeCl_4]=10^{-2}$ M to 10^{-3} M the value of $(k_2k_\epsilon I)^{\frac{1}{2}}/k_1C(V)^{\frac{1}{2}}$ becomes negligible. Henceforth $(2k_s)/(k_d+k_s)-\gamma\approx0$ and $\gamma=(2k_s)/(k_d+k_s)$.

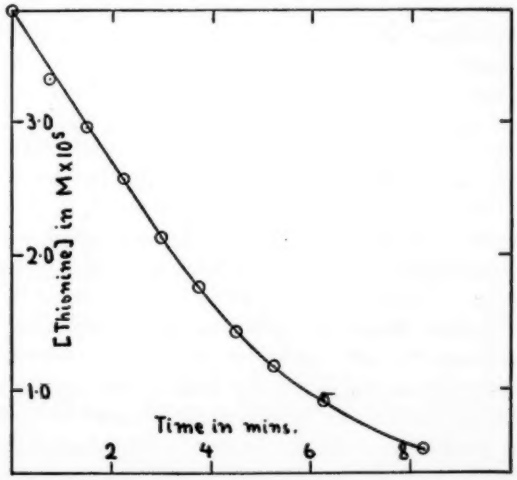

FIG. 7. Photobleaching of thionine (concentration of $[FeCl_4^-]=\sim10^{-2}$ M); Initial $[FeCl_4^-]$ 0.994×10^{-2} M; Initial $[Fe^{3+}]=2\times10^{-5}$ M; Initial [thonine] 0.382×10^{-4} M; $[HClO_4]=1.05\times10^{-2}$ M; [LiCl]=0.40 M; Volume of solution = 22 ml; ($I=3.01\times10^{-6}$ $Nh\nu$/min).

[10] A. Farkas and L. Farkas, Trans. Faraday Soc. **34**, 113 (1938).
[11] J. Franck (footnote in paper by L. Farkas and F. S. Klein, J. Chem. Phys. **16**, 886 (1948)).

These are the conditions of the maximum quantum yield, which was evaluated at 0.31. γ is independent of the light intensity and the concentration of $FeCl_4^-$ in the range of the experimental conditions of Section 2(a). This means that a zero-order reduction of $FeCl_4^-$ is obtained (Fig. 3). The zero-order reduction and the fact that an experiment started at half the $FeCl_4^-$ concentration coincides with the lower part of the line of the original experiment indicate not only that no reaction products effect the course of the reaction (thus excluding a secondary back reaction involving ferrous ion or acetaldehyde); moreover, it also indicates that any light absorption interaction between $FeCl_4^=$ formed and $FeCl_4^-$ which might be expected from the work of McConnell and Davidson[12] is negligible below 450 mμ under these conditions.

In the range of $FeCl_4^-$ concentrations of 10^{-4} to 10^{-6} M it appeared that $(k_2k_\epsilon I)^{\frac{1}{2}}/k_1C(V)^{\frac{1}{2}}$ was no longer negligible. Reaction (4) becomes significant. At low $FeCl_4^-$ concentrations and very high light intensities the reciprocal value, i.e., $k_1C(V)^{\frac{1}{2}}/(k_2k_\epsilon I)^{\frac{1}{2}}$ would approach zero; these extreme conditions under which reaction (3) is negligible and quantum yield reaches its minimum, i.e., $k_s/(k_d+k_s)$ were not achieved in practice. The lowest quantum yield observed was 0.165 which is close to the theoretical minimum. The dependence of the quantum yield on both the $FeCl_4^-$ concentration and the light intensity is, however, a function conforming with the above equation, as far as the accuracy of the experiments would allow us to judge. $k_s/(k_d+k_s)$ is best evaluated as $\gamma_{max}/2=0.155$ and corresponds to the theoretical γ_{min}.

The ratio of the rate constants $k_1/k_2^{\frac{1}{2}}$ was evaluated from a plot of

$$\gamma-\frac{\gamma_{max}}{2}\Big/\left(\frac{(\gamma_{max}-\gamma)V}{k_\epsilon I}\right)^{\frac{1}{2}}$$

against C. $k_1/k_2^{\frac{1}{2}}$ corresponds to the slope of this line and was found to be $\sim$2.7 (mol/liter)$^{-\frac{1}{2}}$ (sec)$^{-\frac{1}{2}}$ at 20°C. As already indicated, the accurate interpretation of experiments with $FeCl_3$ is much more difficult, mainly because of the formation of $FeCl_4^-$ during the reaction. Only at low concentrations of $FeCl_3$ ($<10^{-4}$ M) can this be neglected. The decrease in the net quantum yield, when $FeCl_4^-$ is compared with $FeCl_3$, is not yet understood. Experimentally it is in agreement with a similar decrease in the system $Fe^{2+}Cl_2^=$-vinyl monomer in water as compared with $Fe^{2+}Cl^-$ as initiator.[13] The observations which we made in the system $FeCl_4^-$-thionine-alcohol-light present a rare case of true photocatalysis. While $FeCl_4^-$ is the light absorbing species, the net reaction is the reduction of thionine by alcohol which would not occur in the dark or by direct photoexcitation with the wavelengths used. It appears to be based on a shift in the oxidation-reduction potential $FeCl_4^-/FeCl_4^=$ in alcohol as compared Fe^{3+}/Fe^{2+} in water. Weiss[14] and Rabinowitch[15] studied the reversible photobleaching of thionine in the system thionine-ferrous ion in water. The light absorption leads to photoexcited thionine which oxidizes ferrous ion. In the dark the reaction is reversed; the ferric ion formed in the photoreaction reoxidizes leucothionine. Under our conditions this photoreaction is of no importance as the bulk of light is absorbed by $FeCl_4^-$. Moreover, in the dark $FeCl_4^=$ is such a strong reducing agent that it is instantaneously oxidized by thionine in the dark. We evaluated the equilibrium constant

$$[FeCl_4^-]^n[\text{leucothionine}]/[FeCl_3^=]^n[\text{thionine}]$$

by a comparison of the bleaching of $FeCl_4^-$ in the absence of thionine and the amount of ferrous complex formed in the presence of thionine calculated from the bleaching of the latter. The solutions were allowed to reach equilibrium before the bleaching was measured. The equilibrium in the dark is actually established within a few seconds. When $\log[FeCl_4^-]/[FeCl_4^=]$ was plotted against $\log[\text{thionine}]/[\text{leucothionine}]$ (at room temperature (20°C) and a perchloric acid concentration of 1.05×10^{-2} M), a straight line was obtained, with a slope of $n=1.89$ (the deviation from 2 indicates the presence of a small percentage of semithionine) and K was calculated from the intercept as 2.3×10^3. The dotted portion of curve B (with square points), Fig. 6, was obtained from the bleaching of thionine (curve A, Fig. 6) when the equilibrium constant is taken into account. The deviation in the fully drawn curve (crosses) is thought to be caused by the unknown contribution of the light absorption by semithionine.

Although there is no direct evidence, there are strong indications that it is $FeCl_4^=$ which is the reducing species: (a) An alcoholic solution of ferrous perchlorate (in the presence of $HClO_4$) would not react with thionine; reduction is, however, immediately effected on addition of lithium chloride. (b) When, after reduction has occurred, the solution is diluted with water (by a few percent) the reaction is reversed and the color of the thionine reappears. We have shown that the concentration of $FeCl_4^-$ is practically unaffected by this dilution. On the other hand, analogy with the observations made by Bobtelsky and Spiegler[16] on the stability of the $CoCl_4^=$ complex in alcohol and its decomposition by traces of water, makes it very likely that a similar complex with ferrous ion could also be sensitive to the addition of water. These observations made us assume that it is $FeCl_4^=$ which is reducing and which shows this marked shift in the oxidation-reduction potential of $\sim$0.5 volt.

N.U. would like to acknowledge the tenure of an I.C.I. fellowship and G. J. B. the receipt of a D.S.I.R. maintenance grant.

[12] H. McConnell and N. Davidson, J. Am. Chem. Soc. **72**, 5557 (1950).
[13] Evans, Santappa, and Uri (unpublished work).
[14] J. Weiss, Nature, **136**, 794 (1935).
[15] E. Rabinowitch, J. Chem. Phys. **8**, 551 (1940).
[16] M. Bobtelsky and K. S. Spiegler, J. Chem. Soc. **143** (1949).

The Physical Properties of Molecules in Relation to Their Structure. I. Relations between Additive Molecular Properties in Several Homologous Series

H. J. BERNSTEIN
Division of Chemistry, National Research Council, Ottawa, Canada
(Received September 28, 1951)

Relations between the additive physical properties of the substituted methanes, ethanes, ethylenes, benzenes, and the acyclic saturated hydrocarbons have been derived assuming strict additivity for the contributions from nonbonded atoms as well as for the contributions from bonded atoms.

INTERACTIONS between nonbonded atoms have been introduced into the potential function for the substituted methanes and found to be important in evaluating vibrational frequencies.[1–3] Nonbonded interactions in the substituted methanes and ethylenes have been useful also in the correlation of the diamagnetic susceptibilities of these molecules.[4,5] Even in the saturated acyclic hydrocarbons the nonbonded interactions would seem to be of considerable importance since the heats of atomization of the isomers are quite different.[6]

Relations between the additive properties of the acyclic aliphatic hydrocarbons having been derived[7] by considering all interactions between bonds but neglecting effects due to rotational isomers; and also in a less rigorous manner in terms of the number of carbon atoms which are three bonds apart and the sum of all the CC distances in the molecule.[8]

It is the purpose of this paper to present the relations between the physical properties of molecules in some homologous series. The simple additivity scheme in which only contributions from bonded atoms are considered[9] is extended to include contributions from all nonbonded atoms. It is worth mentioning that although there is a physical distinction between considering nonbonded interactions between atoms and considering interactions between bonds[7] the algebraic results are identical. These relations may be useful in calculating the additive physical properties of molecules in a homologous series or for detecting nonadditivity (due to changes in bond lengths and/or nonadditive effects due to resonance or hyperconjugation, for example).

THE SUBSTITUTED METHANES $CX_{4-n}Y_n$

A preliminary note on the relations for the substituted methanes has been published.[10] The notation has been altered since here we use X and Y instead of A and B, respectively. The derivation of these relations is carried out most easily for the substituted methanes and will be shown in more detail below.

In what follows, P = the additive property of the molecule, p_{CX_1} = the contribution to P from the interaction of atom C with atom X when they are one bond apart, i.e., C and X are bonded, and p_{CX_2} = the contribution to P from the interaction of atom C with atom X when they are two bonds apart, etc., and all contributions are assumed strictly additive. The molecular property of the nth substituted methane of the series $CX_{4-n}Y_n$ is given by

$$P_{CX_{4-n}Y_n}=A_{CX_1}p_{CX_1}+A_{CY_1}p_{CY_1}+A_{XX_2}p_{XX_2}+A_{YY_2}p_{YY_2}+A_{XY_2}p_{XY_2}, \quad (1)$$

where the values of the coefficients of these additive contributions are given in Table I.

It is readily seen that

$$A_{CX_1}=4-n, \quad A_{CY_1}=n, \quad A_{XX_2}=(4-n)(3-n)/2, \quad A_{YY_2}=n(n-1)/2, \quad \text{and} \quad A_{XY_2}=n(4-n). \quad (2)$$

The five equations for $n=0$, 1, 2, 3, and 4 are not independent since the determinant of the coefficients in Table I is zero. The relations between these equations are

$$\begin{aligned} 2P_{CX_3Y}-(P_{CX_4}+P_{CX_2Y_2}) &= 2P_{CX_2Y_2}-(P_{CX_3Y}+P_{CXY_3}) \\ &= 2P_{CXY_3}-(P_{CX_2Y_2}+P_{CY_4}) \\ &= -p_{XX_2}-p_{YY_2}+2p_{XY_2}=\Delta_{XY} \text{ (say)}. \end{aligned} \quad (3)$$

By substituting from (2) into (1) and using Δ_{XY} as

TABLE I. Additive contributions in the series $CX_{4-n}Y_n$.

Molecule	P	A_{CX_1}	A_{CY_1}	A_{XX_2}	A_{YY_2}	A_{XY_2}
CX_4	P_{CX_4}	4	0	6	0	0
CX_3Y	P_{CX_3Y}	3	1	3	0	3
CX_2Y_2	$P_{CX_2Y_2}$	2	2	1	1	4
CXY_3	P_{CXY_3}	1	3	0	3	3
CY_4	P_{CY_4}	0	4	0	6	0

[1] H. C. Urey and C. A. Bradley, Phys. Rev. **38**, 1969 (1931).
[2] T. Simanouti, J. Chem. Phys. **17**, 245, 734 (1949).
[3] D. F. Heath and J. W. Linnett, Trans. Faraday Soc. **44**, 561, 873, 878, 884 (1948); **45**, 264 (1949).
[4] J. R. Lacher, J. Am. Chem. Soc. **69**, 2067 (1947); Lacher, Scruby and Park, J. Am. Chem. Soc. **72**, 333 (1950).
[5] Lacher, Pollock, Johnson, and Park, J. Am. Chem. Soc. **73**, 2838 (1951).
[6] The heats of atomization may be calculated in the usual way from the heats of formation given in the "Selected Values of Properties of Hydrocarbons" (A.P.I. Research Project 44), Natl. Bur. Standards, Washington, D. C. (1947). See also F. D. Rossini, Chem. Rev. **27**, 1 (1940).
[7] J. R. Platt, J. Chem. Phys. **15**, 419 (1947).
[8] H. Wiener, J. Chem. Phys. **15**, 766 (1947); J. Am. Chem. Soc. **69**, 17, 2636 (1947).
[9] L. Pauling, *Nature of the Chemical Bond* (Cornell University Press, Ithaca, New York, 1942), p. 47 *et seq.*
[10] H. J. Bernstein, J. Chem. Phys. **19**, 140 (1951).

TABLE II. Relations in the series $CX_{4-n}Y_n$.

	P_{CX_4}	α	Δ_{XY}
P_{CX_4}	1	...	...
P_{CX_3Y}	1	1	...
$P_{CX_2Y_2}$	1	2	−1
P_{CXY_3}	1	3	−3
P_{CY_4}	1	4	−6

defined by (3),

$$P_{CX_{4-n}Y_n}=P_{CX_4}+(n/4)[P_{CY_4}-P_{CX_4}+8\Delta_{XY}]-(n^2/2)\Delta_{XY}. \quad (4)$$

Thus for these methanes the additive physical property is a parabolic function of the number of substituents. If Δ_{XY} is small, then (4) becomes

$$P_{CX_{4-n}Y_n}=P_{CX_4}+(n/4)(P_{CY_4}-P_{CX_4}), \quad (5)$$

which is the linear relation obtained from the simple additivity scheme in which valence-bond contributions only are considered.

For purposes of calculation it is perhaps more convenient to express these relations in terms of P_{CX_4}, Δ_{XY} and α where α is defined as $P_{CX_3Y}-P_{CX_4}$. In Table II the coefficients of P_{CX_4}, α and Δ_{XY} are given for each molecular property, thus $P_{CXY_3}=P_{CX_4}+3\alpha-3\Delta_{XY}$, for example. These properties can be calculated therefore in terms of three unknowns whereas in the simple additivity scheme two data were sufficient to determine the properties of the series.

Solving for n from Eq. (4) gives

$$n\approx(\rho/A_p)+(\rho^2/A_p^3)\cdot\Delta_p, \quad (6)$$

where

$$\rho=P_{CX_{4-n}Y_n}-P_{CX_4},$$
$$A_p=(P_{CY_4}-P_{CX_4})\tfrac{1}{4}+2\Delta_p,$$

and

$$\Delta_p=-p_{XX_2}-p_{YY_2}+2p_{XY_2}.$$

Since $n\sim\rho/A_p$, Eq. (6) may be rewritten

$$n\approx(\rho/A_p)+(n^2/A_p)\cdot\Delta_p. \quad (7)$$

Similarly, for some other additive property Q a relation similar to (7) may be written, *viz.*:

$$n\approx(q/A_q)+(n^2/A_q)\cdot\Delta_q \quad (8)$$

where

$$q=Q_{CX_{4-n}Y_n}-Q_{CX_4}$$
$$A_q=(Q_{CX_4}-Q_{CY_4})\tfrac{1}{4}+2\Delta_q,$$

and

$$\Delta_q=-q_{XX_2}-q_{YY_2}+2q_{XY_2}.$$

After subtracting (7) and (8) it is found that $P_{CX_{4-n}Y_n}$ and $Q_{CX_{4-n}Y_n}$ are related by

$$P_{CX_{4-n}Y_n}=P_{CX_4}+(A_p/A_q)\{Q_{CX_{4-n}Y_n}-Q_{CX_4}\}+\frac{(Q_{CX_{4-n}Y_n}-Q_{CX_4})^2}{A_q^2}\left\{\frac{A_p}{A_q}\cdot\Delta_q-\Delta_p\right\}. \quad (9)$$

In general then, the relation between any two additive physical properties is parabolic but in the cases when both Δ_q and Δ_p are small or when $\Delta_pA_q\approx A_p\Delta_q$, there is a linear relation between the additive properties.

Relations analogous to (3), (4), and (9) may be obtaned for the methanes of the series $CX_{3-n}Y_nZ$, and $CX_{2-n}Y_nZ_2$. The relations between the 15 substituted methanes containing X, Y, and Z are most readily expressed in terms of the following six unknowns:

$$P_{CX_4},$$
$$\alpha=P_{CX_3Y}-P_{CX_4},$$
$$\beta=P_{CX_3Z}-P_{CX_4},$$
$$\gamma=P_{CX_2Y_2}-P_{CX_3Z},$$
$$\Delta_{XY}=-p_{XX_2}-p_{YY_2}+2p_{XY_2} \text{ as in (3)},$$

and

$$\Delta_{XZ}=-p_{XX_2}-p_{ZZ_2}+2p_{XZ_2}.$$

The coefficients of these unknowns are given in Table III. Thus for example $P_{CXY_2Z}=P_{CX_4}+\beta+2\gamma-\Delta_{XY}$.

These relations may be used to calculate such physical properties of the molecules as molar refraction, diamagnetic susceptibilities, heats of atomization, etc. Since the heat of atomization of the nth substituted methane is equal to

$$Q_{CX_{4-n}Y_n}=L+[(4-n)/2]D_{X_2}+[(n)/2]D_{Y_2}-\Delta H_f^{(n)},$$

where L is the latent heat of sublimation of carbon, D_{X_2} and D_{Y_2} are the bond energies of X_2 and Y_2, and $\Delta H_f^{(n)}$ is the heat of formation of the nth substituted methane, it is readily seen that ΔH_f may be substituted for P in the above relations.

THE SUBSTITUTED ETHANES $C_2X_{6-n}Y_n$

The additive physical property of the nth substituted ethane is given by

$$\begin{aligned}P_{C_2X_{6-n}Y_n}=&A_{CC_1}p_{CC_1}+A_{CX_1}p_{CX_1}+A_{CY_1}p_{CY_1}\\&+A_{CX_2}p_{CX_2}+A_{CY_2}p_{CY_2}+A_{XX_2}p_{XX_2}\\&+A_{XX_3^{\pi/3}}p_{XX_3^{\pi/3}}+A_{XX_3^{\pi}}p_{XX_3^{\pi}}+A_{YY_2}p_{YY_2}\\&+A_{YY_3^{\pi/3}}p_{YY_3^{\pi/3}}+A_{YY_3^{\pi}}p_{YY_3^{\pi}}+A_{XY_2}p_{XY_2}\\&+A_{XY_3^{\pi/3}}p_{XY_3^{\pi/3}}+A_{XY_3^{\pi}}p_{XY_3^{\pi}} \quad (10)\end{aligned}$$

TABLE III. Relations for the substituted methanes.

	P_{CX_4}	α	β	γ	Δ_{XY}	Δ_{XZ}
P_{CX_4}	1	0	0	0	0	0
P_{CX_3Y}	1	1	0	0	0	0
$P_{CX_2Y_2}$	1	2	0	0	−1	0
P_{CXY_3}	1	3	0	0	−3	0
P_{CY_4}	1	4	0	0	−6	0
P_{CX_3Z}	1	0	1	0	0	0
$P_{CX_2Z_2}$	1	0	2	0	0	−1
P_{CXZ_3}	1	0	3	0	0	−3
P_{CZ_4}	1	0	4	0	0	−6
P_{CX_2YZ}	1	0	1	1	0	0
P_{CXY_2Z}	1	0	1	2	−1	0
P_{CY_3Z}	1	0	1	3	−3	0
P_{CXYZ_2}	1	−1	2	2	0	−1
P_{CYZ_3}	1	−2	3	3	0	−3
$P_{CY_2Z_2}$	1	−2	2	4	−1	−1

TABLE IV. Additive contributions in the series $C_2X_{6-n}Y_n$.

	A_{CC_1}	A_{CX_1}	A_{CY_1}	A_{CX_2}	A_{CY_2}	A_{XX_2}	$A_{XX_3^{\pi/3}}$	$A_{XX_3^{\pi}}$	A_{YY_2}	$A_{YY_3^{\pi/3}}$	$A_{YY_3^{\pi}}$	A_{XY_2}	$A_{XY_3^{\pi/3}}$	$A_{XY_3^{\pi}}$
$P_{C_2X_6}$	1	6	...	6	...	6	6	3	...	...	...	...	...	...
$P_{C_2X_5Y}$	1	5	1	5	1	4	4	2	...	...	...	2	2	1
$P_{1,1C_2X_4Y_2}$	1	4	2	4	2	3	2	1	1	...	...	2	4	2
$P_{1,2\text{-}trans C_2X_4Y_2}$	1	4	2	4	2	2	2	2	...	...	1	4	4	0
$P_{1,2\text{-}gauche C_2X_4Y_2}$	1	4	2	4	2	2	3	1	...	1	...	4	2	2
$P_{1,1,1C_2X_3Y_3}$	1	3	3	3	3	3	...	...	...	...	...	3	6	3
$P_{1,1,2\text{-}trans C_2X_3Y_3}$	1	3	3	3	3	1	1	1	1	1	1	4	4	1
$P_{1,1,2\text{-}gauche C_2X_3Y_3}$	1	3	3	3	3	1	2	...	1	2		4	2	3
$P_{1,1,1,2C_2X_2Y_4}$	1	2	4	2	4	1	...	...	3	2	1	2	4	2
$P_{1,1,2,2\text{-}trans C_2X_2Y_4}$	1	2	4	2	4	...	...	1	2	2	2	4	4	
$P_{1,1,2,2\text{-}gauche C_2X_2Y_4}$	1	2	4	2	4	...	1	...	2	3	1	4	2	2
$P_{C_2XY_5}$	1	1	5	1	5	...	...	...	4	4	2	2	2	1
$P_{C_2Y_6}$	1	...	6	...	6	...	...	...	6	6	3	...	...	...

where the notation is as before with the additional superscript $\pi/3$ or π denoting interactions between atoms on different carbon atoms which are rotated by $\pi/3$ or π about the CC axis with respect to one another. The coefficients are given in Table IV. When there are rotational isomers the form with lower electric moment is called *"trans"* and the form with higher moment called *"gauche."* Let

$$P_{C_2X_5Y} - P_{C_2X_6} = \alpha$$
$$P_{1,1C_2X_4Y_2} - P_{C_2X_5Y} = \beta,$$
$$P_{1,2\text{-}trans C_2X_4Y_2} - P_{C_2X_5Y} = \gamma,$$
$$P_{1,2\text{-}gauche C_2X_4Y_2} - P_{C_2X_5Y} = \delta,$$

and

$$2P_{1,1C_2X_4Y_2} - (P_{C_2X_5Y} + P_{1,1,1C_2X_3Y_3}) = \epsilon,$$

where

$$\alpha - \beta = -p_{XX_2} - p_{YY_2} + 2p_{XY_2} = \Delta_{XY} \text{ of Eq. (3)}$$
$$\alpha - \gamma = -p_{XX_3^{\pi}} - p_{YY_3^{\pi}} + 2p_{XY_3^{\pi}},$$

and

$$\alpha - \delta = -p_{XX_3^{\pi/3}} - p_{YY_3^{\pi/3}} + 2p_{XY_3^{\pi/3}}.$$

The molecular properties of the substituted ethanes are given then in terms of the six unknowns, $P_{C_2X_6}$, α, β, γ, δ, and ϵ. The coefficients of these unknowns are given in Table V.

For the molecules possessing rotational isomers the value observed for the property in the gas phase may be calculated from

$$\bar{P} = \frac{(\text{number of } \textit{trans}) \times P_{trans} + (\text{number of } \textit{gauche}) \times P_{gauche}}{\text{total number of molecules}}$$

where

$$\frac{\text{number of } \textit{gauche}}{\text{number of } \textit{trans}} = A \exp(-\Delta H/RT) = 2\frac{f_{gauche}}{f_{trans}} \exp(-\Delta E_0^0/RT).$$

ΔH is the heat of isomerization in the gas,

ΔE_0^0 is the zero point energy difference,

and f_{gauche} and f_{trans} are the combined rotational and vibrational partition functions for the *gauche* and *trans* forms, respectively. In the liquid phase, the equilibrium constant is proportional to $\exp(-\Delta H_{liquid}/RT)$ so the heat of isomerization in the liquid must be used in the calculation.

From Table V it is apparent that the assumption of strict additivity leads to the same energy difference, δ, between the rotational isomers of the 12-di-, 112-tri-, and 1122-tetra- substituted ethanes. Steric effects may cause departures from additivity which may be accounted for by considering the energy difference for the rotational isomers to be different and equal to δ, δ', and δ'', respectively. These steric effects have been considered later under the section dealing with the acyclic saturated hydrocarbons, in which the energy difference between the rotational isomers of 12-dimethyl, 112-trimethyl, and 1122-tetramethyl ethane are assumed different and equal to ΔH_1, ΔH_2, and ΔH_3 respectively.

THE SUBSTITUTED ETHYLENES $C_2X_{4-n}Y_n$

The molecular property of the nth substituted ethylene is given by

$$\begin{aligned} P_{C_2X_{4-n}Y_n} = {} & A_{CC_1}p_{CC_1} + A_{CX_1}p_{CX_1} + A_{CY_1}p_{CY_1} \\ & + A_{CX_2}p_{CX_2} + A_{CY_2}p_{CY_2} + A_{XX_2}p_{XX_2} \\ & + A_{XX_3^0}p_{XX_3^0} + A_{XX_3^{\pi}}p_{XX_3^{\pi}} + A_{YY_2}p_{YY_2} \\ & + A_{YY_3^0}p_{YY_3^0} + A_{YY_3^{\pi}}p_{YY_3^{\pi}} + A_{XY_2}p_{XY_2} \\ & + A_{XY_3^0}p_{XY_3^0} + A_{XY_3^{\pi}}p_{XY_3^{\pi}}, \quad (11) \end{aligned}$$

where the superscripts 0 and π indicate the interactions between atoms in the planar *cis* and *trans* positions, respectively. The coefficients in (11) are given in Table VI.

Let

$$a = P_{C_2X_3Y} - P_{C_2X_4},$$
$$b = P_{1,1C_2X_2Y_2} - P_{C_2X_3Y},$$
$$c = P_{trans\text{-}C_2X_2Y_2} - P_{C_2X_3Y},$$

TABLE V. Relations for the substituted ethanes.

	$P_{C_2X_6}$	α	β	γ	δ	ϵ
$P_{C_2X_6}$	1	...	...	...	...	...
$P_{C_2X_5Y}$	1	1	0	0	0	0
$P_{1,1,C_2X_4Y_2}$	1	1	1	0	0	0
$P_{1,2\text{-}trans\text{-}C_2X_4Y_2}$	1	1	0	1	0	0
$P_{1,2\text{-}gauche\text{-}C_2X_4Y_2}$	1	1	0	0	1	0
$P_{1,1,1C_2X_3Y_3}$	1	1	2	0	0	−1
$P_{1,1,2\text{-}trans\text{-}C_2X_3Y_3}$	1	0	1	1	1	0
$P_{1,1,2\text{-}gauche\text{-}C_2X_3Y_3}$	1	0	1	0	2	0
$P_{1,1,1,2C_2X_2Y_4}$	1	−2	3	1	2	0
$P_{1,1,2,2\text{-}trans\text{-}C_2X_2Y_4}$	1	−2	2	2	2	0
$P_{1,1,2,2\text{-}gauche\text{-}C_2X_2Y_4}$	1	−2	2	1	3	0
$P_{C_2X_5Y}$	1	−5	4	2	4	
$P_{C_2Y_6}$	1	−9	6	3	6	0

and

$$d = P_{cis\text{-}C_2X_2Y_2} - P_{C_2X_3Y},$$

where

$$a - c = -p_{XX_3}{}^{\pi} - p_{YY_3}{}^{\pi} + 2p_{XY_3}{}^{\pi},$$

$$a - d = -p_{XX_3}{}^{0} - p_{YY_3}{}^{0} + 2p_{XY_3}{}^{0},$$

and

$$a - b = -p_{XX_2} - p_{YY_2} + 2p_{XY_2}.$$

The molecular properties are given in terms of $P_{C_2X_4}$, a, b, c, and d. The coefficients are given in Table VII.

THE SUBSTITUTED BENZENES $C_6X_{6-n}Y_n$

$$\begin{aligned} P_{C_6X_{6-n}Y_n} = {} & A_{CC_1}p_{CC_1} + A_{CC_2}p_{CC_2} + A_{CC_3}p_{CC_3} \\ & + A_{CX_1}p_{CX_1} + A_{CX_2}p_{CX_2} + A_{CX_3}p_{CX_3} \\ & + A_{CX_4}p_{CX_4} + A_{CY_1}p_{CY_1} + A_{CY_2}p_{CY_2} \\ & + A_{CY_3}p_{CY_3} + A_{CY_4}p_{CY_4} + A_{XX_3}p_{XX_3} \\ & + A_{XX_4}p_{XX_4} + A_{XX_5}p_{XX_5} + A_{YY_3}p_{YY_3} \\ & + A_{YY_4}p_{YY_4} + A_{YY_5}p_{YY_5} + A_{XY_3}p_{XY_3} \\ & + A_{XY_4}p_{XY_4} + A_{XY_5}p_{XY_5}. \end{aligned} \quad (12)$$

The subscripts 3, 4, and 5 on the terms involving XX, YY, and XY are identical with *ortho*, *meta*, and *para* contributions, respectively. The coefficients in (12) are given in Table VIII.

Let

$$\alpha = P_{C_6X_5Y} - P_{C_6X_6},$$

$$\beta = P_{o\text{-}C_6X_4Y_2} - P_{C_6X_5Y},$$

$$\gamma = P_{m\text{-}C_6X_4Y_2} - P_{C_6X_5Y},$$

and

$$\delta = P_{p\text{-}C_6X_4Y_2} - P_{C_6X_5Y},$$

TABLE VII. Relations for the substituted ethylenes.

	$P_{C_2X_4}$	a	b	c	d
$P_{C_2X_4}$	1	0	0	0	0
$P_{C_2X_3Y}$	1	1	0	0	0
$P_{1,1C_2X_2Y_2}$	1	1	1	0	0
$P_{trans\text{-}C_2X_2Y_2}$	1	1	0	1	0
$P_{cis\text{-}C_2X_2Y_2}$	1	1	0	0	1
$P_{C_2XY_3}$	1	0	1	1	1
$P_{C_2Y_4}$	1	−2	2	2	2

where

$$\alpha - \beta = -p_{XX_3} - p_{YY_3} + 2p_{XY_3},$$

$$\alpha - \gamma = -p_{XX_4} - p_{YY_4} + 2p_{XY_4},$$

and

$$\alpha - \delta = -p_{XX_5} - p_{YY_5} + 2p_{XY_5}.$$

The properties of the substituted benzenes are given in terms of $P_{C_2X_6}$, α, β, γ, and δ. In Table IX the properties are expressed in terms of these unknowns.

THE ACYCLIC ALIPHATIC HYDROCARBONS C_nH_{2n+2}

Whereas the treatment of the preceding homologous series has been perfectly rigorous, it is expedient to consider those interactions which arise between atoms more than three bonds apart as negligible for the aliphatic acyclic hydrocarbons.

More recently the additive properties of the alkanes have been described in terms of ten types of C–C bonds and three types of CH bonds.[11] Since the C–C bonds are of the type found in the substituted ethanes $C_2X_{6-n}Y_n$ in which X=H and Y=C, their properties may be expressed in terms of the quantities $P_{C_2H_6}$, α, β, γ, δ, and ϵ of Table V if strict additivity is assumed. Thus, if additivity is assumed, the nine constants used to determine the data in the work on the alkanes[11] in which the effects of rotational isomerism are neglected, may be reduced to five of the six given above, namely, $P_{C_2H_6}$, α, β, ϵ, and γ or δ.

The molecular property is expressed as

$$\begin{aligned} P = {} & A_{CC_1}p_{CC_1} + A_{CC_2}p_{CC_2} + A_{CC_3{}^{\pi/3}}p_{CC_3{}^{\pi/3}} \\ & + A_{CC_3{}^{\pi}}p_{CC_3{}^{\pi}} + A_{CH_1}p_{CH_1} + A_{CH_2}p_{CH_2} \\ & + A_{CH_3{}^{\pi/3}}p_{CH_3{}^{\pi/3}} + A_{CH_3{}^{\pi}}p_{CH_3{}^{\pi}} + A_{HH_2}p_{HH_2} \\ & + A_{HH_3{}^{\pi/3}}p_{HH_3{}^{\pi/3}} + A_{HH_3{}^{\pi}}p_{HH_3{}^{\pi}}. \end{aligned} \quad (13)$$

The coefficients of (13) are given in Table X for the molecules in the staggered or *trans* configurations.

TABLE VI. Additive contributions in the series $C_2X_{4-n}Y_n$.

	A_{CC_1}	A_{CX_1}	A_{CY_1}	A_{CX_2}	A_{CY_2}	A_{XX_2}	$A_{XX_3{}^{0}}$	$A_{XX_3{}^{\pi}}$	A_{YY_2}	$A_{YY_3{}^{0}}$	$A_{YY_3{}^{\pi}}$	A_{XY_2}	$A_{XY_3{}^{0}}$	$A_{XY_3{}^{\pi}}$
$P_{C_2X_4}$	1	4	0	4	0	2	2	2	0	0	0	0	0	0
$P_{C_2X_3Y}$	1	3	1	3	1	1	1	1	0	0	0	1	1	1
$P_{1,1C_2X_2Y_2}$	1	2	2	2	2	1	0	0	1	0	0	0	2	2
$P_{cis\text{-}C_2X_2Y_2}$	1	2	2	2	2	0	1	0	0	1	0	2	0	2
$P_{trans\text{-}C_2X_2Y_2}$	1	2	2	2	2	0	0	1	0	0	1	2	2	0
$P_{C_2XY_3}$	1	1	3	1	3	0	0	0	1	1	1	1	1	1
$P_{C_2Y_4}$	1	0	4	0	4	0	0	0	2	2	2	0	0	0

[11] V. M. Tatevskii, Doklady Akad Nauk S.S.S.R. **75**, 819 (1950).

TABLE VIII. Additive contributions in the series $C_6X_{6-n}Y_n$.

	A_{CC_1}	A_{CC_2}	A_{CC_3}	A_{CX_1}	A_{CX_2}	A_{CX_3}	A_{CX_4}	A_{CY_1}	A_{CY_2}	A_{CY_3}	A_{CY_4}	A_{XX_3}	A_{XX_4}	A_{XX_5}	A_{YY_3}	A_{YY_4}	A_{YY_5}	A_{XY_2}	A_{XY_4}	A_{XY_5}
PC_6X_6	6	6	3	6	12	12	6	0	0	0	0	6	6	3	0	0	0	0	0	0
PC_6X_5Y	6	6	3	5	10	10	5	1	2	2	1	4	4	2	0	0	0	2	2	1
P_o-$C_6X_4Y_2$	6	6	3	4	8	8	4	2	4	4	2	3	2	1	1	0	0	2	4	2
P_m-$C_6X_4Y_2$	6	6	3	4	8	8	4	2	4	4	2	2	3	1	0	1	0	4	2	2
P_p-$C_6X_4Y_2$	6	6	3	4	8	8	4	2	4	4	2	2	2	2	0	0	1	4	4	0
$P_{1,2,4}$-$C_6X_3Y_3$	6	6	3	3	6	6	3	3	6	6	3	1	1	1	1	1	1	4	4	1
$P_{1,2,3}$-$C_6X_3Y_3$	6	6	3	3	6	6	3	3	6	6	3	2	1	0	2	1	0	2	4	3
$P_{1,3,5}$-$C_6X_3Y_3$	6	6	3	3	6	6	3	3	6	6	3	0	3	0	0	3	0	6	0	3
P_o-$C_6X_2Y_4$	6	6	3	2	4	4	2	4	8	8	4	1	0	0	3	2	1	2	4	2
P_m-$C_6X_2Y_4$	6	6	3	2	4	4	2	4	8	8	4	0	1	0	2	3	1	4	2	2
P_p-$C_6X_2Y_4$	6	6	3	2	4	4	2	4	8	8	4	0	0	1	2	2	2	4	4	0
PC_6XY_5	6	6	3	1	2	2	1	5	10	10	5	0	0	0	4	4	2	2	2	1
PC_6Y_6	6	6	3	0	0	0	0	6	12	12	6	0	0	0	6	6	3	0	0	0

Let

$$\alpha = P_2 - P_1,$$

$$\beta = P_3 - P_2,$$

$$\gamma = P_4 - P_3,$$

and

$$\epsilon = P_{5a} - P_5,$$

where

$$\alpha - \beta = 2p_{CH_2} - p_{HH_2} - p_{CC_2} + 4p_{HH_3}{}^{\pi/3} + 2p_{HH_3}{}^{\pi} - 4p_{CH_3}{}^{\pi/3} - 2p_{CH_3}{}^{\pi},$$

$$\beta - \gamma = -p_{HH_3}{}^{\pi} + 2p_{CH_3}{}^{\pi} - p_{CC_3}{}^{\pi},$$

and

$$2\beta - \alpha - \gamma - \epsilon = -p_{HH_3}{}^{\pi/3} - p_{CC_3}{}^{\pi/3} + 2p_{CH_3}{}^{\pi/3}.$$

For the normal hydrocarbons for $n \geq 3$

$$P_n = P_3 + (n-3)\gamma. \tag{14}$$

It is not possible to extend Eq. (14) to include methane and ethane in a rigorous manner since $\alpha \neq \beta \neq \gamma$. An empirical term may be introduced into Eq. (14), however, to give an equation suitable for $n \geq 1$, *viz.*:

$$P_n = P_1 + a_1(n-1) + a_2[f_{(n)} - 1], \tag{14a}$$

where a_2 is a constant for this particular property and $f_{(n)}$ is a function of n for which $f_{(1)} = 1$, and $f_{(\infty)} = 0$. Such functions as n^{-m} and e^{-n} immediately suggest themselves for $f_{(n)}$. It is not improbable that Eq. (14a) would be a very good fit for the data.

The properties of some hydrocarbons and their isomers are given in Table XI in terms of P_1, α, β, γ, and ϵ.

It is worth emphasizing here that the general physical property of the substituted methane in which X is a hydrogen atom and Y a CH_3 group is a parabolic function of the number of CH_3 groups.

This may be seen quite readily from Table XI since the second differences

$$2P_2 - (P_1 + P_3) = 2P_3 - (P_2 + P_{4a}) = 2P_{4a} - (P_3 + P_{5b}) = \alpha - \beta.$$

Thus it is not necessary to assume that the CH_3 group behaves as a single particle in order to treat methane, ethane, propane, isobutane, and neopentane as a series of substituted methanes.

When the above results, for the various series treated, are applied to thermochemical quantities such as heats of atomization, etc., it must be remembered that corrections must be made for zero point energy differences[12,13] before strict comparison between observed and calculated results can be made. In the case of the C_nH_{2n+2} hydrocarbons further corrections have to be made for rotational isomerism.

The rotational isomers of the paraffins can be divided broadly into three types: (1) those occurring in *n*-butane with an energy difference ΔH_1, (2) those of the type occurring in 1,1,2-trimethylethane with energy difference ΔH_2, and (3) those occurring in 1,1,2,2-tetramethylethane with energy difference ΔH_3. Let the contributions due to rotational isomers be *a*, *b*, *c* in cases (1), (2), and (3), respectively, so that the observed value for *P*, namely $\bar{P}$, is

$\bar{P} = P_{trans} - a$ for butane-like isomers,

$\bar{P} = P_{trans} - b$ for isomers as in 1,1,2-trimethylethane,

and

$\bar{P} = P_{trans} - c$ for isomers as in 1,1,2,2-tetramethylethane.

TABLE IX. Relations for the substituted benzenes.

	PC_6X_6	α	β	γ	δ
PC_6X_6	1	...	...	...	...
PC_6X_5Y	1	1	...	...	...
P_o-$C_6X_4Y_2$	1	1	1	...	...
P_m-$C_6X_4Y_2$	1	1	...	1	...
P_p-$C_6X_4Y_2$	1	1	...	...	1
$P_{1,2,4}$-$C_6X_3Y_3$	1	...	1	1	1
$P_{1,2,3}$-$C_6X_3Y_3$	1	...	2	1	...
$P_{1,3,5}$-$C_6X_3Y_3$	1	...	...	3	...
P_o-$C_6X_2Y_4$	1	−2	3	2	1
P_m-$C_6X_2Y_4$	1	−2	2	3	1
P_p-$C_6X_2Y_4$	1	−2	2	2	2
PC_6XY_5	1	−5	4	4	2
PC_6Y_6	1	−9	6	6	3

[12] V. Dietz, J. Chem. Phys. **3**, 58 (1935).
[13] T. L. Cottrell, J. Chem. Soc. 1448 (1948).

TABLE X. Additive contributions in the paraffins C_nH_{2n+2}.

Compound	Molecular property	A_{CC_1}	A_{CH_1}	A_{CH_2}	A_{HH_2}	A_{CC_2}	$A_{HH_3}{}^{\pi/3}$	$A_{HH_3}{}^{\pi}$	$A_{CH_3}{}^{\pi/3}$	$A_{CH_3}{}^{\pi}$	$A_{CC_3}{}^{\pi/3}$	$A_{CC_3}{}^{\pi}$
Methane	P_1	0	4	0	6	0	0	0	0	0	0	0
Ethane	P_2	1	6	6	6	0	6	3	0	0	0	0
Propane	P_3	2	8	10	7	1	8	4	4	2	0	0
n-Butane	P_4	3	10	14	8	2	10	6	8	2	0	1
2-Methylpropane	P_{4a}	3	10	12	9	3	6	3	12	6	0	0
n-Pentane	P_5	4	12	18	9	3	12	8	12	2	0	2
2-Methylbutane	P_{5a}	4	12	16	10	4	9	5	14	6	1	1
2,2-Dimethylpropane	P_{5b}	4	12	12	12	6	0	0	24	12	0	0
n-Hexane	P_6	5	14	22	10	4	14	10	16	2	0	3
2-Methylpentane	P_{6a}	5	14	20	11	5	11	7	18	6	1	2
3-Methylpentane	P_{6b}	5	14	20	11	5	12	7	16	6	2	2
2,2-Dimethylbutane	P_{6c}	5	14	16	13	7	4	2	24	12	2	1
2,3-Dimethylbutane	P_{6d}	5	14	18	12	6	8	5	20	8	2	2
n-Heptane	P_7	6	16	26	11	5	16	12	20	2	0	4
2-Methylhexane	P_{7a}	6	16	24	12	6	13	9	22	6	1	3
3-Methylhexane	P_{7b}	6	16	24	12	6	14	9	20	6	2	3
3-Ethylpentane	P_{7c}	6	16	24	12	6	15	9	18	6	3	3
2,2-Dimethylpentane	P_{7d}	6	16	20	14	8	6	4	28	12	2	2
2,3-Dimethylpentane	P_{7e}	6	16	22	13	7	11	7	22	8	3	3
2,4-Dimethylpentane	P_{7f}	6	16	22	13	7	10	6	24	10	2	2
3,3-Dimethylpentane	P_{7g}	6	16	20	14	8	8	4	24	12	4	2
2,2,3-Trimethylbutane	P_{7h}	6	16	18	15	9	4	2	28	14	4	2
n-Octane	P_8	7	18	30	12	6	18	14	24	2	0	5
2-Methylheptane	P_{8a}	7	18	28	13	7	15	11	26	6	1	4
3-Methylheptane	P_{8b}	7	18	28	13	7	16	11	24	6	2	4
4-Methylheptane	P_{8c}	7	18	28	13	7	16	11	24	6	2	4
3-Ethylhexane	P_{8d}	7	18	28	13	7	17	11	22	6	3	4
2,2-Dimethylhexane	P_{8e}	7	18	24	15	9	8	6	32	12	2	3
2,3-Dimethylhexane	P_{8f}	7	18	26	14	8	14	9	24	8	4	4
2,4-Dimethylhexane	P_{8g}	7	18	26	14	8	13	8	26	10	3	3
2,5-Dimethylhexane	P_{8h}	7	18	26	14	8	12	8	28	10	2	3
3,3-Dimethylhexane	P_{8i}	7	18	24	15	9	10	6	28	12	4	3
3,4-Dimethylhexane	P_{8j}	7	18	26	14	8	14	9	24	8	4	4
2-Methyl-3-ethylpentane	P_{8k}	7	18	26	14	8	14	9	24	8	4	4
3-Methyl-3-ethylpentane	P_{8l}	7	18	24	15	9	12	6	24	12	6	3
2,2,3-Trimethylpentane	P_{8m}	7	18	22	16	10	7	4	30	14	5	3
2,2,4-Trimethylpentane	P_{8n}	7	18	22	16	10	5	3	34	16	3	2
2,3,3-Trimethylpentane	P_{8o}	7	18	22	16	10	8	4	28	14	6	3
2,3,4-Trimethylpentane	P_{8p}	7	18	24	15	9	10	7	28	10	4	4
2,2,3,3-Tetramethylbutane	P_{8q}	7	18	18	18	12	0	0	36	18	6	3

In the last three columns of Table XI the corrections for rotational isomerism are given.

When the additive property under consideration is the heat of atomization or heat of formation then

$$P_{trans}=P_{gauche}+\Delta H$$

and

$$\bar{P}=\frac{[trans]\times P_{trans}+[gauche]\times P_{gauche}}{[trans]+[gauche]}$$

so that

$$\bar{P}=P_{trans}-\frac{[gauche]\times\Delta H}{[gauche]+[trans]}.$$

For these properties then a, b and c have the values:

$$a=\frac{[gauche]_1\times\Delta H_1}{[gauche]_1+[trans]_1},$$

$$b=\frac{[gauche]_2\times\Delta H_2}{[gauche]_2+[trans]_2},$$

and

$$c=\frac{[gauche]_3\times\Delta H_3}{[gauche]_3+[trans]_3}.$$

Lack of agreement between the observed values and those calculated from these relations when corrections have been made for zero point energy and rotational isomerism are best explained as a break-down of the assumption of strict additivity. For example, the effects of interaction between H atoms on the terminal C atoms in propane have been neglected. Further, the methyl groups in 1,1,2-trimethylethane are no longer in the *trans* configuration with respect to one another. Addition of another methyl group to give 1,1,2,2-tetramethylethane changes the azimuthal angle between methyl groups still further and by no means in an additive way.

A LINEAR RELATION BETWEEN DIFFERENT ADDITIVE PROPERTIES?

From the point of view of the simple additivity scheme in which all contributions from interactions of nonbonded atoms or localized charge distribution are

neglected, it is apparent that the additive physical property of a molecule in a homologous series is a linear function of the number of substituents n. Elimination of n between two such equations for two physical properties P and Q, gives a linear relation between the two properties of the type

$$\Delta P = c_1 \Delta Q, \tag{15}$$

where c_1 is a constant, or in the integrated form

$$P = c_1 Q + c_2, \tag{15a}$$

where c_2 is a constant.

It is of interest to inquire whether such a relation is valid when nonbonded interactions are considered. From Eq. (9) it is evident for the substituted methanes that a linear relation between P and Q exists if $A_q \Delta_p = A_p \Delta_q$, or if $\Delta_p = \Delta_q = 0$. It is apparent from Table V for the substituted ethanes, that one must have

$$\alpha_p/\alpha_q = \beta_p/\beta_q = \gamma_p/\gamma_q = \delta_p/\delta_q = \epsilon_p/\epsilon_q = c_1,$$

in order for a relation of the type given in Eq. (15) to exist. This is obviously not true in general so that Eq. (15) cannot be a rigorous relation for the substituted ethanes.

In the case of the substituted ethylenes in order to have a linear relation between P and Q we must have

$$a_p/a_q = b_p/b_q = c_p/c_q = d_p/d_q = \text{constant}.$$

Again this cannot be true in general so that Eq. (15) cannot be rigorously true for the ethylenes. In a similar fashion it is readily seen that Eq. (15) cannot be rigorously true for the substituted benzenes nor for the isomers and first two members of the acyclic aliphatic hydrocarbons.

The normal aliphatic hydrocarbons for $n \geq 3$ are a somewhat special case since, as can be seen from Table X, there is an exact linear relation between the property and n of the type given in (14). Elimination of n between two such linear equations for two physical properties would of course give the relation $\Delta P = c \Delta Q$. Thus, to quite a high degree of approximation (since all nonbonded interactions up to and including interactions between atoms three bonds apart have been considered) one expects a linear relation of the type shown in Eq. (15) to be valid for the normal acyclic hydrocarbons starting with propane. It is readily seen that this will be true also for the normal compounds of the series $C_nH_{2n+1}X$. Linear relations have indeed been obtained between several additive properties and molecular sound velocity[14] for the acyclic normal paraffins and a proof based on the simple additivity scheme has also been given.[15]

TABLE XI. Relations for the acyclic saturated parafins.

	P_1	α	β	γ	ϵ	a	b	c
P_1	1	0	0	0	0	...	...	...
P_2	1	1	0	0	0	...	...	...
P_3	1	1	1	0	0	...	...	...
P_4	1	1	1	1	0	−1	...	...
P_{4a}	1	0	3	0	0	...	...	...
P_5	1	1	1	2	0	−2	...	...
P_{5a}	1	1	1	2	1	...	−1	...
P_{5b}	1	−2	6	0	0	...	...	...
P_6	1	1	1	3	0	−3	...	...
P_{6a}	1	1	1	3	1	−1	−1	...
P_{6b}	1	2	−1	4	2	...	−2	...
P_{6c}	1	0	2	3	2	...	...	...
P_{6d}	1	1	0	4	2	...	...	−1
P_7	1	1	1	4	0	−4	...	...
P_{7a}	1	1	1	4	1	−2	−1	...
P_{7b}	1	2	−1	5	2	−1	−2	...
P_{7c}	1	3	−3	6	3	...	−3	...
P_{7d}	1	0	2	4	2	−1	...	...
P_{7e}	1	2	−2	6	3	...	−1	−1
P_{7f}	1	1	1	4	2	...	−2	...
P_{7g}	1	2	−2	6	4	...	...	...
P_{7h}	1	1	−1	6	4	...	...	...
P_8	1	1	1	5	0	−5	...	...
P_{8a}	1	1	1	5	1	−3	−1	...
P_{8b}	1	2	−1	6	2	−2	−2	...
P_{8c}	1	2	−1	6	2	−2	−2	...
P_{8d}	1	3	−3	7	3	−1	−3	...
P_{8e}	1	0	2	5	2	−2	...	...
P_{8f}	1	3	−4	8	4	−1	−1	−1
P_{8g}	1	2	−2	7	3	...	−3	...
P_{8h}	1	1	1	5	2	−1	−2	...
P_{8i}	1	2	−2	7	4	−1	...	...
P_{8j}	1	3	−4	8	4	...	−2	−1
P_{8k}	1	3	−4	8	4	...	−2	−1
P_{8l}	1	4	−6	9	6	...	...	...
P_{8m}	1	2	−3	8	5	...	−1	...
P_{8n}	1	0	2	5	3	...	−1	...
P_{8o}	1	3	−5	9	6	...	...	...
P_{8p}	1	2	−3	8	4	...	...	−2
P_{8q}	1	1	−3	9	6	...	...	...

In the manner outlined here, relations for bond dissociation energies and activation energies have been derived for these homologous series. Also, when small departures from additivity are taken into account, relations between bond distances are obtained. These results will be presented in subsequent publications.

I am pleased to acknowledge valuable discussion with W. LeB. Ross on the acyclic hydrocarbons.

[14] R. T. Lagemann and W. S. Dunbar, J. Phys. Chem. **49**, 428 (1945).

[15] F. W. Lima, J. Am. Chem. Soc. **70**, 3141 (1948).

The Infrared Spectra of Naphthalene Crystals, Vapor, and Solutions

GEORGE C. PIMENTEL AND A. L. MCCLELLAN*
Department of Chemistry and Chemical Engineering, University of California, Berkeley, California
(Received August 28, 1950)

The infrared spectra of naphthalene in the gas phase, in solutions of carbon tetrachloride, carbon disulfide, and methyl cyclopentane, and as single crystals have been obtained in the region 3300–450 cm^{-1}. The dichroism of three different single crystal planes, including the cleavage plane, has been studied using polarized infrared radiation. The frequencies were segregated into their respective symmetry classes on the basis of an assumed oriented gas model. Band contour data, together with a statistical comparison of the spectrum of the gas phase with the spectra of the condensed phases, establish the usefulness of this model.

As spectroscopic studies are extended to more complicated molecules, the problem of assignment of vibrational frequencies becomes quite difficult. The accumulation of sufficient spectra to allow determination of recurrent frequencies does not usually determine a large enough number of fundamentals to allow a complete assignment. Emphasis must be placed on methods which aid in segregating the observed bands into the appropriate symmetry classes to allow the selection of the fundamentals from just the restricted number of frequencies in the proper class.

The methods available for such a division include the determination of infrared and Raman activity, the measurement of the depolarization of Raman active lines, the study of Raman spectra of single crystals using polarized incident light, the investigation of infrared band contours, the consideration of changes of selection rules in the condensed phases, and the study of polarized infrared absorption spectra of single crystals. For crystals of suitable optical properties, polarized infrared spectra offer a powerful method of attack for this problem, since each infrared active band can be characterized according to its symmetry, bands of different symmetry lying close together can be distinguished, and the symmetry of Raman active lines can frequently be deduced from the symmetry of the infrared active combinations.

Infrared studies of naphthalene are extensive. Elliott and Ambrose[1] recently studied a single crystal of naphthalene using polarized infrared radiation, but restricted their work to the region 5000–2850 cm^{-1}. Bârcă-Gălăteanu[2] investigated the vapor phase spectrum in the region 5000–670 cm^{-1}, detecting only eight bands at frequencies below 3300 cm^{-1}. The spectrum of liquid naphthalene was taken by Bell[3] while solutions of naphthalene were spectroscopically studied by several workers.[4–9] Completely deuterated naphthalene has been prepared by Corrsin[10] and its spectra in solutions taken by Plyler and Lamb.

EXPERIMENTAL

Crystals

Resublimed naphthalene was recrystallized several times from absolute ethyl alcohol and this purified material was used to grow a single crystal.† Sufficient naphthalene was melted in a vertical glass tube which was pointed at the lower end and contained silica gel. The tube was evacuated to eliminate dissolved air, an atmosphere of nitrogen introduced, and the tube slowly lowered (30 cm in 72 hours) from a cylindrical heater maintained at 85°C. A crystal about 1.5 cm in diameter and 10 cm long was obtained. For some crystals, thin sheets were made by cutting parallel to the cleavage plane. Other crystals were prepared at an arbitrary orientation determined by the angle at which the bulk crystal was held in contact with the polishing surface. All crystals were polished to the desired thickness by rubbing on a flat surface covered with lens tissue dampened with carbon disulfide or ethyl alcohol.

Since solid naphthalene forms a biaxial crystal, it is possible to use a polarizing microscope to identify single crystals. For a perfect single crystal, uniform extinction occurs at four positions as the crystal is rotated through 360° around the direction of observation. Although the crystals used in this study showed a mosaic pattern, the extinction characteristics in the most unfavorable case indicated alignment within 15° of rotation.

Naphthalene crystallizes in the $C_{2h}{}^5-P2_1/a$ space group[11,12] and the principal cleavage plane is the *ab* plane. Examination of the isogyre pattern with a petroscopic microscope equipped with a Bertrand lens fixed the orientation of the *b* axis. The studies of

* Present address, California Research Corporation, Richmond, California.
[1] A. Elliott and E. J. Ambrose, Nature **159**, 641 (1947).
[2] D. Bârcă-Gălăteanu, Bull. Soc. Roumaine Phys. **37**, 19 (1936).
[3] F. K. Bell, J. Am. Chem. Soc. **47**, 2811 (1925).
[4] W. W. Coblentz, Carnegie Inst. Publication **35**, 127 (1905).
[5] A. H. Stang, Phys. Rev. **9**, 542 (1917).
[6] J. Lecomte and P. Lambert, Ann. combustibles liquides **13**, 111 (1938).
[7] J. J. Fox and A. E. Martin, J. Chem. Soc. 318 (1939).
[8] F. T. Wall and G. W. McMillan, J. Am. Chem. Soc. **62**, 2225 (1940).
[9] D. Bârcă-Gălăteanu, Bull. Soc. Roumaine Phys. **43**, 5 (1942).
[10] L. Corrsin, Phys. Rev. **79**, 235 (1950).
† We wish to express our gratitude to Mr. Otto Schnepp for the preparation of the crystals of naphthalene.
[11] K. Banerjee, Nature **125**, 456 (1930); Indian J. Phys. **4**, 557 (1930).
[12] Abrahams, Robertson, and White, Acta Cryst. **2**, 233 (1949).

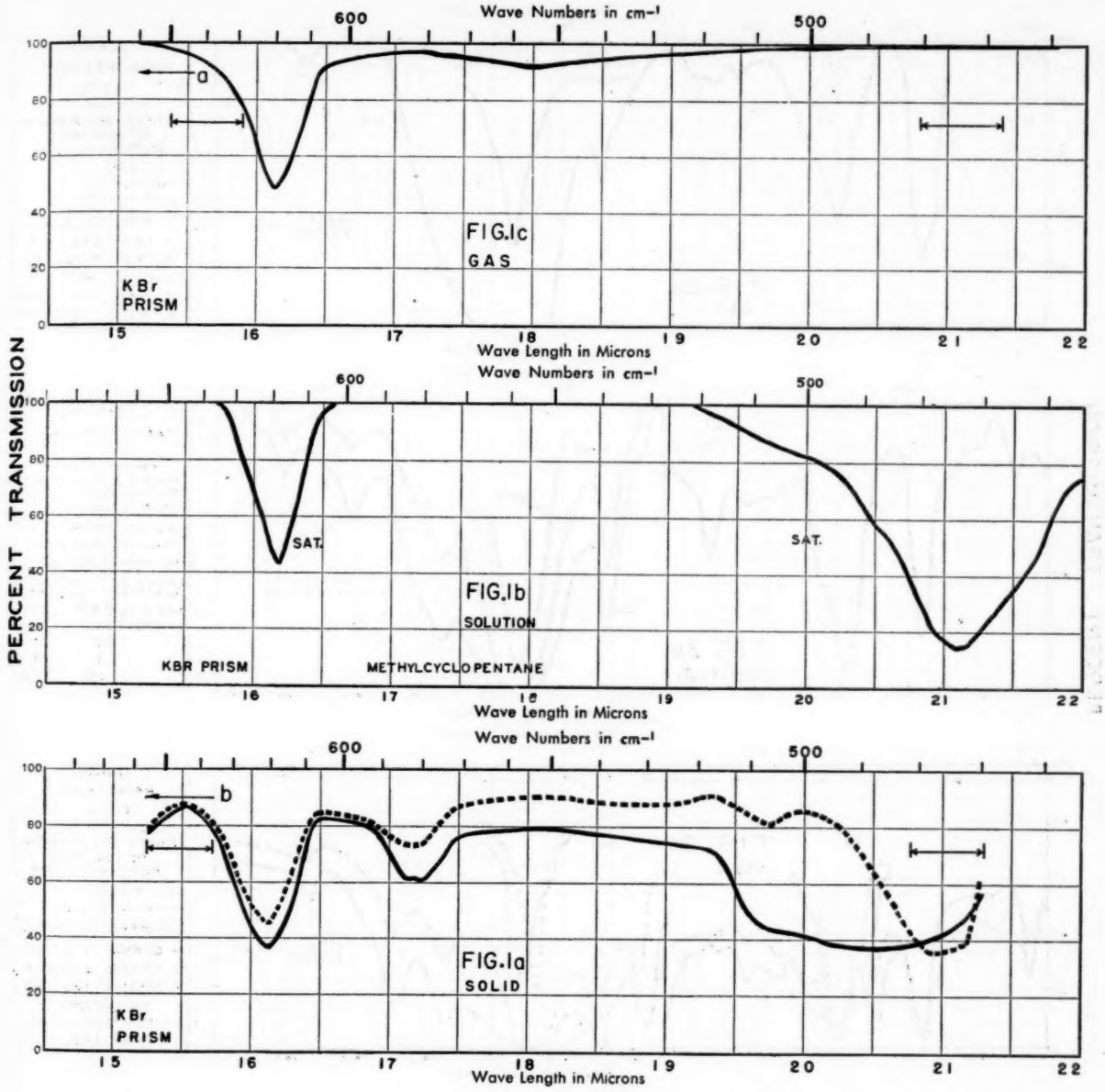

FIG. 1. Spectra of naphthalene between 670 cm^{-1} and 450 cm^{-1}. (a) $C_{10}H_8$ solid. ——— *b* axis perpendicular to plane of polarization. – – – – *b* axis parallel to plane of polarization. (b) $C_{10}H_8$ in solution. (c) $C_{10}H_8$ gas.

Elliott and Ambrose[1] on the dichroism of the band at 3030 cm^{-1} confirm our location of the *b* axis.

Spectra

All the spectra reported here were taken on a Perkin-Elmer Corporation Infrared Spectrometer Model 12-C equipped with LiF, NaCl, and KBr prisms. The accuracy of the frequency measurements was estimated at several specific frequencies to be within ± 2 cm^{-1} at 600 cm^{-1}, ± 5 cm^{-1} at 1000 cm^{-1}, ± 10 cm^{-1} at 2000 cm^{-1}, and ± 15 cm^{-1} at 3000 cm^{-1}. Spectral slit widths used in each region are indicated on the spectra. The polarization of the infrared radiation was accomplished by means of a transmission polarizer consisting of six plates of silver chloride ($5 \times 6 \times 0.025$ cm) placed in the optical path directly after the "Globar" source at a 25° angle to the beam. A holder was used which allowed 360° rotation about the axis of the incident beam and 90° rotation about an axis perpendicular to this beam. The crystal was firmly clamped in the holder and the orientation of the *b* axis was determined.

Spectra of all crystals were recorded at normal incidence for the *b* axis both perpendicular and parallel to the plane of polarization. Other spectra were taken at plus and minus 15° from normal incidence for the perpendicular orientation of the *b* axis. The two spectra of the cleavage plane taken at normal incidence are shown in Figs. 1(a), 2(a), 3(a), and 4(a).

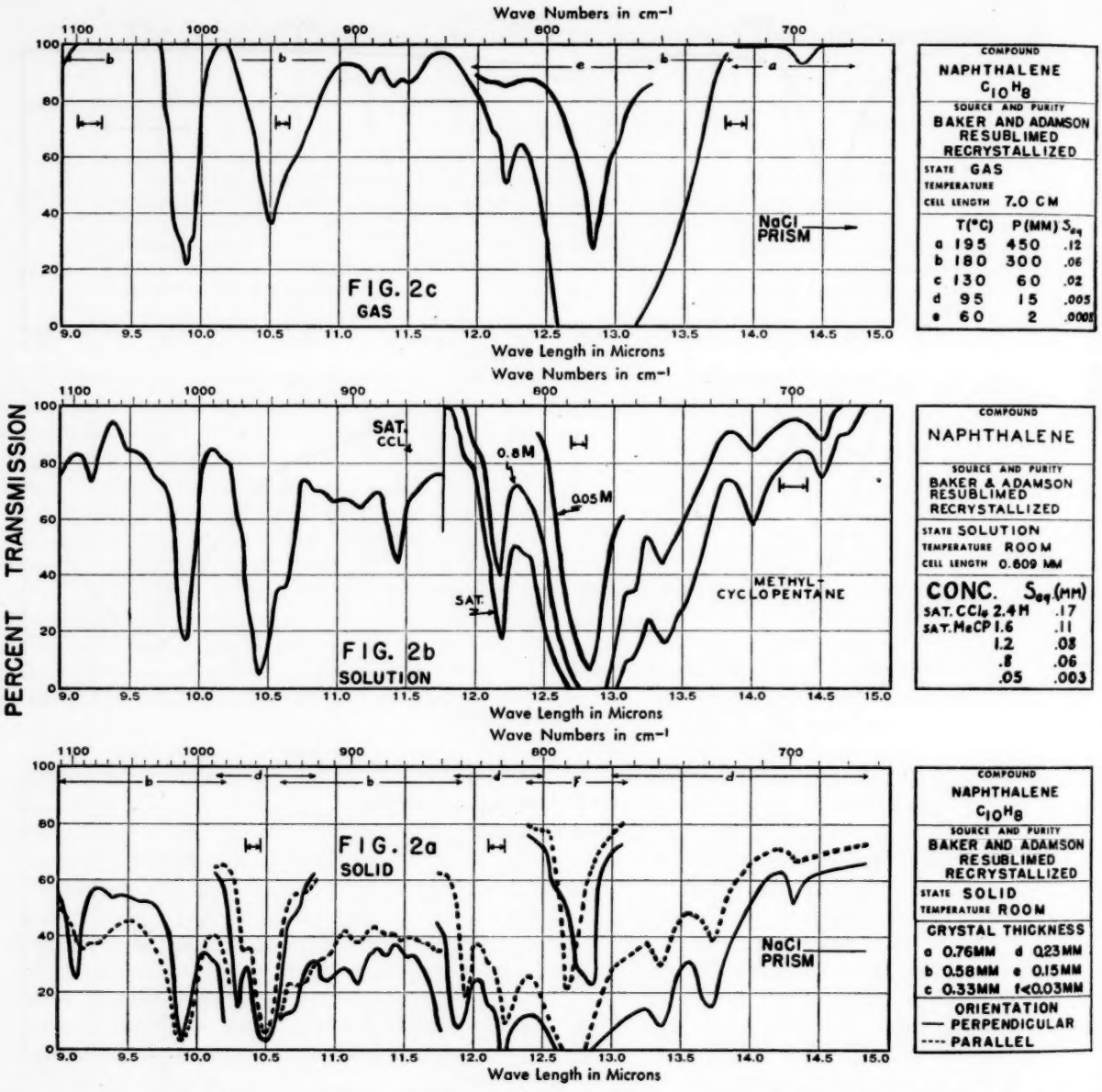

FIG. 2. Spectra of naphthalene between 1100 cm^{-1} and 670 cm^{-1}. (a) $C_{10}H_8$ solid. ——— *b* axis perpendicular to plane of polarization. – – – – *b* axis parallel to plane of polarization. (b) $C_{10}H_8$ in solution. (c) $C_{10}H_8$ gas.

For those crystals other than the cleavage plane the exact orientation of the *b* axis was not determined, but the orientation characteristics were studied. In general the dichroic effects are less pronounced in these crystals. The bands with the most clear-cut symmetry classification in the cleavage plane spectra were correlated with the behavior of the same bands in the other planes.

Spectra of solutions of naphthalene in carbon disulfide, methylcyclopentane, and carbon tetrachloride were obtained by standard methods. The results are shown in Figs. 1(b), 2(b), 3(b), and 4(b). The equivalent crystal thickness, S_{eq}, is given in Fig. 2(b) for each concentration. The spectra for the CS_2 solutions are not presented since they give no additional information.

In addition, the spectrum of naphthalene in the gaseous state was investigated. A 7-cm heated cell with silver chloride windows was used to obtain the spectrum presented in Figs. 1(c), 2(c), 3(c), and 4(c). The equivalent crystal thickness, S_{eq}, is given for each pressure and temperature in Fig. 2(c).

DISCUSSION

A complete collection of observed bands is given in Table I for all phases studied. The frequencies listed for the solid state were restricted to the bands visible in Figs. 1–4. In addition, about sixty very weak bands were located on the spectra of the various crystals studied. In general, the orientation effects of these weak bands were not conclusive. In the case of the solid state, intensity values are listed for the cleavage plane

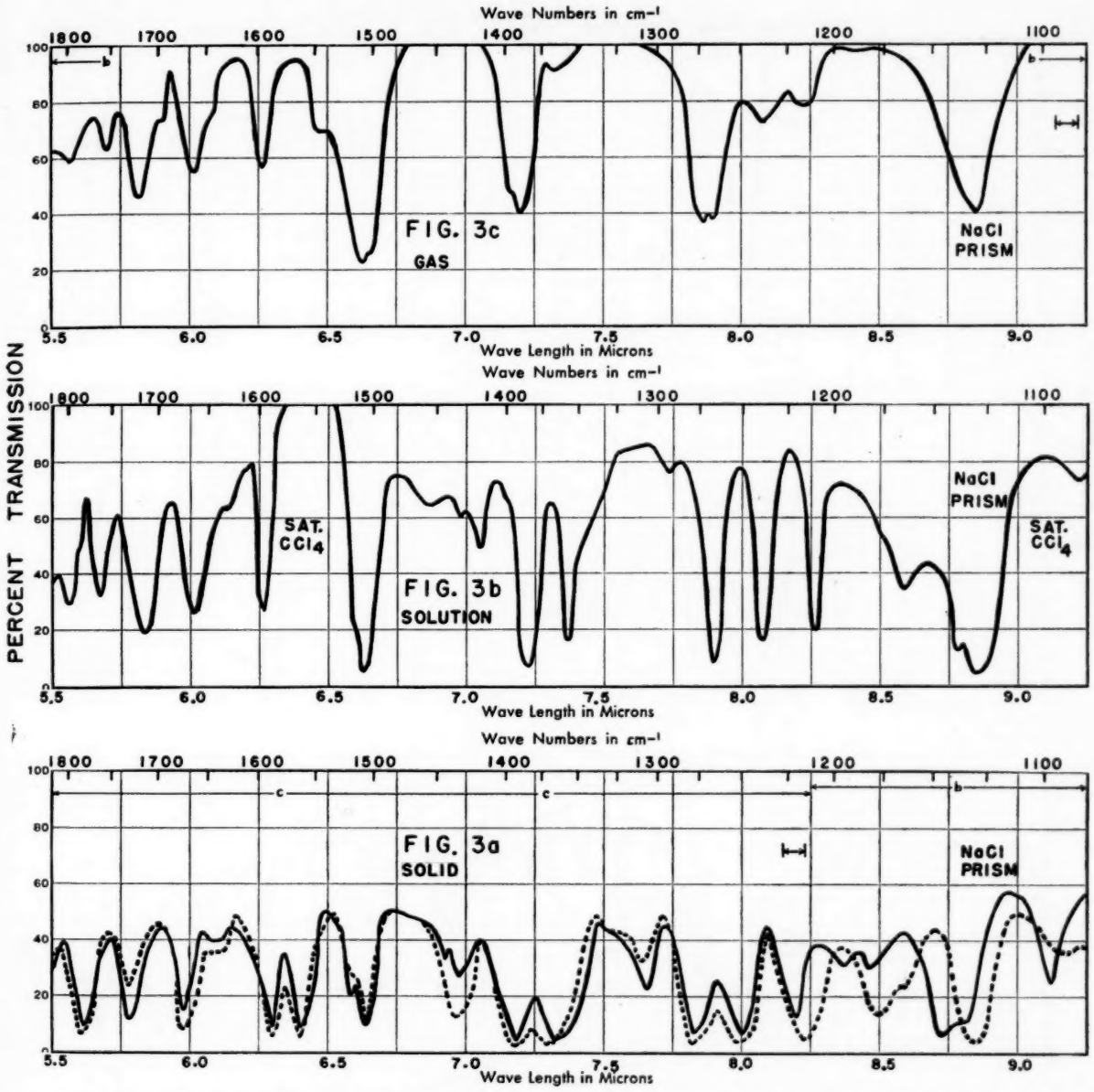

FIG. 3. Spectra of naphthalene between 1800 cm^{-1} and 1100 cm^{-1}. (a) $C_{10}H_8$ solid. ——— b axis perpendicular to plane of polarization. – – – – b axis parallel to plane of polarization. (b) $C_{10}H_8$ in solution. (c) $C_{10}H_8$ gas.

in the four spatial arrangements described above. The intensity values given for the four orientations are internally consistent only for each observed band since reduction of the intensities of all bands to a common basis tends to obscure the dichroism of the weaker bands. These values allow determination of the dichroism, or intensity variation with orientation, of each band.

The molecular symmetry of naphthalene is that of the D_{2h} group and the application of group theoretical postulates provides selection rules for the gas phase and the number of fundamentals of each vibrational type. These results are summarized in Table II.

The effect of the crystalline field may be determined by the methods proposed by Halford,[13] Hornig,[14] and Winston and Halford.[15] Figure 5 shows the relationships among the vibrational classes of the free molecule, those of a molecule subject to the perturbations of the crystal field (site group C_i), and those of two molecules in the symmetry of the unit cell (factor group C_{2h}). In either analysis of the effect of the solid lattice, all of the gerade vibrations are expected to remain inactive in the infrared and all of the ungerade vibrations are expected to be active. Thus it should be possible to locate the gas phase inactive vibrations of A_u class in

[13] R. S. Halford, J. Chem. Phys. **14**, 8 (1946).
[14] D. F. Hornig, J. Chem. Phys. **16**, 1063 (1948).
[15] H. Winston and R. S. Halford, J. Chem. Phys. **17**, 607 (1949).

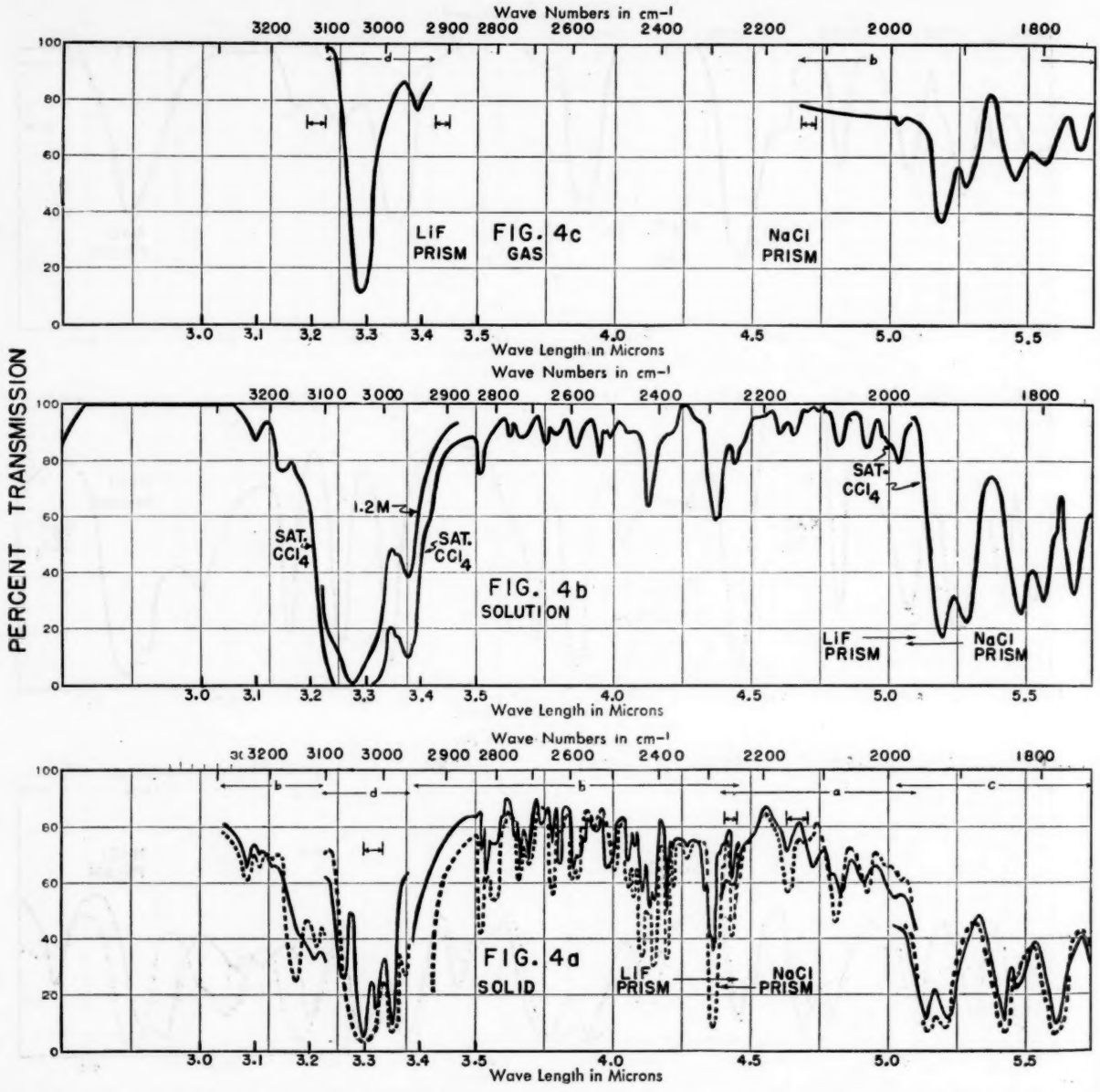

FIG. 4. Spectra of naphthalene between 3300 cm^{-1} and 1800 cm^{-1}. (a) $C_{10}H_8$ solid. ——— b axis perpendicular to plane of polarization. – – – – b axis parallel to plane of polarization. (b) $C_{10}H_8$ in solution. (c) $C_{10}H_8$ gas.

the spectrum of solid naphthalene (as indicated in Table II).

The factor group analysis predicts that each vibration of gaseous naphthalene will be split into two components. In the case of the infrared active vibrations, the A_u component should show a dichroism with maximum absorption when the plane of polarization is parallel to the b axis of the crystal. The corresponding B_u component should have maximum absorption somewhere in the plane perpendicular to the b axis. Since the magnitude of the splitting is not predicted and the dichroism is not expected to distinguish the gas phase symmetry classes, it is possible that the spectrum of solid naphthalene would be hopelessly complex. By comparison between the gas phase and solid phase spectra, it is apparent that this is not the case. For every prominent band appearing in the gas spectrum there is a corresponding band in the solid spectrum. In the heavily occupied region between 690 and 1600 cm^{-1}, 37 bands are observed in the solid spectrum and 18 in the gas spectrum. While the average spacing in the solid spectrum is about 25 cm^{-1}, the average difference in frequency between a gas phase absorption and the nearest band in the solid spectrum is only 2.6 cm^{-1}. A statistical analysis (the chi-squared test) based on the assumption of uniformly spaced solid phase absorptions and completely uncorrelated gas phase absorptions indicates the probability of such a distribution is 0.001.

TABLE I. Observed infrared bands of naphthalene.

Vapor	Solution	Solid	Normal incidence ⊥	Normal incidence ∥	−15° incidence ⊥	+15° incidence ⊥	Symmetry
		Freq					
	473(8)	478(10)	4	6	4	4.5	B_{2u}
		506(8)	5	2	5	5	$B_{1u}B_{3u}$
		581(4)	3	3	2	3	B_{3u}(?)
620(5)	618(5)	620(9)	6	5	5.5	6	B_{3u}
698(1)	689(2)	699(2)	1.7	0.7	1.3	1.3	B_{1u}[a]
	715(4)	726(6)	7	5	6.5	6.5	$B_{1u}B_{3u}$
747(3)	750(8)	749(6)	7	5	7	6	B_{1u}
	761(5)	766(5)	6.5	2	6	5.5	B_{1u}
779(10)	779(10)	778(10)					B_{3u}[a]
		787(10)					B_{2u}[a]
821(5)	821(8)	819(6)	7.5	7	7	7	B_{1u}[a]
		841(6)	8	6	8.5	8	B_{1u}
868(1)	864(2)	870(1)	1	1	1.5	1.5	?
878(1)	878(4)	880(1)	1	0.5	0.4	0.8	B_{2u}
891(1)		895(3)	4	1.5	4	3.5	B_{1u}
		915(3)	3.5	1	2	4	B_{3u}
		932(2)	0	2	6	4	B_{2u}
	943(3)	937(1)	4	1	6.5	6	B_{1u}
949(6)	957(10)	953(6)	9	9	9	9	B_{1u}[a]
		970(3)	9	4	7	9	B_{3u}
1012(8)	1012(9)	1014(5)	9.5	9.5	7	9	B_{3u}[a]
		1068(2)	0.5	1.5	1.0	0.5	B_{2u}
	1085(3)	1094(2)	6	3	4	6	B_{3u}
1130(6)	1130(10)	1133(5)	8	10	10	5	B_{2u}
	1138(2)	1146(5)	9	0	9	9	$B_{1u}B_{3u}$
	1165(2)	1167(2)	0	4	0	0	B_{2u}?
		1180(3)	2	7	7	1	B_{2u}
		1195(1)	2	0	0	3	B_{3u}
1214(2)	1210(7)	1217(3)	7	8	5.5	8.5	B_{3u}[a]
1238(2)	1238(8)	1244(10)	9	9.5	9	9	B_{2u}
1266	1267(9)						
1271(6)		1271(10)	9	9.5	9	8	B_{2u}
	1293(3)	1307(2)	5	3	4	5.5	B_{2u}
1366(1)	1358(7)	1362(9)	8	9	8.1	8.2	B_{2u}
1389(6)	1388(10)	1385(10)	9	9.4	9.4	9.1	B_{2u}
	1420(4)	1424(2)	4	4.5	4.5	4.1	B_{2u}
	1435(2)	1434(2)	5	7.5	5	4.5	B_{2u}
	1455(2)	1446(1)	8	4	2.5	4	B_{3u}
1504							
1509(8)	1510(10)	1506(3)	8	8	6.5	9.5	B_{3u}[a]
		1519(½)	6.5	5.7	4.5	8	B_{3u}
1543(3)		1542(2)	3	4	3.5	3	B_{2u}
		1563(3)	8	9	9	8	B_{2u}
1596(4)	1595(6)	1594(3)	7.5	8.5	8.5	6.5	B_{2u}
		1642(2)	3.5	4.5	4	3	B_{2u}
1661(4)	1665(5)	1673(3)	7	8.5	7.5	6	B_{3u}
		1678(3)	5	5	3	7	B_{3u}?
1720(4)	1715(8)	1737(3)	7.5	5.5	4	8	B_{3u}
1763(1)	1762(5)	1786(3)	7.5	8.5	7.5	6.7	B_{2u}
1798(½)	1797(5)	1817(1)	4.2	2.7	2.5	6	B_{3u}
1835(1)	1826(6)	1845(3)	8	9	7.8	8	$B_{2u}B_{3u}$
1896(3)	1892(7)	1919(3)	7.5	8.5	7.7	7.5	B_{2u}
1938(4)	1925(8)	1944(3)	7.8	8.5	7.5	8	$B_{2u}B_{3u}$
1988(½)	1988(2)	1992(½)	1	0.7	1	1	$B_{1u}B_{3u}$
	2036(2)	2032(0)	1.2	2	1.5	1	B_{3u}
		2064(2)	2.5	1.5	2.5	1.5	B_{1u}
	2075(1)	2080(3)	1.5	4	2	1	B_{2u}
		2118(½)	1.5	0.5	2	1.5	B_{1u}
	2149(½)	2163(½)	1.5	3	2	2	B_{2u}?
	2173(½)						
	2251(2)	2257(3)	2.5	5	2.5	2.3	B_{2u}
	2292(3)	2292(4)	5.5	8.5	6	5	B_{2u}
		2342(2)	1.5	1.5	2	2.5	B_{3u}?
		2372(2)	2.5	4.5	2.5	2.5	B_{2u}?
	2385(1)	2383(3)	4	6	4.2	4.4	?
	2424(2)	2420(2)	4	3	2.5	5	B_{3u}
		2435(3)	3	5	3	2.7	B_{2u}
		2455(2)	1	2	1	0.7	B_{2u}
		2467(2)	1.7	2	2	1.5	B_{3u}
	2510(½)	2514(2)	2.2	2	2	2.5	B_{3u}
	2530(1)	2544(1)	1	1	1	1.5	B_{3u}?
		2570(½)	1.5	0.5	1.4	1.3	$B_{1u}B_{3u}$
	2588(1)	2584(½)	2	2.5	2	2	B_{2u}?
		2594(1)	2.5	2.6	2.5	2.6	$B_{2u}B_{3u}$[a]
		2628(2)	2.5	1	2	2.5	B_{3u}
	2643(½)	2646(2)	1.5	3.5	1.5	1.5	B_{2u}?
	2662(½)	2665(½)	0.6	0.3	0.7	1.2	B_{3u}
		2708(2)	2.5	2.0	2.0	2.5	B_{3u}
	2726(1)	2732(2)	3	3	3	3	?
	2758(½)						
		2826(2)	3	3	2.5	3.5	B_{3u}?
	2838(3)	2837(3)	1.7	5	1.7	2	B_{2u}?
2948(1)	2962(6)	2968(5)	0.5	3	0.5	0.3	B_{2u}
	2973(1)	2984(9)	9	9	8	9	B_{3u}?
3034(9)	3051(10)	3033(10)	9.5	9.8	9.5	9.3	B_{2u}
	3060(1)	3070(8)	5.9	6	3.4	7.5	B_{3u}?
		3114(½)	5	4.5	5	5	$B_{1u}B_{3u}$
		3142(4)	4	6.5	3.5	3.5	B_{2u}?
	3175(2)						
	3230(1)	3213(½)	0.5	1.0	0.3	0.6	B_{2u}?
		3240(2)	1.3	1.5	1.5	1	$B_{2u}B_{3u}$

[a] Symmetry decided using alternate crystals; see discussion.

Hence the assumption of uncorrelated gas and solid absorptions is very improbable. Rather each absorption observed in the spectrum of gaseous naphthalene is observed in the spectrum of the solid at essentially the same frequency.

It is still possible to assume that the additional bands observed in the solid are to be attributed to splitting of the gas-phase frequency into two components, one essentially unchanged and the other shifted by about 25 cm^{-1}. This alternative may be eliminated by consideration of the spectra of solutions of naphthalene. Since all but nine of the bands of the solid phase are observed in the solution spectra (where doublet splitting does not occur), it is apparent that the additional bands are observed because longer path lengths are available in the condensed phases and some of the selection rules of the molecular symmetry are no longer operative. It may be concluded that the perturbation of the vibrational frequencies of gaseous naphthalene upon solidification is about 3 cm^{-1} and the doublet splitting is quite small compared to the average spacing of observed bands. Several absorption bands show an apparent

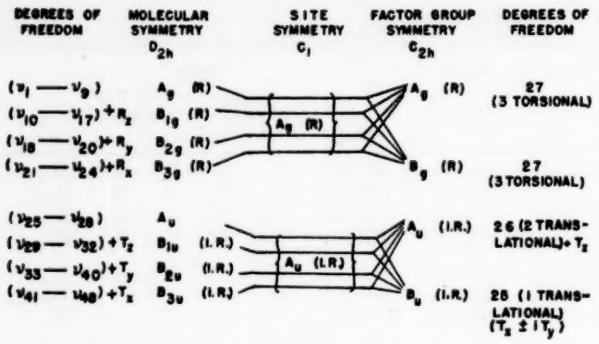
DEGREES OF FREEDOM
MOLECULAR SYMMETRY D_{2h}
SITE SYMMETRY C_i
FACTOR GROUP SYMMETRY C_{2h}
DEGREES OF FREEDOM
$(\nu_1 - \nu_9)$ A_g (R)
$(\nu_{10} - \nu_{17}) + R_z$ B_{1g} (R)
$(\nu_{18} - \nu_{20}) + R_y$ B_{2g} (R)
$(\nu_{21} - \nu_{24}) + R_x$ B_{3g} (R)
A_g (R)
B_g (R)
27 (3 TORSIONAL)
27 (3 TORSIONAL)
$(\nu_{25} - \nu_{28})$ A_u
$(\nu_{29} - \nu_{32}) + T_z$ B_{1u} (I.R.)
$(\nu_{33} - \nu_{40}) + T_y$ B_{2u} (I.R.)
$(\nu_{41} - \nu_{48}) + T_x$ B_{3u} (I.R.)
A_u (I.R.)
B_u (I.R.)
26 (2 TRANSLATIONAL) + T_z
28 (1 TRANSLATIONAL) ($T_x \pm iT_y$)

FIG. 5. Symmetry classes for gaseous and solid naphthalene.

shift of the minimum percent transmission on rotating the crystal, probably evidence of the magnitude of this splitting. On this assumption, the average shift is about 2.5 cm^{-1} with the band at 779 cm^{-1} showing the largest apparent splitting, about 8 cm^{-1}.

Since the crystal field perturbation seems to be quite small, it is possible to estimate the magnitude of the dichroism by assuming the behavior is that of a gas whose molecules remain oriented in space just as they are in the crystal. The dichroism of such an oriented gas model will be the superposition of the individual dichroisms of the two types of molecular orientations indicated by the unit cell. The dichroic effects contributed by one molecule will depend on the orientation of a unit vector parallel to the direction of molecular dipole change (associated with the vibration) relative to the direction of polarization of the light. Each molecule will absorb at any particular gas phase frequency with an intensity proportional to the square of the magnitude of the projection of this unit vector onto the polarization vector of the incident light. By summing the contributions from each molecule of the unit cell, a figure proportional to the total intensity of a band for any crystal orientation may be obtained. Using this model, the calculated curves in Fig. 6 were obtained, in qualitative agreement with the empirically observed dichroism patterns shown by the solid curves. The increased absorption observed at angles of incidence more than 15° from normal incidence is undoubtedly due to mechanical blocking of the beam by the crystal holder.

It is important to note that only qualitative agreement can be expected in view of several uncertain factors relating to the optical properties of the crystal. Reflection and scattering losses are presumably dependent upon angle of incidence, the refractive index varies in some complicated fashion near absorption bands, and the optic axes of the crystal may be frequency-dependent. The assumption has been made that the predominant effect is that of the dichroism associated with molecular orientation, and the empirical agreement with the band contour assignments shown in Table III supports this assumption. Further study of the optical properties of naphthalene crystals is in progress in this laboratory to provide additional information on the relative importance of the other factors.

In general, the classification was taken from the dichroism of the cleavage plane crystal since these data were more definitive. In addition, the spectra of the crystals from two arbitrary, noncrystallographic planes allowed the determination of the symmetries of several bands (reference a in Table I) for which the dichroism of the cleavage plane was not conclusive. Since the orientation of the *b* axis was not known accurately in either of these two crystals and because of possible interference resulting from optical effects, the dichroism of each symmetry type was determined empirically by correlating with the well-identified bands listed in Table III.

The oriented gas model ignores the predictions of the factor group analysis and must be used only after careful consideration of the probable magnitude of the crystalline field perturbations. Fortunately, there is opportunity to check several assignments made on the basis of the dichroism against those obtained by consideration of band contours. The dichroism of nine strong bands was studied in detail and the three distinct patterns shown in the solid curves of Fig. 6 could be correlated with the calculated curves to allow assignments to symmetry classes. These same bands, studied in the gas phase, could be partially classified according to symmetry classes by the band contours. Table III compares the two assignments.

TABLE II. Selection rules of naphthalene.

Class	No. vibrations	No. skeletal vibrations	Gas	Solid
A_g	9	5	*R*	*R*
A_u	4	2	inactive	*IR*
B_{1g}	8	4	*R*	*R*
B_{1u}	4	2	*IR*	*IR*
B_{2g}	3	1	*R*	*R*
B_{2u}	8	4	*IR*	*IR*
B_{3u}	4	2	*R*	*R*
B_{3u}	8	4	*IR*	*IR*

For the nine frequencies to which both methods could be applied there are eight correlations, and the only disagreement involves a doubtful band contour assignment. This apparent success of the assumed model for naphthalene suggests that the method may be valuable in interpreting the dichroism of other molecular crystals where the factor group analysis is not definitive. It should be applied only to crystals with weak intermolecular forces (as indicated spectroscopically by small frequency shifts and small splitting of multiplets) and only after consideration is given to the optical properties of the crystal involved.

It is important to note that the oriented gas model in itself takes no cognizance of the predictions of the factor group analysis concerning splitting of multiplets,

dichroism of the components, or solid phase selection rules. For example, the oriented gas model makes use of gas phase selection rules and incorrectly predicts that the gas phase A_u vibrations of naphthalene remain totally inactive in the solid phase. This is in apparent disagreement with the observation that several bands which do not seem to be multiplet components appear with reasonable intensity in the solid phase spectra and are unobserved in either the gas phase spectra or the Raman spectra (e.g., 581 and 841 cm^{-1}). Consequently, it seems that one may assume applicability of the oriented gas model only after it has been shown that the crystalline field perturbations are negligible. It remains a problem for further study to determine the degree of applicability of the predictions of this model when they are superimposed upon the predictions of the factor group analysis if the crystalline field perturbations are found to be large.

TABLE III. Correlation of band species derived from dichroism and gas-phase-band contours.

Frequency	Dichroism class	Band contour class
620 cm^{-1}	B_{3u}	B_{1u}, B_{3u}
779	B_{3u}	B_{1u}, B_{3u}
821	B_{1u} (?)	B_{1u}, B_{3u}
949	B_{1u}	B_{1u}, B_{3u}
1012	B_{3u}	B_{1u}, B_{3u}
1130	B_{2u}	B_{1u}, B_{3u} (?)
1269	B_{2u}	B_{2u}
1389	B_{2u}	B_{2u}
1590	B_{2u}	B_{2u} (?)

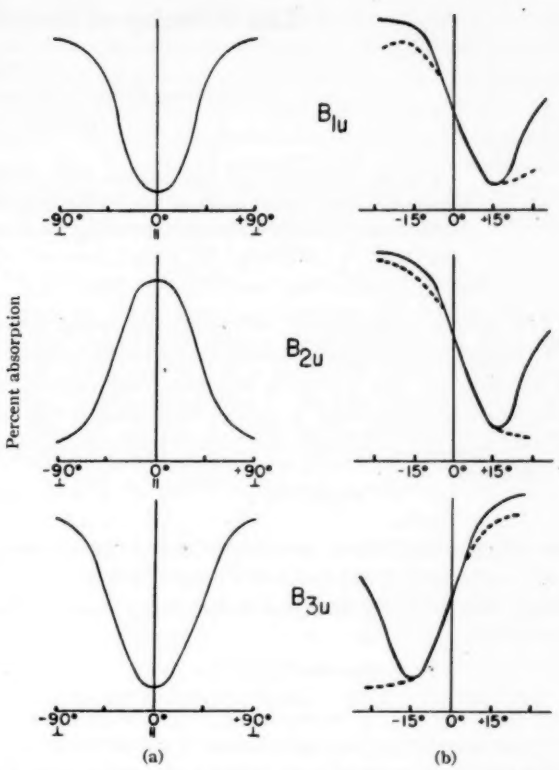

FIG. 6. Dichroism of the cleavage plane of solid naphthalene. (a) Effect of rotation of the b axis with respect to the plane of polarization, crystal at normal incidence, experimental and calculated dichroism. (b) Effect of change of the angle of incidence with the b axis kept perpendicular to the plane of polarization. ——— experimental dichroism. - - - - calculated dichroism.

ACKNOWLEDGMENT

We wish to express our appreciation to the American Petroleum Institute, Research Project 44, for financial support of phases of this investigation. We wish to thank Professor A. Pabst of the Mineralogy Department for his aid in determining the crystal orientations.

The Velocity of Sound in Electrolytic Solutions

SIDNEY BARNARTT
Westinghouse Research Laboratories, East Pittsburgh, Pennsylvania
(Received October 18, 1951)

A relationship between the velocity of sound in electrolytes and concentration has been derived for extremely dilute solutions from the Debye-Hückel limiting law. The equation fits the observed data at higher concentrations when the theoretical coefficients are replaced by empirical constants.

No simple relationship between the velocity of sound u in electrolytic solutions and the molarity c of the solution has yet been reported. For extremely dilute solutions, however, a simple relationship can be derived using the interionic attraction theory to expand the equation

$$u^2=k/\beta d, \tag{1}$$

where β is the isothermal compressibility of the solution, d its density, and k the ratio of its specific heats.

From the limiting Debye-Hückel law, it has been shown[1] that

$$\phi_V=\phi_V^0+S_V c^{\frac{1}{2}}, \tag{2}$$

where $\phi_V=(V-n_1\bar{V}_0)/n_2$ is the apparent molal volume of the dissolved salt, V is the volume of the solution, and $\bar{V}_0$ the molal volume of pure solvent; n_1 and n_2 are the number of moles of solvent and solute in the solution. For a given solvent at a fixed temperature, the slope S_V is the same for all salts of the same valence type. In terms of density, Eq. (2) takes the form,[2]

$$d=d_0+Ac-Bc^{\frac{3}{2}}, \tag{3}$$

where $A=10^{-3}(M_2-d_0\phi_V^0)$ and $B=10^{-3}d_0S_V$; M_2 is the molecular weight of the dissolved salt, and subscript zero denotes pure solvent.

Similarly it has been shown[3] that the apparent molal compressibility $\phi_K=(\beta V-n_1\beta_0\bar{V}_0)/n_2$ is given by the limiting Debye-Hückel theory as

$$\phi_K=\phi_K^0+S_K c^{\frac{1}{2}}. \tag{4}$$

Again the slope S_K is constant for all salts of the same valence type. Combination of Eqs. (2) and (4) yields[4]

$$\beta=\beta_0-Dc+Ec^{\frac{3}{2}}, \tag{5}$$

where $D=10^{-3}(\beta_0\phi_V^0-\phi_K^0)$ and $E=10^{-3}(S_K-\beta_0S_V)$.

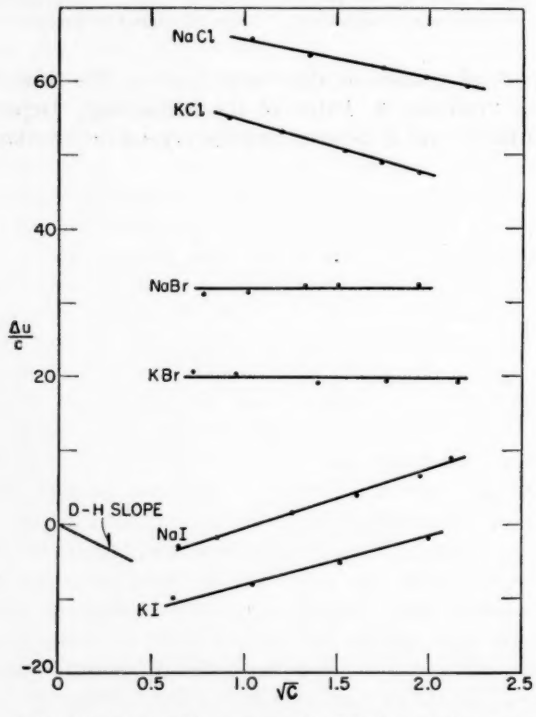

FIG. 1. Velocity of sound in aqueous alkali halide solutions at 20°C. Data of Freyer (see reference 8).

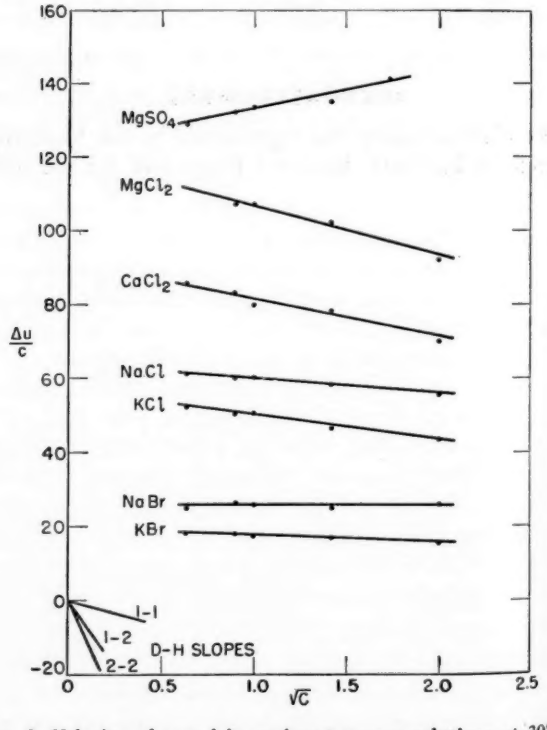

FIG. 2. Velocity of sound in various aqueous solutions at 30°C. Data of Weissler and Del Grosso (see reference 9).

[1] O. Redlich and P. Rosenfeld, Z. physik. Chem. **A155**, 65 (1931).

[2] W. C. Root, J. Am. Chem. Soc. **55**, 850 (1933).

[3] F. T. Gucker, Chem. Revs. **13**, 111 (1933).

[4] F. T. Gucker, J. Am. Chem. Soc. **55**, 2709 (1933).

For extremely dilute solutions Eq. (1) may be written

$$-2\Delta u/u_0=\Delta\beta/\beta_0+\Delta d/d_0, \tag{6}$$

where $\Delta u=u-u_0$, etc. Substitution for $\Delta\beta$ from Eq. (5) and for Δd from Eq. (3) gives the desired result,

$$u=u_0+Fc-Gc^{\frac{3}{2}}, \tag{7}$$

where

$$F=\frac{u_0}{2}\left(\frac{D}{\beta_0}-\frac{A}{d_0}\right)=\frac{u_0}{2000}\left(2\phi_V{}^0-\frac{\phi_K{}^0}{\beta_0}-\frac{M_2}{d_0}\right) \tag{8}$$

and

$$G=\frac{u_0}{2}\left(\frac{E}{\beta_0}-\frac{B}{d_0}\right)=\frac{u_0}{2000}\left(\frac{S_K}{\beta_0}-2S_V\right). \tag{9}$$

Thus the slope of the linear plot of $\Delta u/c$ against $c^{\frac{1}{2}}$ is the same for all salts of the same valence type.

Figures 1 and 2 show limiting Debye-Hückel slopes,[5] together with empirical data[6,7] covering wide ranges of concentration. The experimental curves refer to solutions more concentrated than 0.3 molar (for more dilute solutions the percentage error in Δu increased rapidly). It is not surprising, therefore, that the curves exhibit considerable deviations from the limiting slopes at the lowest concentrations shown. An adequate comparison with the limiting Debye-Hückel theory must await improved techniques for the measurement of sound velocity, since a minimum precision of $\pm5\times10^{-3}$ meter per second ($\pm3\times10^{-4}$ percent) is required.

A method of obtaining the required accuracy is suggested by the following technique which has been used by Holbrook[8] to measure small changes of velocity in solids. A pulse of acoustic energy is transmitted through a fixed length of solution by means of a pulsed oscillator at one end. At the other end the pulse is received and returned to the oscillator to trigger the next pulse. Thus the velocity of sound in the solution is determined from the number of pulses per second, a frequency measurement which can be made with great relative precision.

The two figures reveal the striking fact that the experimental data are well represented by Eq. (7) if F and G are replaced by empirical constants. Hence this equation provides a convenient means of recording and interpolating sound velocities in electrolytic solutions.

[5] Evaluated from recalculated values of S_K and S_V given by H. S. Harned and B. B. Owens, *The Physical Chemistry of Electrolytic Solutions* (Reinhold Publishing Corporation, New York, 1950), p. 587.

[6] E. B. Freyer, J. Am. Chem. Soc. **53**, 1313 (1931).

[7] A. Weissler and V. A. Del Grosso, J. Acoust. Soc. Am. **23**, 219 (1951).

[8] R. D. Holbrook, J. Acoust. Soc. Am. **20**, 590 (1948).

THE JOURNAL OF CHEMICAL PHYSICS VOLUME 20, NUMBER 2 FEBRUARY, 1952

Correlation of Hammett's σ-Values with Electron Densities Calculated by Molecular Orbital Theory*

H. H. Jaffé

Venereal Disease Experimental Laboratory, U. S. Public Health Service, School of Public Health and Department of Chemistry, University of North Carolina, Chapel Hill, North Carolina

(Received September 25, 1951)

It is shown that Hammett's σ-values can be correlated with electron densities calculated by the MO LCAO method. Since Coulomb and exchange integrals for atoms other than carbon are not accurately known, an absolute calculation of σ's is not possible. Nevertheless, σ-values permit derivation of a self-consistent and reasonable set of parameters which can be used to calculate reasonable values for absorption frequencies, mesomeric moments, and orienting power of the substituents.

THE molecular orbital (MO) method, in the LCAO approximation, has long been used for the calculation of electron distribution in unsaturated organic compounds. Such calculations have been quite successful with hydrocarbons and free radicals derived from them, but have been less successful when applied to heterocyclic compounds. Fewer attempts have been made to apply the same methods to benzene derivatives substituted by heteroatoms. Hückel,[1] and Wheland and Pauling[2] have used electron distribution calculations to explain the orienting and activating influences of substituents in the benzene ring. Sherman and Ketelaar[3] have calculated bond lengths of carbon-chlorine bonds in chlorine substituted benzenes. Similar calculations include those of Sandorfy,[4] Coulson and Jacobs,[5] Ploquin[6] and Matsen and co-workers.[7]

Coulson and Dewar[8] have summarized the short-

* Presented before the XIIth International Congress of Pure and Applied Chemistry, New York City, September, 1951.

[1] E. Hückel, Z. Physik **72**, 310 (1931).

[2] G. W. Wheland and L. Pauling, J. Am. Chem. Soc. **57**, 2086 (1935).

[3] J. Sherman and J. A. A. Ketelaar, Physica **6**, 572 (1939).

[4] C. Sandorfy, Bull. soc. chim. France, 615 (1949).

[5] C. A. Coulson and J. Jacobs, J. Chem. Soc. 1983 (1949).

[6] J. Ploquin, Compt. rend. **231**, 133 (1950), Bull. soc. chim. France, *D*359 (1949).

[7] F. A. Matsen, *et al.*, J. Am. Chem. Soc. **72**, 5243, 5248, 5250, 5252, 5260 (1950).

[8] C. A. Coulson and M. J. S. Dewar, Disc. Faraday Soc. **2**, 54 (1947).

TABLE I. Ionization potentials and Coulomb integrals.

Substituent	α^a from Table III	Ionization potential[b] of HX	MeX	EtX
F	1.60 to 2.00		15.0	
Cl	1.63	12.8	11.3	10.9
Br	1.63	12.0	11.2	10.9
I	1.55	10.3	9.5	9.3
OH	0.51	12.6	10.8	10.7
SH	−0.05 to 0.70	10.5		9.7
NH_2	−0.70	10.8	9.8	

[a] See reference a, Table III.
[b] All ionization potentials are in eV. The values are taken from W. C. Price, Chem. Revs. 41. 257 (1947), with the exception of the value for methyl fluoride, which is taken from reference 8.

comings of the MO method. While all of the objections they raise against the method apply in calculations on substituted benzenes, the introduction of heteroatoms further requires a choice of numerical values for several parameters, which at the present time cannot be derived easily from theoretical considerations. These parameters are:

(1) The Coulomb Integral of the Heteroatom (α)

In MO calculations the Coulomb integral of carbon is usually taken as 0; this assignment determines the zero-point of the energy scale. Introduction of a heteroatom into the conjugated system requires a choice of a numerical value for its Coulomb integral relative to that of carbon. Wheland and Pauling[2] have derived such integrals for nitrogen and oxygen by comparison of calculated and experimental resonance energies. Though their values were crude, they were sufficiently accurate for the qualitative conclusions reached and have been used by the majority of subsequent authors. Another treatment consists of identifying the Coulomb integrals with the ionization potentials of the atom in the same valence state.[9] While this is probably the most valid assumption, an arbitrary choice of reference compound is required (See Table I).

(2) The Effect of the Heteroatom on the Coulomb Integrals of the Carbon Atoms

Wheland and Pauling[2] have assumed that a carbon atom adjacent to an heteroatom of Coulomb integral α has a Coulomb integral of 0.1α. Most workers have accepted this value or values close to it. The effect on all other carbon atoms was neglected in these treatments.

A different approach to a treatment of this effect is suggested by experimental work summarized by Branch and Calvin.[10] They propose that a polar effect of $\epsilon^n D$ is induced in the nth atom from a heteroatom, where D is the effect on an adjacent atom. The constant ϵ is given a value of $\frac{1}{3}$. This treatment permits an approximate calculation of the dissociation constants of a large number of acids. It seems reasonable to assign a corresponding increment of $\epsilon^n\alpha$ to the Coulomb integral of the nth atom from the heteroatom of Coulomb integral α. This method, which has been used successfully by Dewar[11] and by Gold,[12] was applied in the present work.

(3) Resonance Integral of the Heteroatom-Carbon Bond (γ)

The majority of authors have made the approximation that the resonance integral of the heteroatom-carbon bond is equal to that of a carbon-carbon bond. This assumption does not appear reasonable in substituted benzenes, where the bond from the ring to the substituent has largely single bond character. Lennard-Jones[13] has derived a general expression for resonance integrals:

$$\gamma/\beta=(E_{C=X}-E_{C-X})/(E_{C=C}-E_{C-C}),$$

where E is the energy of the bond defined by the subscript, and β is a carbon-carbon bond resonance integral. His treatment is justified where the bond in question has largely double bond character, but is not applicable to the present problem. Sandorfy[4] has set the resonance integrals proportional to the negative 4th power of the bond distance involved, but such an approximation completely neglects the differences in atomic orbitals of different elements.

The completely theoretical calculation of resonance integrals has recently been achieved,[14] but application of such methods is not feasible in the present problem.

Longuet-Higgins and Wheland[15] have pointed out that the results of most previous MO calculations were not sensitive to the choice of numerical values for the parameters α and γ. For this reason it would be desirable to find a property of molecules which, when calculated by the MO method, is reasonably sensitive to the choice of the parameters. Values of such a property, calculated with different sets of parameters, could be compared with experimental data. Considerable information concerning the best choice of parameters could be obtained in this way.

Such a sensitive property is available in Hammett's σ-values.[16] These constants correlate the reaction rates and equilibrium constants of a large number of side chain reactions of *meta* and *para* substituted aromatic compounds

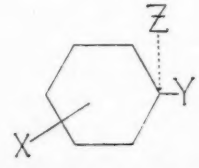

[9] M. Goeppert-Mayer and K. J. McCallum, Revs. Modern Phys. 14, 248 (1942).
[10] G. E. K. Branch and M. Calvin, *The Theory of Organic Chemistry*, (Prentice-Hall, Inc., New York, 1946), Section 25.
[11] M. J. S. Dewar, J. Chem. Soc. 463 (1949).
[12] V. Gold, Trans. Faraday Soc. 46, 326 (1950).
[13] J. E. Lennard-Jones, Proc. Roy. Soc. (London) A158, 280 (1937).
[14] R. G. Parr and R. S. Mulliken, J. Chem. Phys. 18, 1338 (1950).
[15] H. C. Longuet-Higgins and G. W. Wheland, Ann. Rev. Phys. Chem. 1, 138 (1950).
[16] L. P. Hammett, *Physical Organic Chemistry*, (McGraw-Hill Book Company, Inc., New York, 1941), Chapter VII.

with the nature of the substituent X and its position relative to the reacting group Y. For such reactions

$$\log(k/k^0)=\sigma\rho, \qquad (1)$$

where k^0 and k are the rate (or equilibrium) constants for the unsubstituted and the substituted aromatic compound, respectively, ρ is a constant characteristic of the reaction and the conditions under which it occurs, and σ depends only on the substituent group and its position.

The effect of a substituent (X) in the benzene ring on a side chain reaction in Y is assumed to be the result of the influence of X on the electron density of the reacting center.[16] Thus introduction of the substituent changes the electron distribution in the benzene ring; the change of the electron density on carbon atom Z is transmitted to the reacting center in a manner determined by the nature of the side chain Y. The general validity of Eq. (1) demonstrates that the change produced in atom Z by group X is essentially independent of the side chain Y. Therefore, it will be assumed that a similar change in electron density will be produced by X in a monosubstituted benzene (i.e., where Y is a hydrogen atom). Accordingly, the electron density increments in the *meta* and *para* position of monosubstituted benzenes should be a monotonic function of the corresponding σ-values. We shall expand this function in a power series, and shall assume that higher powers of the electron density increments may be neglected for the small values considered. This assumption leads to a direct proportionality between σ's and electron density increments.

When the necessary calculations were performed, it became evident that the electron densities (q_m and q_p) were reasonably sensitive to the choice of parameters, and particularly that the ratio of the electron density increments in *meta* and *para* positions $[\xi=(1-q_p)/(1-q_m)]$ was extremely sensitive.

CALCULATIONS

In this paper we have considered only the simplest type of monosubstituted benzene derivative, namely, that in which the substituent contributes only one π-orbital to the resonating system. This group comprises aniline, phenol, thiophenol, and the halobenzenes. Because of the difficulty of assigning numerical values to the parameters (α and γ) of these groups, we have constructed contour diagrams representing the electron densities in the various positions as a function of α and γ.

The Coulomb integral (α) of the heteroatom was varied from -2.5 to $+2.5$, the resonance integral (γ) of the carbon-heteroatom bond from 0 to 1.2. All energy quantities are expressed in units of the resonance integral (β) of the carbon-carbon bond in benzene. The Coulomb integral of the ring carbon atoms was taken as $\epsilon^n\alpha$ and ϵ was given Branch and Calvin's[10] value of $\frac{1}{3}$. Very similar calculations have been carried out by Sandorfy[4] using $\epsilon=1/10$ and neglecting higher powers of ϵ, and his data will serve to demonstrate the effect of a change in ϵ.

The calculations were carried out by standard MO LCAO method (see e.g., Coulson and Longuet-Higgins[17]). Overlap integrals were neglected throughout. The secular equations may be factored into a second- and a fifth-order equation. The fifth-order equations were solved by successive approximations by the Newton-Raphson[18] method. The second-order equations are independent of the resonance integral γ, and depend on the Coulomb integral of the heteroatom only through its effect on the Coulomb integral of the carbon atoms. This was to be expected since these equations lead to the energies of orbitals which are antisymmetric with respect to the axis of symmetry of the compound, and therefore involve only the atomic orbitals of the carbon atoms which do not fall on the axis of symmetry. The solutions of these secular equations gave the energy levels of the compounds. The coefficients by which the atomic orbitals enter into the molecular orbitals were calculated by evaluation of the subdeterminants of the original secular determinants. The electron densities were obtained as the sum of the squares of these coefficients of a given atomic orbital over all the electrons in the resonating system.

Frequencies of the first absorption band were calculated as an average of the four lowest transitions in a manner similar to that used by Matsen.[7]

RESULTS AND DISCUSSION

According to our basic hypothesis, the change of the electron densities in the *meta* and *para* position of benzene upon monosubstitution should be related to Hammett's σ-values through a single proportionality factor. This constant has no theoretical significance since it depends on the arbitrary choice of a reference reaction for Hammett's scale. The ratio of σ_p/σ_m, how-

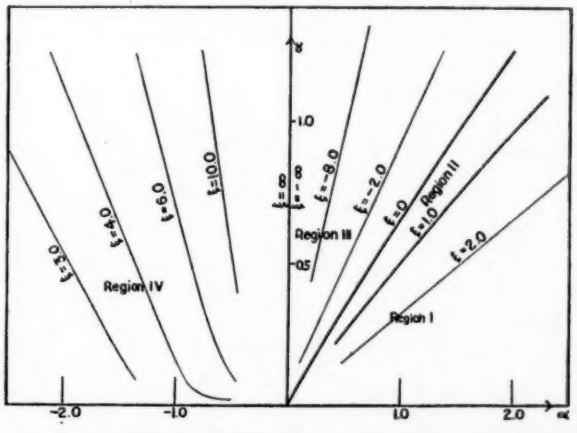

FIG. 1. Contour diagram for the quantity $\xi=(1-q_p)/(1-q_m)$ as a function of α and γ.

[17] C. A. Coulson and H. C. Longuet-Higgins, Proc. Roy. Soc. (London) **A191**, 39 (1947).

[18] *Cf.* H. Margenau and G. M. Murphy, *The Mathematics of Physics and Chemistry* (D. Van Nostrand Company, Inc., New York, 1943), p. 475.

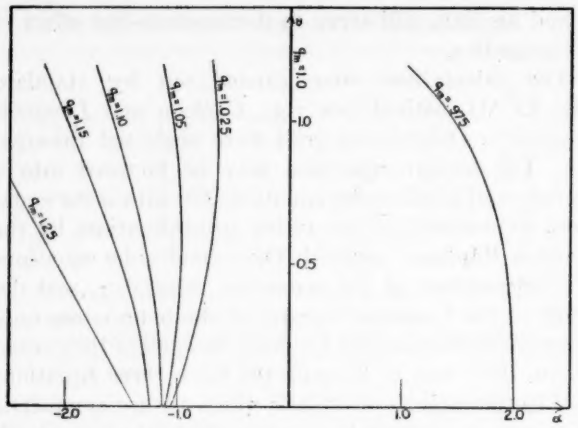

FIG. 2. Contour diagram for q_m as a function of α and γ.

ever, is independent of the proportionality factor, and accordingly may be compared directly with the ratio (ξ) of the increments of electron density in the two positions. The contour diagram for this magnitude is given in Fig. 1.[19] It is seen that the diagram consists of four distinct regions I to IV, which are separated by contour lines $\xi=1$, $\xi=0$, and the γ-axis, for which $\xi=\pm\infty$.

Results obtained from data in a large portion of region IV appear improbable; and calculations with parameters corresponding to this region lead Sandorfy to conclusions which do not appear reasonable. This fact may be understood by consideration of one of the basic assumptions involved in the MO LCAO method. Coulson and Longuet-Higgins[17] point out that the use of a Coulomb integral α_x of an atom X assumes that this quantity is not dependent on the electron density q_x of the atom. While this is doubtlessly not true, it is a fair approximation as long as the changes in q_x are small, and is always implicitly assumed in carrying out

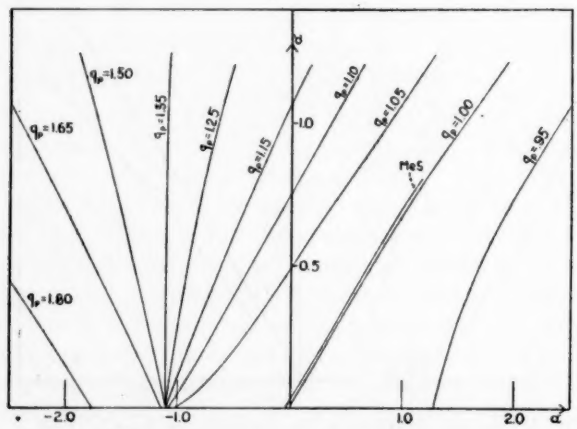

FIG. 3. Contour diagram for q_p as a function of α and γ.

[19] All calculated values of q_p, q_m, and ξ were plotted against α at constant γ, and against γ at constant α, and the resulting plots were used for the interpolations necessary in constructing the diagrams (Figs. 1–5).

LCAO calculations.[20] But in region IV, as α decreases, the energy of the MO arising from the substituent atomic orbital approaches and then exceeds the energy of the first unoccupied MO arising out of the ring orbitals. Therefore, the substituent atomic orbital contributes little to the occupied MO's, and the values of the electron density (q_x) on the substituting atom are greatly reduced. The assumption of small changes in q_x breaks down, and results involving large changes of q's must be viewed with suspicion.

The contour diagrams for the electron densities in the *meta* and *para* position (q_m and q_p) are given in Figs. 2 and 3. Figure 4 shows the contour lines corresponding to the ξ-values equal to the σ_p/σ_m ratios. This diagram fixes the value of either parameter (α or γ) if the other parameter is given. From Fig. 4 several pairs of corresponding parameters were arbitrarily chosen for each compound considered. The q_p-values corresponding to these parameters were then obtained from Fig. 2[19] and plotted against the corresponding α-values in

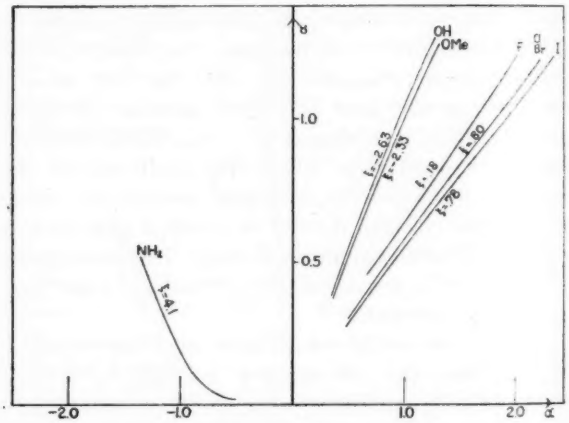

FIG. 4. Contour lines for $\xi=\sigma_p/\sigma_m$ for various compounds.

Fig. 5. The choice of a consistent set of parameters for all compounds is facilitated by the fact that q_p-values for the fluorine substituent are constant for all permitted pairs of parameters, as can be seen from Fig. 5. The q_p-value of fluorine determines the proportionality factor relating density increments ($1-q$) and σ's. Then q_p-values can be calculated for all the compounds from the corresponding σ_p-values, and lead to a unique set of α's and γ's by use of Figs. 4 and 5. These values are summarized in Table I. The lack of dependence of the q_p-values of fluorine on the possible parameter-pairs is due to the nearly parallel course of the contour lines for q_p, q_m, and ξ. Accordingly, no particular pair of parameters can be assigned to fluorine. The only information gained is that the choice of one parameter (α or γ) fixes the value of the other in accordance with the contour line in Fig. 4.

[20] G. W. Wheland and D. E. Mann, J. Chem. Phys. 17, 264 (1949), have recently used a method of iteration to eliminate this assumption.

TABLE II. Transition frequencies, mesomeric moments, and electron distribution.

Compound	Transition frequencies[a] Calc.	Found[b]	Mesomeric moments in D.U. Calc.	Found[c] I	II	III	Electron density[d] *Ortho*	*Meta*	*Para*
C_6H_6	(2.00)	(2.00)	(0)						
C_6H_5F	1.86–1.88	1.986		0.24		0.35			
C_6H_5Cl	1.88	1.945	0.42	0.14	0.59	0.31	1.037	0.976	0.985
C_6H_5Br	1.88	1.942	0.49	0.09	0.68	0.37	1.037	0.976	0.985
C_6H_5I	1.89	—	0.48	0.30	0.83		1.035	0.977	0.982
C_6H_5OH	1.79	1.908	1.13	0.29			1.038	0.993	1.020
$C_6H_5NH_2$	1.20	1.787	1.62	0.16			1.020	1.012	1.057
C_6H_5SH	1.30–1.50	1.836	—						

[a] See reference a, Table III. [b] From K. F. Herzfeld, Chem. Revs. **41**, 233 (1947). [c] From H. B. Watson, *Modern Theories of Organic Chemistry* (Oxford University Press, London, 1941), second edition, p. 60. The three columns differ by the reference compound used: I: Me*X*; II: R_3CX; III: The value for alkyl *X* is the limiting value of the homologous series $C_nH_{2n+1}X$. [d] In units of the electronic charge.

Hammett does not report σ-values for the hydroxy group. The values reported in Table I were obtained as averages from an analysis of a number of reactions reported in the literature. For comparison Hammett's values for the methoxy group are also included. This amounts to a neglect, in the MO treatment, of hyperconjugation of the methyl group.

Branch and Calvin[21] suggest that the experimental evidence does not warrant assigning different σ-values to chlorine, bromine and iodine, since the values are very similar, and the probable errors considerably larger than the differences. The ratio of σ_p/σ_m for chlorine and bromine are 0.61 and 0.59, respectively, and an average of 0.60 was used for both of these substituents. For iodine the experimental value of 0.78 was used.

Hammett[16] does not report σ-values for the SH-group, and for the MeS only a σ_p-value is given. Furthermore, no data are available in the literature to calculate σ-values for SH, or for MeS in the *meta* position. The contour line for MeS, obtained from the electron densities in the *para* position, is included in Fig. 3. This contour line does not permit a choice of a set of parameters (α and γ), but only determines one in terms of the other, and places certain limitations on both. The possible values seem reasonable, since a small resonance integral, which would be expected from an element in the second row of the periodic table, would lead to a Coulomb integral somewhat smaller than that of the OH group.†

The resonance integral for aniline can be expected to be quite small, since the nitrogen atom is in an sp^3 state and the free pair of electrons are not π-electrons; therefore, they contribute to the resonance only to the extent to which they have *p*-character.[22] The negative sign of the Coulomb integral for nitrogen is at first surprising, since nitrogen is generally considered electronegative with respect to carbon. But a negative α-value for amino nitrogen seems justified by several considerations: (1) the electronegativity of the nitrogen atom is reduced by the hydrogen atoms bound to it, and (2) the dipole moment of aniline arises from a dipole having its positive end in the direction of the nitrogen.[23]

The Coulomb integrals assigned to various atoms are compared with ionization potentials in Table I. A satisfactory correlation exists, which shows that the values of our parameters are reasonable. Mesomeric moments and absorption frequencies for the various compounds are given in Table II. It has been shown that the simple LCAO approximation does not lead to good values for the absorption frequencies.[24] Nevertheless, a good correlation exists between experimental and predicted frequencies, though the calculated bathochromic shifts are too large by a factor of four. The mesomeric moments are of the correct order of magnitude, but an exact comparison with experimental values is impossible since these are not known with sufficient accuracy. The electron densities in *ortho*, *meta*, and *para* position are also given in Table III; they are consistent with the orienting powers of the substituents. The activation or

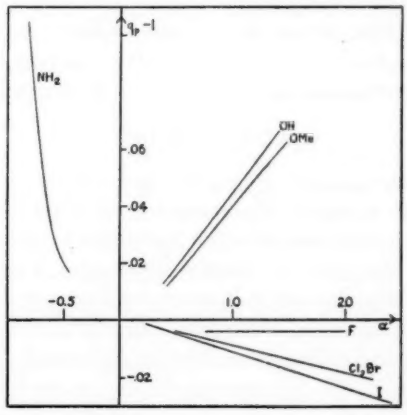

FIG. 5. q_p as a function of α for parameter pairs defined by contour lines of Fig. 4.

[21] Reference 11, p. 248.

† *Note added in proof:* Since this paper was submitted for publication, Price (Abst. XII Int. Congr. Pure and Applied Chem.) has reported the following σ-values for the methylmercapto group in the *meta* and *para* positions: $\sigma_p=-0.075$, $\sigma_m=+0.102$, $\xi=-0.74$. These values lead to the following parameters: $\alpha=0.41$, $\gamma=0.35$, and to the following values for the comparison of Table III: $\nu=1.77$, $q_p=1.005$, $q_m=0.993$, $q_0=1.025$.

[22] A. L. Sklar, J. Chem. Phys. **7**, 984 (1939).

[23] S. Glasstone, *Textbook of Physical Chemistry*, (D. Van Nostrand Company, Inc., New York, 1946), second edition, p. 552.

[24] C. A. Coulson and H. C. Longuet-Higgins, Phil. Mag. (7), **40**, 1172 (1949).

TABLE III. Coulomb and resonance integrals.

Compound	σ_p	σ_m	σ_p/σ_m	α^a	γ^a	ξ from Sandorfy[b]
C_6H_5F	0.062	0.337	0.18	[e]	[e]	∞
C_6H_5Cl	0.227	0.373	0.61[d]	1.63	0.89	∞
C_6H_5Br	0.232	0.391	0.59[d]	1.63	0.89	∞
C_6H_5I	0.276	0.352	0.78	1.55	0.83	∞
C_6H_5OH	−0.317[e]	0.114[e]	−2.78	0.51	0.57	−13
C_6H_5OMe	−0.268	0.115	−2.33	0.52	0.55	
$C_6H_5NH_2$	−0.660	−0.161	4.1	−0.70	0.06	−18
C_6H_5SMe	−0.047			[f]	[f]	11.3

[a] In units of the resonance integral (β) of the carbon-carbon bond in benzene.
[b] See reference 5.
[c] A value of γ between 1.0 and 1.25, which appears reasonable, would lead to α between 1.60 and 2.00.
[d] An average value of 0.60 was used.
[e] Calculated from data in the literature.
[f] A value of γ between 0 and 0.5, which appears reasonable, would lead to a value of α between −0.05 and 0.70.

deactivation in the *para* position is also correctly predicted; the *ortho* position appears to be activated in all compounds, but here specific *ortho* effects must be taken into account.

Sandorfy[4] performed very similar calculations, using $\epsilon=0.1$ and neglecting higher powers of ϵ. The Coulomb integral was varied from −3 to +3, and the resonance integral from 1/16 to 4. A ξ-contour diagram constructed from these data does not show the four regions characteristic of our diagram, and the ξ-values are much too large throughout. The values obtained with his choice of parameters are included in Table III. No correlation with σ-values is obtained, and no self-consistent set of parameters can be chosen from his data. Particularly, in the region of positive Coulomb integrals, where most of the common substituents are found, the electron densities in the *meta* position vary barely from unity, while the σ_m values vary widely. In Wheland and Pauling's[2] calculations also, the electron density values in the *meta* position closely approximate unity. This fact suggests that the fault is to be found in the small inductive constant (ϵ) used by these authors, since the primary effect on the meta position is due to the inductive effect, as may be visualized by consideration of valence-bond structures.

CONCLUSIONS

The calculations presented demonstrate that it is possible to correlate Hammett's σ-values with electron densities in monosubstituted benzenes as calculated by the MO method. An absolute calculation of σ-values is impossible, since the electron densities are very sensitive to the choice of the parameters (α and γ) required for numerical calculations by the MO method, and no good method for the determination of these parameters exists. Comparison of calculated electron densities with σ-values nevertheless leads to a reasonable and consistent set of parameters, even though two independent properties must be correlated with the result of a single calculation for each compound. This is taken as evidence that the basic assumption of a monotonic dependence of σ on the electron density is essentially correct. This conclusion is further substantiated by the reasonable results obtained by using the parameters determined to calculate absorption frequencies, mesomeric moments, and directing power of the substituents. After this work was completed Gutowsky and co-workers have provided experimental evidence for the same conclusion.[25]

Since the results of most previous MO calculations have not been sensitive to the numerical values assigned to the parameters α and γ,[15] relatively crude approximations to their values have been sufficient. The σ-values on the other hand have permitted us to determine sets of parameters within narrow limits; these parameters should prove of value in future calculations.

The results of the present paper permit a comparison of two different treatments of the inductive effect. The treatment we have used permits correlation of σ-values with electron densities, while the older treatment proposed by Wheland and Pauling[2] does not permit such a correlation. Several authors have pointed out that their calculations based on the older treatment would be improved by application of larger increments to the Coulomb integrals of the ring carbon atoms.[26] Ri and Eyring[27] found in calculations based on purely electrostatic considerations that the substituents appreciably affected electron densities in the meta position of monosubstituted benzenes. Such effects can be duplicated in MO calculations only by assigning a reasonably large value to the inductive constant ϵ.

The MO LCAO treatment breaks down for Coulomb integrals (α) below a value of approx −1.0, since then electron densities on the heteroatom (and in the rest of the molecule) are greatly affected, and the assumption of constancy of the Coulomb integral is not valid.

ACKNOWLEDGMENTS

The author wishes to acknowledge the continued interest and helpful advice of Drs. O. K. Rice, G. O. Doak, Leon D. Freedman, and R. A. Marcus.

[25] H. S. Gutowsky (private communication).
[26] G. W. Wheland, J. Am. Chem. Soc. **64**, 900 (1942); see also reference 7.
[27] T. Ri and H. Eyring, J. Chem. Phys. **8**, 433 (1940).

On the Calculation of Electronic Levels in Pyridine and the Isomeric Picolines*

GERTRUD P. NORDHEIM† AND H. SPONER
Department of Physics, Duke University, Durham, North Carolina
(Received October 22, 1951)

The molecular orbital method was used for calculating electronic levels in pyridine and the picolines. The change of the benzene Coulomb integrals caused by the nitrogen atom in the ring and the CH_3 substitution is treated by introducing into the secular determinant perturbation parameters δ_k at the appropriate positions. Bonding and antibonding single-electron molecular orbitals are calculated neglecting the overlap integral and electronic repulsion. The average heights are determined for the four one-electron transitions corresponding to the fourfold degenerate level in benzene. By using the assumption that the centers of gravity of the actual singlets are proportional to these average heights, these centers of gravity are predicted for pyridine and the three picolines using two different perturbation parameters δ_N. The values for pyridine show satisfactory agreement with the experimental mean value 6.14 ev.

INTRODUCTION

IN connection with absorption studies in the vapors of the three isomeric picolines,[1] theoretical calculations were begun more than two and one-half years ago on the position of the electronic levels in pyridine and the picolines. In this paper the first part, which considers only the π-electrons of the ring, is briefly presented. Although the calculations have recently been extended using a generalized perturbation method,[2] the first calculations, in which the secular determinants were solved numerically for the one-electron wave functions, may be of interest as an introduction to the problem of obtaining an energy level scheme for pyridine and its simple derivatives.

METHOD

The molecular orbital method as first described by Hückel[3] for benzene and its monoderivatives is employed in the manner used by Wheland and Pauling[4] in their treatment of the ground state of pyridine. The same method was used later by Longuet-Higgins and Coulson[5] in describing the electronic distribution in the ground state of other heterocyclic molecules containing nitrogen.

The one-electron molecular wave functions of the π-electrons expressed in atomic p orbitals (LCAO) are

$$\varphi_j=\sum_k c_{jk}\psi_k, \tag{1}$$

where the coefficients c_{jk} satisfy the equations

$$\sum_{k=1}^{6} c_{jk}(H_{mk}-\Delta_{mk}E_j)=0 \quad \text{with} \quad j, m=1, 2, \cdots 6. \tag{2}$$

E_j is the energy of the electron in orbital j, $H_{mk}=\int\psi_m^*H\psi_k d\tau$, where H is the effective one-electron Hamiltonian, $\Delta_{mk}=\int\psi_m^*\psi_k d\tau$ (overlap integral). The six roots of the secular determinant

$$|H_{mk}-\Delta_{mk}E_j|=0 \tag{3}$$

are substituted back in (2), and, together with the normalization condition $\int\varphi_j^*\varphi_j d\tau=1$, determine the coefficients c_{jk}. The following customary assumptions were made by Wheland and Pauling:

$$H_{kk}=\alpha+\delta_k\beta$$
$$H_{mk}=\begin{cases}\beta \text{ if } \psi_m \text{ and } \psi_k \text{ belong to adjacent atoms}\\ 0 \text{ otherwise for } m\neq k\end{cases}$$
$$\Delta_{kk}=1$$
$$\Delta_{mk}=0 \text{ for } m\neq k.$$

Here α = the so-called Coulomb integral in benzene, β = resonance or exchange integral between adjacent orbitals, δ_k is a constant introduced to distinguish between the electron affinities of different atoms. $\delta_k>0$ means carbon atom k has a larger, and $\delta_k<0$ means it has a smaller electron affinity than in unsubstituted benzene.

In this paper the method is extended to the picolines, and it is also used for the calculation of excited molecular orbitals. As in Wheland and Pauling's treatment the overlap integral Δ_{mk} was put equal to zero. The parameter δ_N at the position of the N atom was varied between 2 and 0.5, but the ratio between the smaller perturbations $\delta_2=\delta_6$ in the neighboring positions 2 and 6 of the ring and δ_N was kept constant, namely, $\frac{1}{8}$. Wheland and Pauling had found that a relation $(1/28)\delta_N<\delta_2<\frac{1}{4}\delta_N$ and a ratio of about $\frac{1}{10}$ for δ_2/δ_N would account reasonably for observations on substitutions and their rates in pyridine. In the picolines an additional parameter δ_{CH_3} was introduced in the appropriate position of the secular determinant. The ratio δ_{CH_3}/δ_N was estimated from comparisons made between the dipole moments of toluene[6] and the xylenes,[7] and of

* Supported by the ONR under Contract N6ori-107, T.O. I with Duke University.
† Deceased in 1949.
[1] J. H. Rush, Ph.D. thesis, Duke University (1950); J. H. Rush and H. Sponer (paper in preparation).
[2] Per-Olov Löwdin (paper in preparation).
[3] E. Hückel, Z. Physik **72**, 310 (1931).
[4] G. W. Wheland and L. Pauling, J. Am. Chem. Soc. **57**, 2086 (1935).
[5] H. C. Longuet-Higgins and C. A. Coulson, Trans. Faraday Soc. **43**, 87 (1947).
[6] K. B. McAlpine and C. P. Smyth, J. Am. Chem. Soc. **55**, 453 (1933); Le Fèvre, Le Fèvre, and Robertson, J. Chem. Soc., 480 (1935).
[7] E. C. Hurdis and C. P. Smyth, J. Am. Chem. Soc. **64**, 2212 (1942); L. Tiganik, Z. physik. Chem. **B13**, 425 (1931).

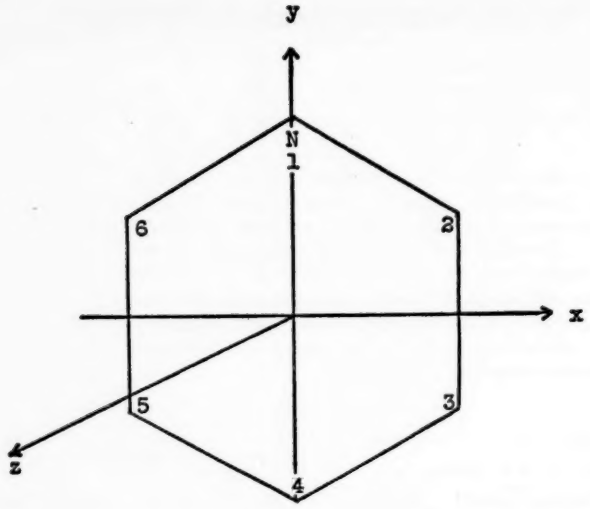

FIG. 1.

pyridine[8] and the picolines.[9] A value of $-\frac{1}{6}$ was chosen for this ratio. Although δ_N, δ_2, and δ_6 are positive quantities, δ_{CH_3} was given a negative sign since the CH_3 substitution influences the charge distribution of the ring in a direction opposite to that of the ring nitrogen.

The secular determinants (3) were solved by numerical methods. For pyridine and γ-picoline, both of which belong to symmetry group C_{2v}, the sixth-order determinant will split into a fourth-order and a second-order determinant. This is easily seen from Eqs. (2) which are

$$\begin{aligned}
&c_1(\alpha+\delta_N\beta-E)+\beta(c_2+c_6)=0\\
&c_2(\alpha+\delta_2\beta-E)+\beta(c_1+c_3)=0\\
&c_3(\alpha-E)\qquad+\beta(c_2+c_4)=0\\
&c_4(\alpha-E)\qquad+\beta(c_3+c_5)=0\\
&c_5(\alpha-E)\qquad+\beta(c_4+c_6)=0\\
&c_6(\alpha+\delta_6\beta-E)+\beta(c_5+c_1)=0.
\end{aligned}\tag{4}$$

We have only to remember that the 4 one-electron benzene orbitals of which two are doubly degenerate, split into 6 nondegenerate orbitals in pyridine. Four of these are of b_2 symmetry (symmetric to a plane through the 1–4 positions $\perp$ to the molecular plane), and two are of a_2 symmetry (asymmetric to the same plane) (Fig. 1). We have then the following relations between the coefficients c_k of Eq. (4),

for b_2 orbitals: $c_2=c_6$, $c_3=c_5$
for a_2 orbitals: $c_2=-c_6$, $c_3=-c_5$, $c_1=c_4=0$.

TABLE I. Orbital energies $E-\alpha$ in units of β.

Symmetry	Pyridine		α-Picoline		β-Picoline		γ-Picoline	
	$\delta_N=2$	$\delta_N=1$	$\delta_N=2$	$\delta_N=1$[a]	$\delta_N=2$	$\delta_N=1$[a]	$\delta_N=2$	$\delta_N=1$[a]
b_2	−1.785	−1.857	−1.828	−1.883	−1.876	−1.898	−1.894	−1.903
a_2	−0.883	−0.939	−0.970	−0.970	−0.976	−0.972	−0.883	−0.944
b_2	−0.383	−0.659	−0.458	−0.706	−0.388	−0.686	−0.480	−0.713
a_2	1.133	1.064	1.046	1.033	1.052	1.035	1.133	1.056
b_2	1.510	1.319	1.509	1.292	1.452	1.275	1.386	1.257
b_2	2.907	2.322	2.860	2.286	2.898	2.300	2.903	2.303

[a] These columns were calculated by means of second-order perturbation theory (reference 2) but were corrected for terms of higher order.

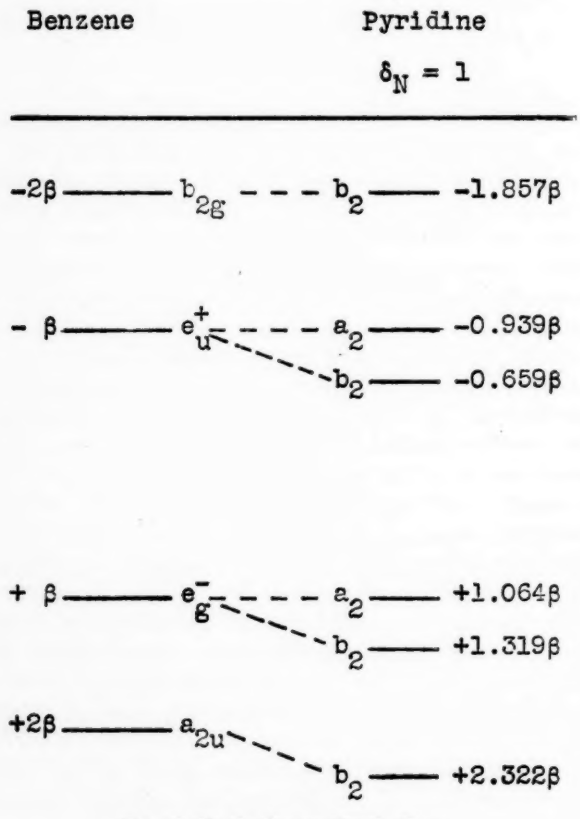

FIG. 2. Single-electron levels $E-\alpha$.

As an example, the one-electron energies of the pyridine molecular orbitals are shown for $\delta_N=1$ in their relation to the benzene orbitals (β is negative, Fig. 2).

For α-picoline and β-picoline the sixth-order determinants were algebraically solved. Naturally, they do not split into determinants of lower order, but it was noticed that they reduce approximately to second- and fourth-order determinants, if the small perturbation quantities δ_{CH_3} when occurring alone are neglected. The errors in the values so obtained from those of the rigorous numerical calculations are small. With bonding and antibonding single-electron molecular orbitals known, a first approach to calculating electronic transitions in these molecules becomes possible. Distribution of the six p electrons over the bonding orbitals according to the Pauli principle gives for the ground state the totally symmetric configuration $(2b_2)^2(2b_2)^2(2a_2)^2$, $^1A_1$ for pyridine and γ-picoline. This notation is true for γ-picoline only if the CH_3 group is regarded as one atom. Excitation of an a_2 electron to the lowest antibonding orbitals b_2 and a_2 gives transitions $A_1\rightarrow B_1$ and $A_1\rightarrow A_1$, respectively, and excitation of an electron from the upper b_2 bonding level to the same two non-

[8] B. A. Middleton and J. R. Partington, Nature **141**, 516 (1938).
[9] M. A. G. Rau and B. N. Narayanaswamy, Z. physik. Chem. **B26**, 23 (1934); D. G. Leis and H. C. Curran, J. Am. Chem. Soc. **67**, 79 (1945).

TABLE II. Average height of the four one-electron transitions.

Molecule	Calc from Table I $\delta_N=2$	Calc from Table I $\delta_N=1$	Predicted in ev $\delta_N=2$	Predicted in ev $\delta_N=1$	Observed in ev
Benzene	(2β)		...	...	6.28
Pyridine	1.95β	1.99β	6.12	6.25	6.14
α-Picoline	1.99β	2.00β	6.25	6.28	...
β-Picoline	1.93β	1.98β	6.07	6.23	...
γ-Picoline	1.94β	1.99β	6.09	6.25	...

bonding orbitals corresponds to $A_1 \rightarrow A_1$ and $A_1 \rightarrow B_1$ transitions, respectively, (Fig. 2). α-picoline and β-picoline belong, even if the CH_3 groups are approximated by one-atom substitutions, to group C_s, which retains as the only element of symmetry the reflection plane of the molecule. The symmetry classes A_1 and B_1 of group C_{2v} go over into the class A' for C_s.

DISCUSSION

The simple approach described here corresponds to the benzene treatment in which the first electronic excitation is taken as 2β. The four electronic transitions just mentioned correspond to the benzene transitions originating from putting an e_g^- electron into the e_u^+ orbital. Without taking into account the differences in electronic interaction in the different orbitals, the resulting level is fourfold degenerate in benzene but splits into the nondegenerate levels B_{2u} and B_{1u}, and the doubly degenerate level E_u^- because of such interaction. It has been suggested[10] that the average height of the corresponding observed levels, singlets and triplets combined, represents the height of the fourfold degenerate level.

It is not intended here to go into the calculation of the different transitions, which would involve the evaluation of a large number of electronic repulsion integrals.[11] Certain statements and predictions are, however, possible concerning the average height of the two A_1 and B_1 levels in pyridine and the picolines. Because of scarcity of the experimental material for the molecules under discussion, we cannot apply the suggestion mentioned above. Instead we will make the additional assumption that the center of gravity of the singlets alone (as well as of the triplets alone) is proportional to the average height of the fourfold degenerate level or of the corresponding transitions resulting from splitting.

The average height of the observed benzene singlets is 6.28 ev which according to our assumption is proportional to 2β. From Table I the average height of the four transitions in pyridine corresponding to the fourfold degenerate transition in benzene lies at 1.95β for $\delta_N=2$. This gives 6.12 ev for the predicted average height of the actual levels in good agreement with the value 6.14 ev from the observations.[11]

Similar calculations were carried out for the picolines (Table II). The symmetry notations a_2 and b_2 are only approximately correct for α-picoline and β-picoline, and the same is true for the notations A_1 and B_1 of the levels, but this is of no importance for the calculations. If the observed center of gravity of the pyridine singlets would be really accurately known, then pyridine should be used as reference substance rather than benzene. For the value 6.14 ev such a calculation would hardly change the column with $\delta_N=2$ but the predicted heights for $\delta_N=1$ would all lie in the neighborhood of 6.14 ev. A comparison of the predicted average heights of the actual picoline levels with experimental values is at present not possible since only one π-electron transition is definitely known in each case.[1] This transition represents the second observed absorption region at 2700–2400A. The first absorption region at 2900–2700A is regarded to originate from excitation of a nonbonding sp^2 electron of the nitrogen into the first unfilled π-ring orbital[12,1] and will not be considered here.

TABLE III. Relative shifts of lowest singlet $\pi-\pi$ transitions.

Molecule	Lowest $\pi-\pi$ singlet in cm^{-1}	$\frac{\nu_{benz}-\nu}{\nu_{benz}}$ obs	$\frac{2\beta-\text{av height}}{2\beta}$ calc $\delta_N=2$	$\frac{2\beta-\text{av height}}{2\beta}$ calc $\delta_N=1$
Pyridine	(38350)	−0.007	0.023	0.005
α-Picoline	37620	0.012	0.004	0.000
β-Picoline	37380	0.016	0.033	0.008
γ-Picoline	38320	−0.006	0.029	0.007

It seemed interesting to test Matsen's assumption[13] concerning substituted benzenes that the relative shift of the calculated average heights with respect to the fourfold degenerate benzene level (2β) also gives the relative shifts of the observed lowest singlet $(\pi-\pi$ transition) from the lowest benzene singlet state. Table III contains the results. They show that Matsen's assumption does not apply to the heterocyclic molecules investigated here.

ACKNOWLEDGMENT

The final writing of the present paper has been delayed by the death of Dr. Gertrud P. Nordheim. Many thanks are due to Dr. P. O. Löwdin, University of Uppsala, Sweden, for valuable and helpful discussions.

[10] C. C. J. Roothaan and R. S. Mulliken, J. Chem. Phys. **16**, 118 (1948). See also C. C. J. Roothaan, Revs. Modern Phys. **23**, 69 (1951), particularly Eq. (68). Special care must be taken in defining the orbital energies and the quantity β, see also R. S. Mulliken, J. chim. phys. **46**, 675 (1949), particularly p. 707 and ff.

[11] A discussion with Dr. J. R. Platt (University of Chicago) was very helpful in clarifying some points.

[11] See for example Fig. 15 in J. R. Platt, J. Chem. Phys. **19**, 101 (1951).

[12] M. Kasha, Symp. at Meeting of Am. Phys. Soc., Washington, D. C., 1949, and Disc. Faraday Soc. **9**, 14 (1950).

[13] F. A. Matsen, J. Am. Chem. Soc. **72**, 5243 (1950).

The Origin of the Ultrasonic Absorption in Liquids. II.

KARL F. HERZFELD
Catholic University of America, Washington, D. C.
(Received September 5, 1951)

Excess absorption in nonassociated liquids has been explained by the same mechanism as is responsible for molecular absorption in gases, namely, slow exchange of energy between internal and external degrees of freedom.

In this paper the rate of energy exchange is calculated for benzene and found to be three times too rapid. The Lennard-Jones interaction potential and model of the liquid are used; the fourth-order terms in the interaction provide the coupling between internal vibrations and Debye waves.

I. INTRODUCTION

MOST liquids show an absorption coefficient for ultrasonic waves larger than the classical one, which can be calculated from shear viscosity and heat conductivity according to Stokes and Kirchhoff. There exist at present three theories for this excess absorption. According to Pinkerton[1] and Bauer,[2] liquids with anomalous absorption may be divided into two classes, to which a third can be added; each of the three theories is supposed to fit one of the classes.

The oldest theory is that of Kneser,[3] which according to Pinkerton and Bauer applies to unassociated liquids. It assigns as reason for excess absorption the slowness of energy exchange between internal and external degrees of freedom, just as in gases. For these liquids, the dispersion region lies at higher frequencies than can be reached experimentally. In that case, the excess absorption coefficient per cm, α' is

$$\alpha'=\frac{1}{2V}\frac{C_p-C_v}{C_p}\frac{C'}{C_p-C'}\tau\omega^2, \qquad (1)$$

where the specific heats C_p, C_v are static, C' is that of the internal degrees of freedom, τ the relaxation time, and V the sound velocity. The present author[4] has calculated from (1) τ for several liquids. For benzene it is 3.10^{-10} sec for other normal liquids one gets the same order of magnitude. However, he showed also that the excess absorption of water could not be so explained, because of the low value of C'. Following the suggestion of Debye, he suggested the existence of a true volume viscosity, because of slow structural changes. This was experimentally proved by Fox and Rock,[5] who showed that the excess absorption of water persisted at 4°C, where, because of the density maximum, C_p-C_v is zero, i.e., isothermal and adiabatic processes are identical. Hall[6] developed a quantative theory for this case. Pinkerton and Bauer put water, together with other associated liquids, into the second anomalous group, for which the excess absorption is not more than three times the classical one.

Finally there exists a third group of liquids,[7] like acetates and acids, which show dispersion and a frequency dependence of α'/ω^2. In these the relaxation is ascribed to the slowness of a chemical reaction, e.g., the establishment of the equilibrium between monomers and dimers.

Recently A. Gierer and Wirtz[8] have expressed the doubt that the first hypothesis gives significant results even for normal liquids. They base their argument on the fact that absorption in solids is very small, while the exchange of energy between internal and external degrees of freedom should not be much different between solids and liquid.

The present paper outlines principles for the calculation of τ according to theory one.

II. THE MODEL OF THE LIQUID

We take as model of the liquid the cell model of Lennard-Jones,[9] in which a molecule is supposed to move in a spherical cell of radius a, formed by the smeared out surrounding molecules. Assume there are N_1 other molecules in the wall of the cell. We assume the other molecules arranged in concentric spherical layers, so that N_1 and a are connected by (N_A Avogadro number)

$$(N_1/4\pi)(M/\rho)(1/N_A)=a^3. \qquad (2)$$

However, for the following only the inner layer matters. If the interaction energy between two molecules is given by $\epsilon(r_0/r)^s$, one finds easily that the interaction energy of a molecule which is a distance R from the center of the hole may be written

$$E_0+\epsilon N_1\left(\frac{r_0}{a}\right)^s \times\left[\frac{(s-1)s}{6}\left(\frac{R}{a}\right)^2+\frac{(s-1)s(s+1)(s+2)}{120}\left(\frac{R}{a}\right)^4\right].$$

[1] J. M. Pinkerton, Proc. Phys. Soc. (London) **B62**, 129 (1949).
[2] E. Bauer, Proc. Phys. Soc. (London) **A62**, 141 (1949).
[3] H. O. Kneser, Ann. Phys. **16**, 337 (1933); **32**, 277 (1938).
[4] K. F. Herzfeld, J. Acoust. Soc. Am. **13**, 33–35 (1941).
[5] F. E. Fox and G. D. Rock, Phys. Rev. **70**, 68–73 (1946).
[6] L. Hall, Phys. Rev. **73**, 775 (1948).
[7] E.g. J. Lamb and J. M. Pinkerton, Proc. Roy. Soc. (London) **199**, 114 (1949).
[8] A. Gierer and K. Wirtz, Z. Naturforsch. **5a**, 270 (1950); Phys. Rev. **79**, 906 (1950).
[9] For a discussion of this model and for numerical data, see e.g., Hirschfelder, Bird, and Spotz, J. Chem. Phys. **16**, 968 (1948). Since we are far below the critical point, we do not make a serious error by neglecting hole formation.

Using now as interaction energy the Lennard-Jones expression

$$-4\epsilon[(r_0/r)^6-(r_0/r)^{12}], \tag{3}$$

one finds

$$E-E_0=A(R/a)^2+B(R/a)^4, \tag{4a}$$

with

$$A=88\epsilon N_1(r_0/a)^{12}[1-\tfrac{5}{22}(a/r_0)^6], \tag{4b}$$

$$B=800.8\epsilon N_1(r_0/a)^{12}[1-(1/14.3)(a/r_0)^6]. \tag{4c}$$

Accordingly, in first approximation the motion of the molecule is a simple harmonic vibration, with a frequency given by

$$4\pi^2m\nu^2=2A/a^2. \tag{5}$$

However, this is calculated on the assumption of fixed cell walls. Actually, we expect a Debye spectrum, with a limiting frequency[10] $\nu_m=\sqrt{2}\nu$, so that

$$\nu_m=1/\pi a(A/m)^{\frac{1}{2}}.$$

Introducing ϵ/k (which is tabulated by Hirschfelder in °K) and $N_1/12$ (since N_1 often is near 12) this becomes

$$\nu_m=\frac{3.56\times10^{12}}{a}\left(\frac{\epsilon}{k}\frac{N_1}{12}\frac{1}{M}\right)^{\frac{1}{2}}\left(\frac{r_0}{a}\right)^6\left[1-\tfrac{5}{22}\left(\frac{a}{r_0}\right)^6\right]^{\frac{1}{2}}, \tag{6}$$

with a in angstrom units and M = molecular weight. For benzene, $\epsilon/k=440$, $r_0=5.270$, $a=5.201$; this gives $\nu_m=4.05\times10^{12}$. This compares with 3.1×10^{12}, the frequency used by Andrews and Lord[11] to represent the low temperature specific heat for solid benzene.

III. THE EXCHANGE PROBABILITY OF ENERGY BETWEEN INTERNAL AND EXTERNAL VIBRATIONS

The quadratic term in (4a) does not produce an energy exchange between different degrees of freedom. One ought to make a transformation to principal axes, which will result in a slight frequency shift of internal and external degrees of freedom, which we will neglect. The fourth-order term, however, gives the required result, by applying standard methods. One says that the significant motion R is made up of two parts, the motion of the center of the molecule R_c and the internal vibration bx, where x is the amplitude of the internal vibration (frequency ν_i) and b a direction cosine. The interaction energy H' is therefore

$$H'=\frac{B}{a^4}(R_c+bx)^4=\cdots\frac{B}{a^4}4bxR_c^3\cdots.$$

The term written above is the only significant one. It means that one quantum of internal vibration will be divided among three Debye waves.

[10] This relation between the limiting frequency and the frequency which would exist if only one particle were allowed to move, is valid in a chain.

[11] R. C. Lord, and D. H. Andrews, J. Chem. Phys. **5**, 649 (1937).

Standard quantum theoretical perturbation[12] calculation leads then to the following result for the probability of a transition

$$\frac{1}{\tau}=\frac{64\pi}{3}\frac{M}{M_i}\frac{\nu_m}{k\Theta_i}\frac{1}{kT}(Bb)^2u^4 \tag{7}$$

with

$$\Theta_i=\frac{h\nu_i}{k}$$

$$u=\frac{3kT}{8\pi^2m\nu_m^2a^2}=\frac{1}{12}\frac{\text{mean square thermal amplitude}}{a^2}. \tag{8}$$

For benzene, $u=2.74\times10^{-4}$. $1/\nu_m\tau$ is the probability of energy transfer during one vibration of the molecule. With (4) one finds, putting $\bar{b}^2=\frac{1}{3}$

$$\frac{1}{\tau}=2.06\times10^{11}\nu_m\frac{M}{M_i}\frac{\epsilon}{k\Theta_i}\frac{\epsilon}{kT}\left(\frac{N_1}{12}\right)^2\left(\frac{r_0}{a}\right)^{24}\times\left[1-\frac{1}{14.3}\left(\frac{a}{r_0}\right)^6\right]^2u^4. \tag{9}$$

For benzene, this leads to $\tau=1.2\times10^{-10}$ sec.

This result is in astonishingly good agreement with experiment, in view of the crude approximations made. However, it is still too crude to explain details for different liquids. For transitions needing n Debye quanta, n being the next higher even number, (9) is changed as follows:

The numerical factor is multiplied by

$$\left(\frac{n}{4}\frac{(10+n)!}{14!}\frac{5!}{(n+1)!}\right)^2;$$

u^4 is replaced by u^n. The [ ] may be omitted.

[12] One has first for the transition probability

$$\frac{64B^2b^2}{a^8}x_i^2x_1^2x_2^2x_3^2\frac{\sin^2\pi(\nu_i-\nu_1-\nu_2-\nu_3)t}{(\nu_i-\nu_1-\nu_2-\nu_3)^2t},$$

where x_1^2, etc., is the transition probability from quantum number j to $j+1$ in the first Debye mode. If one sums over the j values assuming classical specific heat, one gets

$$\bar{x}_1^2=kT/8\pi^2m\nu_1^2.$$

For the internal vibration one gets, assuming only one quantum present

$$x_i^2=h/8\pi^2m_i\nu_i,$$

where m_i is the mass associated with the internal vibration.

The Debye spectrum is assumed to be given by

$$\frac{3}{\nu_m^3}\nu^2d\nu.$$

Therefore,

$$\frac{1}{\tau}=\frac{64B^2b^2}{a^8}x_i^2\left(\frac{3}{\nu_m^3}\right)^3\left(\frac{kT}{8\pi^2m}\right)^3\int_0^{\nu_m}\frac{\nu_1^2}{\nu_1^2}d\nu_1\int_0^{\nu_m}\frac{\nu_2^2}{\nu_2^2}d\nu_2\times\frac{1}{t}\int_0^{\nu_m}\frac{\sin^2\pi(\nu_i-\nu_1-\nu_2-\nu_3)t}{(\nu_i-\nu_1-\nu_2-\nu_3)^2}\frac{\nu_3^2}{\nu_3^2}d\nu_3.$$

The Prediction of Thermodynamic Properties of Nonideal Solutions from Turbidity Measurements

A. L. Babb* and H. G. Drickamer
Department of Chemistry, University of Illinois, Urbana, Illinois
(Received July 25, 1951)

Turbidity measurements have been made on the systems

$CH_3OH-i\text{-}C_5H_{12}$
$CH_3OH-n\text{-}C_5H_{12}$
$CH_3OH-n\text{-}C_6H_{14}$

near the critical solution temperature at seven atmospheres pressure and at a considerably higher pressure. The effect of pressure is to elevate the critical solution temperature and to decrease the minimum transmission. The wavelength dependence is consistent with the theory of Ornstein and Zernike. The change of fugacity with concentration is calculated as a function of temperature, pressure, and composition.

NOMENCLATURE

$\mathfrak{A}$	phenomonological coefficient
C_i	concentration of component i, g/per cc
D	diffusion coefficient
f	fugacity
g	correlation coefficient
I	intensity of transmitted light
I_0	intensity of incident light
l	path length cm
M	molecular weight
n	exponent on λ in the equation $I/I_0 \sim \lambda^{-n}$
N_a	Avogadro's number
R	gas constant, cc atmos per g mole °K
t_s	apparent saturation temperature, °C
T	temperature, °K
$\bar{V}_i$	partial molar volume of component i
X_i	mole fraction of component i
λ	wavelength, cm
μ	refractive index
ρ	density, g per cc
τ	turbidity, cm^{-1}

THE measurement of the attenuation of transmitted light offers a means for the prediction of thermodynamic properties near the critical solution temperature. This has been most clearly illustrated in the recent work of Zimm,[1] whose paper also contains references to earlier work. The present paper presents the results of an investigation of the effect of pressure and of structure on these properties.

The turbidity τ is defined by the equation

$$I/I_0 = e^{-\tau l}, \tag{1}$$

where l is the path length and I/I_0 is the fraction of the incident light transmitted.

Einstein[2] treated the scattering of light near the critical solution temperature using the theory of fluctuations. He obtained a relationship which predicted a λ^{-4} law wavelength dependence and infinite scattering at the critical solution temperature. Ornstein and Zernike[3] introduced a correlation coefficient between fluctuations in neighboring volumes and obtained an equation of the following form

$$\tau = A/(B\lambda^4 + C\lambda^2), \tag{2}$$

where

$$A = \frac{8\pi^3}{3}\frac{RT}{N_A}\bar{V}_2\left(\mu\frac{\partial\mu}{\partial X}\right)^2 X_1^2 X_2^2 \tag{3}$$

$$B = X_1X_2(\partial \ln f_2/\partial X_2) \tag{4}$$

$$C = [2\pi g \sin(\pi/A)]^2 C_1. \tag{5}$$

If measurements are made for light of two different wavelengths (α and β) obtains

$$\frac{\partial \ln f_2}{\partial X_2} = \frac{32\pi^3\bar{V}_2}{3N_A(\lambda_\beta^2 - \lambda_\alpha^2)} \times \left\{\frac{1}{\tau_\beta^2\lambda_\beta^2} - \frac{1}{\tau_\alpha^2\lambda_\alpha^2}\right\}\left(\mu\frac{\partial\mu}{\partial X}\right)^2 X_1X_2. \tag{6}$$

From this relationship many thermodynamic properties can be predicted.

It must be recognized that neither the work of Einstein nor that of Ornstein and Zernike rest on completely sound theoretical grounds. The use of the Lorentz-Lorenz law and the form of correlation coefficient assumed by Ornstein and Zernike are both open to question. It should also be pointed out that fluctuations in density as well as in composition are possible. This general case was treated by Raman and Ramanathan.[4] It is assumed that near the critical solution temperature the density fluctuations are small compared with the composition fluctuations.

A plan of the equipment used in this investigation is shown in Fig. 1. The light source was an AH-4 mercury lamp. The 4050A, 4360A, and 5460A lines were isolated by appropriate combinations of Corning glass filters. The light beam was made approximately parallel by a lens and filter system. Measurements were made using

* Present address: Rayonier, Inc., Shelton, Washington.
[1] B. Zimm, J. Phys. and Colloid Chem. **54**, 1306 (1950).
[2] A. Einstein, Ann. Phys. **33**, 1275 (1910).
[3] L. S. Ornstein and F. Zernike, Proc. Roy. Acad. Sci. (Amsterdam) **17**, 793 (1914).
[4] C. V. Raman and K. R. Ramanathan, Phil. Mag. **45**, 213 (1923).

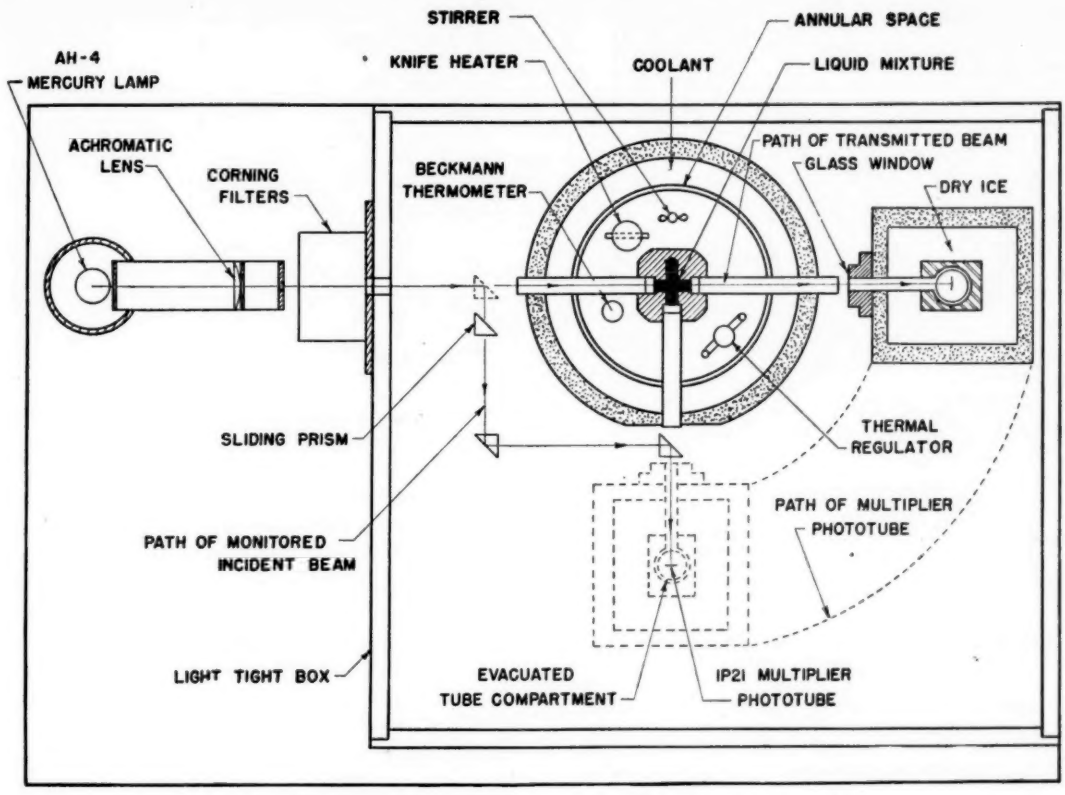

FIG. 1. Plan of equipment for measuring transmitted and scattered light.

a IP21 photomultiplier tube cooled to dry ice temperature. The resulting signal was measured with a type *R* galvanometer having a sensitivity of 7×10^{-5} microampere per mm of scale. The phototube and housing could be rotated 90° to measure either transmitted or 90° scattered light. By appropriate manipulation of the prisms the original beam could be monitored.

The bath temperature was controlled to 0.005°C except near the critical solution temperature where it was manually controlled to 0.001°C. The temperatures were read on a calibrated Beckmann thermometer.

Although both transmitted and scattered light were measured, all calculations were based on the transmitted light because of the difficulty of making satisfactory corrections for multiple scattering on the scattered beam at high attenuations.

The effective path length for transmitted light was determined by using a dilute polymer solution of known turbidity. It turned out to be essentially the measured path length.

The systems studied were: I. Methyl Alcohol-isopentane II. Methyl Alcohol-*n*-pentane III. Methyl Alcohol-*n*-hexane. The hydrocarbons were Phillips Research Grade, while the methanol was Eastman Kodak Pure Grade.

The first system was run at 7 atmospheres and at 102 atmospheres; the latter two were run at 7 and at 85 atmospheres.

The samples were made up by weight and loaded into the evacuated system through a stoppered separatory funnel. Elaborate precautions were taken to remove moisture from the liquids and to keep them dry. Pressure was applied by a piston and cylinder arrangement not shown in the plan. The piston fit the cylinder to ±0.0002 in. and was sealed by an "0" ring. A nitrogen cylinder was used as a source of pressure. The system was heated to about 10°C above the critical solution temperature and held there for at least eight hours. Readings were then taken at this temperature and used as the basis for turbidity calculations, i.e., one hundred percent transmission was assumed at this point. Since a change in temperature in this region gave essentially no change in readings, this assumption was within the accuracy of our measurements.

The bath temperature was then lowered slowly (about 0.2° per hour) and readings were taken until the transmitted light started to fluctuate wildly. One could then see small bubbles forming and collecting in the continuous phase. It was assumed that saturation had been reached. In some cases this temperature differed by a tenth of a degree or more from the saturation temperature reported in the literature[5] for the corresponding composition. Therefore, we refer to this temperature, below which no readings could be made, as the "apparent saturation temperature." Systems II and III appeared to be reversible until very close to saturation,

[5] *International Critical Tables*, (McGraw-Hill Book Company, Inc., New York, 1926), Vol. 3. (See also reference 7.)

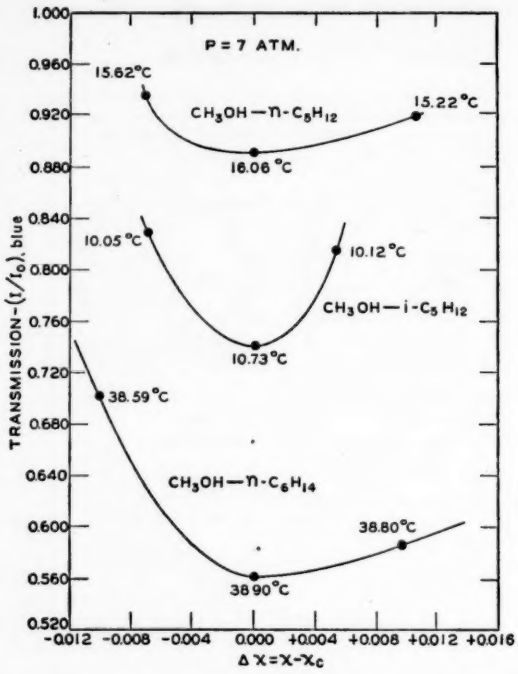

FIG. 2. Minimum transmission as a function of composition. The pressure was constant at 7 atmospheres, and the temperature varied as indicated. The minimum transmission temperature is essentially the saturation temperature.

but the isopentane-methanol system appeared to be irreversible at all temperatures. After reheating to the base line temperature the transmitted readings were considerably higher than the original readings and it was necessary to allow at least twelve hours to elapse before repeating a run.

A tabulation of the detailed results may be obtained by consulting the original thesis.[6]

Figure 2 shows lines of minimum transmission as a function of composition for the three systems. This is the maximum turbidity obtained at each composition before two phases appeared. Temperatures are indicated along each curve. In general, the temperature of minimum transmission was 0.01°C above the "apparent saturation temperature," as defined previously. The CH_3OH-n-C_6H_{14} system has the lowest transmission because of its high refractive index. It is interesting to note that the system involving the branch-chain hydrocarbon has considerably lower transmission than the system involving the corresponding straight chain compound.

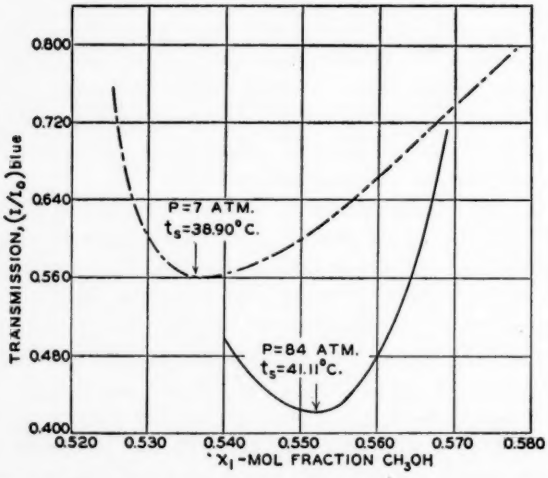

FIG. 3. The effect of pressure on the minimum transmission curve for the system CH_3OH-n-C_6H_{14}.

[6] A. L. Babb, Doctoral thesis, University of Illinois (1951). (The thesis can be obtained by contacting the University of Illinois Library.)

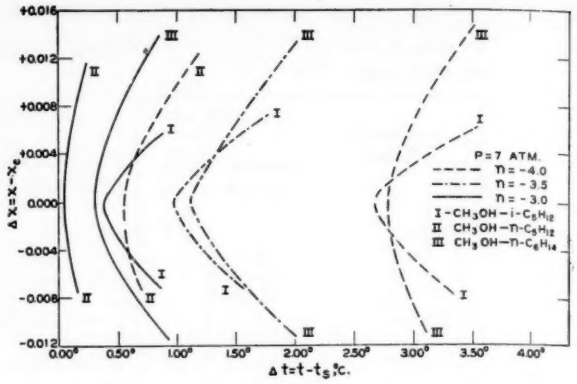

FIG. 4. The wavelength dependence of transmitted light. N is determined from the relationship $I/I_0 \sim \lambda^{-n}$.

Figure 3 illustrates the effect of pressure on the transmission for the system CH_3OH-n-C_6H_{14}. The original solution temperature increases as predicted from the data of Timmermann,[7] the critical composition shifts, and the minimum transmission is lower. The decrease in

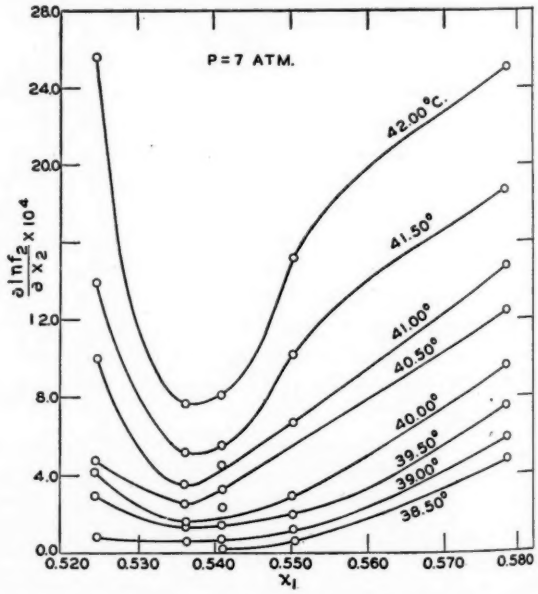

FIG. 5. Fugacity isotherms for mixtures of CH_3OH (Component 1) and $n-C_6H_{19}$ (Component 2).

[7] J. Timmermann, J. chim. phys. **20**, 602 (1923).

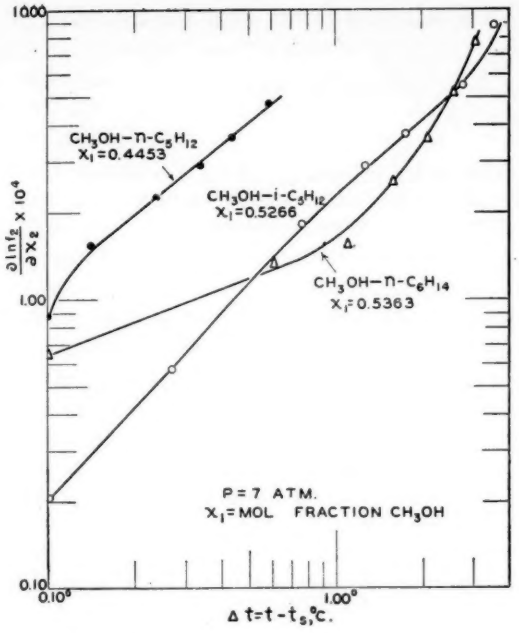

FIG. 6. Variation of $\partial \ln f_2/\partial X_2$ with $\Delta t(t-t_s)$ for critical mixtures.

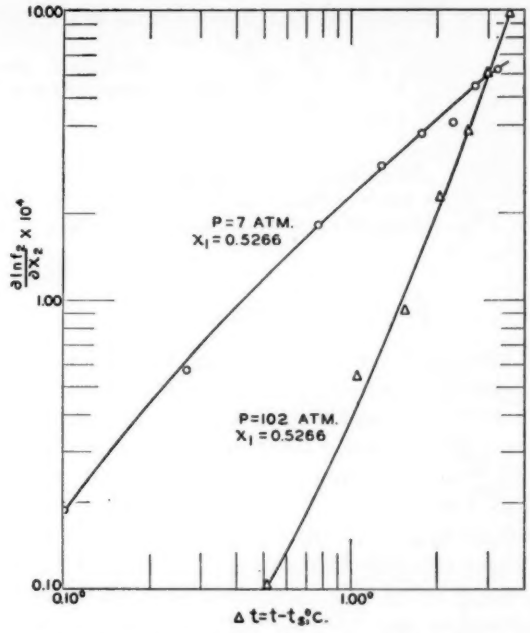

FIG. 7. The effect of pressure on the variation of $\partial \ln f_2/\partial X_2$ with ΔT in the system CH_3OH (Component 1) $-i$-C_5H_{12} (Component 2).

transmission may indicate an effect of density fluctuations neglected in this work. The effect of pressure for the other systems was qualitatively similar.

In Fig. 4, the wavelength dependence is plotted based on the relationship $I/I_0 \sim \lambda^{-n}$. In general the results are consistent with the theory of Ornstein and Zernike. It is interesting to note that the region of deviation from the λ^{-4} law is much larger for the isopentane system than for the normal pentane.

Figure 5 shows typical plots of $\partial \ln f_2/\partial X_2$ as a function of temperature and composition for the system CH_3OH-n-C_6H_{14} at 7 atmospheres pressure. This quantity approaches zero at the critical solution temperature and composition as it should.

Figure 6 is a plot of $t-t_s$ *versus* $\partial \ln f_2/\partial X_2$. This gives a straight line at temperatures sufficiently removed from the critical solution temperature. The deviations are probably because of slight super cooling. Figure 7 illustrates the effect of pressure on such a plot.

From the thermodynamics of irreversible processes[8] a relationship for the diffusion coefficient is derived,

$$D=\alpha \bar{M}^3 RT/X_1X_2M_1^2M_2^2\rho[1+X_1X_2(\partial^2 \ln f/\partial X_1^2)] \quad (7)$$

where

$$X_2(\partial \ln f_2/\partial X_2)=1+X_1X_2(\partial^2 \ln f/\partial X_1^2). \quad (8)$$

If the phenomenological constant α could be established it would then be possible to predict from light scattering data the dependence of the diffusion coefficient on the nonideality of the solution.

In summary it may be said that the results are consistent with the work of Zimm,[1] and the theory of Ornstein and Zernike.[3] They illustrate the possibility of predicting thermodynamic properties from light scattering.

[8] R. Hease, Z. Physik **127**, 1 (1949).

Effect of Various Gases on Potassium Ion Emission from Hot Platinum

EDWARD L. BRADY AND PAUL D. ZEMANY
Research Laboratory, General Electric Company, Schenectady, New York

(Received May 18, 1951)

The effect of several gases on the emission of potassium ions from a hot platinum surface has been studied. It has been found that oxygen, carbon tetrachloride, bromine, and helium cause a marked decrease in the potassium emission; nitrogen has a smaller effect; and hydrogen causes an increase in the emission.

INTRODUCTION

IT has been known for many years that fresh metallic platinum of the highest purity readily available will emit potassium ions when heated to any temperature above a dull red heat.[1] More recent investigations[2] have shown that almost all red hot metals emit potassium and sodium ions. At still higher temperatures ions of the metal being heated are sometimes given off. All ions are singly charged. The present paper reports the results of a study of the effect of various gases on the emission of potassium ions from a hot platinum surface.

EXPERIMENTAL

The ion source of a Nier-type mass spectrometer[3] made by the General Electric Company was modified by replacing the ion repeller plate with a platinum ribbon ($\frac{1}{8}$ inch wide by 0.00015 inch thick) which could be heated by the passage of electric current while simultaneously being used as the ion repeller plate. The ribbon was cut from a sheet rolled between stainless steel plates and was not touched by hand after rolling. The temperature of the filament was adjusted so that the potassium ion emission was of an easily measured magnitude. The temperature was roughly estimated by visual observation through a window in the glass spectrometer head. Any ions emitted by the platinum ribbon and passing through the exit slit from the ionization chamber would undergo the same acceleration, focusing, and collimation as ions formed in standard fashion by the spectrometer.

Various gases were admitted to the spectrometer by means of a standard leak in the vacuum line associated with the instrument. Pressures were measured on the high pressure side of the leak with a thermistor gauge[4] and in the spectrometer with an ionization gauge. Since the ionization gauge was not immediately adjacent to the ion source and since its calibration changes with the gas present, pressure measurements in the spectrometer were considered to have little significance. Comparative pressures were obtained from the thermistor gauge measurements. Since the thermistor readings for different gases are roughly inversely proportional to the square root of the molecular weight and since effusion through the leak into the spectrometer occurs at a rate having the same dependence on molecular weight, it was considered that the pressures inside the spectrometer were proportional to the thermistor gauge reading. The thermistor gauge was calibrated for air, so all pressures reported here are in terms of what might be called "microns air equivalent."

The oxygen used in the experiments was 99.5 percent pure with nitrogen as the principal impurity. Similarly, the tank nitrogen contained about 0.5 percent oxygen. Carbon tetrachloride was purified by fractional distillation, and the bromine was commercial reagent grade. Mass spectrometer analysis of the hydrogen and helium used showed no substances other than those normally present in the spectrometer at the best vacuum attainable.

For observation of the effect of the gases on the potassium ion emission the spectrometer magnet current was adjusted so that the mass 39 ions were focused on the detector. A record of the peak height as a function of time after admission of the gas was obtained from the chart of the Brown potentiometer fed by the spectrometer amplifier.

All potassium peak height measurements were slightly complicated by the slow decay of the emission due to depletion of potassium in the platinum. In order to maintain the peak height at an easily measurable level the temperature was gradually increased during the series of experiments reported here. At the end of the experiments the temperature was about two hundred degrees higher than the initial temperature.

RESULTS

Emission of Potassium Ion

After the ion source had been modified and replaced, the spectrometer was pumped down, and all preliminary focusing operations were carried out using the normal ionization mechanism of the ion source. Argon and mercury vapor were used as calibrating substances. During these operations the bombardment of the platinum surface with the 80-volt electrons used for producing ionization would presumably help to remove adsorbed gases so that the surface would be relatively

[1] O. W. Richardson, *Emission of Electricity from Hot Bodies* (Longmans, Green and Company, New York, 1921).
[2] B. H. Wahlin, Phys. Rev. **34**, 164 (1929); **35**, 653 (1930); **37**, 467 (1931); **38**, 1974 (1931); **45**, 886 (1934). Nature **123**, 912 (1929). L. L. Barnes, Phys. Rev. **42**, 487, 492 (1932). L. P. Smith, Phys. Rev. **35**, 381 (1930).
[3] A. O. Nier, Rev. Sci. Instr. **18**, 398 (1947).
[4] Becker, Green, and Pearson, Trans. Am. Inst. Elec. Engrs. **65**, 711 (1946).

clean. It is impossible to state, however, that the surface was free of adsorbed gases because even at the lowest pressure attainable in the spectrometer (about 10^{-8} mm) the rate of collision of gas molecules with the platinum surface is high enough to form a surface layer in a few minutes. The effect of slight impurities and surface layers on the properties of platinum is illustrated by the extremely wide variation in the list of the values of the electronic work function for platinum obtained by different workers.[5] After the ion beam had been focused, the platinum ribbon was heated to about 800°C, and the mass range from 4 to 220 was swept over with the usual ionizing beam turned off. Over this mass range, only masses at 39 and 41 were detected, with the observed peak height ratio of mass 39 to mass 41 equal to 13.3. The most recently reported values for this abundance ratio range from 13.5 to 13.8;[6] the agreement is considered satisfactory. The pressure in the spectrometer at this time was about 10^{-8} mm.

Effect of Oxygen on Potassium Ion Emission

When oxygen was admitted to the spectrometer, the potassium peak height decreased for two to four minutes, finally becoming fairly constant at a value which was a function of the oxygen pressure. In Figs. 1A and 1B, the ratio of the potassium peak height to the initial peak height is plotted as a function of time after admission of oxygen to the system. The potassium emission decreases exponentially at first and then levels off to a constant value. The data of Fig. 1A indicated by squares were obtained several days after the data indicated by circles; in the interval a number of other gases were admitted to the spectrometer and the filament temperature was raised to maintain the potassium current high enough to measure. Hence, the two sets of data cannot be compared quantitatively. Qualitatively, the behavior towards oxygen on the two occasions was similar.

A proof that the oxygen did not cause the potassium to be emitted in an un-ionized state was obtained by turning on the ionizing mechanism of the mass spectrometer with oxygen in the system. There was no change in the potassium peak height.

Effect of Nitrogen on Potassium Emission

When nitrogen at a leak pressure of 4.5μ was admitted to the spectrometer, the potassium peak height decreased to about 90 percent of its initial value over a period of a minute and then leveled out. This pressure was considerably greater than the pressure of oxygen which reduced the potassium emission to less than 20 percent of its initial value. Increase in pressure of the nitrogen to 11.0μ caused the peak height to drop to 74 percent of its initial value; that is, the decrease in peak height was directly proportional to the pressure. The oxygen impurity in the nitrogen is insufficient to account for the observed effect.

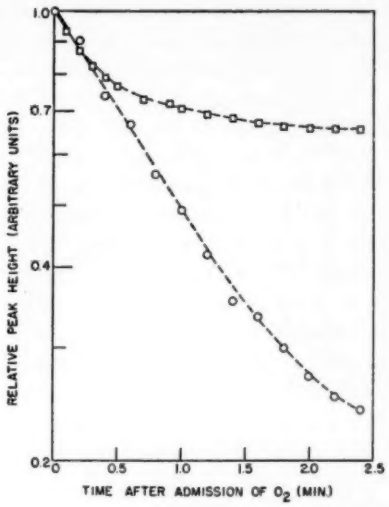

FIG. 1A. Effect of oxygen on potassium ion emission.

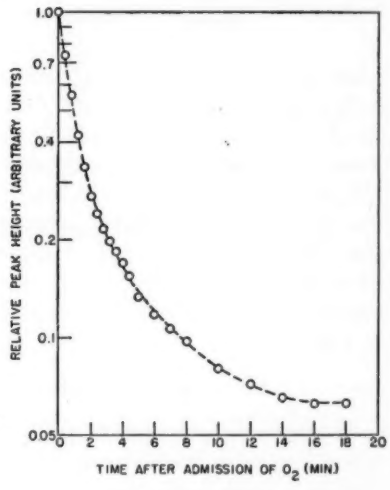

FIG. 1B. Effect of oxygen on potassium ion emission.

Effect of Carbon Tetrachloride and Bromine

Both carbon tetrachloride and bromine at leak pressures of less than 1 micron caused the potassium peak height to drop very rapidly, eventually reaching zero. The data are plotted in Fig. 2, along with the data obtained when helium was admitted to the system.

Effect of Helium

When helium was first admitted to the spectrometer at a leak pressure of 4μ, there was a 17 percent increase in the potassium peak height over a period of two minutes. When the pressure was increased to 18μ, the peak height increased to 64 percent higher than its initial value; that is, the increase in peak height was approximately linear with helium pressure. When the helium was pumped out, there was a small decrease amounting to six percent of the maximum height, followed by an increase over a period of some minutes to a value 27 percent higher than the previous maximum

[5] S. Dushman, Revs. Modern Phys. 2, 381 (1930).
[6] "Nuclear data," U. S. Natl. Bur. Standards Circular 499, U. S. Superintendent of Documents, 1950.

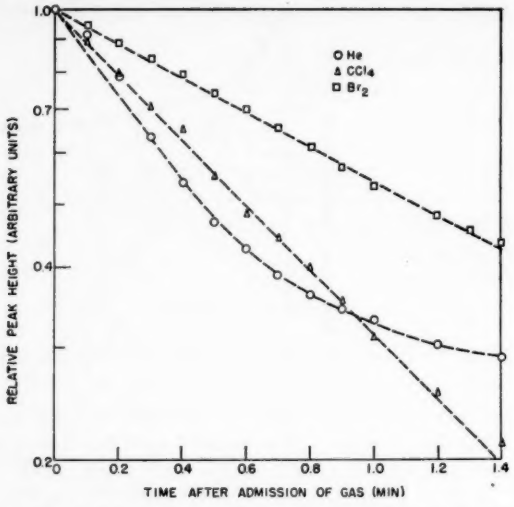

FIG. 2. Effect of helium, carbon tetrachloride, and bromine on potassium ion emission.

with helium in the system. Subsequent admission of helium at a leak pressure of 9.5μ resulted in a decrease to 87 percent of the value with the system evacuated. From this time on the response of the potassium peak height to the helium was consistent—addition of helium caused a decrease in emission down to 30–50 percent of the initial peak height and evacuation produced an increase. Qualitatively, then, the effect of helium is similar to that of oxygen. Typical behavior is shown in Fig. 2.

Effect of Hydrogen

When hydrogen was admitted to the system, the potassium emission *increased* for one to four minutes and then leveled out to a constant value. The behavior is shown in Fig. 3 where the percentage increase in peak height is plotted as a function of time after admission of hydrogen to the system.

When the hydrogen was pumped out of the system, the potassium peak height dropped rapidly for about a minute and then leveled out at about the value observed before the admission of hydrogen. The first two times that hydrogen was pumped out the peak height increased after leveling and rose almost to the value obtained with hydrogen in the system. In four subsequent cases (not all the data were analyzed in detail), there was no increase in the peak height. There was observed only the slow decrease presumably due to depletion of the potassium in the platinum. No explanation is suggested for the increase twice obtained.

Discussion of Results

The effect of the various gases on the emission of potassium ions can be caused by electrostatic fields produced by an adsorbed surface layer, or the effect may be due to a more specific interaction between the gas and the potassium. The results obtained with helium in the system are especially interesting. One is very reluctant to suggest that helium is adsorbed by platinum at a temperature of 800–900°C, forming a layer which inhibits the emission of potassium. One is even more reluctant to suggest that helium forms some sort of compound with potassium. A possible explanation for the effects is the presence of impurities in the gas reaching the spectrometer, perhaps dislodged from the walls of the system by the action of the helium. However, mass spectrometer analysis of the helium showed no mass peaks other than those found when the spectrometer is pumped out as completely as possible.

Evidence that helium is adsorbed to some extent by a bright platinum surface is provided by the work of Rolf[7] who found that the accommodation coefficient of helium on platinum varied with the length of time of contact, increasing quite rapidly for about three minutes (at pressures of 10^{-2}–10^{-3} mm Hg and temperatures from 77°K to 373°K) and then more slowly for ten or fifteen minutes. It has been found in this Laboratory that a platinum surface at 400°C will pick up argon atoms which will be released at a higher temperature.[8] Contact of platinum with argon at room temperature does not result in any retention of the gas. A similar phenomenon may occur with helium.

A possible explanation for the increase of potassium emission when helium was first admitted to the system can be based on the assumption that the helium atoms had a dislodging effect on the atoms already present on the hot platinum. If it is also assumed that the inhibition of the potassium emission due to the previously adsorbed atoms is greater than that of the helium, then, as was observed, the first effect of the helium will be to increase the potassium peak height.

The potassium emission decrease cannot be explained on the basis of thermal effects, since the heat loss of the filament due to gaseous conduction at the experimental pressures is only of the order of 10^{-5} or 10^{-6} times the total heat loss of the filament. Unless there is some source of experimental error which has not been taken

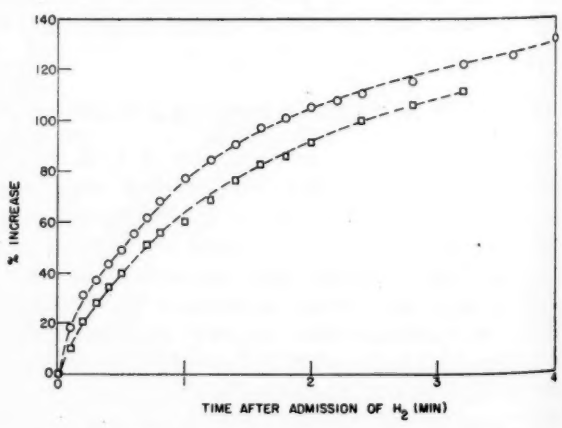

FIG. 3. Effect of hydrogen on potassium ion emission.

[7] P. Rolf, Phys. Rev. **65**, 185 (1944).
[8] P. D. Zemany (unpublished results).

into account, helium must be considered to produce a real effect.

The increase in the potassium emission under the influence of hydrogen could be attributed to a cleaning up of the oxygen or halogen covered surface. Hydrogen is known to dissociate into atoms on a hot platinum surface[9] and would probably react readily with many kinds of gas molecules adsorbed on the metal surface. It could also be assumed that the adsorbed hydrogen has the effect of decreasing the work function for removal of a positive ion from the surface.

The response of the potassium emission to the other gases is not at all surprising. The formation of strongly held gas layers on hot metal surfaces and their influence on electronic work functions have been known and studied for many years. Experiments of the type described here, together with accurate measurements of temperature, could serve as a means of determining positive ion work functions from surfaces of various kinds and conditions.

It is interesting to note that all of the peak height data in the figures will fit a first-order rate law if it is assumed that there are two opposing reactions when a gas is admitted, one tending to decrease and the other to increase the emission. In the case of oxygen, helium, carbon tetrachloride, and bromine it can be assumed that the reaction which decreases the emission is the adsorption of the gas on the surface, while the reaction which increases the emission is the desorption of the gas. A final steady-state rate of potassium emission is reached when the rates of adsorption and desorption are equal. In the case of hydrogen the adsorption process would be considered to cause an increase, while the desorption caused a decrease in emission, with a steady state again being reached when the rates of adsorption and desorption are equal.

[9] See, for instance, I. Langmuir, *Phenomena, Atoms, and Molecules* (Philosophical Library, Inc., New York, 1950); C. J. Smithells, *Gases and Metals* (Chapman and Hall, Ltd., London, 1938).

THE JOURNAL OF CHEMICAL PHYSICS VOLUME 20, NUMBER 2 FEBRUARY, 1952

Study of X-Ray Induced Optical Absorption Bands in CaF_2

SAM BARILE
Lewis Laboratory, NACA, Cleveland, Ohio

(Received September 10, 1951)

The absorption spectrum of CaF_2 crystals containing color centers was investigated as a function of temperature and time elapsed after having been irradiated with x-rays under various conditions. A weak absorption band previously unobserved has been found near 2280A. The intensities of the four absorption bands of crystals irradiated at room temperature decreased to the same extent after having been heated at various temperatures for various time intervals. Irradiation with light at room temperature does not cause any appreciable bleaching. At elevated temperatures the bleaching rate is increased by light. The color of the absorbed light does not however produce any preferential bleaching of any one of the bands. The type of decay and the energies involved were calculated from results obtained by bleaching the crystals at several temperatures. In view of these facts, it would seem that the bands are due to either one type of center, or else to several types incapable of existing independently. The results of the computation of the number of color centers responsible for three of the bands are not incompatible with this point of view.

INTRODUCTION

A CONSIDERABLE amount of work has been done on crystals containing color centers, produced by irradiating with x-rays, by electrolysis, or by heating in the presence of a cation metal vapor. While most of the effort was spent on monovalent ionic crystals, relatively little work has been done on CaF_2 or other more complex crystals. An explanation for this fact might be that these crystals are more complicated from a theoretical point of view so that in most cases the experimental results could not have been compared with results following from the theory. This made their investigation unattractive.

Mollwo[1] was the first to study such crystals by investigating the electron conductivity resulting from the absorption of light by color centers in CaF_2 and $SrCl_2$. In his investigation the color centers were produced by applying a potential at high temperatures between a pointed cathode and a flat anode covering one surface of the crystal or by heating the crystals in the presence of the cation metal vapor (additive coloring). Recently Smakula[2] investigated the absorption spectrum resulting from color centers in CaF_2 and BaF_2 produced by 200-kv x-rays. He found three absorption bands in the region between 2200A and 10,000A. There was furthermore an indication of a band in the far ultraviolet since the absorption coefficient increased in the spectral range from 2600A to 2200A, the latter wavelength representing the violet limit of the spectrophotometer used.

The purpose of this investigation was to obtain in-

[1] E. Mollwo, Göttinger Nachrichten 1, 79 (1934).

[2] A. Smakula, Phys. Rev. 77, 408 (1950).

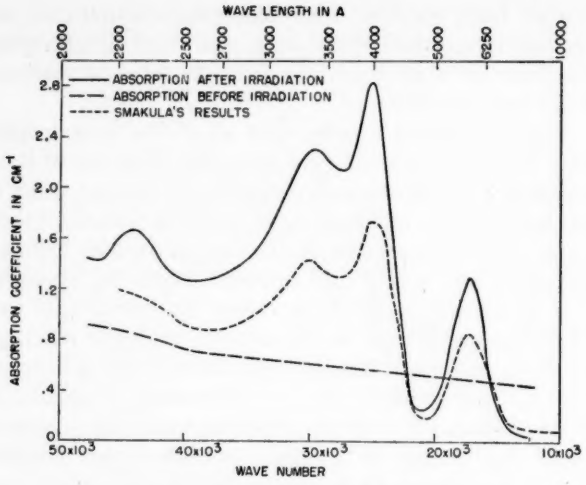

FIG. 1. Absorption coefficient of CaF_2 between 2100 and 10,000A.

formation concerning the mechanisms responsible for the appearance of the various bands and especially to investigate whether the mechanisms are similar to the ones found in the case of the more simple ionic crystals. In order to achieve this objective the absorption spectrum in the spectral range between 2100A and 10,000A was carefully re-examined, the spectrum was resolved into its various components and the bleaching of the individual bands was investigated as a function of temperature and as a function of the color of the absorbed light.

EXPERIMENTAL PROCEDURES

The crystals used throughout this work were obtained from the Harshaw Chemical Company. They were cleaved to produce rectangular pieces of approximate dimensions 1×1×0.5 cm. Instead of leaving them as they were obtained after cleaving, as is usually done, the surfaces were polished using standard techniques. This reduces the light absorption and gives a uniform thickness.

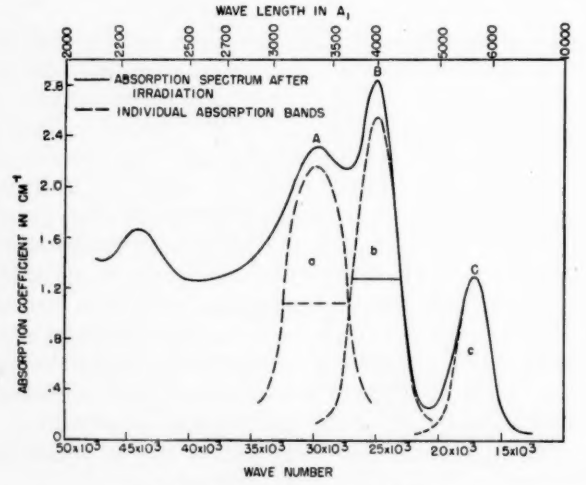

FIG. 2. Analysis of the absorption curve.

The crystals prepared in this manner were irradiated with x-rays from an AEG 50 T Machlett beryllium window tube operated at 50 kv and 30 ma. The crystals were irradiated on both sides for 20 hours after which further irradiation caused no change in the optical absorption of the crystals. This assures a uniform distribution of color centers independent of the absorptivities of the x-rays and their efficiency in producing color centers. After the irradiations, the crystals were kept in the dark for five to thirty minutes to allow the luminescence to decay.

The obvious way to study the decrease in the number of color centers at elevated temperatures (bleaching) would be to make absorption measurements with the crystal at these temperatures. This is, however, impossible. First, CaF_2 exhibits the property of thermoluminescence at elevated temperatures which makes absorption measurements rather difficult. Second, at elevated temperatures the light used for the absorption measurements causes an increase in the rate of bleaching. On the other hand, at room temperatures, almost no bleaching occurs even in the presence of light, as will be shown later. Third, with the instrument at our disposal (Beckmann spectrophotometer), the process of measuring is so slow that, especially at higher temperatures, the rate of bleaching (even without the presence of light) is such that essentially the absorption at different wavelengths would be obtained at a different state of bleaching. Therefore, the specimens were cooled down to room temperature before making the absorption measurements. It can be shown by leaving samples in the spectrophotometer for ten or more hours with light of a color corresponding to the absorption bands incident on them, that at room temperature the bleaching is negligible. There is, however, an error involved in this method because of the fact that it takes of the order of one minute for a crystal either to cool from the temperature of the furnace to room temperature, or to reach the temperature of the furnace after being placed into it. Since the crystals were left in the furnace for intervals of 10 minutes or more, the error introduced by the time required for cooling and heating is of minor importance. As will be shown later, the "time of bleaching" represents the total time that the crystal was in the furnace, which is, therefore, slightly longer than the time that the crystal was actually held at the temperature in question.

TABLE I.

Band	Absorption coeff. K in cm^{-1} at peak	Half-width W in ev	No. of color centers per cm^3
a	2.162	0.6449	1.48×10^{16}
b	2.553	0.4960	1.34×10^{16}
c	1.196	0.3721	0.39×10^{16}

The absorption spectrum was first determined before the irradiation. The absorption measured in this way was subtracted from the absorption measured after the

introduction of the color centers. Measurements were taken at wavelength intervals of 50A throughout the investigated spectral range.

EQUIPMENT

In order to heat the crystals to the desired temperature of 215°C, a furnace was used with automatic temperature controls able to keep the furnace within ±1.5°C. For the other two temperatures, the crystal was placed in a test tube which was immersed in boiling ethylene glycol at 180°C and in boiling water at 100°C. A special small furnace with an open top was constructed for exposing crystals at elevated temperatures to x-rays and to light of various frequencies.

The absorption measurements were made with a Beckman spectrophotometer which, according to the specifications of the manufacturer, can be used in the range 2200A to 10,000A. However, as has already been pointed out by Gibson and Balcom,[3] the instrument is probably very reliable down to 2100A and possibly farther. The results down to 2100A were checked in this laboratory by measuring the absorption of CaF_2 using three different techniques. (1) The sensitivity dial was set three turns counterclockwise from its end position and the slit width was varied in order to obtain a balance of the galvanometer. This procedure is recommended by the manufacturer as being the most accurate. The instrument is very sensitive at this position but large slit widths must be used. (2) The sensitivity dial was set at the extreme counterclockwise position and again the slit width was varied for a balance of the galvanometer. With this method smaller slit widths can be used. (3) The slit width was fixed and a balance of the galvanometer was obtained with the sensitivity knob.

The three different methods gave the same results. Measurements made with various light intensities also gave the same results.

RESULTS

Figure 1 shows the absorption coefficient as a function of the wave number and wave length for a CaF_2 crystal that has been irradiated by x-rays. The dotted curve represents the spectrum obtained by Smakula who irradiated his samples for five hours, while the solid curve represents the results of this investigation. The two curves are reasonably similar for wavelengths higher than 2500A. Our measurements, however, show an absorption band with a peak at 2280A, which does not occur in Smakula's measurements. As can be seen from the figure, this new band is rather weak. An explanation for the fact that Smakula did not observe this band, might be that he took readings at wavelengths father apart than was done in this investigation. The band does not show up very well unless careful measurements are made of the absorption of the crystal before the irradiation, and subtracted from the absorption of the crystal after the irradiation. Our investigation, furthermore, extends to smaller wavelengths than Smakula's (2100A rather than 2200A) so that it is now clear that the peak of the absorption band in the far ultraviolet must be even below 2100A. That there is such a band below 2100A is indicated by the rise in the absorption coefficient to the left of the new band.

[3] K. S. Gibson and M. M. Balcom, J. Opt. Soc. Am. **37**, 593 (1947).

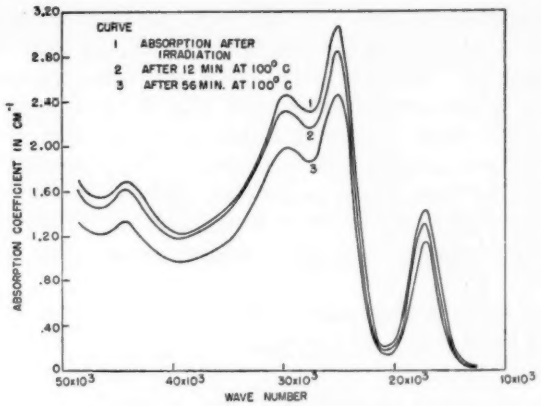
CURVE
1 ABSORPTION AFTER IRRADIATION
2 AFTER 12 MIN AT 100° C
3 AFTER 56 MIN. AT 100° C
ABSORPTION COEFFICIENT IN CM⁻¹
WAVE NUMBER

FIG. 3. Bleaching of CaF_2 at 100°C.

To determine the number of color centers responsible for the various bands in a crystal from its optical absorption, a knowledge of the width of the absorption band at half-maximum and the absorption coefficient at its peak must be known. These values can be obtained from the rather complicated absorption spectrum shown in Fig. 2 with only a limited accuracy. It is evident from this figure that this spectrum is the result of at least five separate absorption bands, the peaks of four of them being in the investigated range between 2100A and 10,000A. In order to determine the heights and half-widths of as many of the bands as possible, it was first assumed that each of them has a Gaussian distribution in wave number. It is evident that the right side of the peak *C* is identical with the distribution of the band *c* itself, since the absorption coefficient eventually comes

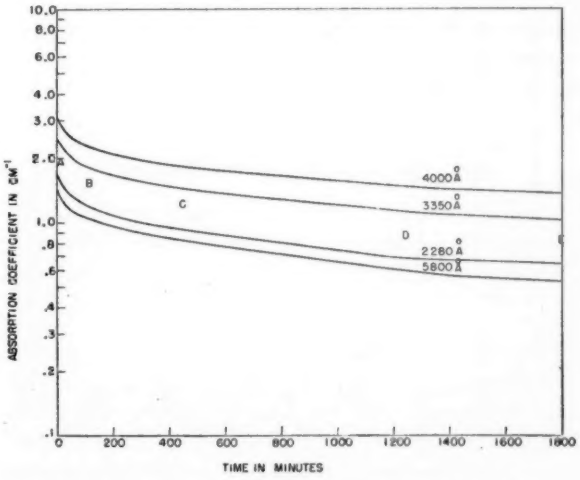

FIG. 4. The absorption coefficient at the 4 peaks is plotted as a function of time.

fairly close to zero. This side of c was reflected at the point C to give the left side of the band. The band thus completed, was subtracted from the total spectrum. Two points on the lower right side of band b, which resulted from this subtraction were selected. Using these two points (again assuming a Gaussian distribution) the band b was constructed. Band b was then also subtracted to obtain band a. The new band cannot be resolved from an adjoining band at wavelengths below 2100A.

If K is the absorption coefficient in cm^{-1} at the peak of a band and W its half-width in ev, then N, the number of color centers per cm^3 responsible for the band, can be calculated by the use of the following expression derived by Smakula.[4]

$$Nf=18mnKW/\pi e^2h(n^2+2)^2. \quad (1)$$

In this expression m, e, and h have the usual meaning and n is the index of refraction ($n=1.434$ for CaF_2).

In order to evaluate this expression for our case, assumptions must be made regarding the oscillator strength f. By assuming $f=1$, we obtain for the number of color centers per cm^3 in our specific case,

$$N=1.06\times10^{16}\times KW. \quad (2)$$

Table I contains the absorption coefficients and half-widths of the bands a, b, and c and the number of color centers calculated by the use of Eq. (2).

From the last column in the table we see that there are approximately the same number of color centers responsible for band a as for band b, but less than one-third of this number for band c. The results of the annealing experiments, which will be described below, make it seem quite possible that all the absorption bands are the result of one type of color center having different energy levels. The fact that the number of color centers calculated to be responsible for band c is smaller than the number responsible for a and b, would then have to be explained in terms of a difference in the oscillator strength f of band c with respect to bands a and b.

Figures 3 and 4 contain the results of the bleaching experiments. The upper curve in Fig. 3 represents the absorption spectrum of CaF_2 which was irradiated for twenty hours. The lower curves represent the spectra after the crystal was kept at 100°C for 12 and 56 minutes respectively. The curves show that the relative decrease in the absorption coefficient is approximately the same for all wavelengths; after 12 minutes there is a decrease of approximately 7 percent, and after 56 minutes, approximately 20 percent.

In order to study over longer periods of time, a series of measurements was made only at wavelengths corresponding to the peaks of the absorption bands. Such measurements were performed at 100°, 180°, and 215°C. In Fig. 4 the absorption coefficient at 2280, 3350, 4000, and 5800A is plotted logarithmically as a function of time for a crystal bleached at 100°C.

Any annealing process involving distinct activation energies, $E_1, E_2, \cdots, E_n$, can be represented by

$$dN/dt=\sum_{i=1}^{n} dN_i/dt, \quad (3)$$

with

$$dN_i/dt=-N_i\gamma_i\nu_i \exp(-E_i/kT). \quad (4)$$

In the case of color centers the annealing or bleaching has usually been observed to follow this law with the values of γ being ordinarily 1 or 2.[5]

An analysis of the curves in Fig. 4 was made in the following manner. The straight sections DE represent simple first-order decays ($\gamma=1$). These sections were extended to $t=0$, and subtracted from the total curves. This process was repeated until the individual components of the composite curves in Fig. 4 were obtained. This is better illustrated in Fig. 5 for the band at 3350A. Decay curves have already been subtracted from the total curve to give the curve ABC in Fig. 5. Now ABC is composed of two straight lines BC and $A'B'$. The absorption coefficient of $A'B'$ has been multiplied by ten. The results show γ to be equal to one for the sections AB, BC, and DE, and equal to 0.2 for the section CD. The remaining three curves in Fig. 4 give similar results.

The activation energies computed under the assump-

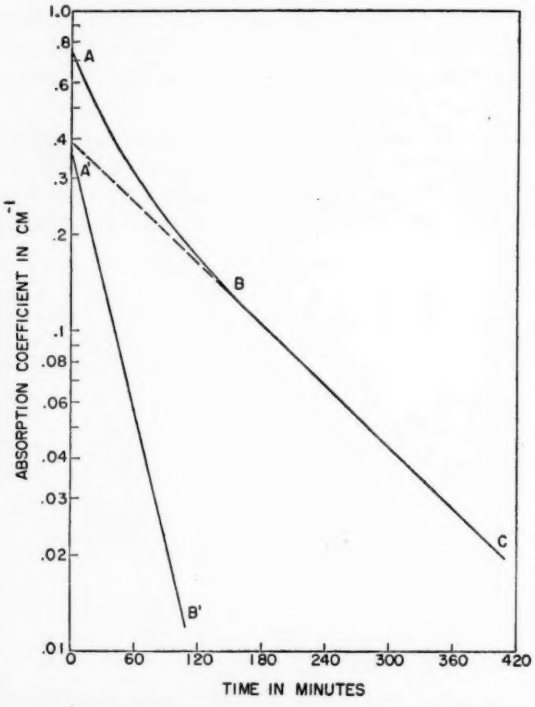

FIG. 5. The absorption coefficient at 3350A after the last two decay curves were subtracted.

[4] A. Smakula, Z. Physik **59**, 603 (1930).

[5] "Preparation and Characteristics of Solid Luminescent Materials," Cornell Symposium of the American Physical Society (John Wiley and Sons, Inc., New York, 1948).

tion that all the ν's are equal to 10^{13} for the decay of the color centers responsible for the four bands are given in Table II. It can be seen that the activation energies connected with the four bands agree fairly well. The activation energies for the decay in which $\gamma=0.2$, sections *CD*, could not be obtained since an accurate analysis, such as was done for Fig. 2, would have to be made several times during the bleaching. It may be remarked that processes of essentially zero order while new to color center studies have been previously observed in investigations of catalysis.

As was mentioned before, a certain error is introduced by the time required for the crystal to cool down to room temperature and to be heated to the temperature of the furnace. This error, of course, becomes larger when the bleaching temperature is higher since it takes a longer period of time for the crystal to reach this temperature or to cool down to room temperature. Furthermore, bleaching at lower temperatures does not require measurements at frequent intervals since decay occurs rather slowly. For this reason our measurements at 100°C are hardly affected by errors of this kind. The bleaching experiments made at 180° and 215°C should be affected to a greater degree. In spite of this fact, a decomposition of the decay curves was readily possible, the results indicating again four decay processes of the same type with fairly good agreement between the activation energies.

As mentioned previously, light has very little effect on the bleaching of CaF_2 at room temperature. Simple experiments were also performed concerning the effect of light of various wavelengths on bleaching at 100°C. The light was passed through filters whose transmission maximum corresponded approximately to the wavelengths of the bands. It was found that the rate of bleaching increased slightly but contrary to the results obtained with alkali halides, there was no evidence of preferred bleaching of any one of the bands so that the absorption spectrum cannot be changed even in this manner.

DISCUSSION

In comparing the properties of color centers in CaF_2 with those in the alkali halides, certain similarities are observed along with several outstanding differences. First, all the various methods used to color the alkali halides can also be used to color CaF_2; however, it is more difficult to color CaF_2 than most of the alkali halides. In most of the alkali halides there are slight differences in the absorption spectra for crystals colored by different methods. In the case of NaCl for instance, different spectra can be obtained by irradiating with x-rays, by electrolysis at elevated temperatures and by heating in a metal vapor. In the latter two cases the spectra can be influenced by the rate of cooling. In this investigation, spectra obtained by electrolysis were compared with spectra obtained by x-ray irradiation and were found to be identical.

TABLE II.

Wavelength	Activation energies in ev		
	AB	*BC*	*DE*
2280A	1.20	1.26	1.38
3350A	1.20	1.25	1.38
4000A	1.18	1.25	1.38
5800A	1.17	1.24	1.37

CaF_2 can, as in the case of alkali halides, be bleached by heating. However, as was shown in our results, CaF_2 shows a rather complicated decay law. The alkali halides can also be readily bleached by light either at room temperature or at elevated temperatures and it is possible to change the absorption spectrum by bleaching one of the bands with light of a wavelength corresponding to the band. There is very little bleaching by light in the case of CaF_2 at room temperature. At elevated temperatures, exposure to light causes a small increase in the rate of bleaching. However, varying the color of the light does not alter the relative bleaching rate of any one of the bands with respect to the rates of the other bands. The fact that the shape of the absorption spectrum in the visible range is unaffected by either the method of coloration or the method of bleaching makes it seem likely that either several types of centers which always appear and disappear together are present or, more simply, that only a single type of color center occurs. In the latter case, the different bands are presumably associated with different energy levels of the electron trapped in the vacancy. The fact that the estimates given for the numbers of color centers associated with the different bands do not agree may be explained by the fact that the same value of the oscillator strength (namely a typical one) was used for all the bands whereas the true value may differ from band to band by an amount sufficient to remove this discrepancy.

The complex nature of the bleaching process is difficult to explain. Assuming that only one type of color center is present, one would infer that there are available different mechanisms for their disappearance. It would be difficult to speculate at this point on the exact mechanisms.

ACKNOWLEDGMENT

The author wishes to express his appreciation to Dr. Gerhart Groetzinger for his help and advice throughout this investigation and to Dr. Philip Schwed for his advice in analyzing the results.

Note added in proof: Since submitting this paper for publication, the writer has learned by private communication that Smakula has also found the peak at 2280A which he has been able to resolve into a pair of bands.

The Raman Effect of Vinylidene Chloride*

POWELL JOYNER† AND GEORGE GLOCKLER
Department of Chemistry and Chemical Engineering, State University of Iowa, Iowa City, Iowa.
(Received September 28, 1951)

The Raman spectrum of vinylidene chloride is reported. An assignment of fundamental vibrational frequencies is made and the overtone and combination frequencies interpreted. A method of accurately marking faint Raman lines for measurement is described.

I. INTRODUCTION

THE molecular spectra and structure of halogenated hydrocarbons have been a subject of considerable interest in this laboratory for a number of years. Recently Edgell, Roberts, and Byrd[1–4] have studied the Raman and microwave spectra of vinylidine fluoride, and this research is a continuation of the study of vinylidene halides. Previously reported studies of the Raman effect of vinylidene chloride[5–7] were incomplete and the assigned fundamental frequencies could not be correlated with those of vinylidene fluoride,[1–4,8] and vinylidene bromide and its deutero derivatives as observed by Hemptinne, Velghe, and Van Riet.[9,10] Previous workers were also bothered by polymerization of their samples initiated by blue and ultraviolet light. It was possible in this research to observe many more of the lines of this unstable molecule due to the use of a very fast spectrograph and further refinements of experimental techniques.

II. EXPERIMENTAL TECHNIQUE

The sample of vinylidene chloride used in this research was obtained from the Dow Chemical Company, Midland, Michigan, through the courtesy of Dr. E. C. Britton, and came stabilized by a trace of an alkyl phenol. Because of the ease with which vinylidene chloride polymerizes, and its susceptibility to oxygen, the samples were purified by several distillations in a vacuum system, and then distilled through a barium oxide containing tube into the sample tube. It has been established by Mallory[11] that the dust carried in by the few milliliters of air that re-enter the sample tube after the final rinse of usual cleaning techniques gives rise to virtually all of the continuous background so troublesome in the study of the Raman effect. Therefore, a modification of an apparatus of the type used by Mallory was employed for cleaning and loading the sample tube. The essential feature of the process is that the final rinses, the air that reenters after the final rinses, and the sample which is later vacuum distilled into the sample tube must all first pass through two fritted glass disks sufficiently fine to eliminate all dust particles. Details of this technique are described elsewhere.[12] The boiling point of the purified vinylidene chloride was 32°C.

A trace of inhibitor was sublimed into the sample tube previous to the distillation of the vinylidene chloride. The most effective inhibitors used were hydroquinone and *p*-cresol. The concentrations were always less than 0.1 percent, and no Raman displacements attributable to any inhibitors used were ever observed.

A Lane-Wells Raman spectrograph and excitation unit was used, having an effective aperture of *f*:3, and a dispersion of 100 cm^{-1} per mm at 4500A. The sample tubes were of conventional design and had a diameter of 1 cm and an effective length of 15 cm. The samples were exposed at a temperature of approximately 30°C. Various arc intensities were used, resulting in exposures of a few minutes to several of 6 hours. These later exposures were under low arc intensities and produced the best results. Rhodamine and paranitrotoluene in alcohol were used as a filter solution to isolate the 4358A mercury triplet, eliminate the polymerization initiating ultraviolet light, and further reduce the continuous background. Qualitative polarization data were obtained by making two exposures: the first with polaroid *J* sheeting wrapped around the sample tube with the electric vector of the transmitted polarized light parallel to the axis of the tube, and the second exposure with the electric vector perpendicular to the axis according to the method of Edsall and Wilson.[13]

Eastman Kodak Tri-x Panchomatic film was used, and developed to maximum contrast in Kodak DK-60a. The Raman displacements were read with a comparator

* This paper is based on a portion of a thesis presented by Powell Joyner in partial fulfillment of the requirements for the degree of Doctor of Philosophy in the State University of Iowa, Iowa City, Iowa.

† Research Department, Minneapolis-Honeywell Regulator Company, Minneapolis, Minnesota.

[1] W. Byrd, Ph.D. thesis, State University of Iowa (1949).
[2] W. F. Edgell and W. Byrd, J. Chem. Phys. **17**, 740 (1949).
[3] W. F. Edgell and A. Roberts, Phys. Rev. **76**, 178 (1949).
[4] W. F. Edgell and A. Roberts, J. Chem. Phys. **17**, 742 (1949).
[5] J. Cabannes, J. chim. phys. **35**, 9 (1938).
[6] H. W. Thompson and P. Torkington, Proc. Roy. Soc. (London) **184**, 21–26 (1945).
[7] V. M. Tatevskii and A. V. Frost, Vestnik. Moscow University, No. **3**, 65–83 (1947).
[8] Smith, Nielsen, and Claasen, J. Chem. Phys. **18**, 326 (1950).
[9] Hemptinne, Velghe, and Van Riet, "Recueil de travaux du Laboratorie de Physique" (Universite de Louvain, 1945). (Reprinted from Bulletin de l'Academie Royale de Belgique (Classe des Sciences) **30**, 40–56 (1944).)
[10] Marc de Hemptinne, Trans. Faraday Soc. **42**, 7 (1946).
[11] H. D. Mallory, Ph.D. thesis (State University of Iowa, 1949).
[12] P. A. Joyner, Ph.D. thesis (State University of Iowa, 1951).
[13] J. T. Edsall and E. B. Wilson, Jr., J. Chem. Phys. **6**, 124 (1938).

and the values calculated using a modification of the Hartmann dispersion formula.

Because of the relatively short exposures used to avoid polymerization, a number of faint Raman lines were observed that were too weak and diffuse to be seen under the magnification of the comparator microscope. In the past it has been the practice in this laboratory to mark these lines by pricking the emulsion with a finely honed needle with the aid of a magnifying glass. This method is not very accurate, and therefore a highly precise method for marking these faint lines was developed which is described in detail elsewhere.[12] The technique consists of drawing a thin filament out of Duco cement and laying it across the film strip and directly on top of the line to be marked. The filament may be drawn much thinner than the Raman lines and can be laid down so as to accurately bisect it. Not only are these filaments quite durable, but they can be easily removed leaving no marks, fresh ones drawn, and the measurement repeated. Figure 1 is a microphotograph of a Raman line marked in this manner. For purposes of illustration, the strong Raman displacement at 1616 cm^{-1} was used, and is approximately 0.055 mm wide on the film strip. The triangular dark area to the right is the point of an ordinary pin.

The precision of this method is excellent. The average deviation of a filament marked line on repeated measurement was 3 cm^{-1} as compared to 1 cm^{-1} for a line strong enought to be measured without marking. A number of weak lines were read by this method before subsequent longer exposures registered them with sufficient intensity to be read without marking. In these cases the average difference between these values was less than 4 cm^{-1} with largest error being 6 cm^{-1} in the region of poorest dispersion. Occasionally one may be in doubt if a particularly weak line actually exists. If a needle mark is made on the plate, then the observer has prejudiced himself. It is suggested that the filament method be used as the criterion in such cases since it leaves no permanent mark. The criterion being that the precision of repeated measurements be less than 5 cm^{-1}. It may be pointed out here that the average error of this method is of the same order as the difference in values for many Raman spectra as reported by different observers.

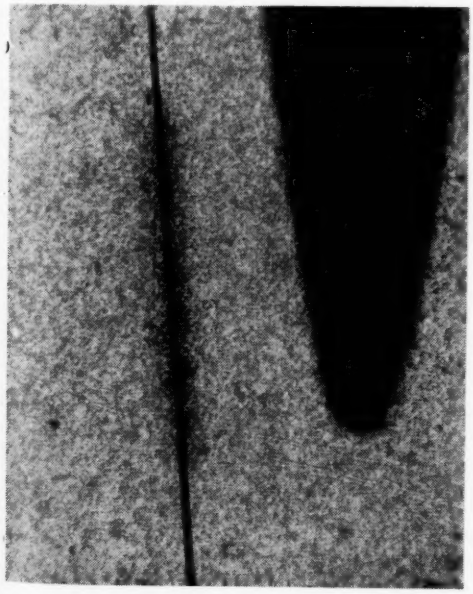

FIG. 1. Microphotograph of Raman line 1616 cm^{-1} of vinylidene chloride, marked with Duco filament.

TABLE I. Raman and infrared spectra of vinylidene chloride.

Raman lines									Infrared		
Cabannes			Thompson and Torkington		Shorygin	Present research					
cm^{-1}	I	p	cm^{-1}	I	cm^{-1}	cm^{-1}	I	p	cm^{-1}	I	C
146	5	p									
293	5	p	295	s	293	299	s	p?			
372	3	d	375	m	371	375	s	d			
			450	w	455	458	m	d			
			540	w							
									580	vw	
600	20	p	595	s	600	601	vs	p	605	s	B
						686	wm	d			
									714	vw	
					750						
						788	wm	d			
									794	s	A
									829	vw	
860	?	d	868	vw	876	874	w		872	s	C
						911	w		916	w	(B)
990	2	p			990				970	vw	
									1020	vw	(C)
			1099	?		1088	vw		1094	s	A
									1142	m	A
1200	?	d									
			1331	?	1317	1320	m	p	1318	w	?A
						1349	m	p			
1393	3	p	1390	m	1388	1391	sm	p	1391	m	
					1393						
						1459	vw				
			1558	m							
						1589	vw		1580	m	
1611	15	p	1611	s	1612	1616	vs	p	1620	s	B
									1742	m	
						1846	vw				
						1867	w		1876	w	
									1920	vw	
									1988	vw	
									2070	vw	
						2162	vw				
						2216	vw		2215	vw	
									2430	vw	
						2687	vw		2670	vw	
3038	10	p	3035	m	3038	3035	vs	p	3035 l.	w	
			3130	m		3130	s	d	3130 l.	w	
						3178	w				
						3228	w				

C = type of contour (T and T)
I = relative intensity
p = polarized
l. = liquid
d = depolarized
vs = very strong
s = strong
sm = strong medium
m = medium
wm = weak medium
w = weak
vw = very weak

III. EXPERIMENTAL RESULTS

The Raman spectrum of vinylidene chloride has been observed by several investigators. Cabannes[5] first reported part of the first-order spectrum in 1938, but experienced considerable trouble due to the polymerization of his sample. H. W. Thompson and P. Torkington[6] studied both the Raman and infrared spectra in 1945 and attempted an assignment of the observed vibrational frequencies. Finally, in 1947 Tatevskii and Frost[7] quote from unpublished work of Shorygin the fundamental frequencies that he assigned to the molecule on the basis of observed Raman spectra. They used this assignment of frequencies to calculate the standard

entropy of vinylidene chloride by statistical thermodynamical methods. The Raman spectra reported by these investigators and that observed in this research are tabulated in Table I, together with estimates of relative intensities and states of polarization. The values for the following lines were determined by marking them with a Duco filament as previously described: 1459, 1846, 2162, 2687, and 3228 cm^{-1}. The lines also excited by Hg 4347 were: 299, 601, 1349, 1616, 3035 cm^{-1}. The lines also excited by Hg 4339 were: 601, 1349 (apparently coinciding with 1349 excited by 4347), 1616 cm^{-1}. The following were observed as anti-stokes lines: 299, 375, 458, and 601 cm^{-1}.

The 145 cm^{-1} and 1200 cm^{-1} frequencies reported by Cabannes are probably spurious since they were neither observed in this research nor by Thompson and Torkington. The existence of the 990 cm^{-1} displacement is doubtful for the same reason, although Thompson and Torkington report an infrared band at 970 cm^{-1}. Not only is it not a fundamental frequency as reported by them, but also no satisfactory combination of fundamentals can give rise to a polarized Raman overtone at 990 cm^{-1}. In the case of the Raman displacements that Thompson and Torkington report at 540 and 1558 cm^{-1} it can be conclusively demonstrated that they are excited by 4347A Hg and not by 4358A. Thompson and Torkington used 4358 Hg as their exciting line. 4347 Hg lies at a displacement of 57 cm^{-1} from 4358 Hg, and frequently excites the strongest of the Raman displacements. Adding 57 cm^{-1} then to 540 and 1558 cm^{-1} one obtains 597 cm^{-1} and 1615 cm^{-1}, respectively. These correspond to the strongest observed Raman displacements. The two displacements in question have been observed in this research and both are polarized as are the 601 and 1616 cm^{-1} displacements. It can further be shown that since the two lines in question are polarized, they would be active in the infrared and no infrared bands are observed near enough to either 540 or 1558 cm^{-1}. The Raman displacement at 1331 (?) reported by Thompson and Torkington is probably either 1320 or 1349 cm^{-1}.

Brockway, Beach, and Pauling[14] reported in 1935 the geometrical configuration of vinylidene chloride as based on electron diffraction observations to be planar with the following dimensions: $R_{CH}=1.08$A, $R_{CC}=1.38$A, $R_{Cl}=1.69$A, and Cl−C−Cl=116°, Cl−C=C=122°, and H−C−H=120°. Thompson and Torkington used these dimensions to compute the moments of inertia as follows: The least moment equals 105×10^{-40} g cm^2 along the x axis (in the plane of the molecule and normal to the C=C bond), the middle moment equals 255×10^{-40} g cm^2 and is along the z axis (the C=C bond), and the greatest moment of inertia equals 360×10^{-40} g cm^2 and is directed along the y axis (normal to the plane of the molecule).

By using this information and extrapolating the curves of Badger and Zumwalt,[15] Thompson and Torkington arrived at the conclusion that vinylidene chloride should display the following band types: A-type bands with 3 submaxima having a spacing between the two outermost of about 14 cm^{-1}, B-type bands being essentially a double band with a central gap and a spacing of about 11–12 cm^{-1} between the submaxima, and C-type bands with a fairly strong central Q branch with two other submaxima on either side of it (O, P, R, and S), the spacing between the pair of outermost maxima, O−S, being about 24 cm^{-1}, and that between the next inner pair being about 12 cm^{-1}.

The infrared spectrum of vinylidene chloride as observed by Thompson and Torkington is listed in Table I with their interpretation of the band types. Apparently some doubt existed in their minds as to the band contours exhibited by the bands at 914 and 1020 cm^{-1} as they did not directly state the type of contours. Therefore, the type of contours that these bands would have to possess was inferred from their overtone interpretation and enclosed in parentheses. Also there must have been some doubt about the contour of the band at 1318 cm^{-1} as they say it has "apparently type A contour."

Emschwiller and Lecomte[16] also reported a few of the infrared bands of CH_2CCl_2 in 1937. However, the work was done under low dispersion so the results are not included here.

Vinylidene chloride belongs to the point group C_{2v} and has 12 normal modes of vibration which will fall into 4 symmetry species. The assignment of the vibrational frequencies was greatly facilitated by comparison to the fundamental frequencies assigned to the other vinylidene halides by various investigators. Edgell, Byrd, and Roberts[1–4] studied the microwave, Raman, and infrared spectra (under low dispersion) in this laboratory. Torkington and Thompson[17] have also studied the infrared spectrum of CH_2CF_2 in 1945. Smith, Nielsen, and Claasen[8] have recently reported a more detailed infrared study of the same molecule under high dispersion as well as its Raman spectra in the gas phase. In particular, the assignment of frequencies was made much easier, because of the unambiguous assignment of the fundamentals of vinylidene bromide and all its deutero derivatives by Hemptinne, Velghe, and Van Riet.[9,10] It should be mentioned that in the case of vinylidene fluoride the least moment of inertia coincides with the C=C bond, and not normal to it as in vinylidene chloride.[4] This gives rise to different band types associated with the various symmetry species. That is, in the case of vinylidene fluoride, type A bands are associated with A_1 vibrations, A_2 vibrations are inactive, type B bands are associated with

[14] Brockway, Beach, and Pauling, J. Am. Chem. Soc. **57**, 2693 (1935).

[15] R. M. Badger and L. R. Zumwalt, J. Chem. Phys. **6**, 711 (1938).

[16] G. Emschwiller and J. Lecomte, J. phys. et radium **8**, 141 (1937).

[17] P. Torkington and H. W. Thompson, Trans. Faraday Soc. **41**, 236 (1945).

B_1 vibrations, and type C bands associated with B_2 vibrations. Further, it should be noted that since $CHDCBr_2$ does not belong to the point group C_{2v}, its vibrations will not fall into the same symmetry species as the other vinylidene halides. According to Thompson and Torkington[6] CH_2CBr_2 should exhibit the same band types as CH_2CCl_2, with different spacings of submaxima.

The agreement between Edgell, Byrd, Smith, Nielsen, and Claasen is good, particularly when one considers that in the first case the Raman effect was observed in the liquid phase at below $-100°C$ and in the second case in the gas phase at much higher temperatures. The only major discrepancy is in the value for the torsional mode and the arguments for each case are summarized by Smith, Nielsen, and Claasen. It seems more likely that the value suggested by Edgell and Byrd is the correct one.

In general one would expect the vibrational frequencies for vinylidene chloride to lie at values intermediate between the corresponding ones for vinylidene fluoride and vinylidene bromide, since both the masses of the chloride atoms and the corresponding force constants would possess intermediate values. Those vibrations which affect the carbon halogen bond lengths and angles would be expected to show a greater change as one progresses from vinylidene bromide to vinylidene fluoride than the vibrations which primarily affect the carbon hydrogen bond distances and angles.

IV. ASSIGNMENT OF VIBRATIONAL FREQUENCIES OF VINYLIDENE CHLORIDE

Assignment of Fundamentals

3130 cm^{-1}: This vibration lies in the region of a CH stretching vibration. The Raman line is depolarized. An infrared band is observed at 3130 cm^{-1}. Therefore, this frequency is assigned to the B_1 CH stretching mode.

3035 cm^{-1}: This line is polarized in the Raman effect, and a corresponding infrared band is present. Therefore, it is the A_1 CH stretching mode.

1616 cm^{-1}: This frequency lies in the region one would expect of a C=C stretching vibration. It is polarized in the Raman and exhibits a strong type B band in the infrared. Therefore, it is assigned to the A_1 C=C stretching mode.

1391 cm^{-1}: The CH_2 deformation in CH_2CBr_2 lies at 1379 cm^{-1}, and that of CH_2CF_2 at 1358 cm^{-1}. This is somewhat contrary to what one would expect. However, CH_2CCl_2 would be expected to more nearly approximate CH_2CBr_2 than CH_2CF_2. The line is polarized in the Raman effect and a corresponding infrared band is present. It is assigned to the A_1 CH_2 deformation mode.

601 cm^{-1}: This displacement is polarized and very strong in the Raman effect, has a type B band in the infrared and is therefore of the symmetry species A_1. It has about the value one would expect of a CCl stretching mode. It is assigned then to the A_1 CCl stretching mode.

229 cm^{-1}: This line should be either a CCl_2 deformation or a CCl_2 rock. It is polarized according to Cabannes. If so, the depolarization factor must be relatively large as it cannot definitely be said to be polarized according to our observations. Although a vibration of species A_1 must be polarized, it is not necessary for it to be strongly so, and according to Cleveland and Murray[18] the values of the depolarization factor as obtained by the method of Edsall and Wilson[13] are definitely too high. Therefore, a weakly polarized line could not be readily detected by this method. One would expect the CCl_2 deformation vibration to have a lower frequency than the CCl_2 rock by analogy to methylene chloride as well as to CH_2CBr_2. It is therefore assigned to the A_1 CCl_2 deformation mode.

375 cm^{-1}: This frequency is depolarized and by analogy to CH_2CBr_2 is classified as the B_1 CCl_2 rocking mode.

458 cm^{-1}: Since it is depolarized and fits nicely between the values for the CBr_2 wag and the CF_2 wag, it is assigned to the B_2 CCl_2 wagging mode.

TABLE II. The fundamental vibrational frequencies of vinylidene chloride.

Sym. species	Approx. descrip.	Raman	p or d obsv.	p or d theory	I.R.[a]	Band type obsv.	Band type theory
A_1	CCl_2 def.	299 s	?	p			B
B_1	CCl_2 rock	375 s	d	d			A
B_2	CCl_2 wag	458 m	d	d			C
A_1	CCl stretch	601 vs	p	p	605	B	B
A_2	Torsion	686 wm	d	d			Inact.
B_1	CCl stretch	788 wm	d	d	794	A	A
B_2	CH_2 wag	874 m	d	d	872	C	C
B_1	CH_2 rock	1088 wm		d	1094	A	A
A_1	CH_2 def.	1391 sm	p	p	1391		B
A_1	C=C stretch	1616 vs	p	p	1620	B	B
A_1	CH stretch	3035 vs	p	p	3035		B
B_1	CH stretch	3130 s	d	d	3130		A

[a] I.R. values from Thompson and Torkington.

686 cm^{-1}: This line is intermediate between the values of the torsional mode in CH_2CBr_2 and the torsional mode in CH_2CF_2 as proposed by Edgell and Byrd. Further, it is depolarized and absent in the infrared. Therefore, it is the A_2 torsional mode.

768 cm^{-1}: This vibration is depolarized, exhibits a type A infrared and, and is violently displaced to higher frequencies as one moves along the CH_2CBr_2, CH_2CCl_2, CH_2CF_2 series. It is then assigned to the B_1 CCl stretching mode.

874 cm^{-1}: This line is depolarized and exhibits a type C band, and closely agrees with the value for the CH_2 wag in CH_2CBr_2. It is assigned to the B_2 CH_2 wagging mode.

1088 cm^{-1}: Since all the polarized fundamentals have been assigned, this must be depolarized. There is a type A infrared band at 1094 cm^{-1}. This frequency is then the B_1 CH_2 rocking mode.

These assignments of the Raman fundamentals are tabulated in Table II along with the corresponding

[18] F. F. Cleveland and M. J. Murray, J. Chem. Phys. 7, 396 (1939).

infrared frequencies. In every case the frequencies satisfy all the requirements as to which are active or inactive in the infrared and Raman effect, as well as the band types in the infrared in so far as they have been resolved. This assignment also satisfies the requirements as to which frequencies should be polarized or depolarized in the Raman effect. The observed intensities are what one would expect. The overtone and combination bands can be successfully interpreted by them. It therefore seems very likely that this assignment is correct.

Figure 2 illustrates the general shift to higher frequencies as one moves up the CH_2CBr_2, CH_2CCl_2, CH_2CF_2 series. The inclusion of CD_2CBr_2 and $CHDCBr_2$ graphically illustrates the shift in the CH and the CD frequencies and is further assurance of their correct assignment. The CH_2 wag, rock, and deformation vibrations all display a shift to lower frequencies in CH_2CF_2. This behavior seems to be characteristic of the fluorocarbons.

Interpretation of Overtone and Combination Frequencies

Table III lists the interpretation of the observed overtone and combination frequencies along with the states of polarization and band types. Since anti-stokes lines were observed for only the four fundamentals of lowest frequency 299, 375, 458, and 601 cm^{-1}, only these states were considered as possibly giving rise to difference bands. In some cases there is more than one possible interpretation on the basis of existing data. In the case of the infrared band at 1020 cm^{-1}, one would infer from Thompson and Torkington's overtone interpretation that it had a type *C* band, as they did not directly state its band type. However, the spacing of the submaxima leaves one in serious doubt as to whether it is of type *C* or type *A*. The nearest possible combinations that could give rise to type *C* bands are,

$$375+686=1061 \text{ type } C \text{ band},$$

$$458+601=1059 \text{ type } C \text{ band},$$

while the best fit is $1391-375=1016$ type *A* band. Thompson and Torkington stated that the infrared band at 1318 cm^{-1} "seems to have type *A* contour," however since the 1320 cm^{-1} Raman is polarized, and also since the corresponding infrared band has two submaxima spaced 15 cm^{-1} apart, it is more likely to be of type *B*. A number of interpretations is possible for the 3228 cm^{-1} Raman line, so it was excluded from the table. The remainder of the interpretation of the overtone and combination bands is straightforward. The good agreement of the interpretation with available experimental data is further evidence in favor of the present assignment of fundamental frequencies.

TABLE III. Interpretation of overtone and combination frequencies of vinylidene chloride.

Raman	Infrared	Interpretation	Theoretical band type	Theoretical p or d
	580	299+ 299= 598	*B*	*p*
		874− 299= 575	*C*	*d*
	714	1088− 375= 713	*B*	*p*
	829	299+ 601= 800	*B*	*p*
911	914 *B*	458+ 458= 916	*B*	*p*
	970	375+ 601= 976	*A*	*d*
	1020 *A* or *C*?	1391− 375=1016	*A*	*d*
		375+ 686=1061	*C*	*d*
		458+ 601=1059	*C*	*d*
	1142 *A*	458+ 686=1144	*A*	*d*
1320 *p*	1318 *B*	1616− 299=1317	*B*	*p*
1349 *p*		458+ 874=1332	*B*	*p*
1459		375+1088=1463	*B*	*p*
1589	1580	788+ 788=1576	*B*	*p*
	1742	874+ 874=1748	*B*	*p*
1846		458+1391=1849	*C*	*d*
1867	1876	788+1088=1876	*B*	*p*
	1920	299+1616=1915	*B*	*p*
	1988	375+1616=1991	*A*	*d*
		601+1391=1992	*B*	*p*
	2070	458+1616=2074	*C*	*d*
2162		788+1391=2179	*A*	*d*
		1088+1088=2176	*B*	*p*
2216	2215	601+1616=2217	*B*	*p*
	2430	788+1616=2404	*A*	*d*
		3035− 601=2434	*B*	*p*
2687	2670	1088+1616=2704	*A*	*d*
		3035− 375=2660	*A*	*d*
3178		1616+1616=3232	*B*	*p*

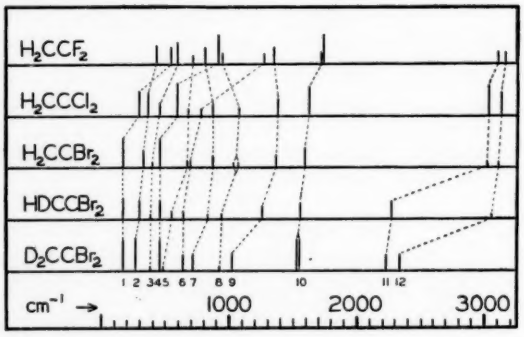

FIG. 2. Fundamental frequencies of the vinylidene halides: (1) A_1-CX_2 deformation; (2) B_1-CX_2 rocking; (3) B_2-CX_2 wagging; (4) A_1-CX stretching; (5) A_2 torsion; (6) B_1-CX stretching; (7) B_2-CH_2 wagging; (8) B_1-CH_2 rocking; (9) A_1-CH_2 deformation; (10) $A_1-(C=C)$ stretching; (11) A_1-CH stretching; (12) B_1-CH stretching.

V. ACKNOWLEDGMENTS

It is with pleasure that the authors acknowledge the following individuals and organizations for valuable aids to this research:

The Graduate College of the State University of Iowa for the research assistantship under which this work was conducted;

The Research Corporation of America for funds for the purchase of the Lane-Wells Raman spectrograph;

Dr. E. C. Britton of the Dow Chemical Company for the sample of vinylidene chloride.

The Infrared Spectra of CF_4 and GeF_4*

P. J. H. Woltz and A. H. Nielsen†
K-25 Laboratories, Carbide and Carbon Chemicals Company, Oak Ridge, Tennessee
(Received September 25, 1951)

The infrared spectrum of CF_4 has been remeasured from 2–19μ and extended to about 33μ, and the infrared spectrum of GeF_4 has been observed from 2–38μ.

Through the use of purer samples and more gas than in previous investigations, a large number of new overtones and combination bands were observed in CF_4, and several bands were eliminated as impurities. Identifications of these bands are given. The infrared-inactive ν_2 was observed, probably because of interaction with ν_4, at 435 cm^{-1} in agreement with the Raman line at 437 cm^{-1}.

In GeF_4 the two active fundamentals ν_3 and ν_4 were observed at 800 cm^{-1} and 260 cm^{-1}, respectively. Eight overtone and combination bands were discovered. From these the values of ν_1 and ν_2 were calculated to be 740 cm^{-1} and 200 cm^{-1}, respectively. Compared with the fundamentals of $GeCl_4$ and $GeBr_4$, these frequencies seem reasonable. The most striking feature of the spectrum of GeF_4 is the scarcity of bands as compared with both CF_4 and SiF_4.

INTRODUCTION

In connection with the recently reported investigation of the infrared and Raman spectra of SiF_4,[1] it became of interest to study other tetrafluorides. This paper deals with the remeasurement and extension of the infrared spectrum of CF_4 and the exploration of the infrared spectrum of GeF_4.

The most recent investigation of the infrared spectrum of CF_4 was that of Bailey, Hale, and Thompson[2] whose measurements extended to about 19μ. They discovered the infrared-active fundamentals ν_3 and ν_4 at 1265 cm^{-1} and 630 cm^{-1} as well as a number of overtones and combination bands. Yost, Lassettre, and Gross[3] observed the Raman spectrum in both gas and liquid, and discovered three lines at 904 cm^{-1}, 635 cm^{-1}, and 437 cm^{-1} which were identified as ν_1, ν_4, and ν_2, respectively.

E. K. Plyler of the National Bureau of Standards, Washington, D. C., and D. G. Weiblen of the Minnesota Mining Company, Minneapolis, Minnesota, independently observed the infrared spectrum of CF_4, but, so far as is known, did not publish their results. Their data were, however, available to the present authors for comparison.

Several discrepancies were noted between the spectra as observed by Bailey, Hale, and Thompson,[2] Plyler, Weiblen, and the present authors. These were ascribed to lack of purity in the samples used in the various earlier experiments.

It was the aim in this investigation to use larger and purer samples of CF_4 in order to ascertain which were the impurity bands, and to discover more overtone and combination bands. It was also deemed of value to extend the measurements throughout the KRS-5 region.

As no previous infrared or Raman work on GeF_4 was discovered in the literature, it was the further aim of this investigation to explore its infrared spectrum. No attempt was made to observe the Raman spectrum when it was learned that GeF_4 sublimes at ordinary pressures, and that rather high pressures would be required to maintain it as a liquid. The fundamental frequencies for $GeCl_4$ and $GeBr_4$ have been given by Heath and Linnett.[4] A comparison of these frequencies with those of GeF_4 will be made in a later section.

EXPERIMENTAL DETAILS

The infrared spectra of CF_4 and GeF_4 were observed with Perkin-Elmer spectrographs models 12C and 21 equipped with NaCl, LiF, CaF_2, KBr, and KRS-5 prisms. Measurements were carried to about 33μ for CF_4 and to about 38μ for GeF_4. The gases were contained in 10 cm fluorothene[5] cells and in a modified Perkin-Elmer meter cell which were fitted with windows of NaCl, KBr, KRS-5 and polyethylene for the appropriate spectral regions. Gas pressures ranged from about 1 mm of mercury in the 10 cm cell to about 2 atmos in the meter cell. The legend accompanying the figures gives the pressures used for specific bands. The envelope of the longest wavelength band of GeF_4 was studied using a fluorothene cell with polyethylene windows 0.001 in. thick. As this cell could not be evacuated the GeF_4 was introduced with dry air at atmospheric pressure. The amount of GeF_4 was estimated to be less than 0.25 inch of mercury by comparing the percent absorption of this arrangement with the absorption in a cell which could be evacuated, and in which actual pressures were measured. Such a cell fitted with KRS-5 windows was, however, not transparent enough at 38.5μ to permit study of the band envelope.

* This document is based on work performed for the AEC by Carbide and Carbon Chemicals Company at Oak Ridge, Tennessee.

† Department of Physics, University of Tennessee, Knoxville, Tennessee.

[1] Jones, Kirby-Smith, Woltz, and Nielsen, J. Chem. Phys. **19**, 242 (1951).

[2] Bailey, Hale, and Thompson, Proc. Roy. Soc. (London) **A167**, 555 (1938).

[3] Yost, Lassettre, and Gross, J. Chem. Phys. **4**, 325 (1936).

[4] D. C. Heath and J. W. Linnett, Trans. Faraday Soc. **44**, 561 (1948).

[5] J. S. Kirby-Smith and E. A. Jones, J. Opt. Soc. Am. **39**, 780 (1949).

TABLE I. Observed frequencies and band assignments for CF_4.

Present work				Bailey, Hale, Thompson[a]		Observed by Plyler, Weiblen
Obs freq cm^{-1}	Calc freq cm^{-1}	Int	Assignment	Obs freq cm^{-1}	Assign	
4710	4753	*vw*	$\nu_1+3\nu_3$			
4062	4102	*vw*	$\nu_1+2\nu_3+\nu_4$			
3850	3849	*vw*	$3\nu_3$			
3794	···	*w*	?			
3450	3451	*vw*	$\nu_1+\nu_3+2\nu_4$			
3184	3198	*w*	$2\nu_3+\nu_4$			
3088	3091	*w*	$2\nu_1+\nu_3$			
3048	···	*vw*	?			
2811	2819	*w*	$\nu_1+\nu_3+\nu_4$			
2556	2566	*s*	$2\nu_3$	2541 (*A*)	$2\nu_3$	*P*, *W*
	2547		$\nu_3+2\nu_4$			
2444	2440	*m*	$2\nu_1+\nu_4$			
2407	···	*vw*	?			
2248	···	*vw*	?			
2187	2187	*s*	$\nu_1+\nu_3$	2179 (*B*)	$\nu_1+\nu_3$	*P*, *W*
2164	2168	*m*	$\nu_1+2\nu_4$			
2147	2153	*m*	$2\nu_2+\nu_3$			
2106	2131	*vw*	$2\nu_3-\nu_2$			
1916	1915	*m*	$\nu_3+\nu_4$	1904 (*C*)	$\nu_3+\nu_4$	*P*, *W*
1893	1896	*m*	$3\nu_4$			
1717	1718	*m*	$\nu_2+\nu_3$	1696 (*D*)	$\nu_2+\nu_3$	*P*, *W*
1538	1536	*s*	$\nu_1+\nu_4$	1535 (*E*)	$\nu_1+\nu_4$	*P*, *W*
···	···	···	Impurity	1516 (*E*)	$2\nu_2+\nu_4$	
1495	1459	*m*	$3\nu_4-\nu_2$			
1337	1341	*m*	$\nu_1+\nu_2$	1360 (*F*)	Impurity	*P*, *W*
1283	···	*vvs*	ν_3	1265 (*G*)	ν_3	*P*, *W*
1275	···	···	?	···	···	···
1261	1264	*m*	$2\nu_4$	1250 (*G*)	$2\nu_4$	*P*, *W*
1252	···	···	?	···	···	···
1235	···	···	?	···	···	···
···	···		Impurity	1156 (*H*)	$\nu_2+\nu_4$	*P*, *W*
···	···		Impurity	1112 (*H*)		*P*
1061	1067	*m*	$\nu_2+\nu_4$			*P*, *W*
(904*R*)	···	···	ν_1			
632 (635*R*)	···	*vs*	ν_4	630 (*L*)	ν_4	
435 (437*R*)	···	*vvw*	ν_2			
373	···	*vw*	$\nu_3-\nu_1$			

[a] See reference 2.

The CF_4 and GeF_4 samples were prepared by Messrs. A. V. Faloon and W. B. Kenna and were of good purity. Further purification by fractionation was effected during the investigation, and various bands of more dubious origin were studied with respect to changes in intensity from one fraction to another. Certain bands were, therefore, fairly easily identified as impurities and were ignored in the identification, while others were less easily designated as impurities. It is believed that the bands listed in Tables I and II belong to CF_4 and GeF_4.

In order to discuss the spectra more clearly the spectral region from 2–38μ has been divided into three intervals, 5000 cm^{-1}–1600 cm^{-1}; 1600 cm^{-1}–700 cm^{-1}; and 700 cm^{-1}–250 cm^{-1}, and the two molecules discussed separately. Figure 1 shows the complete spectrum of CF_4, and Fig. 2 shows that of the GeF_4.

EXPERIMENTAL RESULTS

5000 cm^{-1}–1600 cm^{-1} Region

CF_4

A lithium fluoride prism in a Perkin-Elmer model 12C spectrometer was used for this spectral region. The observed spectrum is shown in the upper and middle sections of Fig. 1. The legend in the figure gives the cell lengths and gas pressures for individual bands. In their earlier work, Bailey, Hale, and Thompson[2] discovered bands which are labeled *A*, *B*, *C*, and *D* in their curves at 2541 cm^{-1}, 2179 cm^{-1}, 1904 cm^{-1} and 1696 cm^{-1}. These bands were also discovered in the present work. Much better dispersion and resolving power was, however, now available and some structure is shown in Fig. 1. Small changes in band centers from the earlier work will be noted. In addition seventeen weaker bands not reported by Bailey, Hale, and Thompson were found. These bands together with their present identifications and the bands observed by the previous authors may be found in Table I. Some of the new bands and additional detail emerged because of better instrumentation, and others because much more gas was used than in the earlier effort. Certain of these new bands were also found by Plyler and Weiblen. They are indicated by a *P* or *W* in Table I.

The essential difference between the earlier work and the present lies in the number of bands observed and in the detail exhibited. Strong *Q* branches may be seen in a number of bands shown in Fig. 1 and some *PR* distances may be measured. The intense band at 2556 cm^{-1} was recorded with a grating spectrometer in connection with some work on F_2O.[6] It is reproduced in Fig. 3 and its envelope is suggestive of a partially resolved *Q* branch converging strongly, and possibly the overlapping of another band.

GeF_4

Only one band located at 1600 cm^{-1} was observed in this region for GeF_4. It is shown in the upper section of Fig. 2 as observed with pressures of 7 inches and 1 atmos, respectively, in the 10 cm cell. No structure is discernible with a CaF_2 prism though the envelope is suggestive of a strong *Q* branch. Table II gives the frequencies and identifications of the bands in GeF_4. The paucity of bands in this region as compared with CF_4 is rather startling.

TABLE II. Observed frequencies and band assignments for GeF_4.

Obs freq cm^{-1}	Calc freq cm^{-1}	Intensity	Assignment
1600	1600	*m*	$2\nu_3$
1535	1540	*m*	$\nu_1+\nu_3$
1000	1020 or 1000	*m*	$\nu_2+\nu_3$ or $\nu_1+\nu_4$
800	···	*vvs*	ν_3
···	740[a]		ν_1
737		*w*	$\nu_2+2\nu_4$
549	540	*vw*	$\nu_3-\nu_4$
518	520	*w*	$2\nu_4$
463	480 or 460	*vw*	$\nu_4-\nu_2$ or $\nu_1-\nu_4$
260		*vs*	ν_4
	200		ν_2

[a] By utilizing the ratio $k_1(XY_4)/k(XY)=1.46$ obtained from the simple valence force field bond-stretching constant of SiF_4 and the force constant of diatomic SiF, and assuming the same ratio to hold for GeF_4 and GeF Andrews and Barrow (Proc. Phys. Soc. (London) **63A**, 185 (1950)) have computed the bond-stretching constant k_1 for GeF_4 and the frequency $\nu_1=715$ cm^{-1}. This value is in good agreement with the value computed from the infrared data.

[6] Jones, Kirby-Smith, Woltz, and Nielsen, J. Chem. Phys. 19, 337 (1951).

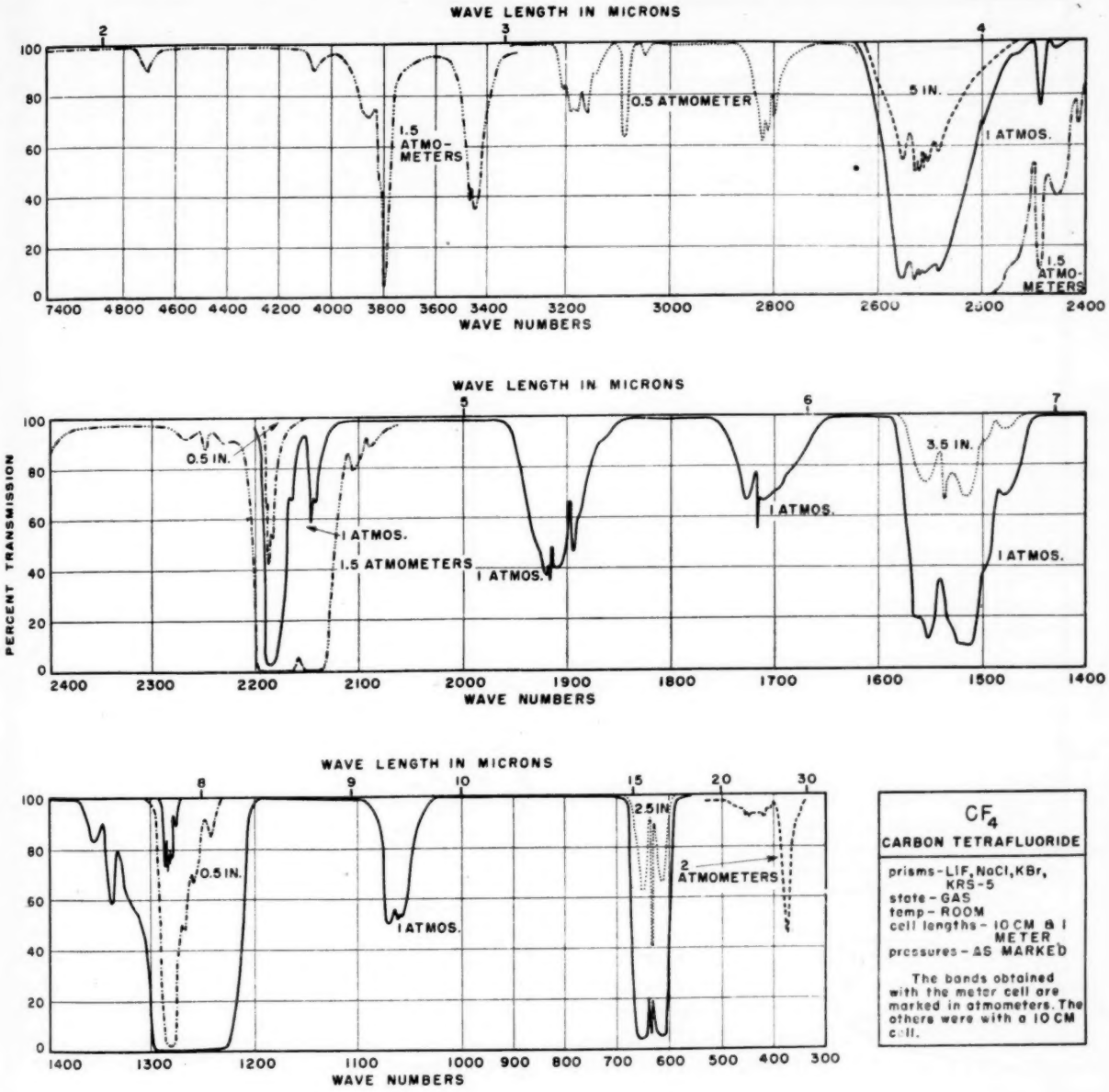

FIG. 1. The infrared prism spectrum of CF_4 from 2–33μ.

1600 cm^{-1}–700 cm^{-1} Region

CF_4

The spectral records of this region were made with the Perkin-Elmer model 21 spectrometer equipped with a NaCl prism. The absorption bands observed are shown in Fig. 1, middle and lower section, and the frequencies are collected in Table I.

Bailey, Hale, and Thompson discovered absorption regions at 1535 cm^{-1}, 1360 cm^{-1}, 1265 cm^{-1}, 1112 cm^{-1}, and 906 cm^{-1} which in their curves are labeled *E*, *F*, *G*, *H*, and *K*, respectively. They suggest that band *F* is very likely an impurity and that in region *H* there is probably a weak band at 1152 cm^{-1} as well as at 1112 cm^{-1}. They suggest further that band *K* may be an impurity. Out of their observed bands they assign frequency identifications only to the bands at 1535 cm^{-1}, 1516 cm^{-1}, 1265 cm^{-1}, 1250 cm^{-1}, and 1112 cm^{-1}.

Plyler's and Weiblen's curves show absorptions corresponding to bands *E*, *F*, *G*, and *H*. In the region *H* Plyler shows, in fact, bands at 1156 cm^{-1} and 1111 cm^{-1}, while Weiblen shows only the one at 1156 cm^{-1}. Neither of these observers found band *K* at 906 cm^{-1}.

In the present investigation the regions *E*, *F*, and *G* were observed, but regions *H* and *K* could not be detected with the purest samples even with considerably more gas than was used in previous experiments. They were, however, observed in the earliest and least pure samples for which records were made in this laboratory. It is, therefore, quite certain that bands at 1156 cm^{-1},

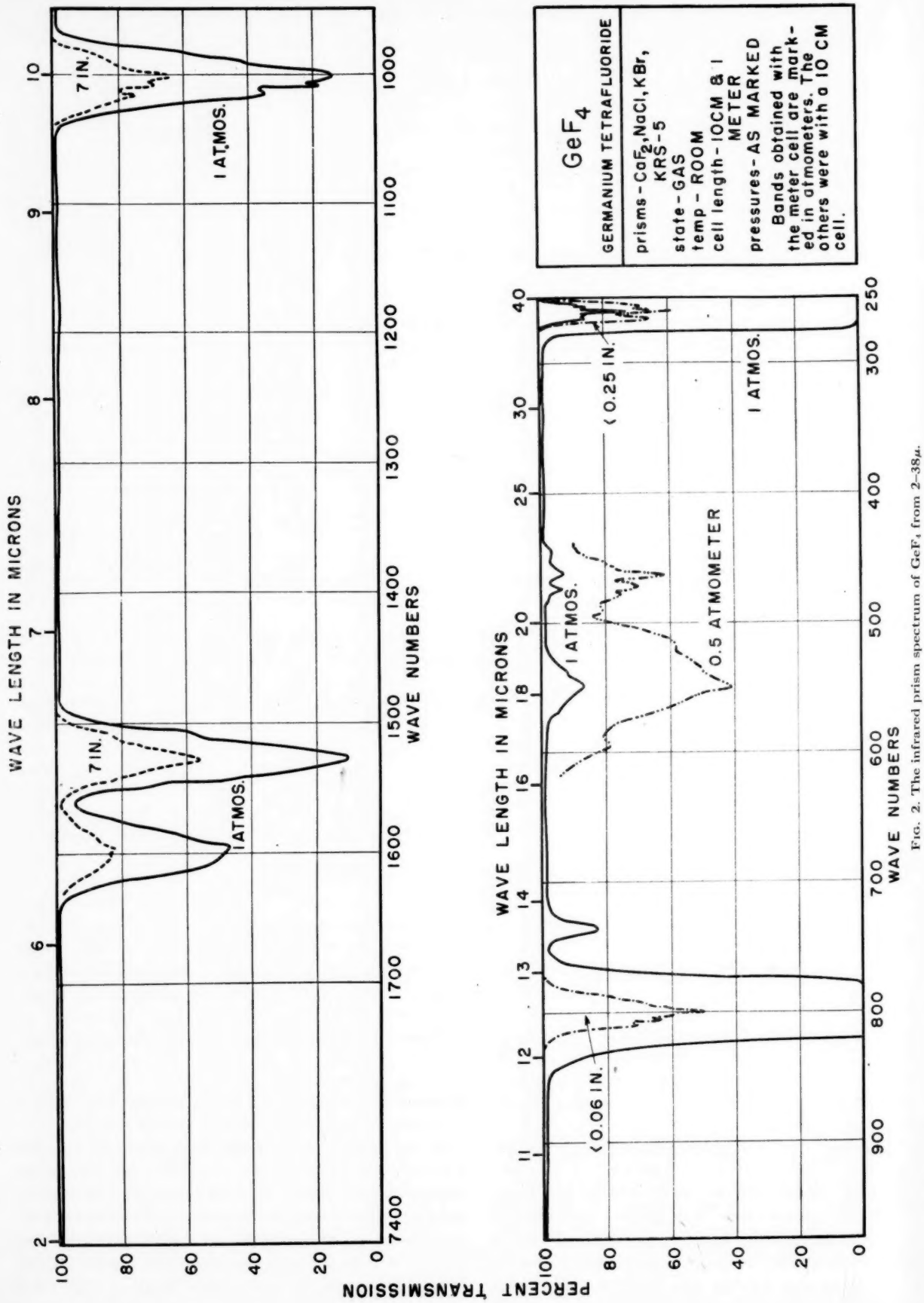

FIG. 2. The infrared prism spectrum of GeF_4 from 2–38μ.

1112 cm^{-1}, and 906 cm^{-1} are impurities, probably CHF_3 or C_2F_6 which are likely contaminants and have bands in this region. On the other hand, band *F* at 1360 cm^{-1} called an impurity by Bailey, Hale, and Thompson was seen also by Plyler and Weiblen and the present authors. It was not possible to show that this band was an impurity and it is, therefore, held to be real.

Altogether six bands belonging to the spectrum of CF_4 were observed in this region. Some structure is evident in all bands and *Q* branches are easily seen in several.

GeF_4

Two prisms were used to explore this region for GeF_4: CaF_2 from 1700 cm^{-1}–1450 cm^{-1} and NaCl from 1450 cm^{-1}–700 cm^{-1}. Three strong bands and one weak one were observed and are shown in Fig. 2.

The band at 1535 cm^{-1} does not exhibit much structure, though a strong *Q* branch and unresolved *P* and *R* branches are indicated. The other strong bands do show some structure suggestive of *PQR* envelopes. It is possible that two bands overlap at 1000 cm^{-1}. The very intense band at 800 cm^{-1} must certainly be a fundamental vibration. The weak band at 737 cm^{-1} shows no structure. The frequencies and assignments are given in Table II.

700 cm^{-1}–250 cm^{-1} Region

CF_4

With the exception of the band labeled *L* at 630 cm^{-1} by Bailey, Hale, and Thompson, this region had not previously been explored. With KRS-5 optics it is now fairly easy to observe out to nearly 40μ. The present remeasurement of band *L* was carried out with a KBr prism. As may be seen in Fig. 1, at low pressures it becomes a beautiful example of a band with *PQR* branches. The *PR* spacing is 38 cm^{-1} in agreement with that observed by Bailey, Hale, and Thompson in a record not so well resolved.

Two additional bands, shown in Fig. 1, were observed at 435 cm^{-1} and 373 cm^{-1}. They were discovered with two atmospheres pressure in the meter cell. The band at 373 cm^{-1} was found to be temperature sensitive and when the cell was cooled to the temperature of solid carbon dioxide the band was considerably weaker. This is suggestive of a difference band. Frequencies and identifications are given in Table I.

GeF_4

Only the KRS-5 prism was used to explore this region for GeF_4. Cells with KRS-5 and polyethylene windows were used as discussed in an earlier section. Bands were discovered at 549 cm^{-1}, 518 cm^{-1}, 463 cm^{-1}, and at 260 cm^{-1} as shown in Fig. 2. Of these bands only the one at 260 cm^{-1}, which is very likely a fundamental, clearly shows *PQR* structure with a fairly sharp *Q* branch. Frequencies and assignments are listed in Table II.

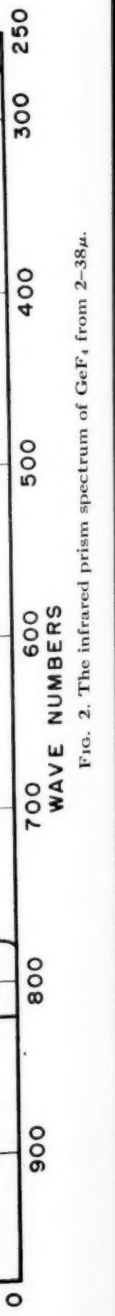

FIG. 2. The infrared prism spectrum of GeF_4 from 2–38μ.

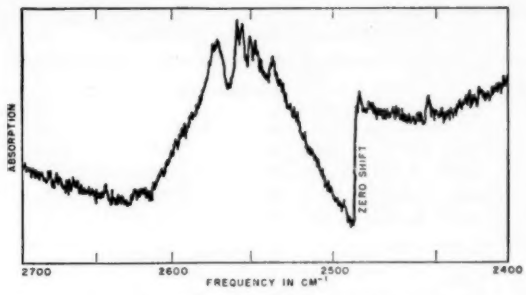

FIG. 3. Grating record of $2\nu_3$ at 2556 cm^{-1}.

DISCUSSION

General

The spectra of CF_4 and GeF_4 resemble each other and that of SiF_4 in that they each have two very intense infrared bands which must be ascribed to the fundamental modes ν_3 and ν_4 with ν_4 having the lower value. For all three molecules ν_4 is the only one of the fundamentals in which the *PQR* band structure is easily discernible in the prism records. The observed *PR* spacings in ν_4 for CF_4, SiF_4, and GeF_4, respectively, are 38 cm^{-1}, 24 cm^{-1}, and 11 cm^{-1}. In general the amounts of gas used to observe the fundamentals at about the same intensity were comparable for the three molecules. Yet, the most characteristic fact about the spectra is that 29 bands were observed for CF_4, 18 for SiF_4, and only 10 for GeF_4.

Only in CF_4 was ν_2, the doubly-degenerate infrared-inactive frequency observed. It was searched for in SiF_4 but was not found. The region in which it would occur in GeF_4 was beyond the instrumental range.

CF_4

The absorption band at 2556 cm^{-1}, shown in Fig. 3 as a grating record, has a fairly complicated appearance. A number of peaks repeat from record to record and appear to be real. Several more peaks occur on the low-frequency side when the cell pressures are increased. The appearance of the band, shown in Fig. 3, made with 7 cm pressure in the 10 cm cell is that of a band with a *Q* branch which is sharp on the high frequency side and shades off into the low frequency side of the band. If the peaks are real it appears that the *Q* branch is splitting. It is difficult to see how this could be observed in this molecule as the lines must be very close together indeed. The lines in the *R* branch are strongly converged as this branch is very narrow. The complicated envelope may, of course, also be caused by an overlapping band.

Careful examination of the interval from 1200 cm^{-1}–1300 cm^{-1} with a CaF_2 prism yielded an absorption region with a number of maxima located at 1235 cm^{-1}, 1252 cm^{-1}, 1261 cm^{-1}, 1275 cm^{-1}, 1280 cm^{-1}, 1283 cm^{-1}, and 1286 cm^{-1}. The most intense absorption is centered around what appears to be a narrow *Q* branch at 1283 cm^{-1}. This *Q* branch has been identified as ν_3. If the

TABLE III. Comparison of vibration frequencies (cm^{-1}) for CF_4, SiF_4, GeF_4, $GeCl_4$, and $GeBr_4$.

Assignment	CF_4	SiF_4[a]	GeF_4	$GeCl_4$[b]	$GeBr_4$[b]
		Fundamentals			
ν_1	904 (*R*)	800 (*R*)	740 (calc)	398	283
ν_2	435 (*R*, *IR*)	268 (*R*)	200 (calc)	132	78
ν_3	1283 (*IR*)	1031 (*R*, *IR*)	800 (*IR*)	450	329
ν_4	632 (*R*, *IR*)	391 (*R*, *IR*)	260 (*IR*)	172	111
		Overtones and combination bands			
$\nu_1+2\nu_3$	3450	2854			
$2\nu_3+\nu_4$	3184	2445			
$2\nu_3$	2556	2057	1600		
$\nu_1+\nu_3$	2187	1827	1535		
$\nu_2+\nu_3$	1717	1294	1000		
$\nu_1+\nu_4$	1538	1191	1000		
$\nu_2+2\nu_4$	...	1065	737		
$\nu_3-\nu_4$	...	...	549		
$2\nu_4$	1261	780	518		
$\nu_1-\nu_4$	...	...	463		
$\nu_2+\nu_4$	1061	...	...		

[a] See reference 1.
[b] See reference 2.

adjacent maxima at 1280 cm^{-1} and 1286 cm^{-1} are taken as the *P* and *R* branch maxima, the *PR* spacing is only 6 cm^{-1} as compared with 11 cm^{-1} for ν_3 in SiF_4. The maximum at 1261 cm^{-1} has been identified as the *Q* branch of $2\nu_4$. The maxima at 1235 cm^{-1}, 1252 cm^{-1}, and 1275 cm^{-1} are presently unexplained, but repeat from record to record. It seems clear that this region requires further examination with a grating in order to learn more about the structure.

The region from 1450 cm^{-1}–1600 cm^{-1} was carefully examined with a LiF prism. Maxima were observed at 1449 cm^{-1}, 1478 cm^{-1}, 1495 cm^{-1}, 1517 cm^{-1}, 1538 cm^{-1}, and 1555 cm^{-1}. It is believed these maxima comprise two overlapping bands $\nu_1+\nu_4$ and $3\nu_4-\nu_2$, the former being by far the more intense. The curve shows quite clearly a band with a *Q* branch at 1538 cm^{-1} with a *PR* spacing of about 38 cm^{-1}.

Seven weak bands at 1235 cm^{-1}, 1252 cm^{-1}, 1275 cm^{-1}, 2248 cm^{-1}, 2407 cm^{-1}, 3048 cm^{-1} and 3794 cm^{-1}, remain unaccounted for in this interpretation.

The *PR* spacings in CF_4 could not be very accurately determined, but it appears that ν_4 and combinations involving ν_4 have spacings of from 38–40 cm^{-1} while ν_3 and combinations involving ν_3 are much smaller. This is also the case in SiF_4.

The frequency ν_2, generally inactive in the infrared spectra of spherical top molecules, may, if fairly close to ν_4, interact with ν_4 and occur with low intensity. Examples for which ν_2 has been observed are CH_4, SiH_4, etc. It was considered worthwhile to search for it in CF_4 although the two frequencies are not as close as in the other cases mentioned. A meter cell with two atmospheres pressure proved to be sufficient to detect a band with about 10 percent absorption at 435 cm^{-1}. This is in excellent agreement with the Raman line at 437 cm^{-1} and the band has been assigned as ν_2. The band at 373 cm^{-1} was also observed with this cell and pressure. It is probably $\nu_3-\nu_1$ as the agreement with the calculated value of 379 cm^{-1} is very good.

Grating measurements will certainly be required to make better *PR* determinations and to investigate the overlap of bands in the regions discussed above.

GeF_4

As has been remarked earlier, the scarcity of bands in this spectrum is its most striking feature. The fundamentals appear with about the same intensities as in CF_4 and SiF_4, but the overtones and combinations are evidently very weak. Of the three, CF_4 is the richest and GeF_4 the poorest in number of bands. Only in the case of ν_4 was a satisfactory band envelope and *PR* spacing obtained. The *PR* spacing of ν_4 appears to be about 12.5 cm^{-1}. If any information about band envelopes is to be obtained for this molecule it must be sought through grating measurements.

No Raman measurements were available to give the infrared-inactive frequencies, and an attempt was made to arrive at these frequencies from the nine observed infrared bands. Two of them, the 800 and 260 cm^{-1}, were easily identified as ν_3 and ν_4, respectively. The remaining seven were, therefore, overtones and combinations. The band at 1600 cm^{-1} was clearly $2\nu_3$ and the one at 518 cm^{-1} was very likely $2\nu_4$.

By subtracting ν_3 and ν_4 from the remaining five bands, the numbers 740 cm^{-1} and 200 cm^{-1} were readily discovered to repeat. The observed bands must be low overtones or combinations because of the general scarcity of absorption bands. This led immediately to the band at 740 cm^{-1} being ν_1 and the band at 200 cm^{-1} being ν_2. All the observed bands can of course be explained in terms of these chosen fundamentals.

Comparison

Table III combines the principal bands of the spectra of CF_4, SiF_4, and GeF_4 in order that the frequencies and assignments may more easily be compared. The fundamentals of $GeCl_4$ and $GeBr_4$ are also included in this table for comparison, and to show that the calculated frequencies in GeF_4 are reasonable.

ACKNOWLEDGMENT

The authors wish to thank Messrs. Faloon and Kenna for preparing the CF_4 and GeF_4 and assisting in sample purifications while measurements were in progress.

The Potential Constants of Ethane

G. E. HANSEN*† AND D. M. DENNISON
Randall Laboratory of Physics, University of Michigan, Ann Arbor, Michigan
(Received August 3, 1951)

The infrared and Raman data of light and heavy ethane (C_2H_6 and C_2D_6) have been reexamined for the purpose of determining as accurately as possible the potential constants of the ethane molecule. In order to fill in some of the gaps in the spectroscopic data, additional high resolution measurements have been made on the infrared spectrum of heavy ethane which have given more precise values for the active fundamental frequencies and zeta-values. Resolution of the fine structure associated with the parallel band ν_5* has given the value of the large moment of inertia of C_2D_6, thus completing the information required for the spectroscopic determination of the dimensions of ethane. The data yield, C−C distance = 1.543A, C−H distance = 1.102A, H−C−C angle = 109°37′, and H−C−H angle = 109°19′. The twenty-two distinct potential constants compatible with the D_{3d} symmetry of ethane have been determined through their relationships to the normal frequencies and zeta-values of C_2H_6 and C_2D_6. The normal frequencies have been obtained by addition of anharmonic corrections to the spectroscopically observed fundamental frequencies. These corrections were estimated by means of the known anharmonic corrections for methane and the conditions imposed by the Teller product rule. The fundamental frequencies and zeta-values have been taken directly from the observed band centers and rotational spacings wherever possible. In the cases of resonance, the influence of the couplings were either calculated or estimated and the corresponding unperturbed values for the frequencies and zeta-values selected. The potential function is determined first in terms of a set of simple symmetry coordinates, and then reexpressed in terms of valence coordinates to permit comparison of the valence force constants of ethane and methane.

I. INTRODUCTION

SHORTLY after the initial measurements of the ethane spectrum,[1] analyses of the observed fundamental frequencies led to the construction of simplified potential functions[2] which not only indicated the magnitudes of the principal restoring forces but also aided in the later assignments of additional fundamental and overtone bands. By 1938, Crawford, Avery, and Linnett[3] were able to give a complete summary of the twelve distinct fundamental frequencies although, as they emphasized, the spectroscopic data were insufficient to determine whether the equilibrium configuration of the molecule is the "staggered" model D_{3d} (center of symmetry) or the "eclipsed" model D_{3h} (reflection plane perpendicular to the symmetry axis).

In 1939 Stitt[4] measured the infrared and Raman spectra of C_2D_6, and determined a set of potential constants for ethane, correlating the data for these two isotopic molecules and illustrating the importance of the forces coupling different bond distortions. Recently, the high resolution measurements by Smith[5] considerably improved and extended the infrared data for ethane. The observed combination bands gave direct evidence for the D_{3d} equilibrium configuration while the rotational spacings gave the moments of inertia for this molecule as well as the zeta-values associated with the degenerate vibrations.

The purpose of the present investigation is the re-evaluation of the present accumulation of spectroscopic data, the filling in of some of the gaps by additional measurements of the infrared spectrum of C_2D_6, and the determination of a set of potential constants for ethane which best describes this information.

At the present time, complete sets of potential constants have been determined for only a few of the simpler polyatomic molecules such as CO_2, H_2O, NH_3, and CH_4.[6] There are two inherent difficulties involved in the calculation, the first of which is that the potential constants are related to the normal vibrational frequencies of the molecule. The observed spectrum, however, yields the fundamental frequencies and these differ from the normal frequencies by amounts of the order of a few percent. These differences are caused principally by the higher order terms, cubic and quartic, in the potential energy and can only be evaluated when all of the overtones involving pairs of fundamental as well as harmonics of fundamental frequencies have been observed. In the case of ethane with its 12 fundamentals, this would require the identification and measurement of 114 overtones and harmonics. This large amount of information is not available, and consequently other methods have been employed which appear to be reliable at least as first approximations. These methods consist in the use of the product rule and the frequencies of such harmonics as are known, together with a plausible assumption regarding the ratio of the anharmonicity factor in isotopic molecules as will be described in Section III.

The second difficulty arises from the fact that while the normal frequencies are functions of the potential constants, there are in general more constants than frequencies. Thus, if a molecule possess n normal vibrations belonging to a particular symmetry class, there will be $\frac{1}{2}n(n+1)$ constants in the general potential

* Based on a dissertation submitted to the Graduate School of the University of Michigan in partial fulfilment of the requirements for the degree of Doctor of Philosophy.

† Present address: Los Alamos Scientific Laboratory, Los Alamos, New Mexico.

[1] A. Levin and C. F. Meyer, J. Opt. Soc. Am. **16**, 137 (1928); P. Daure, Ann. phys. **12**, 375 (1929).

[2] G. Sutherland and D. M. Dennison, Proc. Roy. Soc. (London) A148, 250 (1935); J. B. Howard, J. Chem. Phys. **5**, 442 (1937).

[3] Crawford, Avery, and Linnett, J. Chem. Phys. **6**, 682 (1938).

[4] F. Stitt, J. Chem. Phys. **7**, 297 (1939).

[5] L. G. Smith, J. Chem. Phys. **17**, 139 (1949).

[6] D. M. Dennison, Revs. Modern Phys. **12**, 175 (1940).

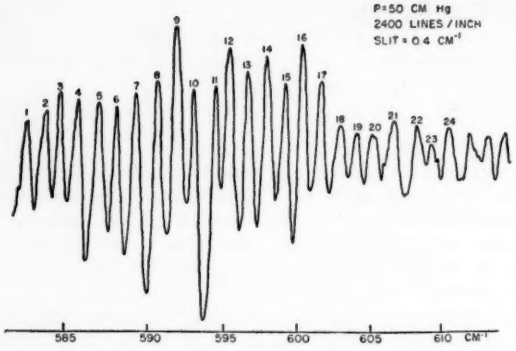

FIG. 1. Absorption by the fundamental $\nu_9^*=593.7$ cm^{-1}. Lines 9, 12, and 16 are enhanced by the presence of water vapor in the absorption path. The rotational spacing $\Delta\nu_9^*=1.197$ cm^{-1} corresponds to the zeta-value $\zeta_9^*=0.182$.

function. There are a number of ways out of this difficulty of which the one which has been most widely used has been to approximate the form of the potential function, for example, by assuming valence type forces, and thus reduce the number of unknown constants. A much more satisfactory method, whenever the experimental data are available, is to employ (1) the normal frequencies of isotopic molecules and (2) the zeta-values. These latter measure the internal angular momenta associated with the degenerate vibrations and are also functions of the potential constants. The data on ethane are at present sufficient to make this method possible in all but one of the symmetry classes. The situation is as follows:

A. Perpendicular Active Vibrations, E_u

There are three frequencies ω_7, ω_8, and ω_9 belonging to this class, and hence six potential constants. The normal frequencies for both light and heavy ethane have been determined as well as the three zetas for light ethane and two of the heavy ethane zetas. The sum of the zetas for any symmetry class is fixed, however, and the product rule imposes a relation between the light and heavy normal frequencies. There are thus nine independent data with which to determine the six constants. A least squares solution gives a very satisfactory fit.

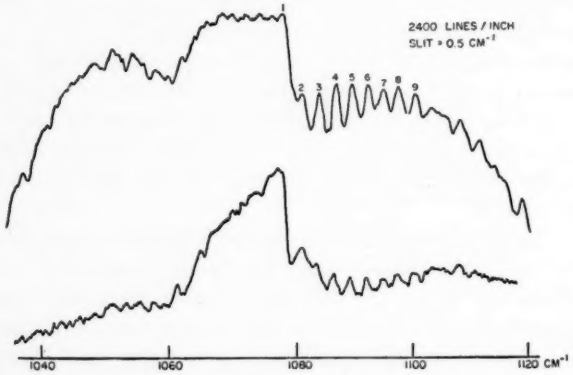

FIG. 2. Absorption by the fundamentals $\nu_8^*\cong1077$ cm^{-1} and $\nu_8^*\cong1082$ cm^{-1}. The rotational spacing $\Delta\nu_8^*=2.76$ cm^{-1} corresponds to the zeta-value $\zeta_8^*=-0.423$.

TABLE I. Wave numbers of the lines shown in Fig. 1.

Line no.	$K''\rightarrow K'$		cm^{-1}
1	10	9	582.3
2	9	8	583.6
3	8	7	584.7
4	7	6	585.9
5	6	5	587.1
6	5	4	588.1
7	4	3	589.3
8	3	2	590.6
9	2	1	591.8
10	1	0	593.0
11	0	1	594.3
12	1	2	595.3
13	2	3	596.5
14	3	4	597.7
15	4	5	598.9
16	5	6	600.2
17	6	7	601.3
18	7	8	602.5
19	8	9	603.8
20	9	10	605.1
21	10	11	606.4
22	11	12	607.8
23	12	13	609.1
24	13	14	610.4

B. Perpendicular Inactive Vibrations, E_g

The three normal frequencies ω_{10}, ω_{11}, and ω_{12} are again known for both the light and heavy ethane and two of the light zetas have been measured. These constitute seven independent data and the six potential constants of this symmetry class may be found.

C. Parallel Inactive Vibrations, A_{1g}

The three normal frequencies ω_1, ω_2, and ω_3 have been found for both the isotopic molecules but, because of the product rule, these constitute only five data. Since the vibrations are not degenerate, there exist no zetas. The six potential constants cannot be calculated without employing a further assumption, and the one that has been made is that the cross product term between the C—C and the C—H stretchings has been taken to be zero.

D. Parallel Active Vibrations, A_{2u}

Two frequencies ω_5 and ω_6 belong to this class and have been measured in both light and heavy ethane.

TABLE II. Wave numbers of the lines shown in Fig. 2.

Line no.	$J''\rightarrow J'$		cm^{-1}
1	0	0	1077.1
	$K''\rightarrow K'$		
2	1	0	1080.4
3	0	1	1083.2
4	1	2	1086.2
5	2	3	1089.0
6	3	4	1091.6
7	4	5	1094.2
8	5	8	1096.9
9	6	7	1099.7

They represent three independent data and hence are just sufficient to find the three potential constants.

E. Torsional Vibration, A_{1u}

There is only one frequency in this class, namely ω_4, and it therefore determines the single potential constant.

In the final section of the paper the potential constants of ethane are expressed in terms of the stretching and bending of the valence bonds and bond angles of the molecule. As might have been expected from previous experience, it is found that the principal contributions come from the stretching of the valence bonds and from the bending of the bond angles, and that the interaction terms between adjacent bonds are, with one or two exceptions, quite small while the interactions between remote bonds are virtually zero.

II. INFRARED MEASUREMENTS ON C_2D_6

The purpose of remeasuring the infrared spectrum of heavy ethane was to obtain (1) more accurate positions

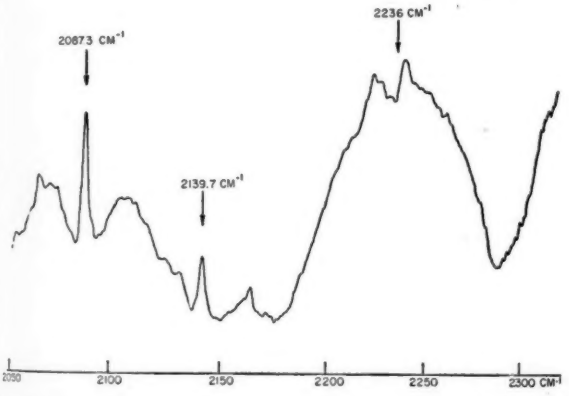

FIG. 3. General record of absorption in the 4.3–5.0 micron region indicating the positions of the parallel doublet bands $\nu_{5a}^* = 2087.3$ cm^{-1} and $\nu_{5b}^* = 2139.7$ cm^{-1} and the perpendicular band $\nu_7^* \simeq 2236$ cm^{-1}.

of the band centers associated with the fundamental vibrations, (2) the zeta-values associated with the rotational spacings of the degenerate vibrations, and (3) the large moment of inertia, this being the last parameter required for the spectroscopic determination of the dimensions of ethane.

The measurements were made with a prism-grating spectrometer and automatic recording attachments such as described by W. E. Anderson.[7] The C_2D_6 was prepared by a method similar to that described by Stitt[5] (generation and catalytic combination of D_2 and C_2D_2 utilizing heavy water as the source of deuterium).

Spectrograms of the absorption by the active fundamentals are given in Figs. 1–4, while Tables I–III give the wave number values and assignments of the principal absorption peaks. The notation for any vibration of heavy ethane is the starred symbol for the analogous

[7] W. E. Anderson, thesis (University of Michigan, 1948).

TABLE III. Wave numbers of the lines shown in Fig. 4.

Line no.	$J'' \rightarrow J'$		cm^{-1}
1	23	22	2066.88
2	22	21	2067.52
3	21	20	2068.51
4	20	19	2069.40
5	19	18	2070.05
6	18	17	2071.15
7	17	16	2072.03
8	16	15	2072.83
9	15	14	2073.67
10	14	13	2074.65
11	13	12	2075.66
12	12	11	2076.48
13	11	10	2077.34
14	10	9	2078.28
15	9	8	2079.03
16	8	7	2080.21
17	7	6	2080.88
18	6	5	2082.10
19	5	4	2082.93
20	0	0	2087.3
21	7	8	2094.59
22	8	9	2095.73
23	9	10	2096.62
24	10	11	2097.51
25	11	12	2098.53
26	12	13	2099.58
27	13	14	2100.58
28	14	15	2101.47
29	15	16	2102.51
30	16	17	2103.40
31	17	18	2104.20
32	18	19	2105.04
33	19	20	2105.97
34	20	21	2107.20
35	21	22	2108.07
36	22	23	2109.02
37	23	24	2109.70
38	24	25	2111.07

vibration of ethane. Similarly for the other quantities such as zeta-values and moments of inertia.

The two parallel bands shown in Fig. 3 arise from the fundamental vibration ν_5^* and a parallel combination band, presumably ν_{8+11}^*. Because of the close proximity of the corresponding frequencies, any coupling between these vibrations is of the resonance type and in this case neither of the observed bands may properly be called the fundamental. Evidence of such coupling is furnished by the appreciable intensity of both of these

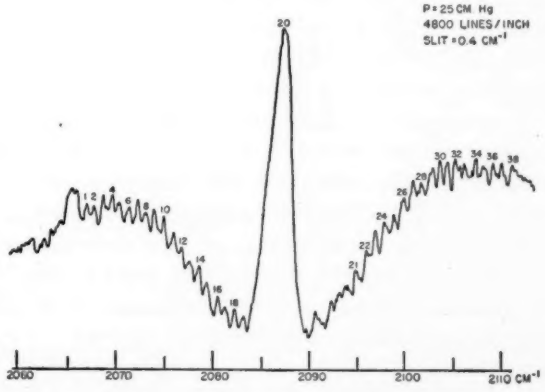

FIG. 4. Fine structure of the fundamental ν_{5a}^*.

bands (and also of the analogous bands of ethane), and consequently they are labelled ν_{5a}^* and ν_{5b}^*.

Figure 4 gives one of the four spectrograms of ν_{5a}^* recorded under conditions of maximum resolution. For each record the rotational constant B_0^* for the vibrational ground state was obtained, using the "method of combination differences" suggested by Herzberg.[8] The resulting mean value, $B_0^*=0.4610\pm0.0010$ cm^{-1}, corresponds to a large moment of inertia, $I_x^*=60.71\times10^{-40}$ g cm^2.

Smith's[6] high resolution measurements of the bands of light ethane have yielded the following values for the large and small moments of inertia of that molecule, $I_x=42.234\times10^{-40}$ and $I_z=10.81\times10^{-40}$ g cm^2. Since the molecule contains only three independent structural parameters, the above data are sufficient for their determination. One obtains for the distances and angles, C−C$=1.543\times10^{-8}$, C−H$=1.102\times10^{-8}$ cm, H−C−C angle$=109°37'$, H−C−H angle$=109°19'$. It will be noted that, whereas the angles differ only slightly from the tetrahedral angle of $109°28'$, the C−H distance is appreciably larger than the C−H distance in methane of 1.093×10^{-8} cm. The moments of inertia of both ethane and methane from which the above figures were derived are the moments in the ground state of vibration and not the equilibrium moments, and hence, strictly speaking, they determine effective but not equilibrium dimensions.

In Fig. 2, eight Q lines of the perpendicular band ν_8^* are visible between 1080 and 1100 cm^{-1}. The absorption maximum rising sharply below 1080 cm^{-1} is interpreted as the strongly broadened Q line of the parallel band ν_6^*. Although quite uncertain because of the anomalous absorption pattern, the band center of the perpendicular band is estimated to lie between the lines 2 and 3 and the assignments of the rotational quantum numbers are given on this basis. An anomalous absorption pattern is indeed expected because of the strong coupling between the vibrations ν_6^* and ν_8^* through the rotation of the molecule. The zeta-value characterizing this coupling has been estimated, on the basis of the final potential constants, to be 0.54, which is sufficiently large to produce the observed amount of distortion when the separation of band centers is small. Although this known interaction supports the qualitative correctness of the above choice of band centers, it is inconsistent with the latter in a quantitative sense (in that, in the absence of other couplings, an absorption head should appear at the unperturbed position of the ⊥ band center. It may be noted that the interaction zeta referred to here gives a measure of the internal angular momentum associated with the superposition of two distinct normal vibrations and hence results in first-order energy contributions only when, as in the above case, such vibrations are accidentally degenerate.)

[8] G. Herzberg, *Infrared and Raman Spectra of Polyatomic Molecules* (D. Van Nostrand Company, Inc., New York, 1945).

The double peak in the envelope of the ν_7^* band is presumably occasioned by resonance interaction with the combination bands ν_{2+6}^* and ν_{2+8}^*. The exact interpretation is obscure and the present measurements do not warrant a change in the value $\nu_7^*=2236$ cm^{-1} reported by Stitt.

III. INITIAL REDUCTION OF THE DATA

The potential energy function for a molecule is generally represented as a power series in the relative atomic displacements, the coefficients associated with the quadratic terms constituting the potential constants which are the subject of this paper.

The normal frequencies, which correspond to atomic vibrations of infinitesimal amplitude, are functions of these potential constants. The fundamental frequencies, however, which are the quantities observed experimentally and which may differ by a few percent from the normal frequencies, depend principally upon the quadratic coefficients, but also to a lesser extent upon the so-called anharmonic terms which are cubic and quartic in the atomic displacements. When all of the simple combination and harmonic bands have been measured, the anharmonic contributions can be found and, through subtraction, the normal frequencies ascertained. It may be remarked that although the normal and fundamental frequencies may be in agreement within a few percent, quadratic potential constants determined by using fundamental rather than normal frequencies may often be in error by several times this amount. In the following discussion, fundamental and normal frequencies will be denoted by the symbols ν_i and ω_i, respectively.

For ethane and heavy ethane, measurements of the very large number of simple combination bands are almost necessarily incomplete and one must rely on estimates of the anharmonicity corrections. A general procedure for the estimation of such corrections has been given by Dennison[6] based on the Teller product rule and approximate relations between anharmonicity corrections of isotopic molecules. Thus, defining the anharmonicity factor, x, through the equation $\nu=(1-x)\omega$, the perturbation treatment of the higher order potential terms of isotopic *diatomic* molecules gives the correction ratio $x^*/x=\omega^*/\omega\cong\nu^*/\nu$. This same ratio is assumed to hold approximately for the similar vibrations of isotopic polyatomic molecules. Designating by μ_{ij} the mass coefficients appearing in the kinetic energy expression for one of the symmetry classes of vibrations, the Teller product rule gives a relation between the ratio of the determinants $|\mu_{ij}|$ and $|\mu_{ij}^*|$ and the products of the normal frequencies, namely,

$$|\mu_{ij}^*|^{\frac{1}{2}}/|\mu_{ij}|^{\frac{1}{2}}=\pi_i(\omega_i/\omega_i^*)\cong\pi_i(\nu_i/\nu_i^*-x_i)/(1-x_i).$$

As there are five symmetry classes for ethane, the product rule gives five additional relations among the anharmonicity factors. Many of the vibrations of ethane, such as the C−H stretching and H−C−H

angle bending vibrations are similar to those of methane, for which the anharmonicity factors are reasonably well known. For such vibrations, the anharmonicity factors of ethane may be chosen to agree with the known factors of methane subject, of course, to the equations given by the product rule. Thus, starting with the fundamental frequencies of ethane and heavy ethane, the anharmonicity corrections may be estimated and the set of normal frequencies obtained by means of the relations

$$x_i^*/x_i = \nu_i^*/\nu_i \tag{1}$$

$$|\mu_{ij}|^{\frac{1}{2}}/|\mu_{ij}^*|^{\frac{1}{2}} = \pi_i(\nu_i/\nu_i^* - x_i)/(1-x_i) \tag{2}$$

$$x_i(\text{ethane}) \sim x_i(\text{methane}) \text{ subject to Eq. (2).} \tag{3}$$

It should be emphasized that these relations are only approximate and there has been no hesitation to make readjustments of the values from the ethane-methane correlation so as to conform to the empirical rules that anharmonicity factors are generally positive and are larger for the higher frequency vibrations.

Although the zeta-values are also slightly affected by the anharmonic potential terms, neither sufficient experimental data nor empirical procedure is available to make corrections. In the absence of resonance, these corrections are expected to be of the order $\Delta\zeta \sim (V_1/V_0)^2 \sim V_2/V_0 \sim 0.01$, where V_0, V_1 and V_2 are typical quadratic, cubic, and quartic potential terms. The squared correction arises from and is proportional to the difference in zeta-values of the coupled vibrations, while the V_2 contribution arises from the interference between the anharmonic terms and the nondiagonal elements of the vibration-rotation interaction energy.

Table IV gives a listing of the fundamental frequencies and zeta-values of ethane and heavy ethane together with the estimated anharmonicity factors and normal frequencies.

The values for the fundamental frequencies and for the zetas have been taken directly from the summary of Raman data listed by Herzberg[3] and from the work of Smith[5] with the following exceptions where it appears that a reinterpretation of the experimental observations will yield more reliable numbers:

(1) Because of resonance interactions with combination vibrations, the fundamentals ν_1, ν_1^*, ν_5, ν_5^*, and ν_{10} appear in the spectrum as doublet bands. The "resonance free" values listed for these fundamentals are estimates furnished by the relative intensities of the doublet components and the relative doublet separations in ethane and heavy ethane. As an example of this process, consider the frequency ν_5. The experimental spectrum shows two bands, one at 2895.60 and the other at 2954.05 cm^{-1}, of which the former is of the order of twice the intensity of the latter. The existence of these two bands is undoubtedly due to the resonance interaction at ν_5 and the overtone level ν_{8+11}. The wave functions describing the resonanting levels are linear combinations of the wave functions for ν_5 and ν_{8+11} and the square of the coefficients of the ν_5 wave function will measure the intensity of the transition to that resonating level. It also measures the extent to which the energy of the resonating level depends upon the unperturbed energy level of ν_5. Thus if the intensity ratio of the bands at 2895.6 and at 2954.0 is as 2:1, one may conclude that the unperturbed level

$$\nu_5 = [2(2895.6) + 2954.0]/3 = 2915 \text{ cm}^{-1}.$$

(2) The vibration ν_2, called the "uncertain frequency" of ethane has not been observed directly and its frequency is estimated from the combination bands $\nu_{2+2} = 2778$ cm^{-1} and $\nu_{2+2}^* = 2300$ cm^{-1} [10] and the approximate isotope relations

$$\nu_{2+2} \equiv 2\nu_2(1-x') \rightarrow \nu_{2+2}^* \cong 2\nu_2^*(1-x'\nu_2^*/\nu_2).$$

The resultant value $\nu_2 = 1400$ cm^{-1} is in good agreement with values estimated from the combination bands $\nu_{2+6} = 2753.3$ and $\nu_{2+9} = 2218$ cm^{-1}.[9]

(3) The value $\nu_{12} = 1190$ cm^{-1} is that obtained by Smith from the combination band ν_{4+12} and is consistent with estimates given by $\nu_{9+12} = 2021.6$ cm^{-1} [10] and $\nu_{7+12} = 4178.9$ cm^{-1}. These latter combination bands, which have the rotational spacings 7.60 cm^{-1} and 6.89

TABLE IV. Fundamental frequencies, anharmonicity factors, normal frequencies, and zeta-values for ethane and heavy ethane.

Fundamental frequencies	Anharmonicity factors	Normal frequencies	Zeta-values
ν_1 = 2915	x_1 = 0.0420	ω_1 = 3042.8	
ν_2 = 1400	x_2 = 0.0340	ω_2 = 1449.3	
ν_3 = 993	x_3 = 0.0225	ω_3 = 1015.8	
ν_4 = 275	x_4 = 0.0933	ω_4 = 303.3	
ν_5 = 2915	x_5 = 0.0477	ω_5 = 3061.0	
ν_6 = 1379.2	x_6 = 0.0405	ω_6 = 1437.5	
ν_7 = 2995.5	x_7 = 0.0460	ω_7 = 3139.9	ζ_7 = 0.095
ν_8 = 1472.2	x_8 = 0.0350	ω_8 = 1525.6	ζ_8 = −0.331
ν_9 = 821.52	x_9 = 0.0004	ω_9 = 821.8	ζ_9 = 0.236
ν_{10} = 2955	x_{10} = 0.0694	ω_{10} = 3175.1	...
ν_{11} = 1460	x_{11} = 0.0590	ω_{11} = 1551.6	ζ_{11} = −0.354
ν_{12} = 1190	x_{12} = 0.0450	ω_{12} = 1246.0	ζ_{12} = 0.490
ν_1^* = 2100		ω_1^* = 2165.5	
ν_2^* = 1158		ω_2^* = 1191.5	
ν_3^* = 852		ω_3^* = 868.8	
ν_4^* = 200		ω_4^* = 214.6	
ν_5^* = 2095		ω_5^* = 2169.4	
ν_6^* = 1077		ω_6^* = 1112.2	
ν_7^* = 2236		ω_7^* = 2315.5	...
ν_8^* = 1082		ω_8^* = 1110.5	ζ_8^* = −0.423
ν_9^* = 593.7		ω_9^* = 593.9	ζ_9^* = 0.182
ν_{10}^* = 2225		ω_{10}^* = 2347.8	...
ν_{11}^* = 1055		ω_{11}^* = 1102.0	...
ν_{12}^* = 970		ω_{12}^* = 1006.9	...

[9] It is the measurement of the ν_{2+9} by Smith which favors a value for ν_2 higher than the value $\nu_2 = 1375$ cm^{-1} originally given in reference 3. It then becomes preferable to assign the 2778 cm^{-1} band as ν_{2+2} rather than ν_{6+6} as given also originally in reference 3.

[10] As mentioned by Smith, the appearance in the infrared spectrum of a perpendicular band with large rotational spacing at 2021.6 cm^{-1} is the strongest argument in favor of the D_{3d} equilibrium configuration of ethane, since this position and rotational spacing forces the band's assignment as ν_{9+12}, a combination band infrared active for the D_{3d} model but infrared inactive for the D_{3h} model.

cm^{-1},[11] respectively, determine the mean zeta-value $\zeta_{12}=0.490$.

(4) The value $\zeta_{12}=0.490$ given above is somewhat higher than the value 0.325 computed by Smith from his measured values of ζ_{10} and ζ_{11} together with the zeta-sum rule for the perpendicular inactive vibrations $(\zeta_{10}+\zeta_{11}+\zeta_{12})=B/2A=0.128$. However, there is strong evidence that the vibration ν_{10} is involved in a resonance interaction with the combination band ν_{8+8} and hence that the associated zeta-value is anomalous. Thus, assuming such a coupling between ν_{10} and ν_{8+8} which gives rise to the complex vibrations $[\nu_{10}]_a$ and $[\nu_{10}]_b$, then an associated zeta-value, say $[\zeta_{10}]_a$ will be an average of the unperturbed values $\zeta_{10}=-0.008$ (as obtained by zeta-sum rule and tabulated values of ζ_{11} and ζ_{12}) and $\zeta_{8+8}=-2\zeta_8=0.662$.[12] weighted according to the composition of $[\nu_{10}]_a$ in terms of ν_{10} and ν_{8+8}. In the different combination vibrations $[\nu_{i+10}]$, the computed $[\zeta_{10}]$ values are expected to be different due to the variation in completeness of resonance. These consequences are amply shown by Smith's measurements on the following combination bands.

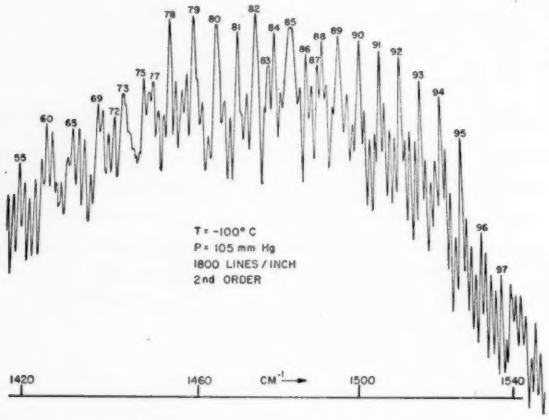

FIG. 5. Absorption by the ν_8 band of ethane (after L. G. Smith, reference 5). The nature of the irregularities in the fine structure of this band furnishes an independent check on the D_{3d} equilibrium configuration of ethane.

$$[\nu_{4+10}]=3258\ cm^{-1} \quad [\nu_{10}]=2968\ cm^{-1}$$
$$\rightarrow$$
$$[\zeta_{4+10}]=0.164 \quad [\zeta_{10}]=0.164$$
$$[\nu_{6+10}]=4334\ cm^{-1} \quad [\nu_{10}]=2955\ cm^{-1}$$
$$\rightarrow$$
$$[\zeta_{6+10}]=0.147 \quad [\zeta_{10}]=0.147$$
$$[\nu_{8+10}]=4416\ cm^{-1} \quad [\nu_{10}]=2944\ cm^{-1}$$
$$\rightarrow$$
$$[\zeta_{8+10}]=-0.039 \quad [\zeta_{10}]=0.370$$
$$[\nu_{7+10}]=5950\ cm^{-1} \quad [\nu_{10}]=2955\ cm^{-1}$$
$$\rightarrow$$
$$[\zeta_{7+10}]=-0.228 \quad [\zeta_{10}]=0.135.$$

Further support for the ν_{10}, ν_{8+8} interaction is offered by the Raman data of Lewis and Houston[13] if the Stokes lines in the vicinity of 3000 cm^{-1} and the single line at 2939 cm^{-1} are interpreted respectively as the ${}^SQ^K$ lines and the first ${}^OQ^K$ line of the band $[\nu_{10}]$. With this interpretation, one obtains $[\nu_{10}]=2947\ cm^{-1}$ and a rotational spacing of 10.0 cm^{-1} which corresponds to the zeta-value $[\zeta_{10}]=0.444$.

(5) As the torsional vibration is both Raman and infrared inactive, the spectroscopic determination of its fundamental frequency can be obtained only from combination bands. For C_2H_6, Smith has determined the average value $\nu_4=290\ cm^{-1}$ from the two bands ν_{4+11} and ν_{4+10} while for C_2D_6, Stitt's measurement $\nu_{4+10}^*=2415\ cm^{-1}$ gives $\nu_4^*=190\ cm^{-1}$. For these two values, the ratio $\nu_4/\nu_4^*=1.526$ differs so markedly from the product rule ratio, $(m^*/m)^{\frac{1}{2}}$, as to indicate a real inconsistency. Although, in general, spectroscopic methods are the more accurate, in this case specific heat measurements give the more concordant results of $\nu_4=275\ cm^{-1}$ and $\nu_4^*=200\ cm^{-1}$,[14] and it is these latter values which are listed in Table IV.

The perturbation of the ν_{10} band prevents the use of the observed rotational spacings of the perpendicular inactive bands for a check on the small moment of inertia of ethane as determined by Smith from the rotational spacings $\Delta\nu_7$, $\Delta\nu_8$, and $\Delta\nu_9$. Although the ν_8 band is also perturbed, as may be seen from the spectrogram given in Fig. 5 and reproduced from Smith's paper, this perturbation is small and the resolution of the fine structure is sufficient to permit simple interpretation and consequent determination of the normal or unperturbed rotational spacing. The general results of an analysis of the ν_8 band have been cited by Smith but, as the perturbation scheme involved requires the D_{3d} equilibrium configuration for ethane (and hence constitutes a check on the correctness of this model), it seems worthwhile to include here a summary of the method as well as the numerical agreement between the observed and predicted positions of the main absorption lines. The procedure consists of two parts. First, the assignment of a quantum number, K, to each Q line, and second, the determination of perturbation parameters required to match the observed and predicted line positions.

For the assignment of quantum numbers, one takes advantage of the feature that the fine structure of ν_8 becomes regular at the high frequency side of the band indicating that the perturbing forces tend to vanish in this direction. Using the Q line spacing in this high frequency region to establish approximate values for the small moment of inertia and the zeta-value for this

[11] Smith reported these spacings as 7.64 and 7.02 cm^{-1} respectively, but reexamination of his data seems to indicate the above listed values to be preferable.

[12] M. Johnston and D. M. Dennison, Phys. Rev. **48**, 868 (1935) show that the dipole coupling between a combination level and the vibrational ground state is such that if $l_1, l_2, \cdots$ represent the internal angular momenta quantum numbers, the apparent zeta-value for the combination band is $\zeta=+(\Sigma l_i\zeta_i)$ or $-(\Sigma l_i\zeta_i)$ as $|\Sigma l_i|=3n+1$ or $3n-1$, where n is any integer.

[13] C. M. Lewis and W. V. Houston, Phys. Rev. **44**, 903 (1933).

[14] Kistiakowsky, Lacher, and Stitt, J. Chem. Phys. **7**, 289 (1939).

band, a theoretical intensity distribution for the equivalent unperturbed band may be calculated. This predicted intensity distribution is pictured in Fig. 6. An unusual situation occurs in the ν_8 band in that, due to a coincidence, the spacing of the lines in the sub-bands for which $\Delta J=\pm 1$ are almost exactly $\frac{1}{4}$ of the Q line spacing. This means that the sub-band lines will bunch together into groups of three equispaced lines lying between the individual Q lines. These groups of lines have characteristic intensity patterns. Thus, for example, between the K lines 5 and 6, the low frequency member of the triplet is the most intense due to the large contribution of the first R line of the $K=4$ sub-band. Similarly between 6 and 7 the middle member is intense, and between 7 and 8 the last member is intense, this being due, respectively, to the first R lines of the $K=5$ and $K=6$ sub-bands. These features are exactly matched by the intensities of the substructure lines found by Smith between the Q lines which he designated as 91 and 92, 92 and 93, and 93 and 94, respectively. It will be noted that between the K lines 10 and 11, the substructure lines are predicted to be as intense as the R lines and that this condition is found to obtain in the corresponding position of the observed band, namely between lines 96 and 97.

From his examination of the ν_8 band, Smith concluded that two distinct regions of perturbation were present and suggested that these perturbations were the result of Fermi and Coriolis interactions with the combination band ν_{4+12} which presumably lies in this region. The stepwise assignments of the Q lines starting from the high frequency side do indeed give two resonance like curves for the function $\nu_8(K)$. However, all the observed Q lines are not accounted for by this procedure and these "extra" Q lines do not fall on the resonance curves. Yet, the existence and positions of these "extra" lines are, as will be shown, actually a consequence of the interaction scheme suggested by Smith. From the line assignments given in Table V, the unperturbed rotational spacing and band center can be determined without any perturbation calculation. For these assignments indicate that the resonances occur near the middle of the band and hence the line positions at the high and low frequency sides are approaching asymptotically the hypothetical positions of the resonance free lines. A measurement of these two asymptotes permits the evaluation of the normal band center, the rotational spacing, and the convergence of the resonance free lines. This procedure gives $\nu_8=1472.2$ cm^{-1} and $\Delta\nu_8=5.563$ cm^{-1} (at the band center).

For the quantitative determination of the structure of ν_8, one has three essential perturbation parameters, (1) the strength, Δ, of the Fermi coupling term (arising from an anharmonic potential term such as $\xi_4\rho_{12}\rho_8\sin(\phi_8-\phi_{12})$ where ξ_4 is the torsional normal coordinate, and ρ_8, ϕ_8 and ρ_{12}, ϕ_{12} are the polar normal coordinates associated with the vibrations ω_8 and ω_{12}),

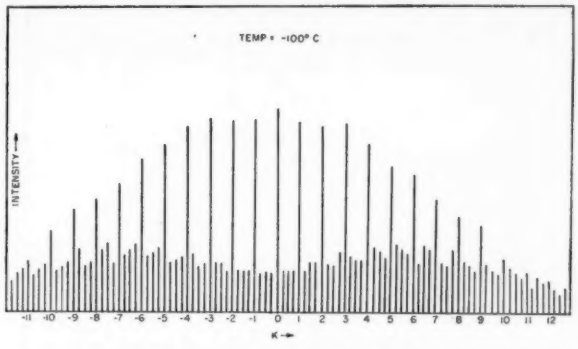

FIG. 6. Theoretical intensity distribution for the unperturbed ν_8 band. The quantum number K refers to that of the ground vibrational state.

(2) the strength, f, of the Coriolis coupling term (arising from the vibration-rotation interaction $(P_xp_x+P_yp_y)/I_x$. Although this interaction strength depends on the rotational quantum numbers as $C[(J-K)(J+K+1)]^{\frac{1}{2}}$, one may use a value averaged over J which near the band center is essentially $C\bar{J}=f$, a number independent of K. In the harmonic oscillator approximation there is no Coriolis coupling between ν_8 and ν_{4+12} and the non-vanishing of the coupling coefficient C depends on the existence of appropriate anharmonic potential terms), and (3) the separation, a, between the unperturbed band centers of ν_8 and ν_{4+12}. The energy contributions due to the Fermi and Coriolis interactions are determined from the eigenvalues of the 4×4 matrices (see Herzberg for the selection rules governing such

TABLE V. Line assignments for the ν_8 band.[a]

Line no.	K''	K'	cm^{-1}	Perturbation (cm^{-1})
55	10	9	1418.71	−0.39
60	9	8	1424.56	−0.33
65	8	7	1430.34	−0.31
69	7	6	1435.65	−0.74
72	6	5	1439.63	−2.47
73	6	5	1441.36	−0.74
75	5	4	1446.38	−1.41
77	5	4	1448.52	0.73
78	4	3	1452.41	−1.04
79	3	2	1457.91	−1.18
80	2	1	1463.48	−1.21
81	1	0	1468.45	−1.84
82	0	1	1472.95	−2.90
83	0	1	1475.87	0.02
84	1	2	1477.78	−3.91
	1	2		0.14
85			1481.49	
	2	3		−5.41
86	1	2	1485.64	4.25
87	2	3	1488.28	1.38
88	2	3	1489.29	2.39
89	3	4	1493.68	1.29
90	4	5	1498.90	1.05
91	5	6	1504.13	0.84
92	6	7	1509.47	0.77
93	7	8	1514.65	0.56
94	8	9	1519.85	0.40
95	9	10	1525.14	0.35
96	10	11	1530.51	0.41
97	11	12	1535.80	0.41

[a] See reference 5.

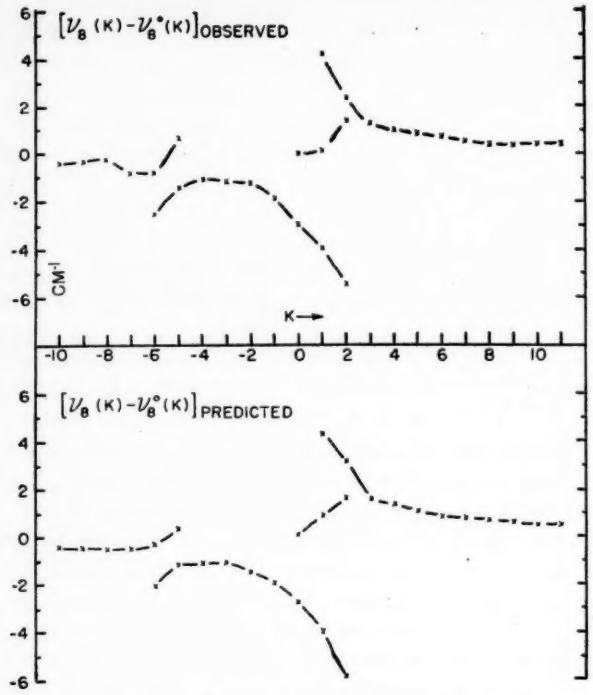

FIG. 7. Observed and calculated perturbation of the Q lines of ν_8.

interactions)

$$\begin{array}{cccc} E_8^+(K) & \Delta & 0 & f \\ -\Delta & E_{4+12}^+(K) & -f & 0 \\ 0 & f & E_8^-(K+1) & -\Delta \\ -f & 0 & \Delta & E_{4+12}^-(K+1) \end{array}$$

where $E_8^+(K)$ is the energy of the Kth rotational level of the state ν_8^+ in the absence of the perturbing terms Δ and f. Thus

$$E_8^+(K)=(A-B)K^2-2A\zeta_8 K.$$

Using Smith's initial values for the moments of inertia and zeta-values,[15] one obtains the perturbation function plotted in Fig. 7 with the choice

$$a=7.0\ \text{cm}^{-1};\ f^2=1\ \text{cm}^{-2};\ \Delta^2=16\ \text{cm}^{-2}.$$

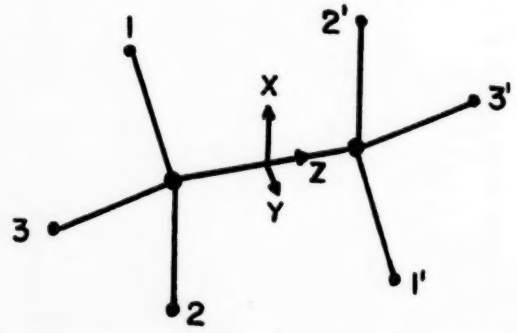

FIG. 8. Schematic diagram of the ethane molecule and the adopted indexing of the hydrogen and carbon atoms.

[15] L. G. Smith and W. N. Woodward, Phys. Rev. **61**, 386(A) (1942).

Although the agreement between the predicted and observed perturbation functions might be improved somewhat by a more careful determination of the parameters a, f, and Δ, the above choice is sufficiently close to show the essential correctness of the perturbation scheme. The "extra" Q lines which are one of the characteristic features of the spectrum arise from the coupling, by way of ν_{4+12}, of two different levels of ν_8 which normally make transitions to two different ground vibrational states (as contrasted, say, to the coupling of two levels of a perpendicular band via rotational interaction with a common third level of a parallel band as in ν_6^* and ν_8^* where no "extra" lines are expected).

IV. DETERMINATION OF THE GENERAL POTENTIAL CONSTANTS

The twenty-two independent potential constants compatible with the symmetry of ethane are defined by means of the set of symmetry coordinates pictured in Fig. 9 and are evaluated in groups—one group for each symmetry class of vibrations. It will be noted that these coordinates uniquely specify the configuration of the molecule whatever the ratio of carbon and hydrogen masses may be. They are thus geometric coordinates in the sense used by Johnston and Dennison[12] (thus, in terms of these coordinates, the potential energy expression is the same for both ethane and heavy ethane). The appropriate expressions for the kinetic and potential energies of each class of vibrations are given in the following order: (1) E_u; (2) E_g; (3) A_{1g}; (4) A_{2u}; and (5) A_{1u}. For the degenerate classes, the z components of internal angular momenta are also given.

In the following, m, m^*, and M will designate, respectively, the masses of the hydrogen, deuterium, and carbon atoms.

A. Perpendicular Active Vibrations (E_u)

The coordinates ξ_1, η_1 represent the well-known degenerate vibrations of a triatomic molecule with equal atoms set at the corners of an equilateral triangle. A displacement of the coordinate ξ_1 is such that the atoms of one of the hydrogen triangles execute the displacements shown in diagram (1a) of Fig. 9, while the atoms of the other triangle are displaced as in (1b). The actual displacement of each of the six atoms may be shown to be equal and is chosen to be $[1/(6)^{\frac{1}{2}}]\xi_1$. The η_1 displacements are the usual complements of ξ_1 and will not be shown. In both ξ_1 and η_1 the carbon atoms are not displaced and hence the kinetic energy is just $\frac{1}{2}m(\dot{\xi}_1^2+\dot{\eta}_1^2)$ for light ethane and $\frac{1}{2}m^*(\dot{\xi}_1^2+\dot{\eta}_1^2)$ for heavy ethane.

The displacements ξ_2 and η_2 are again ones in which neither the carbon atoms nor the center of gravity of each H_3 group move and consist in a rocking of each of the hydrogen triangles through an angle α. If now $\xi_2=S\alpha$ where S is the equilibrium side of a hydrogen triangle, the kinetic energy associated with this motion is $\frac{1}{2}m(\dot{\xi}_2^2+\dot{\eta}_2^2)$ or $\frac{1}{2}m^*(\dot{\xi}_2^2+\dot{\eta}_2^2)$. η_2 is of course

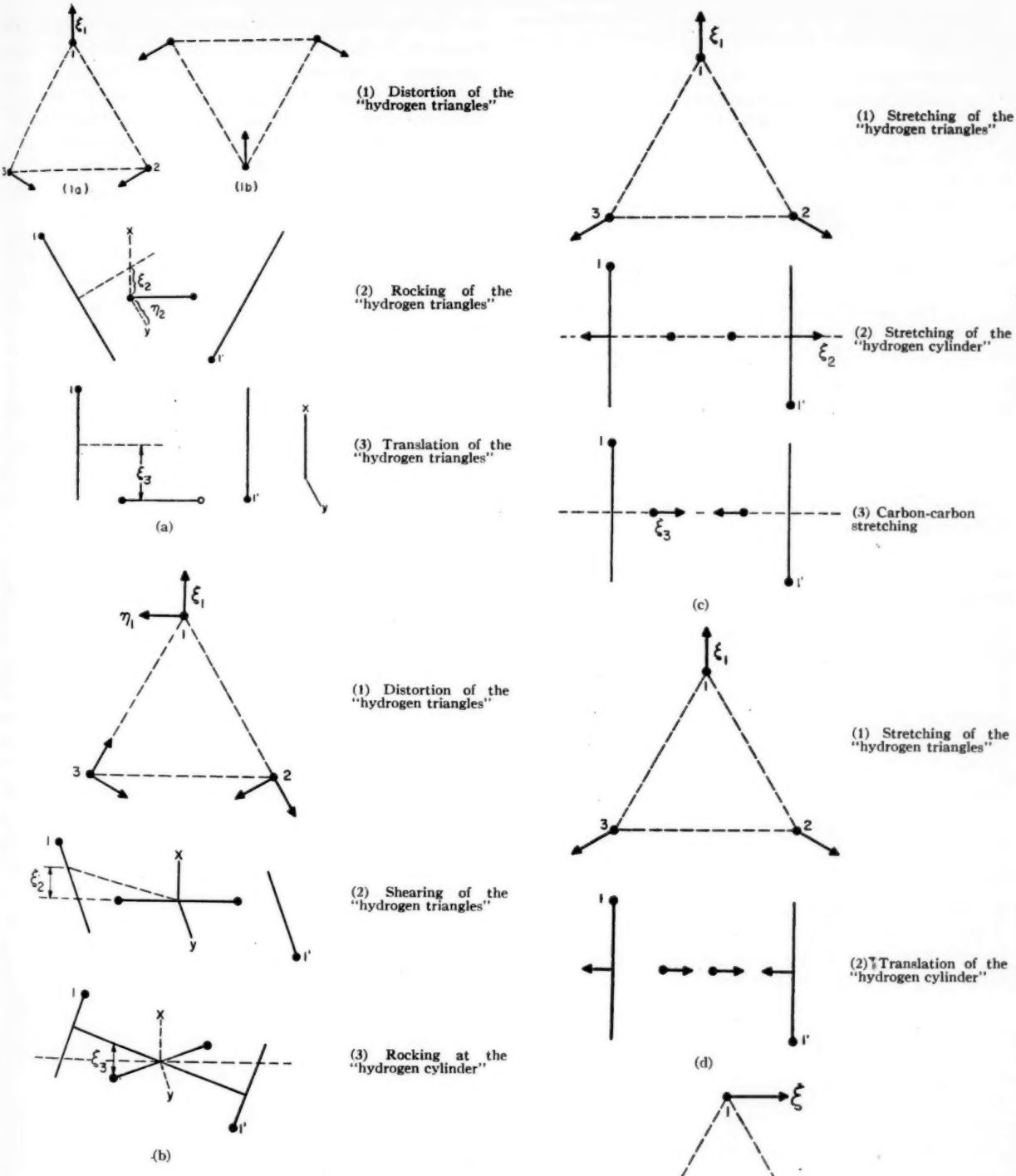

FIG. 9. Definition of the set of symmetry coordinates used for the representation of the potential energy function of ethane. (a) Coordinates for expressing the perpendicular active vibrations. (b) Coordinates for expressing the perpendicular inactive vibrations. (c) Coordinates for expressing the parallel inactive vibrations. (d) Coordinates for expressing the parallel active vibrations. (e) Coordinate for expressing the torsional vibration.

TABLE VI. Potential constants of ethane based on coordinate system defined in Fig. 9. All constants are expressed in units of 10^5 dynes/cm.

(a) Potential constants associated with the perpendicular active vibrations.

$a_{11}=2.992$	$a_{12}=1.182$
$a_{22}=1.436$	$a_{13}=1.790$
$a_{33}=3.203$	$a_{23}=1.693$

(b) Potential constants associated with the perpendicular inactive vibrations.

$b_{11}=3.244$	$b_{12}=1.778$
$b_{22}=3.159$	$b_{13}=1.401$
$b_{33}=1.935$	$b_{23}=1.456$

(c) Potential constants associated with the parallel inactive vibrations.

$c_{11}=5.330$	$c_{12}=0.705$
$c_{22}=1.238$	$c_{13}=0.431$
$c_{33}=0.789$	$c_{23}=0.331$

(d) Potential constants associated with the parallel active vibrations.

$d_{11}=5.484$	$d_{12}=0.578$
$d_{22}=1.305$	

(e) Torsion constant: $e=0.0546$

similar to ξ_2 but the axis of the rocking motion is turned through 90°.

The displacements ξ_3 and η_3 are ones where the hydrogen triangles are both displaced in one direction without rocking and the carbons are displaced in the reverse direction. For convenience, the displacement of the carbon atoms relative to the H-triangles has been chosen to be $(3m+M/6M)^{\frac{1}{2}}$ times ξ_3 or η_3 and hence the kinetic energy for light ethane is $\frac{1}{2}m(\dot{\xi}_3^2+\dot{\eta}_3^2)$ and for heavy ethane is $\frac{1}{2}m^*(3m+M/3m^*+M)(\dot{\xi}_3^2+\dot{\eta}_3^2)$.

In each of these displacements it will be noted that there is neither a net rotation nor change in center of gravity of either the light or heavy ethane molecule. (These requisite features also obtain for the individual displacements defined for the other symmetry classes.) The choice of the coordinates has been such that there exist no cross product terms in the kinetic energy. Collecting the above results we have

$$T=\tfrac{1}{2}m(\dot{\xi}_1^2+\dot{\xi}_2^2+\dot{\xi}_3^2+\dot{\eta}_1^2+\dot{\eta}_2^2+\dot{\eta}_3^2)$$

$$T^*=\tfrac{1}{2}m^*(\dot{\xi}_1^2+\dot{\xi}_2^2+\dot{\xi}_3^2/\sigma+\dot{\eta}_1^2+\dot{\eta}_2^2+\dot{\eta}_3^2/\sigma);$$

$$\sigma=(3m^*+M)/(3m+M)$$

$$V=V^*=\tfrac{1}{2}\Sigma a_{ij}(\xi_i\xi_j+\eta_i\eta_j)$$

$$p_z=p_z^*=-1(\xi_1 p_{\eta 1}-\eta_1 p_{\xi 1})+1(\xi_3 p_{\eta 3}-\eta_3 p_{\xi 3})$$

where $p_{\eta 1}$ is the momentum conjugate to η_1, etc.

For the estimation of the normal frequencies we have adopted the following set of anharmonicity factors: $X_7=0.0460$, $X_8=0.0350$, $X_9=0.0004$. The values of X_7 and X_8 were chosen, in accordance with the principles outlined in Sec. III, to agree roughly with the anharmonicity factors 0.046 and 0.039 of the corresponding triply degenerate frequencies of methane.[7] The value of X_8 was arbitrarily lowered to 0.0350 so that the Teller product rule would give a positive value for X_9. By using least squares and a weighting scheme based on the estimate that a 1 percent error in a normal frequency is equivalent to an error of 0.02 in a zeta-value, the six potential constants, a_{ij}, are readily calculated from the determinant giving the normal frequencies and from the theoretical expressions for the zetas. They are listed in Table VI and yield the following calculated normal frequencies and zeta-values which may be compared with the observed quantities.

	Normal frequencies (cm^{-1})		Zeta-values	
Vibration	Predicted	Observed	Predicted	Observed
ν_7	3136.9	3139.9	0.098	0.095
ν_8	1526.9	1525.6	−0.334	−0.331
ν_9	825.1	821.8	0.236	0.236
ν_7^*	2321.3	2315.5	0.213	···
ν_8^*	1109.3	1110.5	−0.403	−0.423
ν_9^*	595.2	595.3	0.190	0.182

The unitary matrices which connect the normal vibrations with the displacements ξ_1, ξ_2, ξ_3 (or η_1, η_2, η_3) have been calculated to have the following numerical elements.

$$\begin{matrix} S_{71}= & 0.601 & S_{72}= & 0.422 & S_{73}=0.678 \\ S_{81}=-0.797 & S_{82}= & 0.253 & S_{83}=0.548 \\ S_{91}= & 0.059 & S_{92}=-0.871 & S_{93}=0.489 \end{matrix} \begin{pmatrix}\xi_7\\ \xi_8\\ \xi_9\end{pmatrix}=S\begin{pmatrix}\xi_1\\ \xi_2\\ \xi_3\end{pmatrix}$$

$$\begin{matrix} S_{71}^*= & 0.558 & S_{72}^*= & 0.404 & S_{73}^*=0.725 \\ S_{81}^*=-0.826 & S_{82}^*= & 0.193 & S_{83}^*=0.529 \\ S_{91}^*= & 0.074 & S_{92}^*=-0.894 & S_{93}^*=0.442 \end{matrix} \begin{pmatrix}\xi_7^*\\ \xi_8^*\\ \xi_9^*\end{pmatrix}=S^*\begin{pmatrix}\xi_1\\ \xi_2\\ \xi_3/(\sigma)^{\frac{1}{2}}\end{pmatrix}$$

These elements are of value in determining the actual motions of the atoms. For example, the normal vibration ω_7 consists of 0.601 of the displacement ξ_1 on which has been superposed 0.422 of displacement ξ_2 and 0.678 of ξ_3. The zeta-value associated with ω_7 is found by weighting the zeta-values of ξ_1, ξ_2, and ξ_3, namely -1, 0, $+1$, respectively, with the squares of the matrix elements. Thus

$$\zeta_7=(-1)(0.601)^2+(0)(0.422)^2+(1)(0.678)^2=0.098.$$

B. Perpendicular Inactive Vibrations (E_g)

The coordinates ξ_1, η_1 are the same as the identically labelled coordinates of the E_u class except for a reversal of phase in the atomic displacements in the opposing hydrogen triangle [(1b) of Fig. 9].

In the displacement ξ_2, there is a rotation of each hydrogen triangle about its center together with a counter rotation of the triangle centers about the molecule center of such relative magnitude that no change in angular momentum occurs. For convenience, the scale of ξ_2 is chosen such that the displacement of a triangle center is $(I_Z/12I_c)^{\frac{1}{2}}$ times ξ_2 or η_2, where I_Z is the large moment of inertia of ethane and I_c is the large moment of the hydrogen "cylinder," that is, the structure consisting solely of the six hydrogen atoms in their equilibrium positions. The kinetic energy contributions for light and heavy ethane are then $\frac{1}{2}m(\dot{\xi}_2^2+\dot{\eta}_2^2)$ and $\frac{1}{2}m^*(\dot{\xi}_2^2+\dot{\eta}_2^2)$.

In the displacement ξ_3, the hydrogen cylinder rocks through an angle α_1 while the carbon atoms counter rotate about the molecule center through an angle α_2 such that there is no change in angular momentum. Denoting the distance of a carbon atom from the molecule center by S, ξ_3 is chosen such that $S(\alpha_1+\alpha_2)=(mI_x/2MI_c)^{\frac{1}{2}}\xi_3$ and hence the kinetic energy for light ethane is $\frac{1}{2}m(\dot{\xi}_3^2+\dot{\eta}_3^2)$ and for heavy ethane is $\frac{1}{2}m^*(I_x/I_x^*)(\dot{\xi}_3^2+\dot{\eta}_3^2)$. Again the choice of coordinates has been such that there exist no cross product terms in the kinetic energy and one obtains the following expressions.

$$T=\tfrac{1}{2}m(\dot{\xi}_1^2+\dot{\xi}_2^2+\dot{\xi}_3^2+\dot{\eta}_1^2+\dot{\eta}_2^2+\dot{\eta}_3^2)$$

$$T^*=\tfrac{1}{2}m^*(\dot{\xi}_1^2+\dot{\xi}_2^2+\dot{\xi}_3^2/\sigma+\dot{\eta}_1^2+\dot{\eta}_2^2+\dot{\eta}_3^2/\sigma)$$

$$\sigma=I_x^*/I_x$$

$$V=V^*=\tfrac{1}{2}\Sigma b_{ij}(\xi_i\xi_j+\eta_i\eta_j)$$

$$\begin{aligned}p_z=&-1(\xi_1p_{\eta 1}-\eta_1p_{\xi 1})+(I_Z/2I_c)(\xi_2p_{\eta 2}-\eta_2p_{\xi 2})\\&+\{1-(I_Z/2I_c)+(I_Z/2I_x)\}(\xi_3p_{\eta 3}-\eta_3p_{\xi 3})\\&+\{(I_Z/2I_c)[1-(I_Z/2I_c)][1-(I_c/I_x)]\}^{\frac{1}{2}}\\&\times\{(\xi_2p_{\eta 3}-\eta_3p_{\xi 2})+(\xi_3p_{\eta 2}-\eta_2p_{\xi 3})\}.\end{aligned}$$

With the coordinates $\xi_1^*=\xi_1$; $\xi_2^*=\xi_2$; $\xi_3^*=\xi_3/(\sigma)^{\frac{1}{2}}$, the expression for the vibrational angular momentum of C_2D_6 is the same as p_z above but with all quantities starred.[16] The symbol I_c appearing in p_z refers as before to that part of the large moment of inertia of ethane contributed by the six hydrogen atoms. The values for the six potential constants b_{ij} were determined from the five independent normal frequencies and the value of ζ_{11}. The experimental value for ζ_{12}, being obtained from combination bands, was not considered sufficiently accurate to be weighted in the determination of the potential constants. The values of the b_{ij} listed in Table VI thus predict back the normal frequencies and the ζ_{11} value exactly and yield the value $\zeta_{12}=0.413$ as compared with the observed value of 0.490. The as yet unobserved ζ values of heavy ethane are predicted to be $\zeta_{10}^*=0.190$, $\zeta_{11}^*=-0.395$, and $\zeta_{12}^*=0.383$.

The unitary matrices connecting the normal vibrations with the displacements ξ_1, ξ_2, ξ_3 have the following numerical elements.

$$\begin{matrix}S_{10,1}= & 0.636 & S_{10,2}= & 0.630 & S_{10,3}= & 0.446\\ S_{11,1}= & -0.734 & S_{11,2}= & 0.672 & S_{11,3}= & 0.097\\ S_{12,1}= & 0.239 & S_{12,2}= & 0.389 & S_{12,3}= & -0.890\end{matrix}\begin{pmatrix}\xi_{10}\\ \xi_{11}\\ \xi_{12}\end{pmatrix}=S\begin{pmatrix}\xi_1\\ \xi_2\\ \xi_3\end{pmatrix}$$

$$\begin{matrix}S_{10,1}^*= & 0.596 & S_{10,2}^*= & 0.593 & S_{10,3}^*= & 0.542\\ S_{11,1}^*= & -0.783 & S_{11,2}^*= & 0.578 & S_{11,3}^*= & 0.228\\ S_{12,1}^*= & 0.178 & S_{12,2}^*= & 0.560 & S_{12,3}^*= & -0.809\end{matrix}\begin{pmatrix}\xi_{10}^*\\ \xi_{11}^*\\ \xi_{12}^*\end{pmatrix}=S\begin{pmatrix}\xi_1\\ \xi_2\\ \xi_3/(\sigma)^{\frac{1}{2}}\end{pmatrix}$$

C. Parallel Inactive Vibrations (A_{1g})

The displacement ξ_1 is one in which each hydrogen atom moves outward away from the symmetry axis by an amount $[1/(6)^{\frac{1}{2}}]\xi_1$. In the displacement ξ_2 each hydrogen triangle moves away from the molecule center by an amount $[1/(6)^{\frac{1}{2}}]\xi_2$, and in the displacement ξ_3 each carbon atom moves towards the molecule center by an amount $(m/2M)^{\frac{1}{2}}\xi_3$. This choice of internal coordinates gives the following energy expressions:

$$T=\tfrac{1}{2}m(\dot{\xi}_1^2+\dot{\xi}_2^2+\dot{\xi}_3^2)$$

$$T^*=\tfrac{1}{2}m^*(\dot{\xi}_1^2+\dot{\xi}_2^2+\dot{\xi}_3^2/\sigma);\quad \sigma=m^*/m$$

$$V=V^*=\tfrac{1}{2}\Sigma c_{ij}\xi_i\xi_j.$$

For the determination of the six potential constants, only five independent normal frequencies are available, and it is necessary to introduce one simplifying assumption. We have chosen equal to zero the valence force constant k_{Rr} which couples C−C stretching to C−H stretching, and the values of the potential constants c_{ij} listed in Table VI are dependent upon this assumption.

The elements of the unitary matrices connecting the normal vibrations with the displacements ξ_1, ξ_2, and ξ_3 are

$$\begin{matrix}S_{11}= & 0.980 & S_{12}= & 0.170 & S_{13}= & 0.102\\ S_{21}= & -0.198 & S_{22}= & 0.873 & S_{23}= & 0.445\\ S_{31}= & -0.013 & S_{32}= & -0.456 & S_{33}= & 0.890\end{matrix}\begin{pmatrix}\xi_1\\ \xi_2\\ \xi_3\end{pmatrix}=S\begin{pmatrix}\xi_1\\ \xi_2\\ \xi_3\end{pmatrix}_{\text{normal}}$$

$$\begin{matrix}S_{11}^*= & 0.970 & S_{12}^*= & 0.176 & S_{13}^*= & 0.169\\ S_{21}^*= & -0.236 & S_{22}^*= & 0.500 & S_{23}^*= & 0.833\\ S_{31}^*= & 0.062 & S_{32}^*= & -0.848 & S_{33}^*= & 0.527\end{matrix}\begin{pmatrix}\xi_1^*\\ \xi_2^*\\ \xi_3^*\end{pmatrix}=S\begin{pmatrix}\xi_1\\ \xi_2\\ \xi_3/(\sigma)^{\frac{1}{2}}\end{pmatrix}_{\text{normal}}$$

D. Parallel Active Vibrations (A_{2u})

In the displacement ξ_1, the hydrogen atoms of one triangle (the unprimed triangle) move outward while the atoms of the opposing triangle move inward towards the symmetry axis by the same amount $[1/(6)^{\frac{1}{2}}]\xi_1$. In the displacement ξ_2, the hydrogen atoms move in the direction of the $-Z$ axis while the carbon atoms move in the direction of the $+Z$ axis by an amount such that there is no translation of the molecule center. The scale of ξ_2 is chosen such that the sum of the carbon and hydrogen (or deuterium) atom displacements is $(6M/3m+M)^{\frac{1}{2}}\xi_2$ and this choice gives rise to the following energy expressions.

$$T=\tfrac{1}{2}m(\dot{\xi}_1^2+\dot{\xi}_2^2)$$

$$T^*=\tfrac{1}{2}m^*(\dot{\xi}_1^2+\dot{\xi}_2^2/\sigma);\quad \sigma=(3m^*+M)/(3m+M)$$

$$V=V^*=\tfrac{1}{2}\Sigma d_{ij}\xi_i\xi_j=\tfrac{1}{2}(d_{11}\xi_1^2+d_{22}\xi_2^2+2d_{12}\xi_1\xi_2).$$

---

[16] The choice of coordinates such that the kinetic energy expression for ethane has a diagonal form and equal coefficients gives rise to two simplifying features: first, the transformation matrix $S_{i\alpha}$, connecting the symmetry coordinates ξ_i with the normal coordinates (ξ_{10}, ξ_{11}, and ξ_{12}) is unitary, and second, the matrix of the coefficients Z_{ij}, appearing in the expression for p_z is symmetric and related to the zeta-matrix, $\zeta_{\alpha\beta}$ (i.e., the coefficients in the expression for p_z in terms of normal coordinates), by the equation

$$\zeta_{\alpha\beta}=\Sigma Z_{ij}S_{i\alpha}S_{i\beta},$$

where the diagonal elements $\zeta_{\alpha\alpha}$ are the observable values $\zeta_\alpha=\zeta_{10}$, ζ_{11}, and ζ_{12}. The formal advantage of the use of a new set of coordinates ξ_i^* in accomplishing this same simplification for heavy ethane is offset by a consequent necessity for the introduction of a new set of potential constants b_{ij}^* related but not equal to the b_{ij}.

TABLE VII. Definition of valence force constants for ethane (excluding the force constant associated with torsion). r_i denotes the H_i-C distance minus the equilibrium distance, R the C−C distance minus the equilibrium distance, ψ_i the increase in the H_i-C-C angle, θ_i the increase in the $H_{i-1}-C-H_{i+1}$ angle.

	Nature of the constant	Contribution to the potential energy
	(A) Stretching and bending force constants.	
(1)	C−H stretching	$\frac{1}{2}k_r(r_1^2+r_2^2+r_3^2+r_{1'}^2+r_{2'}^2+r_{3'}^2)$
(2)	∠H−C−C bending	$\frac{1}{2}k_\psi r_0^2(\psi_1^2+\psi_2^2+\psi_3^2+\psi_{1'}^2+\psi_{2'}^2+\psi_{3'}^2)$
(3)	∠H−C−H bending	$\frac{1}{2}k_\theta r_0^2(\theta_1^2+\theta_2^2+\theta_3^2+\theta_{1'}^2+\theta_{2'}^2+\theta_{3'}^2)$
(4)	C−C stretching	$\frac{1}{2}k_R R^2$
	(B) Force constants coupling adjacent parts of the molecule.	
(5)	C−H stretching / C−H stretching	$\frac{1}{2}k_{rr}(r_1r_2+r_2r_3+r_3r_1+r_{1'}r_{2'}+r_{2'}r_{3'}+r_{3'}r_{1'})$
(6)	H−C−C bending / H−C−C bending	$\frac{1}{2}k_{\psi\psi}r_0^2(\psi_1\psi_2+\psi_2\psi_3+\psi_3\psi_1+\psi_{1'}\psi_{2'}+\psi_{2'}\psi_{3'}+\psi_{3'}\psi_{1'})$
(7)	H_i-C-C bending / $H_{i+1}-C-H_{i-1}$ bending	$\frac{1}{2}k_{\theta\psi}r_0^2(\theta_1\psi_1+\theta_2\psi_2+\theta_3\psi_3+\theta_{1'}\psi_{1'}+\theta_{2'}\psi_{2'}+\theta_{3'}\psi_{3'})$
(8)	H_i-C stretching / $H_{i+1}-C-C$ bending	$\frac{1}{4}k_{r\psi}\beta r_0\{r_1(\psi_2+\psi_3)+r_2(\psi_3+\psi_1)+r_3(\psi_1+\psi_2)+r_{1'}(\psi_{2'}+\psi_{3'})+r_{2'}(\psi_{3'}+\psi_{1'})+r_{3'}(\psi_{1'}+\psi_{2'})\}$
(9)	H_i-C stretching / $H_{i+1}-C-H_{i-1}$ bending	$\frac{1}{2}k_{r\theta}r_0(r_1\theta_1+r_2\theta_2+r_3\theta_3+r_{1'}\theta_{1'}+r_{2'}\theta_{2'}+r_{3'}\theta_{3'})$
(10)	H_i-C stretching / H_i-C-C bending	$\frac{1}{2}k_{r\psi}r_0(r_1\psi_1+r_2\psi_2+r_3\psi_3+r_{1'}\psi_{1'}+r_{2'}\psi_{2'}+r_{3'}\psi_{3'})$
(11)	H−C stretching / C−C stretching	$\frac{1}{2}k_{rR}R(r_1+r_2+r_3+r_{1'}+r_{2'}+r_{3'})$
(12)	C−C stretching / H−C−C bending	$\frac{1}{2}k_{R\psi}r_0R(\psi_1+\psi_2+\psi_3+\psi_{1'}+\psi_{2'}+\psi_{3'})$
	(C) Force constants coupling remote parts of the molecule.	
(13)	H_i-C stretching / $H_{i'}-C$ stretching	$k_{rr'}(r_1r_{1'}+r_2r_{2'}+r_3r_{3'})$
(14)	H_i-C stretching / $C-H_{(i+1)'}$ stretching	$\frac{1}{2}k_{rr'}\beta(r_1r_{2'}+r_1r_{3'}+r_2r_{1'}+r_2r_{3'}+r_3r_{1'}+r_3r_{2'})$
(15)	H_i-C stretching / $C-C-H_{(i+1)'}$ bending	$\frac{1}{4}k_{r\psi'}\beta r_0\{r_1(\psi_{2'}+\psi_{3'})+r_2(\psi_{3'}+\psi_{1'})+r_3(\psi_{1'}+\psi_{2'})+r_{1'}(\psi_2+\psi_3)+r_{2'}(\psi_3+\psi_1)+r_{3'}(\psi_1+\psi_2)\}$
(16)	H_i-C stretching / $C-C-H_{i'}$ bending	$\frac{1}{2}k_{r\psi'}r_0(r_1\psi_{1'}+r_2\psi_{2'}+r_3\psi_{3'}+r_{1'}\psi_1+r_{2'}\psi_2+r_{3'}\psi_3)$
(17)	H_i-C stretching / $H_{(i+1)'}-C-H_{(i-1)'}$ bending	$\frac{1}{2}k_{r\theta'}r_0(r_1\theta_{1'}+r_2\theta_{2'}+r_3\theta_{3'}+r_{1'}\theta_1+r_{2'}\theta_2+r_{3'}\theta_3)$
(18)	H_i-C-C bending / $C-C-H_{i'}$ bending	$k_{\psi\psi'}r_0^2(\psi_1\psi_{1'}+\psi_2\psi_{2'}+\psi_3\psi_{3'})$
(19)	H_i-C-C bending / $C-C-H_{(i+1)'}$ bending	$\frac{1}{2}k44_{\beta'}r_0^2(\psi_1\psi_{2'}+\psi_1\psi_{3'}+\psi_2\psi_{3'}+\psi_2\psi_{1'}+\psi_3\psi_{1'}+\psi_3\psi_{2'})$
(20)	$H_{i+1}-C-H_{i-1}$ bending / $H_{(i+1)'}-C-H_{(i-1)'}$ bending	$k_{\theta\theta'}r_0^2(\theta_1\theta_{1'}+\theta_2\theta_{2'}+\theta_3\theta_{3'})$
(21)	$H_{i+1}-C-H_{i-1}$ bending / $C-C-H_{i'}$ bending	$k_{\theta\psi'}r_0^2(\theta_1\psi_{1'}+\theta_2\psi_{2'}+\theta_3\psi_{3'})$

The three independent normal frequencies associated with this symmetry class just suffice to determine the values of the d_{ij} listed in Table VI.

The unitary matrices connecting the normal vibrations with the displacements ξ_1 and ξ_2 have the following numerical elements.

$$\begin{matrix} S_{51}= & 0.991 & S_{52}=0.134 \\ S_{61}= & -0.134 & S_{62}=0.991 \end{matrix} \quad \begin{pmatrix}\xi_5\\ \xi_6\end{pmatrix}=S\begin{pmatrix}\xi_1\\ \xi_2\end{pmatrix}$$

$$\begin{matrix} S_{51}^*= & 0.988 & S_{52}^*=0.155 \\ S_{61}^*= & -0.156 & S_{62}^*=0.988 \end{matrix} \quad \begin{pmatrix}\xi_5^*\\ \xi_6^*\end{pmatrix}=S^*\begin{pmatrix}\xi_1\\ \xi_2/(\sigma)^{\frac{1}{2}}\end{pmatrix}$$

E. The Torsional Vibration (A_{1u})

In the displacement ξ one hydrogen triangle rotates clockwise while the other rotates counterclockwaise about the symmetry axis, the displacement of any hydrogen atom being $[1/(6)^{\frac{1}{2}}]\xi$. The energy expressions are thus

$$T=\tfrac{1}{2}m\dot{\xi}^2$$
$$T^*=\tfrac{1}{2}m^*\dot{\xi}^2$$
$$V=V^*=\tfrac{1}{2}e\xi^2.$$

The torsional motion or hindered rotation in ethane represents a rather special case in which the shape of the potential energy function is approximately known over the whole range of the torsion angle θ. Perhaps more significant than the potential constant e is the value of the barrier height $V_0=965$ cm^{-1} [14] appearing in the assumed expression $V(\text{torsion})=V_0(1-\cos 3\theta)/2$.

V. THE VALENCE FORCE CONSTANTS OF ETHANE

By means of the general potential constants already evaluated, it is now possible to determine restoring forces associated with arbitrary small distortions of ethane such as the stretching of a C−H bond or the bending of H−C−H angles. The force constants associated with such specific distortions are of importance mainly for comparisons with other molecules which possess similar components. Complicating such comparisons is the fact that when, for example, one of these bands is stretched, the remaining parts of the molecule deform in such a way as to minimize the poten-

TABLE VIII. The valence force constants of ethane. (All constants are expressed in units of 10^5 dynes/cm.)

Stretching and bending force constants		
(1)	k_r	5.35 ± 0.03
(2)	k_θ	0.51 ± 0.02
(3)	k_ψ	0.63 ± 0.02
(4)	k_R	4.57 ± 0.03
Coupling constants for adjacent components		
(5)	$k_{r\psi\beta}$	-1.89 ± 0.20
(6)	$k_{R\psi}$	0.60 ± 0.04
(7)	$k_{r\theta}$	-0.20 ± 0.02
(8)	$k_{\theta\psi}$	-0.07 ± 0.02
(9)	$k_{r\psi}$	-0.07 ± 0.15
(10)	k_{rr}	-0.04 ± 0.04
(11)	$k_{\psi\psi}$	0.03 ± 0.04
(12)	k_{Rr}	0.00 ± 0.20
Coupling constants for remote components		
(13)	$k_{\psi\psi'}$	0.11 ± 0.02
(14)	$k_{\theta\psi'}$	0.07 ± 0.03
(15)	$k_{r\theta'}$	-0.03 ± 0.02
(16)	$k_{\theta\theta'}$	-0.02 ± 0.02
(17)	$k_{rr'\beta}$	-0.08 ± 0.04
(18)	$k_{rr'}$	0.08 ± 0.04
(19)	$k_{r\psi'\beta}$	0.35 ± 0.20
(20)	$k_{r\psi'}$	-0.13 ± 0.15
(21)	$k_{\psi\psi'\beta}$	0.00 ± 0.05

tial energy. Such deformations are characterized by coupling force constants and indicate the strength of interaction between various parts of the molecule. It is well known, however, that the vibrational spectra of many molecules may be computed quite accurately by use of potential functions in which most of the possible coupling terms are assumed zero. One thus expects, *a priori*, that many of the coupling terms for ethane will be small, especially those terms which represent coupling between the remote parts of the molecule.

These bond stretching, bond angle bending, and coupling force constants are the potential constants associated with a valence coordinate expression of the potential energy function. In the displacement corresponding to the torsional vibration, no bond distances and no bond angles are changed. Thus, on the assumption of pure valence forces, there would be no restoring force and this frequency would be zero. The observed value of the frequency is indeed rather small and the restoring force, which depends on its square, is considerably less than the force required to distort a bond angle. To this extent the measurements of the torsional frequency agree with the simplified valence picture. The remaining eleven frequencies all involve changes in bond distances and angles.

The nineteen bond distances and bond angles of ethane give rise to the nineteen valence coordinates having the following definitions:

(1) R = increase in C−C distance (that is, the C−C separation minus the equilibrium separation)

(2–7) r_i (or $r_{i'}$) = the increase in C−H_i (or C−$H_{i'}$) distance, where the subscript i designates a particular hydrogen atom as labelled in Fig. 8

(8–13) ψ_i = the increase in the H_i−C−C bond angle

(14–19) θ_i = the increase in the H_{i-1}−C−H_{i+1} bond angle. These coordinates are not independent but satisfy the two conditions

(a) $(\theta_1+\theta_2+\theta_3)\sin\theta_0=(\psi_1+\psi_2+\psi_3)(3\sin\psi_0\cos\psi_0)$

(b) $(\theta_{1'}+\theta_{2'}+\theta_{3'})\sin\theta_0=(\psi_{1'}+\psi_{2'}+\psi_{3'})(3\sin\psi_0\cos\psi_0)$

which are equivalent to the conditions of no net rotation about the symmetry axis and no torsion of the methyl groups. Although the redundancy of the coordinate system permits a certain latitude in the expression of the potential energy, twenty-one independent force constants may be defined as in Table VII. As a consequence of the latitude in choice of the twenty-one independent quadratic forms constituting the expression of the potential function, the values of the angle bending force constants k_θ and k_ψ depend on the particular expression of the coupling terms. This dependence, however, is quite weak due to the smallness of the coupling force constants. Table VIII gives the values of the valence force constants as obtained directly from the set

TABLE IX. Definition and values for the valence force constants of methane. r_i denotes the C−H_i distance minus the equilibrium distance, and ψ_{ij} the increase in the H_i−C−H_j angle.

	Nature of constant	Contribution to the potential energy	Value of constant in units of 10^5 dynes/cm
(1)	C−H stretching	$\frac{1}{2}K_r(r_1^2+r_2^2+r_3^2+r_4^2)$	$K_r = 5.394$
(2)	∠H−C−H bending	$\frac{1}{2}K_\psi r_0^2(\psi_{12}^2+\psi_{13}^2+\psi_{14}^2+\psi_{23}^2+\psi_{24}^2+\psi_{34}^2)$	$K = 0.420$
(3)	$\begin{matrix}C-H_i\\C-H_j\end{matrix}$ coupling	$\frac{1}{2}K_{rr}(r_1r_2+r_2r_3+r_3r_4+r_4r_1+r_1r_3+r_2r_4)$	$K_{rr}= 0.037$
(4)	$\begin{matrix}C-H_i\\H_j-C-H_k\end{matrix}$ coupling	$\frac{1}{2}K_4r_0\{r_1(\psi_{23}+\psi_{24}+\psi_{34})+r_2(\psi_{13}+\psi_{14}+\psi_{34})+r_3(\psi_{12}+\psi_{14}+\psi_{24})+r_4(\psi_{12}+\psi_{13}+\psi_{23})\}$	$K_4 =-0.276$
(5)	$\begin{matrix}H_i-C-H_j\\H_k-C-H_l\end{matrix}$ coupling	$\frac{1}{2}K_5r_0^2(\psi_{12}\psi_{34}+\psi_{13}\psi_{24}+\psi_{14}\psi_{23})$	$K_5 =-0.075$

TABLE X. Correlation of the valence force constants of ethane and methane.
(Force constants expressed in units of 10^5 dynes/cm.)

Nature of force constant	Ethane	Methane
C−H stretching	$k_r = 5.35$	$K_r = 5.394$
H−C−H bending	$k_\theta = 0.51$	$K_\psi = 0.420$
C−H_i to C−H_j coupling	$k_{rr} = -0.04$	$K_{rr} = 0.037$
C−H_i to H_{i+1}−C−H_{i-1} coupling	$k_{r\theta} = -0.20$	$K_4 = -0.276$

Formal correlations

Ethane Nature of constant	Ethane Value	Methane Value	Methane Nature of constant
C−C stretching	$k_R = 4.57$	$K_r = 5.394$	C−H stretching
H−C−C bending	$k_\psi = 0.63$	$K_\psi = 0.420$	H−C−H bending
C−H to C−C coupling	$k_{rR} \equiv 0.00$	$K_{rr} = 0.037$	C−H_i to C−H_j coupling
H_{i-1}−C−H_{i+1} to H_i−C−C coupling	$k_{\theta\psi} = -0.07$	$K_5 = -0.075$	H_{i-1}−C−H_{i+1} to H_i−C−H_{i+2} coupling
C−H_i to H_{i-1}−C−C coupling	$k_{r\psi\beta} = -1.99$	$2K_4 = -0.552$	C−H_i to H_{i-1}−C−H_{i+1} coupling
C−H_i to H_i−C−C coupling	$k_{r\psi} = -0.07$	"$k_{r\psi}$" $\equiv 0.000$	C−H_i to H_i−C−H_{i-1} coupling
C−C to H_i−C−C coupling	$k_{R\psi} = 0.60$	$-K_4 = 0.276$	C−H_i to H_i−C−H_{i-2} coupling
H_i−C−C to H_{i-1}−C−C coupling	$k_{\psi\psi} = 0.03$	"$k_{\psi\psi}$" $\equiv 0.000$	H_i−C−H_{i-2} to H_{i-1}−C−H_{i-2} coupling

of general potential constants associated with the previous symmetry coordinate system.

The "uncertainty values" shown in Table VIII are based on the changes in the computed force constants when the individual fundamental frequencies and zeta-values are given upper and lower limits consistent with the spectroscopic data (e.g., although the positions of the components of the resonance doublets ν_{1a} and ν_{1b} have been measured with high precision, the unperturbed value chosen for the fundamental frequency ν_1 is necessarily only an estimate which may be in error by perhaps ± 15 cm^{-1}). These "uncertainty values" are intended to give a measure of how well the present data determine the valence force constants and thus also the extent to which the values of the constants can be used for significant correlations with similar constants of other molecules.

It will be noticed that, for the most part, the principal contributions to the potential energy arise from changes in the bond distances and bond angles and not from the cross product terms. The potential energy associated with a change in a C−C−H angle is approximately but not exactly equal to that coming from a change in H−C−H angle. The coupling constants for adjacent components of the molecule are not very significantly different from zero with the exception of the interaction between a C−C stretching and a C−C−H bending, a H_i−C stretching and a H_{i+1}−C−H_{i-1} bending, and a H_i−C stretching and a H_{i+1}−C−C bending. It seems very puzzling that these last two interactions should be so large.

VI. CORRELATION OF THE VALENCE FORCE CONSTANTS OF ETHANE AND METHANE

The potential function for methane has been determined by Dennison[6] and is characterized by a set of five potential constants. In terms of valence coordinates these constants may be given as in Table IX (the one relation among the six H_i−C−H_j angles, ψ_{ij}, again making possible a number of different explicit expressions for the potential energy). That the coupling terms for methane and ethane have been chosen in a manner appropriate for the direct comparison of the simple force constants can be verified by rewriting the potential function of methane treating the 4th hydrogen atom formally equivalent to the primed carbon (or primed methyl group) of ethane and then comparing the coefficients of the resulting quadratic terms with the corresponding force constants of ethane. The results of such a procedure are given in Table X. The values of the principal force constants of both ethane and methane given here are in general higher than those cited for example in Herzberg which have been obtained by the use of fundamental rather than normal frequencies in the secular determinant.

It is a pleasure to acknowledge the many helpful discussions with Dr. L. G. Smith regarding the infrared spectrum of ethane.

The Kinetics of the Fast Gas-Phase Reaction between Nitryl Chloride and Nitric Oxide*

EDWARD C. FREILING,† HAROLD S. JOHNSTON, AND RICHARD A. OGG, JR.
Department of Chemistry, Stanford University, California

(Received November 5, 1951)

The kinetics of the fast reaction between nitryl chloride and nitric oxide has been studied by absorptiometric methods in two systems of greatly different surface-to-volume ratio and over a temperature range from 1° to 71°. The pressure of each reactant has been varied from 0.1 mm to 18 mm and the total pressure from 0.2 mm to 384 mm. The reaction proceeds quantitatively according to the equation

$$ClNO_2+NO=NO_2+ClNO.$$

It is homogeneous and first order with respect to each reactant. The second-order rate constant is expressed by the equation

$$k=0.83\times10^{12}\exp(-6900/RT)\text{cc mole}^{-1}\text{ sec}^{-1}.$$

An elementary bimolecular mechanism is proposed.

INTRODUCTION

IN the thermal decomposition of nitrogen pentoxide there occurs a rapid reaction[1–3] which must have almost zero energy of activation[4]

$$NO_3+NO=2NO_2. \quad (1)$$

Ogg and Weston[5] sought and found an analogue to this process in the fast reaction between nitryl chloride and nitric oxide

$$ClNO_2+NO=NO_2+ClNO. \quad (2)$$

Ogg and Weston[5] also found that nitrogen pentoxide reacts with nitrosyl chloride to produce nitryl chloride and nitrogen dioxide

$$N_2O_5+ClNO=ClNO_2+2NO_2. \quad (3)$$

This article reports the results of a kinetic study of the first of these reactions, Eq. (2). The nitryl chloride used in this investigation was prepared by way of the second reaction, Eq. (3).

EXPERIMENTAL

The rate of reaction was followed absorptiometrically in two systems of widely different surface-to-volume ratio.

The great majority of runs were carried out in the same low pressure apparatus that has been described by Johnston and Perrine.[6] A 22-liter, spherical Pyrex bulb, which served as the reaction vessel, was connected to two sets of pipets. Each set consisted of two pipets in series, one of which was one-hundredth and the other one-thousandth of the volume of the reaction bulb. Nitric oxide was introduced into one of these sets at a pressure measured directly with a mercury manometer. The pressure of nitryl chloride in the other set of pipets was determined with the aid of a Bourdon null gage. At zero time these reactants were passed together into the evacuated reaction bulb; the optical density of the mixture at 436 mμ was then followed by means of a 1P28 electron-multiplier photoelectric tube and an electronic voltmeter. Time was indicated by an electric metronome which gave both visible and audible signals every three seconds. The progress of the reaction was recorded at three-second intervals for some 39 sec and then at appropriately longer intervals until no further progress could be detected. Blank experiments indicated that the reactants came to temperature and pressure equilibrium in the reaction bulb in less than three seconds. The reaction cell and optical system were calibrated by Johnston and Perrine[6] by the introduction of nitrogen dioxide air mixtures into the reaction cell. The pipets could then be calibrated relative to the reaction cell by filling them to measured pressures of nitrogen dioxide, emptying their contents into the evacuated reaction cell, and determining the resulting pressure absorptiometrically.

A small number of runs were carried out in the intermediate pressure apparatus of Mills and Johnston.[3] In this apparatus reactants were mixed rapidly in a flow system, and a sample of the reacting mixture was isolated at constant volume and temperature. The transmission of 436 mμ radiation was followed on an oscilloscope by the method of Johnston and Yost.[7] The flow system of Mills and Johnston was modified by the introduction of a 66-cm pre-cooling coil of 6-mm glass tubing between the mixing chamber and the reaction cell. Advantage was taken of the nitrogen dioxide-nitrogen tetroxide equilibrium to establish absorptiometrically that the flowing gases came to thermal equilibrium with the surrounding water bath before entering

* Abstracted from a thesis presented in partial fulfillment of the requirements for the degree of Doctor of Philosophy at Stanford University, 1951.

† Present address: Chemistry Branch, U. S. Naval Radiological Defense Laboratory, San Francisco 24, California.

[1] J. H. Smith and F. Daniels, J. Am. Chem. Soc. **69**, 1735 (1947).

[2] R. A. Ogg, Jr., J. Chem. Phys. **15**, 337 (1947); **15**, 613 (1947).

[3] R. L. Mills and H. S. Johnston, J. Am. Chem. Soc. **73**, 938 (1951).

[4] H. S. Johnston, J. Am. Chem. Soc. **73**, 4542 (1951).

[5] R. E. Weston, Jr., doctoral thesis, Stanford University, California, 1950.

[6] H. S. Johnston and R. L. Perrine, J. Am. Chem. Soc. **73**, 4782 (1951).

[7] H. S. Johnston and D. M. Yost, J. Chem. Phys. **17**, 386 (1949).

TABLE I. Results of runs made in the low pressure apparatus at 27°C with unequal initial concentrations of the reactants.

Pressure of gases in mm NO	$ClNO_2$	$k\times10^{-7}$ cc mole^{-1} sec^{-1}
1.14	0.123	0.64
1.14	0.131	0.60
1.01	0.176	0.54
0.587	0.100	0.69
0.390	0.133	0.64
0.362	0.118	0.76
0.182	0.120	0.96
0.124	0.179	0.61
0.134	0.393	0.94
0.121	0.352	0.81
0.157	1.02	0.56
0.098	0.594	0.79
0.121	1.13	0.70
0.122	1.10	0.87

the reaction cell. The optical density was followed for a period of about two seconds during a typical run made in this system. The calibration of the reaction cell and optical system of the intermediate pressure apparatus was in principle identical to that for the low pressure apparatus. For convenience, however, only one quantitative mixture of air and nitrogen dioxide was made up, and successively lower concentrations of nitrogen dioxide were obtained by using this mixture at successively lower total pressures.

Nitric oxide was prepared by using the same method and equipment that has been reported by Mills and Johnston.[3] Nitryl chloride was prepared according to the foregoing reaction (3) by condensing freshly distilled nitrosyl chloride upon a twofold excess of nitrogen pentoxide. When this reaction mixture was stored in a dry ice acetone bath under an atmosphere of nitrogen, the slow oxidation of nitrosyl chloride could be observed by the disappearance of its characteristic orange color. By hastening the reaction with frequent periods of agitation and gentle warming, there remained eventually only a white solid and a clear, colorless, supernatant liquid. The supernatant was separated and twice distilled from $-78°$ to $-196°$, low and high boiling fractions being discarded with each distillation. An aerostatic balance of the type described by Stock and his co-workers[8] was used to determine the molecular weight of the purified product. A value of 81 ± 3 was obtained while the theoretical value is 81.47. Although the distilled nitryl chloride invariably possessed a very pale straw-yellow coloration, the amount of impurity present was insufficient to permit detection by either the molecular weight determination or the quantitative conversion to nitrogen dioxide which will be described later.

RESULTS

The reaction was followed by the appearance of optical density at 436 mμ. Both products, nitrogen dioxide and nitrosyl chloride, absorb at this wavelength.

[8] A. Stock and W. Siecke, Ber. deut. chem. Ges. **57**, 562 (1924); A. Stock and G. Ritter, Z. physik. Chemie **119A**, 333 (1926).

At low temperatures nitrogen dioxide associates to form colorless nitrogen tetroxide. The association of nitric oxide with nitrogen dioxide was negligible under all conditions studied. If the trial assumption is made that the reaction goes according to Eq. (2) with no side reactions, then it follows from stoichiometric considerations that

$$[ClNO]=[NO_2]+2[N_2O_4], \tag{4}$$

where the brackets refer to concentrations. These concentrations are related to the optical density D and the length of light path L by the equation

$$D/L=\epsilon[NO_2]+\epsilon'[ClNO], \tag{5}$$

where ϵ and ϵ' refer respectively to the molar extinction coefficients of nitrogen dioxide and nitrosyl chloride. Combination of these equations with the equilibrium expression

$$K=[NO_2]^2/[N_2O_4] \tag{6}$$

yields the relationship

$$[ClNO]=\frac{D}{L\epsilon'}+\frac{K\epsilon(\epsilon+\epsilon')}{4(\epsilon')^2}\left\{1-\left[1+\frac{8D\epsilon'}{LK(\epsilon+\epsilon')^2}\right]^{\frac{1}{2}}\right\}. \tag{7}$$

Since this expression involves small differences between large numbers, it is expedient to make the definition

$$y=8D\epsilon'/LK(\epsilon+\epsilon')^2 \tag{8}$$

and expand Eq. (7) in a power series

$$[ClNO]=\frac{D}{L(\epsilon+\epsilon')}\left[1+\frac{2\epsilon}{\epsilon'}\times\left(\frac{y}{8}-\frac{y^2}{16}+\frac{5y^3}{128}-\frac{7y^4}{256}+\cdots\right)\right]. \tag{9}$$

The factor enclosed in brackets serves to correct the optical density for the dimerization of nitrogen dioxide. In evaluating this factor all terms of the power series which contributed less than 0.05 percent of the total value of the factor were neglected. Thus, while it was necessary to include terms as high as the fourth power of y in applying Eq. (9) to runs made in the neighbor-

TABLE II. Results of runs made in the intermediate pressure apparatus using diluent nitrogen gas.

Temperature °C	Pressures of gases in mm NO	$ClNO_2$	Total	$k\times10^{-7}$ cc mole^{-1} sec^{-1}
4.1	18.7	18.8	384	0.35
1.4	14.2	14.2	290	0.33
1.8	13.7	13.7	280	0.26
4.1	6.68	6.70	137	0.26
27.1	4.69	4.70	95	0.69
27.0	4.11	4.12	84	0.59
27.3	3.28	3.29	67	0.64
29.5	3.05	3.06	62	0.95
28.6	2.78	2.79	57	0.67

hood of 0°, at 27° and above no more than the first-order term had to be evaluated. ϵ was obtained from the data of Dixon,[9] ϵ' from the data of Goodeve and Katz,[10] and K was evaluated from the results of Verhoek and Daniels.[11]

The purity of nitryl chloride was established by determining its molecular weight. A further check on the purity of either reactant was obtained by comparing the absorptiometrically observed pressure of nitrosyl chloride at the completion of a run with that expected from manometer readings and pipet volumes when the reaction was carried out in the presence of an excess of the other reagent. The results of 9 runs carried out with an excess of nitryl chloride yield a value of 1.008±0.009 for the ratio of observed-to-expected pressure, while the results of 7 runs made with nitric oxide in excess yield a ratio of 1.01±0.01. Each reagent was, therefore, 99±1 percent pure. This agreement indicates further that side reactions, if they exist, are negligible.

A sensitive test which shows the reaction to be complete was an attempt to follow the reverse reaction. A mixture of nitrogen dioxide and nitrosyl chloride was followed absorptiometrically for 48 minutes without detection of decrease in optical density. Under the conditions of the experiment this indicated that the reaction between nitryl chloride and nitric oxide is at least 99 percent complete. Combined with the qualitative observations of substantial amounts of nitrosyl chloride in the reaction products, these results establish that the reaction proceeds quantitatively according to Eq. (2). Thus the rate of the reaction is equal to the rate of formation of nitrosyl chloride and can be determined from the appearance of optical density as indicated previously.

The rate of reaction for any given run was found to fit the appropriate form of the integrated rate expression for a second-order reaction. The ratio of initial concentrations was varied from about 1:10 to 10:1, and the second-order rate constants obtained are given in Table I. The mean is 0.72×10^7 cc mole^{-1} sec^{-1} and the standard deviation 0.14×10^7 cc mole^{-1} sec^{-1}. There is no significant trend in the rate constants, and thus the reaction is second order and first order in each reactant.

The runs made in the 6-mm diameter cell of the intermediate pressure apparatus are shown in Table II. The temperatures were measured rather than controlled, and therefore they vary from run to run. A comparison of the individual values of the rate constants from studies made in this apparatus at temperatures near 27° with those made at 27° in the large bulb shows that the reaction is homogeneous. In spite of a 40-fold change of surface-to-volume ratio, the second-order rate constants are the same in each apparatus. In Table II the results of a few runs made between 1° and 4° are also given.

[9] J. K. Dixon, J. Chem. Phys. **8**, 157 (1940).
[10] C. F. Goodeve and S. Katz, Proc. Roy. Soc. (London) **A172**, 432 (1939).
[11] F. H. Verhoek and F. Daniels, J. Am. Chem. Soc. **53**, 1250 (1931).

TABLE III. Results of runs made in the low pressure apparatus using equal concentrations of the reactants.

Temperature °C	Number of runs	$k_{Av}\times10^{-7}$ cc mole^{-1} sec^{-1}	Standard error of mean $\times10^{-7}$ cc mole^{-1} sec^{-1}
27	28	0.79	0.02
38	20	1.25	0.04
50	9	1.64	0.06
61	16	2.56	0.05
71	25	3.4	0.1

In order to determine the activation energy 98 runs were made in the low pressure apparatus using equal initial concentrations of reactants. These runs covered a temperature range from 27° to 71°. The results are summarized in Table III. All runs in Tables I, II, and III were fitted to the Arrhenius equation by the method of least squares. The rate constant may be expressed as

$$k=0.83\times10^{12}e^{-E/RT}\text{ cc mole}^{-1}\text{ sec}^{-1},$$

where the energy of activation is 6.9 kcal and twice its standard error of estimate is 0.3 kcal.

DISCUSSION

This investigation has shown that the reaction between nitryl chloride and nitric oxide is given quantitatively by Eq. (2), and it is fast, homogeneous, and first order in each reactant. There is no indication that the reaction is complex; and since the energy of activation is less than any bond energy in either reactant, it is not unimolecular. Thus it is proposed that this is an elementary bimolecular reaction.

Even if this mechanism is correct, it still leaves open an interesting ambiguity of path. Nitryl chloride could pass either an oxygen atom or a chlorine atom to nitric oxide with the same chemical result. The following experiment might clarify this question: Label nitryl chloride with isotopic nitrogen N*; make a series of studies to see if the reactants and products undergo exchange; and if the exchange rates can be neglected, carry out this reaction to see which path it takes:

$$ClN^*O_2+NO=N^*O_2+ClNO$$
$$ClN^*O_2+NO=NO_2+ClN^*O.$$

ACKNOWLEDGMENT

We wish to thank Dr. Ralph Weston for permitting us to study this reaction prior to its publication in his thesis, Dr. Harvey Crosby for assistance in use of the intermediate pressure apparatus, Mr. Richard Perrine for help in using his low pressure apparatus, and Mr. Daniel Devor for construction of the aerostatic balance.

The Heat of Dissociation of Fluorine*

RUSSELL N. DOESCHER
Jet Propulsion Laboratory, California Institute of Technology, Pasadena, California
(Received September 24, 1951)

Equilibrium pressure measurements of the dissociation of F_2 have been completed with the use of (1) a nickel vessel coated stepwise by heating in contact with fluorine at temperatures up to 850°C and (2) a differentially applied manometer containing a fluorinated oil. This latter technique made it possible to carry out the measurements in the comparatively low temperature range 759° to 1115°K. The method consisted essentially in a direct comparison of the pressure variation with temperature of a quantity of fluorine with that of a quantity of nitrogen. Twenty-four determinations of the equilibrium constant were made, and in a plot of $\ln K$ as a function of $1/T$, the points gave a straight line. The slope gave $\Delta H = 37.7$ kcal/mole as the mean heat of dissociation in the temperature range of the experiments for the reaction $F_2\,(g) \rightarrow 2F\,(g)$. This ΔH value is in good agreement with values calculated from entropy quantities and values of $\ln K$ obtained from the line.

INTRODUCTION

BEFORE 1947, it apparently was generally accepted that the value of the heat of dissociation of F_2 was above 60 kcal/mole, a value which seemed reasonable as representing a progression in this property of the halogens. According to a table given by Glockler,[1] the results obtained by various investigators ranged from 63 to 81 kcal/mole. The first indication of a considerably lower value appears to have been the work of Wahrhaftig[2] on the dissociation energy of ClF. In 1947, Gaydon[3] arrived at approximately 51 kcal/mole for the dissociation energy of F_2 on the basis of existing experimental evidence, and Schmitz and Schumacher[4] obtained the alternative values 33.4 and 30.6 kcal/mole through a redetermination of the dissociation energy of ClF and of the heat of formation of ClF. Other recent results have been obtained, and some of these are shown in Table I. However, it is believed that until now no direct measurement has been reported. The experiments described in the present paper were undertaken with the purpose of providing a relatively direct measurement.

TABLE I. Dissociation of F_2.

Heat of dissociation or dissociation energy	Scientist and year
35 kcal/mole	Potter,[a] 1949
$\leqslant 45$	Caunt and Barrow,[b] 1950
30	Schumacher,[c] 1950
40	Eucken and Wicke,[d] 1950
37	Evans, Warhurst, and Whittle,[e] 1950

[a] R. L. Potter, J. Chem. Phys. **17**, 957 (1949).
[b] A. D. Caunt and R. F. Barrow, Trans. Faraday Soc. **46**, 154 (1950).
[c] H. J. Schumacher, Anales asoc. quím. argentina **38**, 113 (1950).
[d] A. Eucken and E. Wicke, Naturwiss. **37**, 233 (1950).
[e] M. G. Evans, E. Warhurst, and E. Whittle, J. Chem. Soc. (London) **1950**, 1524.

DESCRIPTION OF APPARATUS

The method consisted essentially in a direct comparison of the pressure variation with temperature of a quantity of fluorine gas with that of a quantity of nitrogen gas, which does not dissociate appreciably at the temperatures involved in these experiments. Figure 1 contains a schematic representation of the principal parts of the apparatus employed. The tube furnace was especially constructed to produce a high uniformity of temperature. The inside wall of the furnace was a sterling silver tube, inside diameter 1.75 in., outside diameter 2.25 in., length 24.0 in., adjoining the inside surfaces of the furnace ends, which were made from $\frac{3}{8}$-in. Transite. Heat was supplied by passing electric currents through two separate windings, two end windings in series, and a center winding. In order to prevent heat transfer from the center through the furnace ends, with consequent large temperature gradient along the tube, the current through the end windings was made larger. The center winding was connected to a variable transformer, which was in turn connected to a 110-volt source through a constant-voltage transformer; the end windings were connected to a variable transformer, which was connected to a 110-volt source. Temperature surveys over the inside of the tube, with the use of a thermocouple, were carried out for the purpose of determining the variable-transformer settings corresponding to the optimum degree of uniformity for each temperature out of a number selected at regular intervals in the range of interest. The proper settings for a given temperature could then be found by interpolation or extrapolation. Temperature measurements were made by means of a chromel-alumel thermocouple in conjunction with a potentiometer.

Inside the tube were two identical nickel cylinders, each having an outside length of 10.0 in., one being for fluorine, the other for nitrogen. The connecting tubes and all other small metal tubes represented in Fig. 1 were made from nickel tubing. The cylinder ends with-

* This paper presents the results of one phase of research carried out at the Jet Propulsion Laboratory, under Contract No. DA-04-495-ORD 18, sponsored by the U. S. Army Ordnance Department.

[1] J. H. Simons, editor, *Fluorine Chemistry* (Academic Press Inc., New York, 1950), Vol. 1, p. 327.
[2] A. L. Wahrhaftig, J. Chem. Phys. **10**, 248 (1942).
[3] A. G. Gaydon, *Dissociation Energies and Spectra of Diatomic Molecules* (John Wiley and Sons, Inc., New York, 1947), pp. 188 and 189.
[4] H. Schmitz and H. J. Schumacher, Z. Naturforsch. **2a**, 359 and 362 (1947).

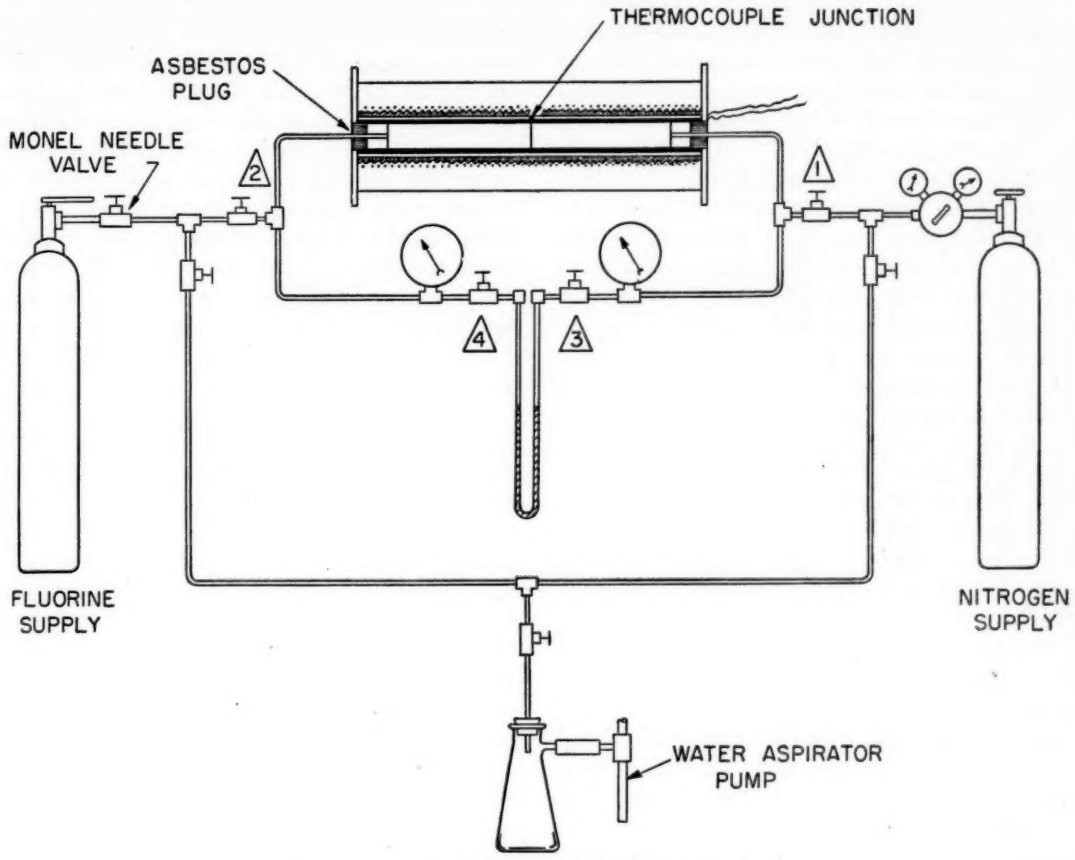

FIG. 1. Apparatus for studying fluorine dissociation.

out connecting tubes touched each other at the center of the furnace, and the clearance between each cylinder and the sterling silver tube was approximately 0.04 in. Nickel was chosen as the material because of its relatively high resistance to fluorine at high temperatures[5] and its inactivity with respect to nitrogen.[6–8] The material of the *T*-connectors was stainless steel, it being satisfactorily resistant to fluorine at room temperatures and 1 atmos.[9] With the exceptions of the Monel needle valve and the valves on the supply cylinders, all valves represented in Fig. 1 were stainless steel bar-stock globe valves in which the ordinary packing had been replaced with accurately machined Teflon rings lubricated by a fluorinated oil, Fluorolube Standard, produced by the Hooker Electrochemical Company. The packing of the Monel needle valve also was Teflon. Two identical Bourdon vacuum gauges were employed for measuring total pressure. These gauges had "*K*" Monel Bourdon tubes, were of high quality, and were carefully calibrated before and during the period of the fluorine-dissociation determinations. The pressure values obtained from each gauge probably differed from the true values by 0.15 in. of mercury or less. They were designated as Ashcroft Duragauge, Cat. No. 1079PV, Manning, Maxwell and Moore, Inc. A Meriam Gland Packed Manometer in which the ordinary gaskets had been replaced with accurately machined Teflon rings was used for measuring the difference in pressure between the fluorine and the nitrogen. The manometer liquid was Fluorolube Standard.

The uncertainty in the measurement of absolute temperature was estimated to be 3 deg, with a much smaller uncertainty in the measurement of temperature differences. The temperature gradient along the tube at the outer ends of the cylinders was approximately 1 deg/in.

EXPERIMENTAL PROCEDURE

A method of rendering the fluorine cylinder resistant to fluorine at temperatures between 500° and 850°C was discovered quite by accident. With the object of coating the inside of the cylinder by heating in the presence of fluorine, this gas was placed in the cylinder at room temperature and approximately ½ atmos with valve 4 closed; valve 2 was then closed, and the cylinder was heated. When a decrease in pressure occurred, showing a consumption of fluorine, an appropriate quantity was added. Below 500°C, the reaction between the fluorine

[5] R. Landau and R. Rosen, Ind. Eng. Chem. **39**, 281 (1947).
[6] A. Sieverts and W. Krumbhaar, Ber. deut. chem. Ges. **43**, 893 (1910).
[7] G. Hägg, Nova Acta Regiae Soc. Sci. Upsaliensis **7** (Series 4), 22 (1929).
[8] R. Juza and W. Sachsze, Z. Chem. **251**, 201 (1943).
[9] W. R. Myers and W. B. DeLong, Chem. Eng. Progress **44**, 359 (1948).

and the nickel finally ceased, but at 525°C, the reaction rate fell to a value which appeared to be nearly constant and which was far too large to permit fluorine-dissociation determinations through suitable corrections. When it seemed that this attempt had failed, an approach through a different method of coating was tried. The first cylinder was not used for this purpose and stood at room temperatures for about eight weeks, containing fluorine for about six weeks of this period, and open to the atmosphere for about two weeks. The second approach was unsuccessful, and with a different use in mind, the first cylinder was again tested. It was found that the corrosion resistance (defined in terms of rate of loss of fluorine) of the first cylinder had increased more than 100-fold during the eight-weeks period. The resistance increased rapidly with additional fluorination, which was carried out in steps at temperatures between 600° and 850°C accompanied by periods at temperatures below 300°C, but a point was finally reached at which the resistance increased very slowly and additional fluorination became unprofitable.

In the following discussions, the system containing the fluorine cylinder, extending to the liquid surface in the manometer, and which is isolated by closing valve 2 is called the fluorine side. The corresponding system containing the nitrogen cylinder is called the nitrogen side. After the fluorine cylinder had been coated, the accuracy of matching of the fluorine side with the nitrogen side was tested. Thermal equilibrium having been established in the furnace, nitrogen was placed in the fluorine side and the nitrogen side at exactly the same pressure. The temperature was changed through a wide range, and when thermal equilibrium had been re-established, the manometer levels were compared. In tests involving temperature increases ranging from 400 to 800 deg, the manometer levels were the same (within ±0.05 in.) at the end. Similar results were obtained in tests involving temperature decreases. Also, tests were made in which fluorine was placed opposite nitrogen at the same pressure with the use of the manometer and the temperature was varied in the range 300° to 400°C, where fluorine does not dissociate appreciably (pressure was approximately 0.6 atmos); similar results were obtained. The position of the cylinders in the furnace proved not to be particularly critical.

A general statement of the procedure in each fluorine-dissociation determination follows. Thermal equilibrium having been established at the desired temperature, a fluorine sample in the fluorine side was brought to the pressure of a nitrogen sample in the nitrogen side, and the furnace was cooled to 500°C. The elapse of nearly 3 hours was required for the re-establishment of thermal equilibrium, after which the difference in pressure between the fluorine and the nitrogen was measured. The 3-hour period and the fact that it was possible to decrease the temperature much more rapidly than to increase the temperature were the reasons for cooling rather than heating. Corrections for the reaction between the fluorine and the nickel would have been excessive in the case of heating, whereas the shortness of the high-temperature period together with the absence of reaction at 500°C caused the corrections to be very low in the cooling procedure.

Details of the procedure are as follows. With thermal equilibrium at the desired temperature, the fluorine cylinder was flushed two to four times with fluorine, this manipulation being required as a result of the fact that the water aspirator pump could not reduce the pressure below approximately 0.8 in. of mercury. Valve 4 was kept closed during this manipulation, but fluorine at about 0.75 atmos had been previously placed in the space between the valve and the liquid surface in the manometer. Likewise, nitrogen at about 0.75 atmos had been previously placed in the nitrogen side. Through the use of the Bourdon vacuum gauges, the fluorine pressure in the fluorine cylinder was made approximately equal to the pressure in the nitrogen cylinder. A final pressure equalization was made with the use of the manometer, saturation of the manometer liquid was established, and the rate of pressure change because of the reaction between the fluorine and the nickel was measured (valves 1 and 2 closed, valves 3 and 4 open). The pressure equalization was again made, and with valves 1, 2, 3, and 4 closed, the furnace currents were interrupted. When the temperature had decreased to 500°C, the furnace currents were switched on at the values corresponding to that temperature value.† Time and temperature data were taken during the period of cooling. After thermal equilibrium had been re-established, valves 3 and 4 were opened, and two manometer readings were made between 2 and 6 min afterward. Steady readings were obtained; evidently, the transfer of gas between the two phases in the manometer was slow. The experiments were performed in an air-conditioned laboratory; consequently, the temperature of the manometer liquid varied only slightly.

A constant quantity of nitrogen was maintained in the nitrogen side, with the result that the fluorine-dissociation determinations formed a continuous series. The rates of pressure change due to the reaction of the fluorine with the nickel, corrected as described in the following section, gave points which lay near a smooth curve when the rates were plotted as a function of temperature. Examples of the corrected rates were 0.241 in. of mercury/hr at 842°C and 0.009 in. of mercury/hr at 688°C.

TABLE II. Composition of fluorine supply.

Component	Mole-fraction
F_2	0.983
O_2	0.010
N_2	0.005
HF	0.002

† In two fluorine-dissociation determinations, the temperature decrease was started at a temperature below 500°C.

TABLE III. Equilibrium constant for dissociation of F_2.

Temp., T	Total press	$K=p_F^2/p_{F_2}$	Temp., T	Total press	$K=p_F^2/p_{F_2}$
1115°K	0.831 atmos	7.55×10^{-2} atmos	961°K	0.758 atmos	3.98×10^{-3} atmos
1112	0.829	7.95×10^{-2}	954	0.755	3.9×10^{-3}
1084	0.816	4.77×10^{-2}	921	0.740	2.06×10^{-3}
1082	0.816	4.58×10^{-2}	920	0.739	2.35×10^{-3}
1061	0.804	2.9×10^{-2}	901	0.730	1.29×10^{-3}
1057	0.802	3.0×10^{-2}	897	0.728	1.18×10^{-3}
1032	0.792	1.7×10^{-2}	870	0.714	8.92×10^{-4}
1030	0.791	1.5×10^{-2}	870	0.713	7.70×10^{-4}
1011	0.781	1.2×10^{-2}	850	0.705	4.12×10^{-4}
1010	0.782	1.4×10^{-2}	849	0.702	4.52×10^{-4}
982	0.770	7.1×10^{-3}	760	0.655	2.0×10^{-5}
979	0.765	6.1×10^{-3}	759	0.654	2.4×10^{-5}

TREATMENT OF EXPERIMENTAL RESULTS

In calculating the degree of dissociation, $\alpha=\frac{1}{2}N_F/(N_{F_2}+\frac{1}{2}N_F)$ in which N_F and N_{F_2} are the numbers of moles of F and F_2 present, respectively, account must be taken of (1) the quantity of nitrogen transferred into the nitrogen cylinder from the external part of the nitrogen side because of the temperature decrease, (2) the corresponding quantity of fluorine, (3) the correction for the reaction of the fluorine with the nickel, (4) the degree of dissociation at the lower furnace temperature (500°C), and (5) the mole-fraction of F_2 in the fluorine supply. All these items except (3) are considered in deriving the equation

$$P_N=\frac{1+c_1\alpha+(1+c_1\alpha)c_2}{1+c_1\alpha_c+(1+c_1\alpha_c)(1+c_1\alpha)c_3}P_F, \qquad (1)$$

where P_N = total pressure of nitrogen at lower furnace temperature, P_F = total pressure of fluorine at lower furnace temperature, c_1 = mole-fraction of F_2 in fluorine supply, c_2 = number of moles of nitrogen transferred per mole of nitrogen in nitrogen cylinder at higher furnace temperature, c_3 = number of moles of fluorine transferred per mole of gas in fluorine cylinder at higher furnace temperature, and α_c = degree of dissociation at lower furnace temperature. Equation (1) expresses the proportionality of the pressure and number of moles and can be derived by considering 1 mole of undissociated fluorine from the fluorine supply as a reference quantity. The factor $1+c_1\alpha_c$ corresponds to the dissociation of the fluorine transferred. Solving Eq. (1) for α with the introduction of the relationship $p=P_N-P_F$ gives

$$\alpha=\frac{\left(1+\frac{p}{P_F}\right)(1+c_1\alpha_c)\frac{1+c_3}{1+c_2}-1}{c_1\left[1-\left(1+\frac{p}{P_F}\right)\frac{c_3(1+c_1\alpha_c)}{1+c_2}\right]}. \qquad (2)$$

Through the perfect-gas law, the quantities c_2 and c_3 are each calculated from the total pressure, the volume of the external part of the nitrogen side or fluorine side, and the room temperature, each item taken before and after the temperature decrease, and also the volume of the cylinder and the higher furnace temperature. In every calculation involving total pressure, an average value from the two Bourdon gauges is employed, the manometer reading being taken into account where the pressures are different. The volume of the external part when the manometer levels were equal was determined gasometrically with the use of the following equation, derived from the perfect-gas law:

$$P_2/P_3=T_2(VT_1+vT_3)/T_3(VT_1+vT_2), \qquad (3)$$

in which P_2 = total pressure at furnace temperature T_2, P_3 = total pressure at furnace temperature T_3, V = volume of cylinder, v = volume of external part, and T_1 = room temperature. The volume of each cylinder, calculated geometrically, is 14.28 cu in.; the average value of the volume of the external part with the manometer levels equal is 3.07 cu in. A volume correction is made for the displacement of liquid in the manometer.

The rates of pressure change due to the reaction of the fluorine with the nickel are applied in corrections to the values of p and P_F, which are identified with the lower furnace temperature. Therefore, the rates are corrected for temperature decrease; Eq. (3) is used in determining the corrections for the rates. The rates are not corrected for dissociation. An arithmetic-integration process is employed in calculating the corrections to be applied to the values of p and P_F. None of these corrections exceeds 4 percent of the value of p.

The degree of dissociation at the lower furnace temperature was found experimentally. This quantity could have been made effectively zero by selecting a somewhat lower value for the lower furnace temperature, but c_2 and c_3 would have been larger. The selection of 500°C represented a compromise.

The composition of the fluorine supply was determined by the "precision analysis" of Kimball and Tufts[10] and is given in Table II. The experimental re-

[10] R. H. Kimball and L. E. Tufts, *The Complete Analysis of Fluorine Gas*, U. S. Atomic Energy Commission Declassified Document MDDC-195 (Office of Technical Services, Publication Board No. 52708, Washington, July 11, 1946).

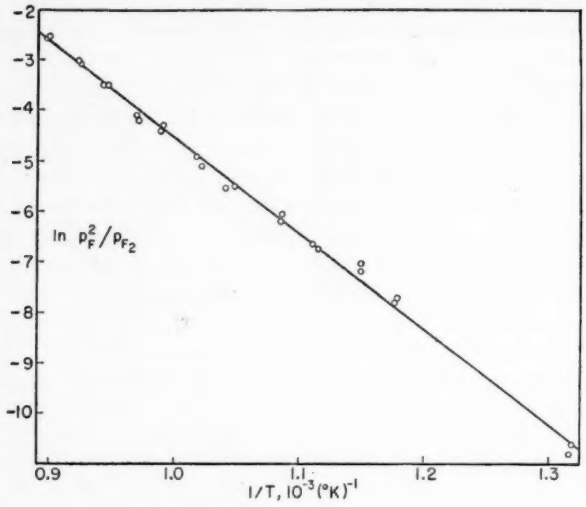

FIG. 2. Dissociation of F_2.

sults are treated as though the O_2, N_2, and HF underwent no chemical change in the experiments. Thermodynamic relationships[11] show that O_2 does not combine with F_2 at the temperatures and pressures of the fluorine-dissociation determinations. Possibly N_2 reacts with F_2 under these conditions, but the error introduced would be very small. It is clear that HF is inert under these conditions.

Table III gives the values obtained for the equilibrium constant. In Fig. 2, showing $\ln K$ as a function of $1/T$, the best straight line‡ according to the method of least squares is given. The slope is $-(19.0\pm0.2)10^3$ deg. The limits of error stated are the probable error due to random errors in $\ln K$. This slope gives $\Delta H=37.7\pm0.4$ kcal/mole as the mean heat of dissociation in the temperature range 759° to 1115°K for the reaction F_2 $(g)\rightarrow 2F$ (g). The value of $\ln K$ at 1000°K obtained from the line, -4.5, together with the standard entropy values[12] for F_2 and 2F at 1000°K, 58.50 and 88.58 cal/deg, respectively, results in $\Delta H=39.0$ kcal/mole. At 900°K, $\ln K=-6.6$, $S_{F_2}{}^0=57.57$ cal/deg, $S_{2F}{}^0=87.52$ cal/deg, and $\Delta H=38.8$ kcal/mole.

DISCUSSION AND CONCLUSIONS

It does not appear possible to explain the observations on the basis of an equilibrium in which a fluoride of nickel decomposes with the production of fluorine since NiF_2 is the only compound of nickel and fluorine according to Emeléus,[13] and NiF_2 is an exceedingly stable compound.[14] Likewise it is improbable that the observations are caused by an adsorption phenomenon since heat of adsorption varies markedly with amount adsorbed in practically all cases,[15] and a curved line results when $\ln K$ is plotted as a function of $1/T$. The experiments reported in the present paper lead to the conclusion that the heat of dissociation of F_2 in the region of 900°K, expressed to two significant figures, is 38 kcal/mole.

ACKNOWLEDGMENTS

The author expresses his appreciation to Mr. Howard F. Keller, Jr., and Mrs. Lois L. Taylor, who analyzed the fluorine, and to Professor Don M. Yost and Mr. Wilmer A. Jenkins II, who reviewed the manuscript.

[11] W. M. Latimer, *The Oxidation States of the Elements and their Potentials in Aqueous Solutions* (Prentice-Hall, Inc., New York, 1938), p. 46.

‡ The difference between the calculated enthalpy increase of 2F for the temperature range 759° to 1115°K and the corresponding increase of F_2 is about 0.5 kcal.

[12] Data calculated by L. G. Cole, M. Farber, and G. W. Elverum, Jr., of this laboratory, included in a paper to be published in J. Chem. Phys.

[13] J. H. Simons, editor, *Fluorine Chemistry* (Academic Press, Inc., New York, 1950), Vol. 1, p. 68.

[14] F. R. Bichowsky and F. D. Rossini, *The Thermochemistry of the Chemical Substances* (Reinhold Publishing Corporation, New York, 1936).

[15] G. Schwab, *Catalysis*, translated by H. S. Taylor and R. Spence (D. Van Nostrand Company, Inc., New York, 1937), pp. 194 to 204.

Far U.V. Spectra of Peptides*

JOE S. HAM AND J. R. PLATT
Department of Physics, University of Chicago, Chicago, Illinois
(Received October 2, 1951)

The spectra of diglycyl, triglycyl, and glycine anhydride have been extended to 1800A in water solution. The peak observed near 1850A is attributed to an almost additive absorption by the −CONH− groups. The oscillator strength f is 0.27±0.07 per peptide group.

GOLDFARB, Saidel, and Mosovich[1] found steeply rising absorption in proteins and simple peptides below 2200A, with intensity approximately proportional to the number of peptide links present. (Fig. 2). They identified this as the long wavelength side of a characteristic peptide electronic transition.

We have now checked their curves for diglycyl and triglycyl and have extended the curves to 1800A in water solution in an 0.13-mm cell, using the fluorite vacuum spectrograph and techniques described earlier.[2] We also obtained the spectrum of glycine anhydride (2,5-diketopiperazine), which has two peptide groups in a six-membered ring. The curves are given in Fig. 1. Diglycyl shows a broad maximum below 1900A, with molar extinction about 7000. This becomes a true peak, with a sharper and more certain maximum at about 1850A in the other compounds.

In Fig. 1 the −CONH− spectra are compared with the spectra of the acid chromophore, −COOH, and the amide chromophore, $-CONH_2$. The peptide group, −CONH−, is a substituted amide and shows the typical red shift from substitution. In accordance with the usual rules,[3] the red shift is larger for the strong $\pi-\pi$ transition with ϵ about 10,000, which we shall designate as $^1A-{}^1B$, than for the weak $n-\pi$ transition near 2100A with ϵ about 100, which we shall designate as $^1A-{}^1U$. As a result, the latter transition, which must still be present in the peptide group, becomes quite concealed by the encroachment of its intense neighbor. The $^1A-{}^1U$ transition can be seen most clearly in the isoelectronic spectrum of the acid, −COOH, where the separation between the $\pi-\pi$ and the $n-\pi$ transitions is greater. According to Saidel and Goldfarb,[4] a long wavelength shoulder can be seen in the spectrum of a 0.01N HCl solution of acetylglycine; which must be this $n-\pi$ transition. Low temperature studies on the peptides might permit resolution of the $n-\pi$ and $\pi-\pi$ transitions.

The system of four π-electrons of the planar −CONH− group makes it isoconjugate with the butadiene group, C=C−C=C, or the acrolein group, C=C−C=O. The strong $^1A-{}^1B$ absorption peak is at shorter wavelengths than the similar peaks for these latter compounds, which lie near 2200A, because of the shortening of the conjugated system with consequent increase in the energy spacing of the π-orbitals.

The absorption per peptide link is plotted in Fig. 2. It is the same for diglycyl as for triglycyl within our experimental uncertainty of about 10 percent. This shows that no conjugation is present in the latter compound and that hyperconjugation of the two peptide groups across the intervening saturated carbon is negligible, at least so far as the spectra are concerned. It might be supposed that the hyperconjugation, if present, would be cumulative with increasing numbers of such groups joined in the same way, as was found for hyperconjugated arachidonic acid (four double bonds),[5] and therefore would be easier to detect in large polypeptides. Goldfarb, Saidel, and Mosovich[1] did find that the absorption per peptide group at a fixed wavelength was not quite the same for the first few polypeptides as for the higher ones, but there was little or no evidence for hyperconjugation. The absorption "per peptide link"

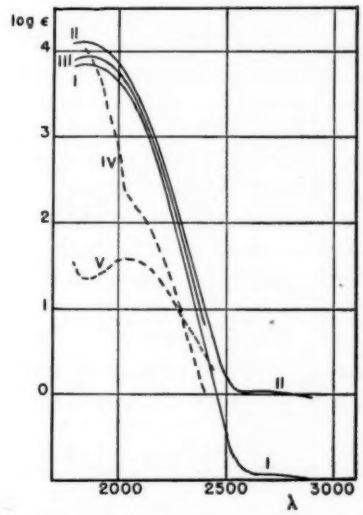

FIG. 1. Absorption of diglycyl (I) (one peptide link) (Beckman data to 2900A on di- and triglycyl furnished by courtesy of Dr. L. J. Saidel and Dr. A. R. Goldfarb); triglycyl (II) (two peptide links); glycine anhydride (III) (two links in a ring); the amide group (IV) [H. Ley and B. Arends, Z. Physik. Chem. **B17**, 177 (1932); W. Herold, Z. physik. Chem. **B18**, 265 (1932)]; and the acid group (V) (see reference 5).

* This work was assisted in part by the ONR under Task Order IX of Contract N6-ori20 with the University of Chicago.

[1] A. R. Goldfarb and L. J. Saidel, Science **114**, 156 (1951); Goldfarb, Saidel, and Mesovich, J. Biol. Chem. (to be published).

[2] L. E. Jacobs and J. R. Platt, J. Chem. Phys. **16**, 1137 (1948).

[3] J. R. Platt, J. Chem. Phys. **19**, 101 (1951).

[4] Private communication.

[5] Rusoff, Platt, Klevens, and Burr, J. Am. Chem. Soc. **67**, 673 (1945).

for bovine serum albumin with about 580 such links is given from their curves in Fig. 2. It is not much higher than the diglycyl curve, and the additional absorption is about what would be expected from the phenyl-chromophores present in several percent of the amino-acid residues in the native protein.

Of course, the apparent absence of hyperconjugation in the spectra does not rule out its possible contribution to the observed photochemical and biochemical energy transfers in proteins.[6]

The oscillator strength of the $^1A-{}^1B$ transition for each $-CONH-$ group is about $f=0.27\pm0.07$ from the area under the two top curves in Fig. 2, extrapolating these curves to zero at 1600A. For the glycyl anhydride, this drops to $f=0.19\pm0.05$. These figures compare with oscillator strengths of about $f=0.30$ for the $^1A-{}^1B$ transition of the C=C bond[7] which is a smaller conjugated system, and about $f=0.60$ for the similar transition of the C=C−C≡C group[2] which is larger.

A certain amount of twist of the $-\underset{\underset{H}{|}}{N}-$ group out of the $-CON-$ plane may be produced in the glycine anhydride,

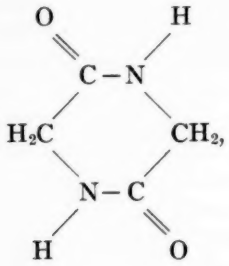

by ring formation. This may partially account for the loss of intensity near 1850A in this compound compared to the chain dipeptide, triglycyl; there is a similar loss of intensity in cyclohexene compared with a chain ethylene.[7] It is somewhat peculiar that the loss of intensity in the anhydride, regardless of its explanation, is not associated with any shift in the peak position or any conspicuous change in the shape of the curve.

The absorption of proteins in the quartz ultraviolet, at wavelengths longer than about 2200A, has been discussed by Rideal and Roberts,[6] Anslow,[8] and others,[9] and by Beaven, Holiday, and Jope.[10] Curve I of Fig. 1 shows the correctness of the conclusion reached by Beaven and co-workers, that the peptide link has negligible absorption to the red of 2500A. (Probably the increased absorption in curve II is caused by an impurity.)

What absorption diglycyl does have in this region may be the orbitally-allowed singlet-triplet transition, $^1A-{}^3B$, corresponding to the allowed 1850A singlet-singlet transition. The intensity and position are about right for such an interpretation, and it might account for the photochemical effects noted at 2537A by Rideal and Roberts. This absorption is too weak by a factor of

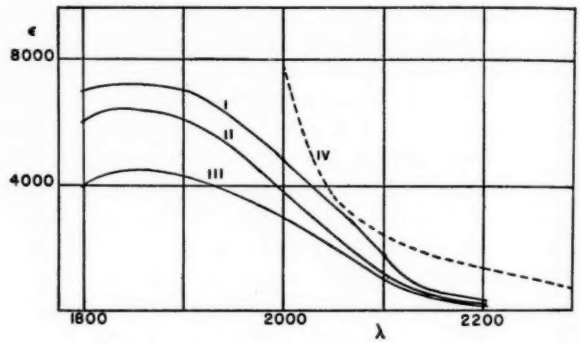

FIG. 2. Absorption per peptide link for different molecules: diglycyl (I), triglycyl (II), glycine anhydride (III), and bovine serum albumin (IV) (see reference 1).

100 to be the singlet-singlet $n-\pi$ transition of a keto (compare acetone) or lactam group.

The far ultraviolet spectrum of glycine itself and of several other important amino acids have been measured in this laboratory and are being prepared for publication.[11]

The samples of di- and triglycyl were kindly supplied by Dr. A. R. Goldfarb. We are indebted to him and to Dr. L. J. Saidel for showing us their manuscript and other results in advance of publication. The glycine anhydride was an Eastman Kodak Company White Label Product.

[6] E. K. Rideal and R. Roberts, Proc. Roy. Soc. (London), **205A**, 391 (1951).
[7] Platt, Klevens, and Price, J. Chem. Phys. **17**, 466 (1949).
[8] G. A. Anslow, Disc. Faraday Soc. **9**, 299 (1951).
[9] See reference 8, pp. 332–4.
[10] Beaven, Holiday, and Jope, Disc. Faraday Soc. **9**, 406 (1951).
[11] H. B. Klevens and J. R. Platt (to be published).

Letters to the Editor

THIS section will accept reports of new work, provided these are terse and contain few figures, and especially few half-tone cuts. The Editorial Board will not hold itself responsible for opinions expressed by the correspondents. Contributions to this section should not exceed 600 words in length and must reach the office of the Editor not later than the 15th of the second month preceding that of the issue in which the letter is to appear. No proof will be sent to the authors. A publication charge of $10.00 per Letter is made which, when honored, will entitle the Institution to 100 free reprints.

Intermolecular Forces in CF_4 and SF_6

J. S. ROWLINSON
Department of Chemistry, The University of Manchester, England
(Received November 12, 1951)

IN their physical properties the perfluorocarbons resemble the hydrocarbons more closely than they do the corresponding chlorine compounds. Too little is known of the forces between polyatomic molecules to give any quantitative explanation of this. The calculations made in this note suggest, though, that one reason for the weakness of the forces between fluorocarbons is the fact that, even for spherically symmetrical molecules, the forces act through points well removed from the centers of the molecules.

It is not strictly accurate to assume that the energy between two molecules AX_n may be found by superimposing the $(n+1)^2$ potentials of the interactions of the $2(n+1)$ atoms, but no better approximation has been suggested. Let the energy between any two atoms be of the form proposed by Lennard-Jones,

$$E(r)=4\epsilon[(d/r)^{12}-(d/r)^6]=\epsilon[(r_{\min}/r)^{12}-2(r_{\min}/r)^6], \quad (1)$$

where $E(d)=0$, $E(r_{\min})=-\epsilon$, and $r_{\min}^6=2d^6$. The mean energy between two AX_n molecules could be found by averaging over-all orientations the $(n+1)^2$ potentials of this form. Corner[1] has used such a method to calculate the second virial coefficients of ellipsoidal molecules which have four interacting centers in a row. A more simple averaging is used here. Let the model of the AX_n molecule be a point center (A atom) surrounded by a spherical surface (nX atoms) whose radius, a, is the $A-X$ bond length. To calculate the energy between two such surfaces, between all parts of which there is a potential given by Eq. (1), divide the surfaces into annuli of uniform area whose centers lie on the line joining the centers of the molecules. Now replace each annulus by its center and so calculate the total potential between the surfaces. This averaging gives an energy which still has spherical symmetry, and represents, in the simplest way, the effect of the "spreading" of the interaction centers in a polyatomic molecule. (The integrations resemble those used by Lennard-Jones and Devonshire[2] in their cell theory of liquids.) The results are to insert coefficients $\rho(12)$ and $\rho(6)$ before the $(d/r)^{12}$ and $(d/r)^6$ terms in Eq. (1).

(a) interaction of two spherical surfaces

$$\rho(n)=[(1-2\alpha)^{-n+2}+(1+2\alpha)^{-n+2}-2]/4n(n-1)\alpha^2. \quad (2)$$

(b) interaction of a point with a surface

$$\rho(n)=[(1-\alpha)^{-n+1}-(1+\alpha)^{-n+1}]/2(n-1)\alpha, \quad (3)$$

where $\alpha=a/r$. As the coefficients ρ are themselves functions of r, the energy is no longer a simple (12:6) potential, but the change in shape is small.

Equations (2) and (3) enable the forces between two AX_n molecules to be found from the X,X, and the A,X, and the A,A interatomic forces. This may be tested by comparison with the recent determination by MacCormack and Schneider[3] of the intermolecular potentials of CF_4 and SF_6. The C–F and S–F bond lengths in these molecules are[4] 1.36A and 1.58A. The energy between F atoms may be found from the viscosity of F_2. It has been shown[5] that the apparent constants of Eq. (1), assuming F_2 is spherical, are $d=3.65$A and $\epsilon/k=112$°K. Comparison with similar results for N_2 shows that the same parameters are found from both viscosity and virial coefficient measurements, and so Corner's[1] tables may be used to deduce the F, F atom interaction from these figures. The F–F bond length is[4] 1.44A. This gives $d=3.29$A and $\epsilon/k=32.0$°K, per pair of F atoms. These parameters are also used for the C and S atoms whose contributions are less important. The results are shown in Table I. The calculation shows that the effective F, F energies are only the fractions 0.24 in CF_4, and 0.18 in SF_6, of those in elementary F_2. There is no "adjustable constant" in this calculation.

TABLE I.

	$r_{\min}$ (A)		ϵ/k (°K)	
	CF_4	SF_6	CF_4	SF_6
Experimental[a]	5.39	6.17	153	201
Calculated	5.53	6.05	178	269
Error	3%	−2%	16%	34%

[a] See reference 3.

The agreement is excellent for $r_{\min}$, but the calculated energies are rather too large. There is good reason for this, apart from the approximations already made. The experimental values are for a (12:6) potential. In the modified potential used here, the effective repulsion index is about 15. Buckingham[6] has shown that, for argon, the ϵ/k for a (14:6) potential is 14 percent higher than for a (12:6) potential, when both are fitted to the same experimental results. The distances are less sensitive. It may be concluded, therefore, that the intermolecular potentials of CF_4 and SF_6 are consistent with the known forces between F atoms.

Probably the forces between CH_4 molecules are more truly central than for CF_4, as the polarizable electrons are all on the C atom or in the C–H bonds. The energy will therefore not be weakened as in CF_4. This would explain why CH_4 and CF_4 are more alike than are H_2 and F_2.

[1] J. Corner, Proc. Roy. Soc. (London) **A192**, 275 (1948).
[2] J. E. Lennard-Jones and A. F. Devonshire, Proc. Roy. Soc. (London) **A163**, 53 (1937), Eq. (37).
[3] K. E. MacCormack and W. G. Schneider, J. Chem. Phys. **19**, 849 (1951).
[4] See P. W. Allen and L. E. Sutton, Acta Cryst. **3**, 46 (1950).
[5] Hirschfelder, Curtiss, Bird, and Spotz, University of Wisconsin CF-1507 (revised, 17th April, 1951).
[6] See R. H. Fowler and E. A. Guggenheim, *Statistical Thermodynamics* (Columbia University Press, New York, 1939), p. 285.

Potential Constants and Thermodynamic Properties of Ozone*

FORREST F. CLEVELAND
Spectroscopy Laboratory, Department of Physics
AND
MORTON J. KLEIN
Department of Chemistry, Illinois Institute of Technology, Chicago 16, Illinois
(Received November 14, 1951)

IN a previous note,[1] potential (force) constants and thermodynamic properties, calculated with $d=$O–O$=1.26$A and $\alpha=$O–O–O$=127°$, were given. These results indicated that a 3 constant potential energy function ($f_{d\alpha}=0$) was a good approximation for ozone.

Recent microwave work,[2] however, shows that $d=1.276$–1.279A and $\alpha=116.5$–$117.0°$. Accordingly, we have recalculated the potential constants and thermodynamic properties, taking $d=1.2775$A and $\alpha=116.75°$. With these, it is no longer possible to use a 3 constant potential function with $f_{d\alpha}=0$, since this leads to imaginary roots. Consequently, it is necessary to assume reasonable values of f_{dd}/f_d and calculate sets of values of all 4 potential constants. The results are given in Table I, and are shown graphically in Fig. 1. (The values of f_α and $f_{d\alpha}$, obtained with

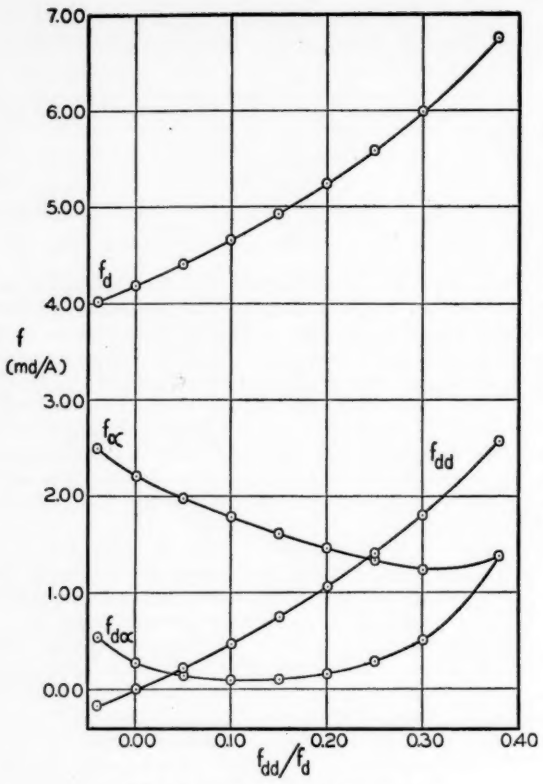

FIG. 1. Potential constants for ozone.

the 2nd root of the quadratic equation, seemed unreasonably large, and were, therefore, not included in Table I.)

The values for $f_{dd}/f_d=0.15$ may be adopted since they seem reasonable in comparison with the results for other molecules. They are:

$$f_d=4.92, \qquad f_\alpha=1.60,$$
$$f_{dd}=0.739, \quad \text{and} \quad f_{d\alpha}=0.095md/A.$$

This choice is somewhat arbitrary, however, since a unique set cannot be determined unless it becomes possible to obtain data for an isotopic molecule. (For comparison the values obtained previously[1] were 4.64, 1.70, 0.695, and 0.002, respectively.)

The product ABC of the 3 principal moments of inertia, calculated from the new bond distance and interbond angle values, is

$$(70.816)(62.869)(7.946)10^{-120}\ \text{g cm}^2$$
$$=(42.651)(37.865)(4.786)\ \text{Awu}A^2=7729.3\ \text{Awu}^3A^6.$$

This 28 percent increase in ABC makes it necessary to add 0.25 cal deg^{-1} M^{-1} to each of the previously given[1] free energy and entropy values. (The heat content and heat capacity values are unchanged.) The revised values are given in Table II. Following

TABLE I. Potential constants for ozone (O_3).

f_{dd}/f_d	f_d	f_α	f_{dd}	$f_{d\alpha}$
−0.04[a]	[b]4.02_{44}	2.49_{20}	-0.160_{98}	0.541_{04}
0.00	4.18_{83}	2.20_{20}	0.000_{00}	0.274_{71}
0.05	4.40_{87}	1.96_{88}	0.220_{29}	0.146_{02}
0.10	4.65_{03}	1.77_{56}	0.465_{03}	0.0932_{69}
0.15[c]	4.92_{37}	1.60_{42}	0.738_{56}	0.0954_{83}
0.20	5.23_{17}	1.45_{15}	1.04_{63}	0.153_{13}
0.25	5.58_{05}	1.32_{18}	1.39_{51}	0.277_{87}
0.30	5.97_{88}	1.23_{01}	1.79_{36}	0.498_{05}
0.38[a]	6.75_{04}	1.36_{99}	2.56_{32}	1.35_{92}

[a] If f_{dd}/f_d is less than −0.04 or greater than 0.38, imaginary values of f_α and $f_{d\alpha}$ are obtained.
[b] The units are md/A.
[c] Adopted values.

TABLE II. Heat content, free energy, entropy, and heat capacity of ozone for the ideal gaseous state at 1-atmos pressure.

T(°K)	$(H°-E_0°)/T$	$-(F°-E_0°)/T$	$S°$	$C_p°$
100	[a]7.95	40.01	47.95	7.95
200	8.02	45.53	53.55	8.38
273.16	8.21	48.05	56.26	9.10
298.16	8.30	48.78	57.07	9.37
300	8.30	48.83	57.13	9.39
400	8.71	51.27	59.98	10.44
500	9.14	53.26	62.40	11.26
600	9.55	54.96	64.51	11.87
700	9.91	56.46	66.37	12.30
800	10.23	57.81	68.04	12.62
900	10.51	59.03	69.54	12.86
1000	10.75	60.15	70.90	13.04

[a] Cal deg^{-1} M^{-1}.

the suggestion of Pennington and Kobe,[3] values were calculated for the ice-point (273.16°K), in addition to the previous temperatures.

* Supported in part by Office of Ordnance Research Contract DA-11-022-ORD-464.

[1] Klein, Cleveland, and Meister, J. Chem. Phys. **19**, 1068 (1951).
[2] R. H. Hughes, Bull. Am. Phys. Soc. **26**, 21, No. 6 (1951).
[3] R. E. Pennington and K. A. Kobe, J. Chem. Phys. **19**, 510 (1951).

Hydrogen Redistribution During Olefin Hydrogenation

C. D. WAGNER, J. N. WILSON, J. W. OTVOS, AND D. P. STEVENSON
Shell Development Company, Emeryville, California
(Received November 20, 1951)

IT has been recognized for some time that hydrogen-exchange between olefin and hydrogen may occur during the metal-catalyzed hydrogenation of olefins.[1] It is known also that catalyzed exchange between paraffin hydrocarbons and hydrogen occurs at temperatures above 50°–100°C.[2] We have recently found, even under conditions where no exchange takes place either between hydrogen and olefin or between hydrogen and paraffin, that the product of a reaction between olefin and deuterium contains several deuterated paraffin species with more than two deuterium atoms per molecule. This result indicates a type of exchange, hitherto not reported, involving migrations of hydrogen atoms among adsorbed hydrocarbon residues. Therefore, to prove that simple addition of deuterium to a double bond has occurred in the synthesis of a deuterated compound, it is not sufficient to show that unreacted olefin is undeuterated and that only the stoichiometric amount of deuterium has been taken up by the olefin.

The distribution of isotopic species obtained with a nickel catalyst (Harshaw No. 78) and *cis*-2-butene with 10 volumes of deuterium at −78°C is shown in Fig. 1. These results were obtained from mass-spectrometric analysis using low energy ionizing electrons. No hydrogen appeared in the deuterium gas during this experiment. (In a separate experiment using butene, hydrogen, and *n*-butane-1-*d*, the absence of butane-d_2 and HD in the products proved that paraffin molecules are inert under these conditions.) The relative amounts of all the observed species (Fig. 1), with the exception of d_2, correspond to those calculated for random distribution among molecules with an average empirical formula of $C_4H_8D_2$. The calculated mole fractions are: $d_0=F(0.8)^{10}$, $d_1=10F(0.8)^9(0.2)$, $d_2=45F(0.8)^8(0.2)^2$, etc., where F is the fraction of butane molecules whose hydrogens have been redistributed. The values of d_i for $F=0.92$ are shown by the dotted line in Fig. 1. A possible mechanism for attaining such a distribution is discussed below. The excess d_2 species that is observed probably arises from the simple addition of deuterium to the double bond by a second mechanism.

A mechanism that explains the observed distribution is the following: There are two distinct reactions on the catalyst.

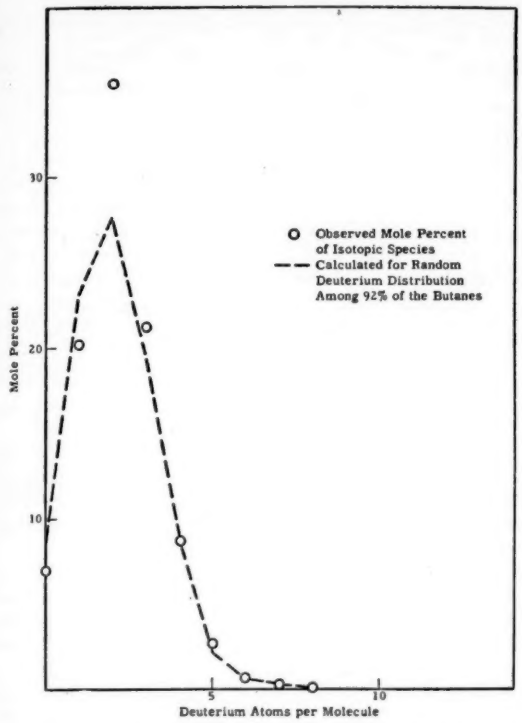

FIG. 1. Distribution of isotopic species from the reaction of *cis*-2-butene with deuterium over nickel at −78°.

(1) Deuterium is adsorbed, it dissociates, reassociates, and is desorbed. (This was shown in a separate experiment in which butene was hydrogenated with a mixture of H_2 and D_2, and HD was produced.) (2) An olefin molecule is irreversibly adsorbed, taking a deuterium atom from (1) and becoming an alkyl radical. Occasionally one of a group of alkyl radicals on the surface acquires an extra hydrogen (or deuterium) atom from a neighboring radical and escapes as alkane. The free valence left on the neighboring radical then diffuses among the remaining radicals by transfer of hydrogen (or deuterium) atoms, until finally it is satisfied by acquiring a deuterium atom from (1). This provides an exchange mechanism and also provides for the reaction of two deuterium atoms per molecule of alkane formed. At the steady state the atom-fraction of deuterium in the hydrogen in the alkyl pool should be $2/2n+2$, where n is the carbon number; the alkanes leaving this pool will have this average deuterium content but will be distributed over a range of isotopic compositions because of the exchange reaction. It is required that no hydrogens (or deuteriums) from (2) exchange with deuterium atoms from (1); deviations from this condition occur at higher temperatures.

The second mechanism, involving direction addition, probably occurs on different catalyst sites. The fraction of *cis*-2-butene molecules reacting in this way at −78°C is $(1-F)$ or 0.08, in terms of the foregoing example. Direct addition was found to be more important with isobutylene over nickel at −78°C (95 percent d_2 formed) and with ethylene over platinum at −20°C (70 percent d_2 formed). At the higher temperatures we have found small amounts of olefin-d_1 in the products, indicating that still another mechanism is operating.

The first mechanism, involving transfer of hydrogens among alkyl radicals, provides an explanation for the observations of Turkevich, *et al.*[3] who found in the reaction of ethylene with deuterium over nickel at 90°C significant amounts of ethane-d_0 and ethane-d_1 in the initial products.

Our results show that the olefin hydrogenation reaction is complex and cannot be satisfactorily represented by any one of the recently discussed processes alone.[4–7] These observations extend and amplify the mechanisms proposed by Beeck.[8]

[1] Farkas, Farkas, and Rideal, Proc. Roy. Soc. (London) **A146**, 630 (1934).
[2] Morikawa, Benedict, and Taylor, J. Am. Chem. Soc. **58**, 1795 (1936).
[3] Turkevich, Bonner, Schissler, and Irsa, Trans. Faraday Soc. 352 (1950).
[4] K. J. Laidler, Disc. Faraday Soc. 47 (1950).
[5] D. D. Eley, Disc. Faraday Soc. 99 (1950).
[6] G. H. Twigg, Disc. Faraday Soc. 152 (1950).
[7] Eyring, Colburn, and Zwolinski, Disc. Faraday Soc. 39 (1950).
[8] O. Beeck, Revs. Modern Phys. **17**, 61 (1945); Trans. Faraday Soc. 118 (1950).

Carrier-Free Radioisotopes from Cyclotron Targets. XXV. Preparation and Isolation of $Au^{195, 196, 198, 199}$ from Platinum*

JEANNE D. GILE, WARREN M. GARRISON, AND JOSEPH G. HAMILTON
Crocker Laboratory, Radiation Laboratory, Divisions of Experimental Medicine, Radiology, and Medical Physics, University of California, Berkeley and San Francisco, California
(Received November 16, 1951)

RADIOACTIVE gold, produced by bombardment of platinum with 19-Mev deuterons, has been isolated without added isotopic carrier. Four known long-lived radioisotopes of gold[1] are produced by (d, n) and $(d, 2n)$ reactions with deuterons of this energy: 180-day Au^{195}, 5.6-day Au^{196}, 2.7-day Au^{198}, and 3.3-day Au^{199}. The shorter-lived activities (Au^{193} and Au^{194}) were allowed to decay out prior to chemical separation. Other possible concurrent reactions include formation of radioisotopes of platinum by (d, p) reactions and radioisotopes of iridium by (n, p) reactions. The carrier-free radiogold was separated from the target material and from possible radioisotopes of iridium by a solvent extraction method using ethyl ether.

Five 1-mil foils of C.P. platinum[2] were clamped to a water-cooled copper target plate and bombarded with 19-Mev deuterons for a total of 20 microampere hours at an average beam intensity of 10 microamperes, in the 60-in. cyclotron at Crocker Laboratory. The bombarded foils were dissolved in a minimum volume of aqua-regia. Twelve N HCl was added to destroy excess HNO_3, the solution was diluted to approximately 15 ml of 3 N HCl, and the radiogold was extracted with ethyl ether which had previously been saturated with 3 N HCl. Four extractions with ethyl ether were needed to remove most of the radiogold from the aqueous phase. The ether layer was washed with 6 N HCl and the activity was quantitatively retained in the organic layer. Fifty milligrams of NaCl were added to the ether phase and the mixture was evaporated to 1 ml on a steam bath. The carrier-free radiogold plus the NaCl was diluted to 5 ml to give an isotonic saline solution for subsequent biological investigations.

The radiogold was identified by half-life determinations, absorption measurements, and by a chemical separation procedure using carriers. The decay was followed for 60 days and showed an initial composite half-period of approximately 3.5 days, presumably due to $Au^{198, 199}$. Four days after chemical separation the decay curve showed mainly the 5.6-day period of Au^{196}.[3] After 15 days the curve began to lengthen perceptibly and 25 days after chemical separation the activity showed only the 180-day period, which was presumably Au^{195}.[3] Aluminum and lead absorption measurements 6 days after bombardment showed the approximately 0.43-Mev beta-particle and the 0.37-Mev gamma-ray previously reported[4] for Au^{196}. An aliquot of the solution was added to a solution containing carrier amounts of Ir, Pt, and Au. The radioactivity was quantitatively recovered in the Au fraction following chemical separation.

We wish to thank Professor G. T. Seaborg for helpful suggestions, the crew of the 60-in. cyclotron at Crocker Laboratory for bombardments, and Miss Margaret Gee for assistance in counting.

* This document is based on work performed under Contract No. W-7405-eng-48-A for the AEC.
[1] G. T. Seaborg and I. Perlman, Revs. Modern Phys. **20**, 585 (1948).
[2] Spect. pure platinum—less than 0.01 percent gold.
[3] Nuclear Data, National Bureau of Standards Circular 499 (September, 1950).
[4] G. Wilkinson, Phys. Rev. **75**, 1019 (1949).

The Explosive Reaction of Carbon Monoxide and Oxygen at the Second Explosion Limit in Quartz Vessels

ALVIN S. GORDON
USNOTS, China Lake, California
(Received October 29, 1951)

KOPP, Kowalsky, Sagulin, and Semenoff[1] have studied this reaction in the presence of water vapor in a flowing system; Hadman, Thompson, and Hinshelwood[2] have studied it with carefully dried gases in a static system. Both teams used quartz reaction vessels. The latter investigators could not get the mixture to explode by the usual method of loading the gases above the second limit and then evacuating the mixture until it crossed the second limit. They had to resort to less satisfactory methods to get their data.

In the present work the furnace was put on a track so that it could be lowered and the reaction vessel exposed. The premixed composition of carbon monoxide-oxygen and sometimes other gases were added to the cooled quartz reaction sphere and the furnace then brought rapidly up around the vessel. This system brought the reaction vessel to explosion temperature in one to two minutes. Air was forced over the surface of the vessel while it was being heated until there was no temperature gradient from the top to the bottom of the vessel. The air was then turned off; as soon as the explosion was noted by the violent kick of the quartz spiral gauge and a simultaneous flash of light the temperature at the top and bottom of the vessel was read to make certain that there was no appreciable gradient. Mercury vapor was excluded from the reaction vessel by employing a quartz spiral pressure gauge and by forcing all gases to pass over a gold leaf trap before entering the reaction vessel. The gases were dried by liquid nitrogen. The mass spectrometer was unable to detect any i-m purity in the CO and a total impurity of about 0.5 percent ($A+N_2$) in the O_2.

Hadman, Thompson, and Hinshelwood[2] claimed that they found no surface dependence in their work, but the results of this work which are plotted in Fig. 1 show quite a pronounced effect of surface. To get reproducible results in this work it was necessary to precondition the surface at the beginning of the day by making about three runs at 350–400-mm pressure. The vessels were then fairly reproducible as long as there was at least one explosion in the vessel every ½ hour. When the surface was reproducible, pretreating the surface with CO_2, CO, or O_2 had no appreciable effect on the explosion temperature.

TABLE I. Effect of added inerts on explosion temperature.

Comp.: 2CO:1O Texp. C.	Pexp. (total)	Bulb radius = 2.89 cm Percent CO_2 added
765	251.8	0
748	251.0	2.8
749	269.2	5.8
760	259.8	9.2
Comp.: 1CO:2O₂ **Texp. C.**	**Pexp. (total)**	**Bulb radius = 1.89 cm Percent CO_2 added**
791	330.4	0
780	325.6	3.1
784.5	309.5	10.7
795.5	300.4	20.3
Comp.: 4CO:1O₂ **Texp. C.**	**Pexp. (total)**	**Bulb radius = 2.89 cm Percent N_2 added**
797	292	0
772.5	278.5	11.1
765.5	300.8	18.0

The graphical results show a striking dependence on the presence of water in contrast to the results of Hadman, Thompson, and Hinshelwood. When as little as 0.33 percent of water is added to the explosion mixture, the explosion temperature is decreased by about 100°C. Larger addition of water vapor lowers the explosion temperature further, but the additional effect is minor compared to the original. It is interesting to note in Fig. 1 that the explosion temperature does not change with the pressure over a range of pressure with certain $CO-O_2-H_2O$ compositions.

In the presence of water vapor, increase of S/V increases the explosion temperature as it does with the dry gases.

The results in Table I show that up to more than 10 percent of CO_2 in the mixture of CO and O_2 lowers the explosion temperature and the presence of up to 18 percent of N_2 in the mixture also lowers the explosion temperature.

As previously noted, Hadman, Thompson, and Hinshelwood did not observe explosion of carbon monoxide-oxygen mixtures when

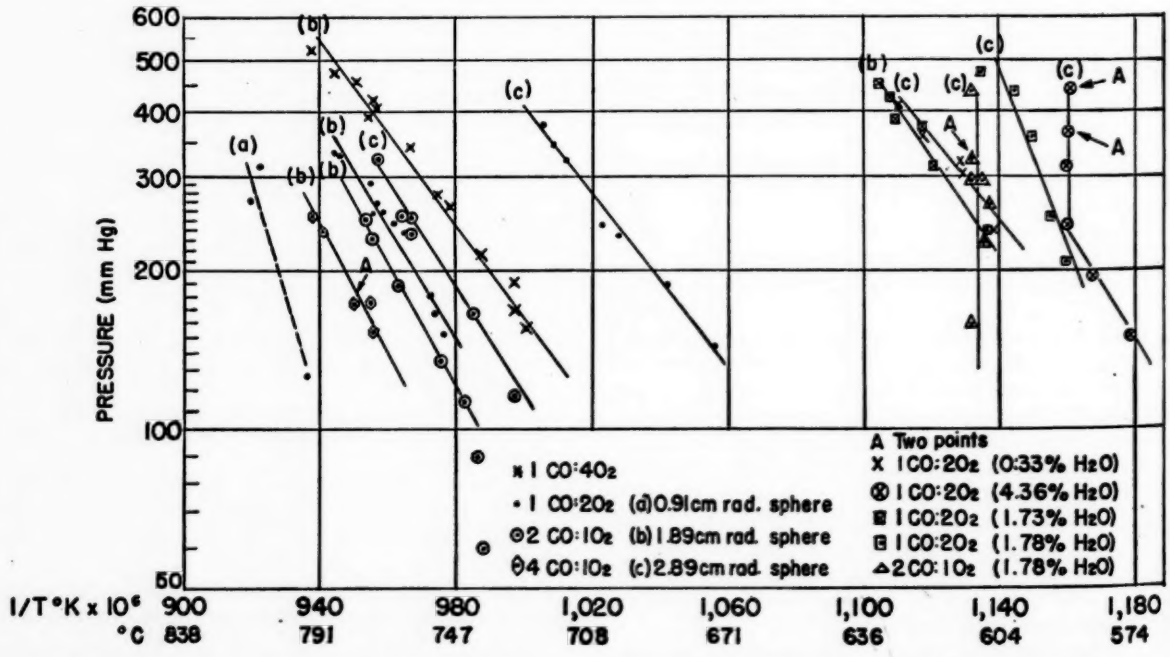

FIG. 1. Effect of composition, bulb diameter, and water vapor on the second limit of the explosive reaction between CO and O_2.

the pressure was reduced below the second explosion limit (the existence of a limit was determined by other experimental methods). These results have been confirmed in this work. In addition, it has been found that if the premixed gases are admitted to the reaction vessel at low temperature and heated to the final temperature such that the pressure is above the critical pressures (in one experiment slightly above atmospheric pressure which is rougly three times the critical pressure in this temperature and composition range), then the mixture always explodes when the pressure is reduced below the second limit. The second limit pressure in this temperature range (*ca* 700°C) is about 250 mm for the compositions investigated. It has been demonstrated that the CO_2 formed during the slow reaction preceding explosion is not responsible for the difference in explosive behavior.

[1] Kopp, Kowalsky, Lagulin, and Semenoff, Z. physik. Chem. **B**, 307 (1930).
[2] Hadman, Thompson, and Hinshelwood, Proc. Roy. Soc. (London) **A137**, 87 (1932).

Note on the Application of Near-Frozen Flow Criteria for One-Dimensional Nonviscous Expansion through a Level Nozzle

S. S. PENNER
Guggenheim Jet Propulsion Center, California Institute of Technology, Pasadena, California
(Received November 16, 1951)

A GENERAL criterion for near-frozen adiabatic expansion in one-dimensional nonviscous flow through a Laval nozzle has been described in a recent publication.[1] Unfortunately it appears that the discussion was so condensed that it is hardly possible to apply the result, Eq. (28a), without a few explanatory remarks.

Near-frozen flow should be defined properly by Eq. (27) in terms of equilibrium constants based on mole fractions. However, in the special case $\Sigma_j(\nu_j''-\nu_j')=0$, which is of interest for most practical applications, the near-frozen flow criterion given in Eq. (28a) becomes identical with the criterion derivable from Eq. (27) with equilibrium constants expressed in terms of mole fractions.

In deriving Eq. (28a) from Eq. (28) it is obvious that the quantity $(d\ln K_e/dT)_{T'\cong T_c}$, which appears on the left-hand side of Eq. (28a), represents $(d\ln K_e/dT)_{T_c}(T_c-T')/(T_c-T)$. The quantity $d\ln K_e/dT$ appearing on the right-hand side of Eq. (28a) should have the single subscript T_c as in Eq. (28). For the important special case $\Sigma_j(\nu_j''-\nu_j')=0$, $(d\ln K_e/dT)_{T_c}=\Delta H/RT_c^2$ where ΔH equals the heat of reaction. It is then a simple matter to obtain an explicit relation for T_c-T'. The result, for $\Sigma_j(\nu_j''-\nu_j')=0$, is

$$T_c-T'=(RT_c^2/\Delta H)[K_e(T_c)/K_e(T)-1]\times\left\{1+[(-DT/Dt)K_e(T_c)/K_e(T)(T_c-T)]\times\left[k_f\Pi_j C_j^{\nu_j'}\Sigma_j\frac{(\nu_j''-\nu_j')^2}{C_j}\right]^{-1}\right\}^{-1} \quad (28b)$$

or, in most cases which are of practical interest,

$$(T_c-T')/(T_c-T)\leqslant(-DT/Dt)^{-1}(RT_c^2/\Delta H)k_f\times\Pi_j C_j^{\nu_j'}\Sigma_j\frac{(\nu_j''-\nu_j')^2}{C_j}. \quad (28c)$$

Thus the reduced temperature lag $(T_c-T')/(T_c-T)$ is proportional to the reaction rate and inversely proportional to the rate of change of temperature with time. For sufficiently large values of $(-DT/Dt)$ the chemical changes occurring during flow are always negligibly small.

For individual chemical reaction steps for which $\Sigma_j(\nu_j''-\nu_j')\neq 0$, near-frozen flow is best defined by the relation

$$K_x(T')\simeq K_x(T_c)-K_x(T_c)(d\ln K_x/dT)_{T_c}(T_c-T'), \quad (27a)$$

where $K_x=K_e(\Sigma_j C_j)^{\Sigma_j(\nu_j''-\nu_j')}$ is the equilibrium constant expressed in terms of mole fractions. From Eqs. (21) and (27a) it is then readily shown that

$$(d\ln K_x/dT)_{T'\simeq T_c}(-DT/Dt)=k_f\Pi_j C_j^{\nu_j'}[\Sigma_K(\nu_K''-\nu_K')^2/C_K]\times\{1-[K_e(T)/K_e(T_c)][\Sigma_j C_j(T')/\Sigma_j C_j(T_c)]^{\Sigma_j(\nu_j''-\nu_j')}\times[1+(d\ln K_x/dT)_{T_c}(T_c-T')]\}. \quad (29a)$$

Equation (28b) is now replaced by the relation

$$[\Delta H/RT_c^2+\Sigma_j(\nu_j''-\nu_j')\gamma/T_c(\gamma-1)]\times(T_c-T')(-DT/Dt)/(T_c-T)=k_f\Pi_j C_j^{\nu_j'}[\Sigma_K(\nu_K''-\nu_K')^2/C_K]\times\{1-[K_e(T)/K_e(T_c)](T'/T_c)^{\Sigma_j(\nu_j''-\nu_j')/(\gamma-1)}\times[1+(\Delta H/RT_c^2)(T_c-T')+\Sigma_j(\nu_j''-\nu_j')\gamma(T_c-T')/T_c(\gamma-1)]\}. \quad (29b)$$

From Eq. (29b) the following conservative near-frozen flow criterion is obtained for $d\ln K_x/dT>0$:

$$(T_c-T')/(T_c-T)\leqslant(-DT/Dt)^{-1}\times[\Delta H/RT_c^2+\Sigma_j(\nu_j''-\nu_j')\gamma/T(\gamma-1)]^{-1}\times k_f\Pi_j C_j^{\nu_j'}[\Sigma_K(\nu_K''-\nu_K')^2/C_K]. \quad (29c)$$

Representative applications of the preceding relations to separate chemical reaction steps can be worked out without difficulty and will be described elsewhere.

[1] S. S. Penner, J. Chem. Phys. **19**, 877 (1951).

Nonstoichiometric Chemisorption of Hydrogen on Tungsten and Nickel

J. C. P. MIGNOLET
Service de Chimie Générale, Institut Spring, Liége, Belgium
(Received November 14, 1951)

RECENT experiments by a contact potential technique[1] of the adsorption of hydrogen at low temperatures on chromium and tungsten evaporated films reveal the same effect as was found in the case of nickel,[2] i.e., the formation of a positive rather volatile film following that of the normal negative one.

The surface potentials for tungsten are:

saturated negative film: −0.65 volt
saturated positive film: +0.2 volt.

These values obtained first with the vibrating condenser method, have been confirmed with the thermoionic method. Incidentally, the latter is easily applicable to metal evaporated film. The cell used (Fig. 1) contained two hairpin tungsten wires: one for the evaporation onto the cell wall, and the other for the measurements.

For some time, the author has thought these positive somewhat unusual films to be molecular and considered their existence as evidence in favor of the Rideal mechanism for the catalytic H_2-D_2 exchange.

There are, however, objections to the molecular interpretation. Firstly, the enormous dipole moment of 3 debye would have to be attributed to the H_2 adsorbed molecules. Secondly, calculation of the stabilization energy due to the polarization of the H_2 film leads to the absurdly high figure of 60 kcal/mole.

There is an alternative interpretation based on the concept of nonstoichiometric chemisorption which, moreover, can help to explain the steep fall in the heat of adsorption near saturation.[3] Upon adsorption, the atoms preferentially occupy the sites of the superficial lattice with a high heat evolution and a negative variation in surface potential. When all sites are occupied, atomic adsorption can proceed a little further with an increasing distortion of the H-lattice. Now, the important point in this second stage is that for each new atom to be adsorbed, many others must shift

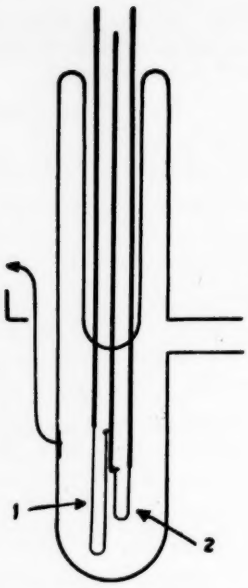

FIG. 1. A cell for measuring surface potentials on evaporated W deposits. L: Lead; 1: W filament for the evaporation; 2: W electron emitter.

appreciably from their positions of lowest energy. This readily explains the steep fall in the differential heat of adsorption, and the strong effect on the surface potential. The surface potentials can be accounted for by assuming that the shift produces a dipole moment reduction by roughly 30 percent, which is not unreasonable in view of the simultaneous reduction in orbitals overlapping.

These considerations may also explain the maximum in the curve surface potential *vs* surface concentration found for alkali metal films on tungsten.[4]

Nonstoichiometry may well be an important favorable factor in catalysis.

A detailed article will appear shortly.

My best thanks are due Professor L. D'Or for help and encouragement.

[1] J. C. P. Mignolet, Disc. Faraday Soc. No. 8, 326 (1950).
[2] J. C. P. Mignolet, Disc. Faraday Soc. No. 8, 105 (1950).
[3] Trapnell, Proc. Roy. Soc. (London) 45 (1950).
[4] E. Bosworth and K. Rideal, Proc. Roy. Soc. (London) **162**, 1 (1937), and references cited therein.

The Association Band of the Hydrogen Bridge

MANSEL DAVIES AND J. C. EVANS
The Edward Davies Chemical Laboratories, Aberystwyth, Wales
(Received November 16, 1951)

RECENT measurements of the association features for a number of amino-compounds in solution give the following wave numbers as the centers of well-defined features in the N−H stretching region:

	Monomer		Associated			
$HCONH_2(CCl_4)$	3533(a)	3411(s)	3499(f)	3307	3228	3176
$CH_3CONH_2(CHCl_3)$	3533(a)	3415(s)	3501(f)	3351	3190	
$NH_2COOC_2H_5(CCl_4)$	3557(a)	3442(s)	3513(f)	3324	3266	3176

(a) and (s) identify the antisymmetric and symmetric modes of the $-NH_2$ group. The numerical differences, $\Delta\omega$ = monomer wave number − associated wave number, between (s) and the first of the associated features (f) (which is quite remarkably sharp in each case) and between (a) and the remaining frequencies are (in cm^{-1}) for formamide 88; 226 (75×3), 305 (76×4), 357 (71×5): for acetamide 86; 182 (91×2), 343 (86×4); for urethane 71; 233 (78×3), 291 (73×4), 381 (76×5).

It is suggested that (f) is a summation tone, the other difference tones arising from combination of the X−H stretching mode with low frequency vibrations within the associated molecules. Reference to the extensive association band plotted for CCl_3COOH by one of us[1] gives the following values of $\Delta\omega$ relative to the monomer peak at 3497 cm^{-1}: 420 (210×2), 464, 623 (208×3), 886 (221×4), 1009 (202×5), 1181, 1238 (206×6).

The deviations from regular wave-number spacings above are perhaps no greater than the uncertainties in locating the centers of these overlapping features. By comparison with other association bands the suggestion arises that such combination tones are more clearly resolved the more definite the structure (e.g., cyclic or saturated) of the associated species—compare the carboxyl dimer and the chain-associating alcohols.

The number of difference tones involved is thus the apparent reason for the over-all width of the association bands in these cases. The relative paucity of addition tones is a matter for further study. The frequency intervals, ω_i (70 to 90 cm^{-1} for NH_2-compounds, 210 cm^{-1} for CCl_3COOH) must be expected to vary from molecule to molecule. As the directly observed hydrogen-bridge frequencies (ν_1 of the linear X−H···Y) in H_2O and HCOOH are 167 cm^{-1} and ~180 cm^{-1} respectively,[2] it is perhaps plausible to identify ω_i with ν_1 for these molecules. Measured by their ΔH values in a given solvent, the hydrogen bridge in acetamide has about one-third the energy found in carboxylic acids,[3] and this accords with the suggested ν_1-values of 86 cm^{-1} and 210 cm^{-1}. The latter, with the corresponding ν_3-values (3475 cm^{-1}, 3497 cm^{-1}) give for the X−H···Y stretching-force constants (in 10^5 dynes/cm) $k_1=6.60$: $k_2=0.03$ for CH_3COONH_2: $k_1=6.60$; $k_2=0.22$ for CCl_3COOH.

In so far as a particular range of combination tones involving ν_1 is a general occurrence, a positive correlation between ν_1 (or strength of the H-bridge) and the total association band width would be expected. From some of the observational data such a correlation has been suggested.[4] A simple relation between the strength of the H-bridge and the frequency shift from monomer to the "center" of the association band could only be anticipated on the further and doubtless unlikely supposition of the unchanging relative intensities of the individual combination tone features.

Finally, a different item further illustrated by our present studies is the much smaller frequency change on association in the δ(X−H) vibration when compared with the ν(X−H) mode. This, at first sight surprising result, we interpret as substantial evidence indicating the predominantly nondirectional (e.g., electrostatic) nature of the forces contributing to the H-bridge.

[1] M. M. Davies, Trans. Faraday Soc. **36**, 1114 (1940).
[2] Gupta, Indian J. Phys. **10**, 313 (1936); J. O. Halford, J. Chem. Phys. **14**, 395 (1946); G. H. Cartwright and J. Errera, Phys. Rev. **49**, 470 (1936); Proc. Roy. Soc. (London) **A154**, 138 (1936).
[3] M. M. Davies and Hallam, Trans. Faraday Soc. (to be published).
[4] C. S. Venkateswaran, Proc. Indian Acad. Sci. **7**, 13 (1938); M. M. Davies, J. Chem. Phys. **8**, 586 (1940).

Ferroelectric Transitions and Heterogenous Catalysis

G. PARRAVANO
Frick Chemical Laboratory, Princeton University, Princeton, New Jersey
(Received November 23, 1951)

FERROELECTRIC substances are known to show anomalous behavior in ϵ and tanδ at transition temperatures, where optical, electrical, and other physical properties undergo profound changes due to a structural and electronic rearrangement. On the other end catalytic reactions, such as carbon monoxide oxidation, have been shown to proceed through some type of electron transfer between the gas and solid phases. This was clearly established in the case of NiO[1] and Cu_2O.[2] It seems therefore plausible to inquire whether the electron exchange occurring during the catalytic process is affected by the electronic rearrangement, which the solid phase undergoes at ferroelectric transition temperatures. Among several ferroelectrics tested for this purpose, sodium and

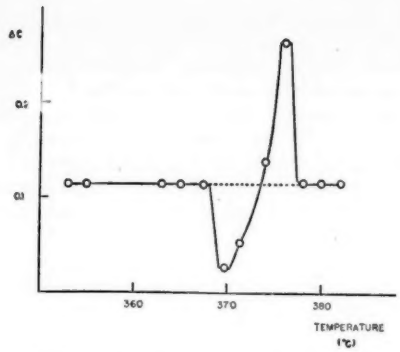

FIG. 1. CO oxidation on $NaNbO_3$ (1.88 g 30–40 mesh). ΔC is the increment of conversion in percent for 2°C temperature rise. $CO+O_2$ 1:1, p_0=300 mm Hg. Heating rate 0.22°C/min.

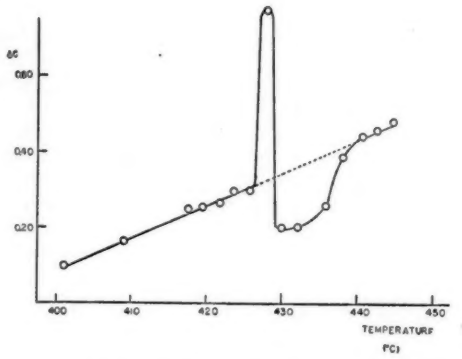

FIG. 2. CO oxidation on $KNbO_3$ (1.88 g 30–40 mesh). $CO+O_2$ 1:1, p_0=300 mm Hg. Heating rate 0.22°C/min.

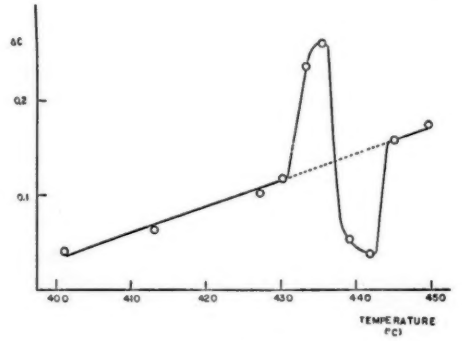

FIG. 3. CO oxidation on $KNbO_3$ (1.88 g 30–40 mesh). $CO+O_2$ 1:1, p_0=300 mm Hg. Heating rate 0.56°C/min.

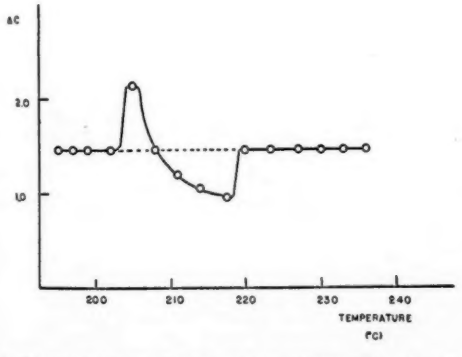

FIG. 4. CO oxidation on $LaFeO_3$ (0.40 g 30–40 mesh). $CO+O_2$ 1:1, p_0=300 mm Hg. Heating rate 0.31°C/min.

potassium niobates and lanthanum ferrite were found active at transition points for carbon monoxide oxidation.

Recent data of Matthias and Remeika[3] have shown that alkali metal niobates can be described as ferroelectric materials. Potassium niobate has two transitions: at 224 and 434°C, the latter being the ferroelectric Curie temperature, in which the largest change in both ϵ and $\tan\delta$ occurs. Sodium niobate has three transitions at −80, 370, and 480°C, the second point showing in this case the largest change in ϵ and $\tan\delta$. Fulfillment of certain structural conditions in lanthanum ferrite leads to the conclusion that this substance also ought to be ferroelectric. Matthias[4] was in fact able to detect in this compound a marked optical anisotropy at ~200°C, although at the same temperature no apparent change of the cubic structure could be observed.

Data for carbon monoxide oxidation on these substances are presented in Figs. 1–4. These results were obtained in a constant volume apparatus, the catalyst being submitted to a linear heating rate. An anomaly in the reaction rate is clearly present in all cases at temperatures in the neighborhood of one of the ferroelectric transitions. The anomaly was found to be reproducible. In one case, using a higher heating rate, the anomalous region of the reaction rate was found to be shifted slightly forward (Fig. 3). This might be explained by consideration of the relaxation effect present in ferroelectric changes.

On the basis of these results it can be concluded that the rate of the catalytic oxidation of carbon monoxide is affected by ferroelectric transitions occurring in sodium and potassium niobates and lanthanum ferrite. This might be interpreted as supporting evidence for an electronic mechanism being rate determining for the catalytic oxidation of carbon monoxide.

I wish to thank Dr. M. Boudart of this Laboratory for stimulating discussions on this subject and Dr. R. M. Burns, Director of the Bell Telephone Laboratories, Murray Hill, New Jersey, for kindly supplying the sodium and potassium niobates.

[1] C. Wagner and K. Hauffe, Z. Elektrochem. **44**, 172 (1938).
[2] Garner, Gray, and Stone, Proc. Roy. Soc. (London) **A197**, 134 (1949); Disc. Faraday Soc. No. 8, 246 (1950).
[3] B. T. Matthias and J. P. Remeika, Phys. Rev. **82**, 727 (1951).
[4] B. T. Matthias, Phys. Rev. **75**, 1771 (1949).

Diffusion Coefficient of Sodium Vapor in Nitrogen

R. J. CVETANOVIĆ* AND D. J. LE ROY
Department of Chemistry, University of Toronto, Toronto, Canada
(Received November 23, 1951)

A KNOWLEDGE of the diffusion coefficient of sodium vapor is of fundamental importance in the determination of rate constants by the diffusion flame method. In the Hartel-Polanyi expression[1] for the rate constant the diffusion coefficient of sodium in the reaction mixture enters to the first power and any error in this quantity will be reflected in the calculated rate constant. The temperature coefficient of the diffusion constant is also important, not only in the evaluation of activation energies from the temperature coefficients of rate constants,[2] but also in evaluating a rate constant for a temperature different from that at which the diffusion data were obtained.

Soon after the development of the diffusion flame technique, Hartel, Meer, and Polanyi[3] undertook a study of the diffusion of sodium in the carrier gases commonly used. Their measurements were confined to a single temperature, 382°C, about 100° higher than the temperatures normally used in diffusion flame work. Subsequent workers have used their data exclusively, and in most cases have assumed that the diffusion coefficient varied as the $\frac{3}{2}$ power of the temperature, as predicted by simple kinetic theory. Polanyi,[4] however, has made the statement that, "The (diffusion flame) data are preliminary ones and their reliability is impaired in particular by the fact that the values of the diffusion constant of Na vapor, which are indispensable to the calculation of the velocity constant, . . . have not yet been determined with sufficient accuracy."

With a view to removing this uncertainty we have developed a method of investigating the diffusion of sodium vapor at temperatures considerably lower than that used by Hartel, Meer, and Polanyi. The complete investigation will take some time, and would include a study of the temperature coefficient of the diffusion constant and of the effect of adding various halides to the carrier gas. At present we wish to report our value for the diffusion coefficient of sodium in pure nitrogen at 253.5°C.

In the present method the diffusion takes place through a nickel capillary approximately 10 cm long and 3 mm i.d. A constant partial pressure of approximately 10^{-3} mm of sodium vapor was maintained at the lower end of the capillary from a pool of molten sodium in a 3-cm i.d. tube. The bottom of the larger tube was kept at a constant temperature somewhat lower than that of the capillary; a small intermediate furnace was used to eliminate cold spots. The sodium diffusing out of the capillary was continuously swept away by the circulating nitrogen and carried into an optical cell in which the absorption of sodium D resonance radiation was measured by a double photocell arrangement. The gradual darkening of the cell windows through the action of sodium vapor was allowed for by reversing the direction of nitrogen flow to take the "100 percent transmission" reading. The light absorption readings were correlated with sodium concentrations in calibration experiments in which the carrier gas was saturated with sodium vapor by passing over molten sodium at a series of known temperatures. The rate of diffusion of sodium out of the capillary was then calculated from the steady-state concentration of sodium in the carrier gas sweeping across the top of the capillary, and the flow rate of this gas. A correction term, amounting to 0.8 percent, was applied to take account of the diffusion in the 3-cm tube.

A total of six experiments were performed at 253.5±0.1°C, using a nitrogen pressure of 4.3 mm. It is generally accepted that at such low pressures the diffusion coefficient is inversely proportional to the total pressure, and it is customary to express the results in terms of values calculated for a total pressure of one atmosphere. Our value, expressed in this way, was 0.68±0.03 $cm^2\ sec^{-1}$ at 253.5°C and one atmosphere. Hartel, Meer, and Polanyi[3] quote a mean value of 0.91 $cm^2\ sec^{-1}$ at 382°C for their two experiments with pure nitrogen.

The new value of the diffusion coefficient is in good agreement with the one calculated from the data of Hartel, Meer, and Polanyi on the assumption of the $\frac{3}{2}$ power law, *viz.*, 0.66 $cm^2\ sec^{-1}$ at 253.5°C. It would therefore appear that there was no serious error in using the earlier number for diffusion flame experiments at temperatures of this order. The problem still remains, however, of determining the exact law of temperature dependence and the influence of halide.

The authors wish to acknowledge the kindness of the International Nickel Company of Canada in supplying the nickel capillary, of the Associate Committee on Scientific Research of the University of Toronto in supporting the research, and of the Senate of the University in granting a Nadine Phillips Scholarship to one of us (R.J.C.).

* Present address: Division of Chemistry, National Research Laboratories, Ottawa, Canada.

[1] H. v. Hartel and M. Polanyi, Z. physik. Chem. **B11**, 97 (1930).
[2] R. J. Cvetanović and D. J. Le Roy, J. Chem. Phys. (to be published)
[3] Hartel, Meer, and Polanyi, Z. physik. Chem. **B19**, 139 (1932).
[4] M. Polanyi, *Atomic Reactions* (Williams and Norgate, London, 1932).

Intramolecular Isotope Effects in the Decarboxylation of Malonic Acid*

PETER E. YANKWICH, EDWARD C. STIVERS, AND ROBERT F. NYSTROM
Department of Chemistry, University of Illinois, Urbana, Illinois
(Received November 21, 1951)

MALONIC acid, singly carboxyl-labeled with C^{14} by a modification of the method of Gal and Shulgin,[1] was decarboxylated at 138.0°C under 1 atmos of helium preheated to the same temperature. Acetic acid was removed from the gas stream by a dry ice trap, carbon dioxide by a liquid nitrogen trap. Acetic acid was burned to carbon dioxide over copper oxide. Samples of carbon dioxide were analyzed for C^{13} content determined with an ionization chamber-vibrating reed electrometer combination. Corrections and precautions described by Bigeleisen and Friedman,[2] and Lindsay, Bourns, and Thode[3] were applied.

In Table I are collected typical results, expressed as the ratio of rate of rupture of $C^{12}-C^{12}$ bonds to that of $C^{12}-C^{x}$ bonds,

TABLE I. Experimental values of k_4/k_3.

	C^{13} effect		C^{14} effect	
	CO_2 basis	Acetic acid basis	CO_2 basis	Acetic acid basis
I	1.026	1.026	1.105	1.105
II	1.027	···	1.101	1.087

where x is 13 or 14; this ratio is k_4/k_3 in the notation of Bigeleisen and Friedman.

The C^{13} results are in agreement with those of previous investigations;[2,3] the C^{14} results are in essential agreement with the work of Yankwich and Calvin[4] but not with that of Roe and Hellmann.[5] The C^{14} results disagree with the predictions of Bigeleisen[6] and are not in much better correspondence with those of Pitzer.[7]

Preliminary experiments on bromomalonic acid indicate C^{13} and C^{14} isotope effects only slightly larger than those found for the unsubstituted acid.

* Supported by the AEC.
[1] Gal and Shulgin, J. Am. Chem. Soc. **73**, 2938 (1951).
[2] J. Bigeleisen and L. Friedman, J. Chem. Phys. **17**, 998 (1949).
[3] Lindsay, Bourns, and Thode, Can. J. Chem. **29**, 192 (1951).
[4] P. E. Yankwich and M. Calvin, J. Chem. Phys. **17**, 109 (1949).
[5] A. Roe and M. Hellmann, J. Chem. Phys. **19**, 660 (1951).
[6] J. Bigeleisen, J. Chem. Phys. **17**, 425 (1949).
[7] K. Pitzer, J. Chem. Phys. **17**, 1341 (1949).

Near Infrared Absorption by Solutions of Inorganic Substances

S. D. CHATTERJEE, N. N. GHOSH, AND A. M. NAHA
University College of Science, and Bose Research Institute, Calcutta, India
(Received October 15, 1951)

THE application of infrared absorption to the study of inorganic compounds has been of a rather limited nature.[1-3] Moreover, the infrared photometry of nearly "colorless" solutions is a well-nigh unexplored field. In the present communication an account of a preliminary study of some copper and nickel compounds, in the presence of some complex forming substances, is given.

The apparatus schematically depicted in Fig. 1 may be called a near infrared colorimeter. The light from a prefocus-type lamp,

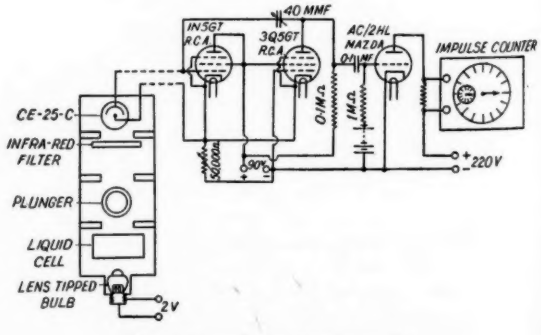

FIG. 1. Experimental arrangement.

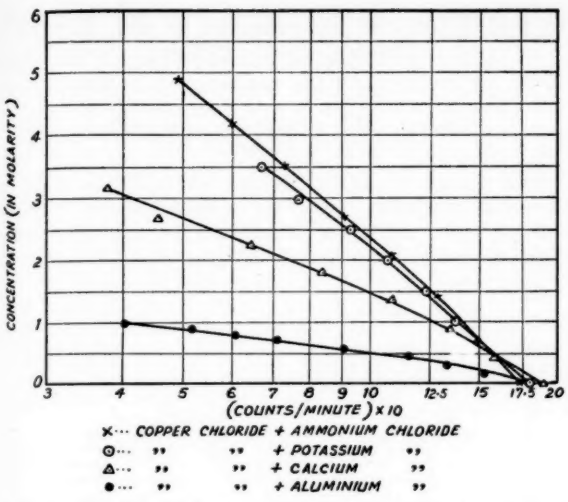

FIG. 2. Change of absorption of cupric chloride 0.01M solution upon the addition of concentrations of various chlorides.

passing successively through a glass-cell containing the solution under examination, and a "Kodak" infrared filter, falls on a photo-emission cell (cesium-oxide cathode). A plunger bolt, which can be screwed up and down, regulates the amount of incident light. The photoemission cell is connected across the grid-input of a feed-back, relaxation oscillator. The intensity of the transmitted light is measured by the number of counts recorded by a suitable numerical counter in a certain interval of time, minus the background count during that interval. The background count can be made conveniently low, if care is taken to make the insulation of the input grid circuit sufficiently high. On account of the inherent characteristics of the cesium-oxide type photocell, the infrared region studied lies between 8000–11,000A units (0.8–1.1μ).

The results obtained may be briefly stated as follows: Both the aqueous and the ammoniacal copper sulfate solutions appear to obey Beer's law. Absorption decreases by the addition of ammonia, which means that the complex cupri-ammonium ions are comparatively less opaque to the infrared region employed. Absorption curves for copper chloride, copper nitrate solutions show no difference from that of copper sulfate of the same concentration, within the region of dilution employed (0.01M).

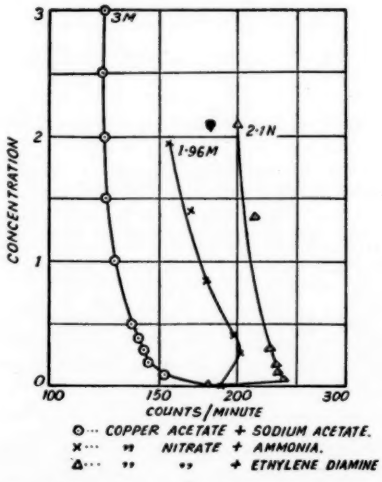

FIG. 3. Change in absorption of various copper solutions upon the addition of the reagents shown.

Both the aqueous and ammoniacal solution of nickel sulfate likewise obey Beer's law, but the nickel ammonium ion, on the contrary, shows a comparatively stronger absorption. No difference in absorption was observed between solutions of copper sulfate and copper ammonium sulfate, between those of nickel sulfate and nickel ammonium sulfate, or between ferrous sulfate and ferrous ammonium sulfate solutions.

Figure 2, shows the influence of ammonium chloride, potassium chloride, calcium chloride, and aluminium chloride upon the absorption by copper chloride solution (0.01M). As far as they have been studied the curves relating the concentration of the foreign chlorides with $\log I_0/I_t$ are all more or less straight. This seems to suggest the gradually increased formation of complex $[CuCl_4]''$ anion with the increased concentration of the chloride added. The complex tetra-chloro-cupric ion appears also to follow Beer's law.

Addition of increasing quantities of ammonium nitrate to a solution of copper nitrate shows no such change in absorption except a slight increase at very high concentrations of ammonium nitrate. Mercuric chloride added to a solution of copper chloride (0.01M) also shows no change in the absorption of the latter, obviously due to the non-ionic character of mercuric chloride. The absorption of nickel chloride solution, on the other hand, is not affected by the addition of ammonium chloride, potassium chloride, or aluminium chloride.

Figure 3 shows the influence of the addition of sodium acetate on the absorption of copper acetate and of ammonia and methylenediamine on that of copper nitrate. The curves give definite indication of complex formation. The breaks in the absorption curves for copper ammonia and copper ethylenediamine solutions seem to suggest stepwise formation of complexes in two stages which differ in their absorption power. The nickel chloride with ethylenediamine in aqueous solution, however, gives a continuous curve with continually increasing absorption with increasing ethylenediamine concentration, till a maximum is reached when it remains practically constant. Similar behavior was also observed with nickel chloride and pyridine solutions. The nickel ethylenediamine and nickel pyridine complexes are, therefore, formed in a single stage, and when their formation reaches a maximum equilibrium value, the absorption remains practically constant.

It is intended to make a systematic and quantitative study of infrared absorption by solutions of inorganic substances with a view to determine the nature of the molecule responsible for the absorption.

[1] Erwin Heintz, Arch. phys. biol. **15**, 303 (1939).
[2] Duval, Bull. soc. chim. (1947, 1948).
[3] Berraz and Virasoro, Chem. Abst. 6225 (1944).

The Location of the Activator in Fluorescent ZnS–Cu

F. A. KRÖGER
Philips Research Laboratories, N. V. Philips' Gloeilampenfabrieken, Eindhoven, Netherlands

(Received November 12, 1951)

IN several papers evidence has been given for the view that ZnS phosphors prepared in the presence of halogen ions (Cl, Br, or I) take up an amount of halogen of the order of the concentration of the activator.[1,2] In a recent note Bube[3] has published results of a chlorine analysis of ZnS-Cu prepared with NaCl which support this view. There are differences, however, in the way in which this fact is explained.

According to Kröger *et al.*,[2] in green fluorescent ZnS-Cu the halogen is incorporated as a monovalent negative ion at a normal anion lattice site, thus making possible the simultaneous incorporation of the monovalent activator ion (Cu^+) at a normal cation lattice site. The charge compensation can also be accomplished

with trivalent cations, two Zn^{2+} ions being replaced by one monovalent and one trivalent cation.[3] The fluorescence promoted by trivalent cations proves to be identical to that promoted by halogens. In ZnS-CuCl containing a high concentration of Cu ($>10^{-4}$) and showing a blue luminescence, the Cl/Cu ratio approaches the value ½. Therefore Kröger *et al.* proposed that the centers responsible for the blue luminescence shown by such products are due to a monovalent complex Cu_2^+ consisting of one monovalent copper ion and a copper atom near by. Bube,[4,5] on the other hand, supposes that the green band is due to Cu^+ at interstitial sites and the blue band to Cu^{2+} at normal lattice sites. Bube arrived at this conclusion mainly on the basis of the observation that the spectral position of the green band is different for the cubic and the hexagonal modifications of ZnS, while for the blue band this is not so. The two modifications having identical first-shell surroundings at a lattice point but not at an interlattice point, it was assumed that the bands showing the difference were due to atoms at interstitial sites and the ones not showing it to atoms at normal lattice sites.

The argument presented by Bube is not convincing for two reasons. In the first place, differences in the spectral position, as found with the green band of ZnS-Cu, also occur with the fundamental absorption edge of pure ZnS and the low temperature fundamental fluorescence band corresponding to it, neither of which are connected with the presence of ions at interstitial sites.[1] In the second place, a similar difference occurs with all non-characteristic fluorescence bands found with ZnS; e.g., with ZnS activated by Ag,[1] Au,[3] Na, Li[6] and, this in contradiction to Bube, also with blue fluorescent ZnS-10^{-4}Cu[1]. Therefore we do not believe that this difference can be used as a clue to the position of the activator.

There are, however, other means to decide the point. If the green of ZnS-Cu is due to Cu^+ at interstitial sites, and Cl^- is to have the favorable effect observed, then this might be explained by the incorporation of one Cl^- in the interlattice for each Cu^+ incorporated there. The favorable effect of trivalent ions, however, cannot be explained on this basis. For Cu^+ incorporated at lattice sites, on the other hand, the favorable effect of both halogens and trivalent ions is straightforwardly explained on the basis of the principle of compensation of charge as outlined above, both ions occupying normal lattice sites. Therefore we believe that the monovalent activators occupy a normal lattice site in all cases.

The model Cu_2^+ proposed by us for the blue copper centers has been criticized[4] because the ratio Cl/Cu$\sim$0.5 required by it is not only found with ZnS-10^{-4}Cu showing a blue luminescence but also by samples containing a higher concentration of copper, which are weakly green fluorescent. This green fluorescence, however, is only predominant at room temperature.[2] Upon cooling, the fluorescence becomes intensely blue. The weak green appearing in the high temperature range is not due to a new kind of centers, but it is the normal green band occurring with all ZnS-Cu phosphors at slightly higher temperatures. The only difference between the samples with medium (10^{-4}) and those with high ($>10^{-4}$) copper concentration being that the temperature at which the blue is suppressed is shifted to lower temperatures with increasing copper content. This is caused by killer centers formed in the products with the higher copper concentrations, which centers probably consist of several copper ions. The blue center Cu_2^+ may be considered as the first step in the direction of such a complex center. It is possible[7] to describe quantitatively the intricate phenomena involved in the formation of ZnS-Cu phosphors in an atmosphere of H_2S-HCl, on the basis of the model of green and blue centers outlined above.

[1] F. A. Kröger and J. E. Hellingman, J. Electrochem. Soc. **93**, 156 (1948); **95**, 68 (1949).
[2] Kröger, Hellingman, and Smit, Physica **15**, 990 (1949).
[3] F. A. Kröger and J. Dikhoff, Physica **16**, 297 (1950).
[4] R. H. Bube, J. Chem. Phys. **19**, 985 (1951).
[5] R. H. Bube, Phys. Rev. **80**, 655 (1950).
[6] F. A. Kröger, J. Opt. Soc. Am. **39**, 670 (1949).
[7] F. A. Kröger and N. W. Smit, Physica **16**, 317 (1950).

Normal Vibration Frequencies of the Trimer of Phosphonitrile Chloride

JULIO V. IRIBARNE AND DORA G. DE KOWALEWSKI
Laboratorio de Fisicoquímica, Facultad de Ciencias Exactas, Físicas y Naturales, Universidad de Buenos Aires, Argentina
(Received November 23, 1951)

THE Raman effect of $(PNCl_2)_3$ has been studied by de Ficquelmont, Magat, and Ochs;[1] they obtained 15 lines, of which 4 were polarized and 1 was a combination line. According to their results, the symmetry group D_{3h} must be assigned to this molecule.

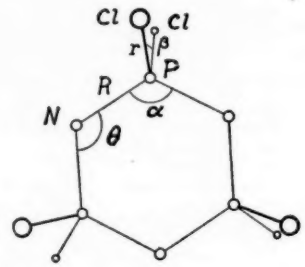

FIG. 1.

The distances and angles were determined by Brockway and Bright, using an electron diffraction method.[2] The structure of the molecule is shown in Fig. 1.

Based on this data a vibrational analysis was made, applying E. B. Wilson's methods,[3] and the numerical values of some force constants were derived. The internal coordinates chosen, of a generalized valence type, were: extension of the P−N and P−Cl bonds, planar deformation of the ring, deformation of the Cl−P−Cl angles, three angles to describe the bending, rocking, and twisting of each PCl_2 group and the nonplanar deformation of the ring. Some interaction terms were included in the expression for the potential energy.

The 14 Raman active fundamental frequencies are the totally symmetrical A_1' (4) and the double degenerated E' (6) and E'' (4). The 4 polarized lines must belong to the A_1' representation, and this is the only assignment that can be made. The partial secular equation corresponding to the A_1' representation

$$|\mathcal{G}_{A_1'}\mathcal{F}_{A_1'}-E\lambda|=0$$

was solved in several approximate ways. In the calculation the problem of assigning the lowest frequency (100 cm^{-1}) arises. Two hypotheses were considered. (I) This vibration corresponds to the planar deformation of the ring; (II) it corresponds to the deformation of the Cl−P−Cl angle. The approximate results are given in the columns headed *A*-I and *A*-II of Table I. In this calculation

TABLE I.

Force constant	*A*-I	*A*-II	*B*-I	*B*-II
$f_R+2f_{RR}\cong f_R$	4.0	3.7	4.16	4.0
$f_r+f_{rr}\cong f_r$	4.0	3.8	4.16	4.0
$\frac{1}{2}(f_\alpha+f_\theta)-2f_{\alpha\theta}\cong f_\alpha\cong f_\theta$	0.0285	0.30	0.031	0.315
f_β	1.1	0.104	1.05	0.113
f_{Rr}	0	0	0.53	0.9

f_R, f_r: force constants for the extension of P−N(R) and P−Cl(r) bonds.
f_α, f_θ, f_β: force constants for variation of the angles N−P−N(α), P−N−P(θ), Cl−P−Cl(β).
f_{RR}, f_{rr}, f_{Rr}, $f_{\alpha\theta}$: interaction constants.
A: approximate solutions, obtained by separation of frequencies and assuming $f_{Rr}=0$.
B: exact solutions, assuming $f_R+2f_{RR}=f_r+f_{rr}$ and including f_{Rr}.
I: low frequency assigned to plane deformation of the ring.
II: low frequency assigned to deformation of angle Cl−P−Cl. The angle constants are divided by the square of the corresponding bond length. All values are given in 10^5 ·dyne/cm.

if the interaction constant f_{Rr} (between both types of bonds) was put equal to zero, the equation had no exact real positive solutions. The second calculation was made putting $f_R+2f_{RR}=f_r+f_{rr}$. With this assumption, the exact solutions given in the columns B-I and B-II were found.

The values of the column B-I would imply a very easy deformation of the ring, compared with a rigid Cl−P−Cl angle, while the bonds P−N and P−Cl are equally strong. Moreover, the value 1.05 seems too large when compared with the value 0.3 obtained by Howard and Wilson[4] for Cl−P−Cl deformation in PCl_3. These considerations point to the values of column B-II as the adequate set of constants. Attention may be called to the large interaction between both types of bonds.

The complete expression for the potential energy, the symmetry coordinates, the factorized matrices for potential and kinetic energies, and the way followed to solve the secular equation for A_1' will be given elsewhere.[5]

[1] de Ficquelmont, Magat, and Ochs, Compt. rend. **208**, 1900 (1939).
[2] L. O. Brockway and W. M. Bright, J. Am. Chem. Soc. **65**, 1551 (1943).
[3] E. B. Wilson, J. Chem. Phys. **7**, 1047 (1939); **9**, 76 (1941).
[4] G. Herzberg, *Infrared and Raman Spectra of Polyatomic Molecules* (D. Van Nostrand Company, Inc., New York, 1945), pp. 177 and 187.
[5] Revista Unión Matem. Arg.

Absorption Spectrum of Free NH_2 Radicals

G. Herzberg and D. A. Ramsay
Division of Physics, National Research Laboratories, Ottawa, Canada
(Received November 23, 1951)

It is well known that ammonia-oxygen and hydrogen-nitrous oxide flames as well as discharges through streaming ammonia emit an extremely complicated many-line spectrum, called the α-bands, in the region 4200–8300A.[1–3] The α-bands have also been observed in fluorescence when ammonia is irradiated with Schumann ultraviolet radiation.[4] It has been suspected for a long time that this spectrum is due to the free NH_2 radical[5] although a transition between two excited states of NH_3 has also been considered.

Photochemical investigations strongly suggest that NH_3 by absorption of light in the region of its diffuse ultraviolet absorption bands decomposes according to[6]

$$NH_3+h\nu\rightarrow NH_2+H.$$

Therefore, if the carrier of the α-bands is the NH_2 radical, one would expect to observe these bands in absorption in photochemically dissociated NH_3. We have carried out such an experiment and have indeed obtained the α-bands in absorption.

NH_3 at 10-mm pressure was decomposed in a flash photolysis apparatus similar to that described by Porter[7] and mentioned by us[8] in an earlier publication. The absorption spectrum of the products was obtained within 1 msec of the photolysis in the second order of a 21-ft grating spectrograph. About 50 absorption lines were observed in the region 5700–6900A. Figure 1a shows two sections of the spectrum. For comparison Fig. 1b shows the emission spectrum of an oxygen-ammonia flame taken with the same spectrograph. The exact coincidence of all the absorption lines with emission lines leaves no doubt that emission and absorption are due to the same molecule.

The fact that the α-bands occur in absorption suggests very strongly that the lower state is the ground state of the molecule involved. The possibility of absorption from a metastable state seems very remote since as far as we are aware there is no case in which absorption by a metastable diatomic or polyatomic molecule has been observed in the gaseous state. In addition the observation of the α-bands in comets by Swings, McKellar, and Minkowski[5] is not compatible with a metastable lower state if the usual fluorescence mechanism for their excitation applies.

The conclusion that the α-bands have the ground state as the lower state immediately eliminates NH and NH_3 as carriers since their absorption spectra are well known. Moreover, the NH band at 3360A does not appear in absorption under the same conditions under which the α-bands appear. The structure of the spectrum both in emission and absorption shows a rather coarse fine structure without obvious regularity and is not compatible with N_2H or other molecules containing more than one N atom. We conclude, therefore, that the molecule responsible for the α-bands is the free NH_2 radical. If NH_2 is nonlinear as would be expected from considerations of directed valence, it is an asymmetric top and can, therefore, readily account for the complicated structure of the α-bands.

The α-bands observed in absorption are definitely simpler than in emission. It appears not impossible that a vibrational and

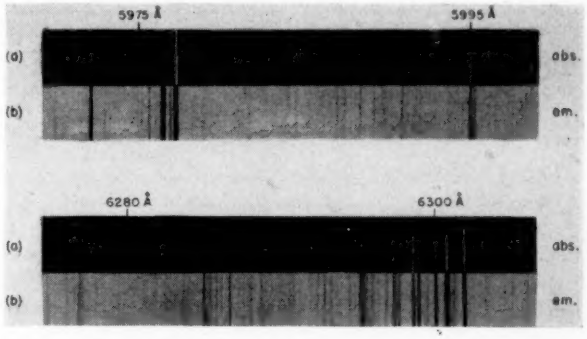

FIG. 1. Two parts of the spectrum of the free NH_2 radical: (a) in absorption by flash photolysis of ammonia; (b) in emission from an ammonia-oxygen flame.

rotational analysis can be obtained particularly when spectra with longer absorbing paths both of NH_2 and ND_2 and possibly $N^{15}H_2$ become available. Preparations for such experiments are in progress.

The observation of the absorption spectrum of the free NH_2 radical opens the possibilities of studying not only the kinetics of many photoprocesses involving this radical but also of other chemical reactions involving it. It also raises the hope that absorption spectra of CH_3, CH_2, and similar radicals may yet be found.

[1] W. B. Rimmer, Proc. Roy. Soc. (London) **A103**, 696 (1923).
[2] A. Fowler and J. S. Badami, Proc. Roy. Soc. (London) **A133**, 325 (1931).
[3] A. G. Gaydon, Proc. Roy. Soc. (London) **A181**, 197 (1942).
[4] A. N. Terenin and H. H. Neuimin, Acta Physicochim. U.R.S.S. **5**, 465 (1935).
[5] See e.g., Swings, McKellar, and Minkowski, Astrophys. J. **98**, 142 (1943).
[6] W. A. Noyes, Jr., and P. A. Leighton, *The Photochemistry of Gases* (New York, 1941).
[7] G. Porter, Proc. Roy. Soc. (London) **A200**, 284 (1950); Disc. Faraday Soc. No. 9, p. 60 (1950).
[8] G. Herzberg and D. A. Ramsay, Disc. Faraday Soc. No. 9, p. 80 (1950).

The Raman Spectra of Methoxychlorosilanes

Hiromu Murata
The Osaka Municipal Technical Research Institute, Osaka, Japan
(Received November 12, 1951)

Out of the series of experiments on the spectral sequence $XY_4\rightarrow XZ_4$ I have already worked on methylchlorosilanes,[1] methylbromosilanes,[2] and ethylchlorosilanes[3] and I shall now report on the Raman spectra of methoxychlorosilanes. The samples were prepared as follows; tetrachlorosilane was added slowly to vigorously stirred anhydrous methanol. After careful fractional distillation, they gave the following boiling point: CH_3OSiCl_3, 79°; $(CH_3O)_2SiCl_2$, 100°; $(CH_3O)_3SiCl$, 112–0.5°. The results for these compounds together with the data available for the two compounds $SiCl_4$ and $Si(OCH_3)_4$[4] are given in Table I. Taking into

TABLE I (for Murata letter). Raman spectra of methoxychlorosilanes (cm^{-1}).

Modes of vibrations	$SiCl_4$	CH_3OSiCl_3	$(CH_3O)_2SiCl_2$	$(CH_3O)_3SiCl$	$(CH_3O)_4Si$
τ(Si−O)*		135(4s)(ek)	140(4s)(ek)	147(2b)(ek)	
δ(Si−Cl)	E 150	E 170(8s)(ek)	A_1 183(5s)(e)		
			A_2 ...	E ...	E ...
δ(Si−OCH_3)	F_2 221	A_1 226(6s)(ek)	A_1 250(2s)(ek)	A_1 264(2b)(ek)	F_2 ...
		E 295(3s)(ek)	B_1 315(3b)(ek)	E 357(2b)(e)	
			B_2 364(1s)(e)		
δ(O−CH_3)		329(3s)(ek)	406(2s)(ek)	420(2b)(ek)	
ν(Si−Cl)	A_1 424	A_1 450(10s)(ek)	A_1 481(10b)(ek)	A_1 510(4s)(ek)	A_1 649
	F_2 608	E 602(1b)(ek)	B_2 590(2s)(ek)	A_1 717(6s)(ek)	F_2 840
ν(Si−OCH_3)		A_1 808(5s)(ek)	A_1 772(5s)(ek)	E 845(4s)(ek)	
			B_1 851(3s)(ek)		
ν(O−CH_3)			1098(1s)(k)	1097(2b)(k)	1099
			1190(1s)(k)	1210(1s)(k)	1178
δ(C−H)		1270(1s)(e)	1274(2s)(ek)	1276(4s)(ek)	
		1362(2s)(ek)	1373(2s)(ek)	1370(3s)(ek)	
		1468(2s)(ek)	1459(3s)(ek)	1465(4b)(ek)	1457
					2777
ν(C−H)		2850(6s)(ek)	2850(8s)(ek)	2850(10s)(ek)	2836
		2945(6s)(ek)	2945(8s)(ek)	2945(10s)(ek)	2935
		3002(2s)(ek)	3002(2s)(ek)	3002(3s)(ek)	

* τ denotes the internal rotation around the axis of Si−O bond.

account the result obtained for methylchlorosilanes,[1,5] I have tentatively assigned the observed lines as shown in Table I, where *A* denotes totally symmetric, *B* antisymmetric, *E* twofold degenerate, and *F* threefold degenerate vibrations of the tetrahedral molecule, respectively.

[1] H. Murata, J. Chem. Soc. Japan, Pure Chem. Sect. (to be published).
[2] H. Murata and S. Hayashi, J. Chem. Phys. **19**, 1217 (1951).
[3] Murata, Okawara, and Watase, J. Chem. Phys. **18**, 1308 (1950).
[4] B. T. Thosar and R. N. Bapat, Z. Physik **109**, 472 (1938).
[5] Shimanouchi, Tsuchiya, and Mikawa, J. Chem. Phys. **18**, 1306 (1950).

A New Approach to Photosynthesis in Vitro

N. URI*
Chemistry Department, University of Manchester, Manchester, England
(Received September 25, 1951)

THE mechanism of photosynthesis *in vivo* is far from being understood. It is thought that the first step is the photo-oxidation of water. This may be effected also by irradiation of suspensions of chloroplasts,[1] even though removed from living cells, accompanied by the reduction of various substances, but not carbon dioxide. The second step is the reduction of carbon dioxide or carboxylic acids, possibly incorporated in large complex molecules, by the substance formed during the photo-oxidation of water. The significance of the malic enzyme and the coenzyme II in the extracellular reaction of isolated chloroplasts was recently discovered by Vishniac and Ochoa,[2] Tolmach,[3] and Arnon.[4]

Attempts to imitate the whole process in vitro have invariably failed. Linstead, Braude, and Timmons[5] showed recently that the claims made by Baur and Niggli[6] to that effect were unfounded. This author considers that by photoexcited electron transfer a highly unstable species can be produced in solution, e.g., $Pb^{2+}Cl^- \xrightarrow{h\nu} Pb^+ + Cl$, first hinted at by Rabinowitch[7] and substantiated by the author's observation of initiation of vinyl polymerization in this system. There is a possibility that under strictly anaerobic conditions and *in the presence of a substrate*, like benzene derivatives, which would react with Cl atoms or other oxidizing radicals by means of a bond breaking mechanism (e.g., (1) $HO_3SC_6H_5 + Cl \rightarrow HCl + HO_3SC_6H_4^{\cdot}$ (2) $HO_3SC_6H_4^{\cdot} + Cl \rightarrow HO_3SC_6H_4Cl$) but would not oxidize by electron transfer the unstable reduced substance (e.g., Pb^+), both carbon dioxide or carboxylic acids might be reduced. The essential condition is a negative oxidation-reduction potential $M^{(n-1)+}/M^{n+}$ in the order of magnitude of −0.5 volt (e.g., like that of Cr^{2+}/Cr^{3+}). The important function of the substrate is to *inhibit a secondary dark back reaction*. The reduction of carboxylic acids could occur via an electron transfer mechanism,[8] *viz.*, $e + RCOOH \rightarrow (RCOOH)^- \rightarrow RCO + OH^-$. The RCO radical could react with R...H of weak bond strength to give 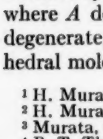 +R or by disproportionation 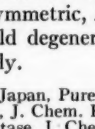 +CO. It is generally assumed that RCO radicals are formed in the photolysis of ketones.

A reaction in which a true photocatalyst takes part was reported by Brealey, Evans, and Uri[9] in the system $FeCl_4^-$-alcohol-thionine-light. A detailed account of this work by Brealey and Uri[10] is in the course of publication. In this case $FeCl_4^-$ can be considered as photocatalyst, while the net reaction is the reduction of thionine by alcohol. The reduction of carbon dioxide or carboxylic acid by water is, of course, energetically much more difficult (the difference is approximately 0.8 volt). Some preliminary experiments were carried out in this laboratory in collaboration with Mr. Copestake, using $PbCl_4^{2-}$ and $Pb^{2+}Cl^-$ as photocatalysts, but failed to give formaldehyde yields clearly distinguishable from blank tests, although it was shown that $PbCl_4^{2-}$ is formed and such dyes as thionine and Janus green are reduced photocatalytically, when the system $PbCl_2$-LiCl-dye-ethyl alcohol is irradiated with ultraviolet light of wavelengths in the region 280–320 mμ. Janus green is more difficult to reduce than thionine. The oxidation-reduction potential is of the order of −0.25 volt in neutral solution. There is no appreciable photobleaching of Janus green in the absence of the photocatalyst. Further work along those lines, e.g., with various fluoride complexes, could, however, lead to some interesting results. The species are, of course, not the same as those *in vivo*, with chlorophyll as photocatalyst, but in principle the photocatalytic system might be similar. The method described here is suggested as a new approach to artificial photosynthesis. The author intends to continue this investigation and would like to acknowledge a very stimulating discussion with Dr. M. J. S. Dewar (Maidenhead) on many aspects of this subject.

* Present address: Institute of Radiobiology and Biophysics, University of Chicago, Chicago 37, Illinois.
[1] J. Franck, Ann. Rev. Plant Physiology **2**, 53 (1951); H. Gaffron and E. W. Fager, Ann. Rev. Plant Physiology **2**, 87 (1951).
[2] W. Vishniac and S. Ochoa, Nature **167**, 768 (1951).
[3] L. J. Tolmach, Nature **167**, 946 (1951).
[4] D. I. Arnon, Nature **167**, 1008 (1951).
[5] Linstead, Braude, and Timmons, Nature **166**, 557 (1950).
[6] E. Baur and F. Niggli, Helv. Chim. Acta **26**, 251 (1943).
[7] E. Rabinowitch, Revs. Modern Phys. **14**, 112 (1942).
[8] N. Uri, Remarks in the Faraday Society Discussion on 'Hydrocarbons,' (to be published).
[9] Brealey, Evans, and Uri, Nature **166**, 959 (1950).
[10] G. J. Brealey and N. Uri, J. Chem. Phys. **20**, 257 (1952).